

**ATTN: ACCESSIONING DEPT. , PARKWAY CENTER
NASA CENTER FOR AEROSPACE INFORMATION (CASI)
7121 STANDARD DRIVE
HANOVER, MD, 21076-1320**

*199808614
W-31
primary*

NAG-1-1310

SUMMARY OF RESEARCH REPORT

by

**Dr. Isaac Elishakoff
Department of Mechanical Engineering
Florida Atlantic University
Boca Raton, FL, 33431-0991**

**Tel: 561-297-2729
Fax: 561-297-2825**

November, 1998



0960-0779(94)00158-8

Buckling Mode Localization in Elastic Plates due to Misplacement in the Stiffener Location

I. ELISHAKOFF and Y. W. LI

Center for Applied Stochastics Research and Department of Mechanical Engineering, Florida Atlantic University,
Boca Raton, FL 33431-0991, USA

and

J. H. STARNES JR

NASA Langley Research Center, Hampton, VA 23664-5225, USA

(Received 26 May 1994)

Abstract—This paper deals with the buckling of the stiffened plate under uni-axial compression. The direct integration of the governing differential equation is performed and the exact solution to the problem is obtained. As examples, a square plate with single stiffener, and a stiffened three-span, continuous plate are investigated, with special attention given to the influence of stiffener misplacement on the buckling load and mode shape of the plate. It is found that a small misplacement of the stiffeners from the nominal configuration may change the buckling mode from a global one to a highly localized one.

1. INTRODUCTION

Traditionally, the stability of the stiffened plate has been studied following three different trends. One approach consists of replacing the stiffened plate by an 'equivalent' orthotropic plate after the stiffeners are smeared out, in an energetic sense, over the entire surface of the plate [1, 2]. This approach appears reasonable for plates with many closely spaced stiffeners but is doubtful for plates with fewer stiffeners. The second approach is based on energy consideration and treats the contributions of the plate and the stiffener separately; the Rayleigh-Ritz method has been utilized widely to estimate the buckling load of the stiffened plate structure [3, 4]. This method may predict well the global buckling but fail to detect the localization of buckling mode due to the small changes in the location of the stiffeners. The third approach is the analytical method for equally spaced stiffeners by the analytical finite difference calculus [5, 6] which, though powerful for studying plates with periodically spaced stiffeners or supports, is totally inapplicable if the periodicity is disturbed as is usually the case when misplacement in the location of the stiffener or support is present through imprecision of construction. Despite their usefulness and simplicity, the above-mentioned methods can only be employed to investigate the global buckling of the structure and appear incapable of revealing the localization phenomena when the structure is sparsely or irregularly stiffened and the buckling mode is likely to be localized.

In this paper, we investigate the effect of small structural irregularity, due to the misplacement of stiffeners or interior supports, on both the buckling load and the buckling

51-39
4108 897
358919

P. 16 NIS

mode of the rib-stiffened plate. Since the buckling mode shape is of main interest here, the interaction between the plate and stiffeners should be properly taken into account; and none of the above-mentioned methods seems successful in this context. Here, the integration of the general governing differential equation is attempted for the stiffened elastic plate. By considering the rib-stiffened plate as a physically continuous plate with as many spans as the number of ribs, the stiffeners are accounted for through the conditions of continuity. Two cases commonly encountered in practice are considered; one with simple support under the ribs and one without. It is found that in the presence of small misplacement of stiffeners or interior supports, the buckling mode shapes experience dramatic changes to become strongly localized. Localization phenomenon was first uncovered by the Nobel Laureate P. W. Anderson [7] in physics. Its occurrence in structures has recently attracted much attention. Among others, Pierre and Plaut [8] considered the two-span column case with deterministic disorder. A more general case, the multi-span column, was recently treated by Nayfeh and Hawwa [9] using the transfer matrix method. Ariaratnam and Xie [10] investigated the localization in the buckling of a system of rigid bars connected with springs in the stochastic setting. Tvergaard and Needleman [11] discussed the development of localized patterns in the elastic-plastic and thermal buckling problems. Cai and Lin [12] studied the localization of wave propagation in randomly disordered periodic structures. The deterministic buckling localization in cylindrical shells was investigated by El Naschie [13–16]. In this study, we deal with the localization phenomenon in the buckling of stiffened plates. As a numerical example, a two-span plate with a single rib is discussed using different parameters for the stiffener. Furthermore, a stiffened three-span plate is also investigated, and the optimal configuration of stiffener placement, which yields the highest buckling strength, is discussed along with the attendant localization sensitivity to deterministic misplacements.

2. STABILITY FORMULATION

We consider a rib-stiffened rectangular plate subjected in its mid-plane to uniform compression P in the x direction (Fig. 1). The differential equation of the deflection surface of the plate under consideration is

$$D \left(\frac{\partial^4 w}{\partial x^4} + 2 \frac{\partial^4 w}{\partial x^2 \partial y^2} + \frac{\partial^4 w}{\partial y^4} \right) + P \frac{\partial^2 w}{\partial x^2} = 0, \quad (1)$$

where w is the transverse displacement, downward positive; D is the flexural rigidity of the

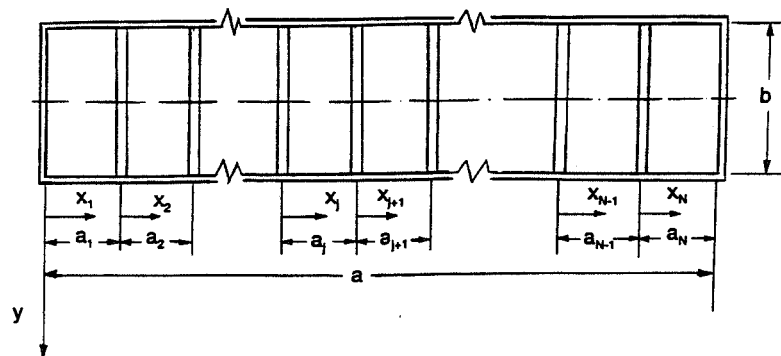


Fig. 1. Simply supported rectangular plate stiffened with N ribs.

plate. The solution of equation (1) can be represented in the following form

$$w(x, y) = X(x) \sin\left(\frac{\pi y}{b}\right). \quad (2)$$

Substitution of equation (2) into equation (1) results in

$$\frac{d^4 X}{dx^4} + \left(\frac{P}{D} - 2\frac{\pi^2}{b^2}\right) \frac{d^2 X}{dx^2} + \frac{\pi^4}{b^4} X = 0. \quad (3)$$

The corresponding characteristic equation reads

$$s^4 + \left(\frac{P}{D} - 2\frac{\pi^2}{b^2}\right) s^2 + \frac{\pi^4}{b^4} = 0 \quad (4)$$

or

$$s^2 = -\left(\frac{P}{2D} - \frac{\pi^2}{b^2}\right) \pm \sqrt{\frac{P}{2D}\left(\frac{P}{2D} - 2\frac{\pi^2}{b^2}\right)}. \quad (5)$$

Even for the unstiffened plate, the buckling load P_{cr} is always equal to or larger than $4\pi^2 D/b^2$ [17]. Thus, for rib-stiffened, or intermediately supported, plates, we have roots $s_i (i = 1, 2, 3, 4)$ as following

$$s_1 = i\beta_1, \quad s_2 = -i\beta_1, \quad s_3 = i\beta_2, \quad s_4 = -i\beta_2, \quad (6)$$

where

$$\beta_1 = \left(\left(\frac{P}{2D} - \frac{\pi^2}{b^2} \right) + \left(\frac{P}{2D} \left(\frac{P}{2D} - 2\frac{\pi^2}{b^2} \right) \right)^{1/2} \right)^{1/2},$$

$$\beta_2 = \left(\left(\frac{P}{2D} - \frac{\pi^2}{b^2} \right) - \left(\frac{P}{2D} \left(\frac{P}{2D} - 2\frac{\pi^2}{b^2} \right) \right)^{1/2} \right)^{1/2}. \quad (7)$$

Solution of equation (1) can be written as

$$w(x) = [A \cos(\beta_1 x) + B \sin(\beta_1 x) + C \cos(\beta_2 x) + D \sin(\beta_2 x)] \sin\left(\frac{\pi y}{b}\right), \quad (8)$$

where A , B , C and D are unknown constants, which are to be determined by use of continuity and boundary conditions. For the arbitrary, j th span, the solution can be written as

$$w_j(x_j) = [A_j \cos(\beta_1 x_j) + B_j \sin(\beta_1 x_j) + C_j \cos(\beta_2 x_j) + D_j \sin(\beta_2 x_j)] \sin\left(\frac{\pi y}{b}\right),$$

$$0 \leq x_j \leq a_j, \quad (9)$$

where a_j is the length of the j th span and j ranges from 1 to N for an N -span plate. We consider the plate simply supported along its periphery. Then the boundary conditions are

$$w_1|_{x_1=0} = 0,$$

$$M_x^{(1)}|_{x_1=0} = -D \left(\frac{\partial^2 w_1}{\partial w_1^2} + \nu \frac{\partial^2 w_1}{\partial y^2} \right) \Big|_{x_1=0} = 0,$$

$$M_x^{(N)}|_{x_N=a_N} = -D \left(\frac{\partial^2 w_N}{\partial x_N^2} + \nu \frac{\partial^2 w_N}{\partial y^2} \right) \Big|_{x_N=a_N} = 0,$$

$$w_N|_{x_N=a_N} = 0, \quad (10)$$

where $M_x^{(1)}$ and $M_x^{(N)}$ are the bending moments in the first and last spans of the continuous plate; ν is the Poisson ratio. In view of (9), the above boundary conditions become

$$A_1 + C_1 = 0, \quad (11)$$

$$\beta_1^2 A_1 + \beta_2^2 C_1 = 0, \quad (12)$$

$$\beta_1^2 \cos(\beta_1 a_N) A_N + \beta_1^2 \sin(\beta_1 a_N) B_N + \beta_2^2 \cos(\beta_2 a_N) C_N + \beta_2^2 \sin(\beta_2 a_N) D_N = 0, \quad (13)$$

$$\cos(\beta_1 a_N) A_N + \sin(\beta_1 a_N) B_N + \cos(\beta_2 a_N) C_N + \sin(\beta_2 a_N) D_N = 0. \quad (14)$$

As to the continuity conditions between two successive spans, two cases of practical interest deserve consideration.

Case A. Simple support under the rib. In some applications, the flexural rigidity of the stiffener is not large enough, and a vertical support is installed under the stiffener to suppress the transverse displacement. In this case, the continuity conditions between the two typical neighboring spans j and $j + 1$ are [2]

$$\begin{aligned} w_{j+1}|_{x_{j+1}=0} &= 0, \\ w_j|_{x_j=a_j} &= 0, \\ \frac{\partial w_j}{\partial x_j} \Big|_{x_j=a_j} &= \frac{\partial w_{j+1}}{\partial x_{j+1}} \Big|_{x_{j+1}=0}, \\ M_x^{(j+1)}|_{x_{j+1}=0} - M_x^{(j)}|_{x_j=a_j} &= (GJ)_j \frac{\partial^3 w_{j+1}}{\partial x_{j+1} \partial y^2} \Big|_{x_{j+1}=0} \end{aligned} \quad (15)$$

or

$$-D \left(\frac{\partial^2 w_{j+1}}{\partial x_{j+1}^2} + \nu \frac{\partial^2 w_{j+1}}{\partial y^2} \right) \Big|_{x_{j+1}=0} + D \left(\frac{\partial^2 w_j}{\partial x_j^2} + \nu \frac{\partial^2 w_j}{\partial y^2} \right) \Big|_{x_j=a_j} = (GJ)_j \frac{\partial^3 w_{j+1}}{\partial x_{j+1} \partial y^2} \Big|_{x_{j+1}=0},$$

where $(GJ)_j$ denotes the torsional rigidity of the j th rib.

Substituting equation (9) into the above conditions of continuity leads to the following four equations:

$$A_{j+1} + C_{j+1} = 0, \quad (16)$$

$$\cos(\beta_1 a_j) A_j + \sin(\beta_1 a_j) B_j + \cos(\beta_2 a_j) C_j + \sin(\beta_2 a_j) D_j = 0, \quad (17)$$

$$\begin{aligned} -\beta_1 \sin(\beta_1 a_j) A_j + \beta_1 \cos(\beta_1 a_j) B_j - \beta_2 \sin(\beta_2 a_j) C_j + \beta_2 \cos(\beta_2 a_j) D_j - \beta_1 B_{j+1} \\ - \beta_2 D_{j+1} = 0, \end{aligned} \quad (18)$$

$$\begin{aligned} -\beta_1^2 \cos(\beta_1 a_j) A_j - \beta_1^2 \sin(\beta_1 a_j) B_j - \beta_2^2 \cos(\beta_2 a_j) C_j - \beta_2^2 \sin(\beta_2 a_j) D_j \\ + \beta_1^2 A_{j+1} + \frac{(GJ)_j}{D} \frac{\pi^2}{b^2} \beta_1 B_j + \beta_2^2 C_{j+1} = \frac{(GJ)_j}{D} \frac{\pi^2}{b^2} \beta_2 D_{j+1} = 0. \end{aligned} \quad (19)$$

Case B. No support under the rib. In this case, the bending, in addition to the torsion, of ribs should be taken into account. The conditions of continuity between two consecutive spans j and $j + 1$ read

$$\begin{aligned}
w_j|_{x_j=a_j} &= w_{j+1}|_{x_{j+1}=0}, \\
\frac{\partial w_j}{\partial x_j} \Big|_{x_j=a_j} &= \frac{\partial w_{j+1}}{\partial x_{j+1}} \Big|_{x_{j+1}=0}, \\
M_x^{(j+1)}|_{x_{j+1}=0} - M_x^{(j)}|_{x_j=a_j} &= (GJ)_j \frac{\partial^3 w_{j+1}}{\partial x_{j+1} \partial y^2} \Big|_{x_{j+1}=0} \\
\text{or } \left(\frac{\partial^2 w_j}{\partial x_j^2} + v \frac{\partial^2 w_j}{\partial y^2} \right) \Big|_{x_j=a_j} - \left(\frac{\partial^2 w_{j+1}}{\partial x_{j+1}^2} + v \frac{\partial^2 w_{j+1}}{\partial y^2} \right) \Big|_{x_{j+1}=0} &= (GJ)_j \frac{\partial^3 w_{j+1}}{\partial x_{j+1} \partial y^2} \Big|_{x_{j+1}=0}, \quad (20) \\
V_x^{(j+1)}|_{x_{j+1}=0} - V_x^{(j)}|_{x_j=a_j} &= (EI)_j \frac{\partial^4 w_{j+1}}{\partial y^4} \Big|_{x_{j+1}=0}
\end{aligned}$$

or

$$\left[\frac{\partial^3 w_j}{\partial x_j^3} + (2-v) \frac{\partial^2 w_j}{\partial x_j \partial y^2} \right] \Big|_{x_j=a_j} - \left[\frac{\partial^3 w_{j+1}}{\partial x_{j+1}^3} + (2-v) \frac{\partial^2 w_{j+1}}{\partial x_{j+1} \partial y^2} \right] \Big|_{x_{j+1}=0} = (EI)_j \frac{\partial^4 w_{j+1}}{\partial y^4} \Big|_{x_{j+1}=0},$$

where $V_x^{(j)}$ and $V_x^{(j+1)}$ are the shearing forces in the j th and $(j+1)$ th spans of the plate; $(EI)_j$ is the flexural rigidity of the j th rib.

These conditions of continuity can, in turn, be expressed by the following equations in terms of the constants of integration:

$$\cos(\beta_1 a_j) A_j + \sin(\beta_1 a_j) B_j + \cos(\beta_2 a_j) C_j + \sin(\beta_2 a_j) D_j - A_{j+1} - C_{j+1} = 0, \quad (21)$$

$$\begin{aligned}
-\beta_1 \sin(\beta_1 a_j) A_j + \beta_1 \cos(\beta_1 a_j) B_j - \beta_2 \sin(\beta_2 a_j) C_j + \beta_2 \cos(\beta_2 a_j) D_j - \beta_1 B_{j+1} \\
- \beta_2 D_{j+1} = 0, \quad (22)
\end{aligned}$$

$$\begin{aligned}
-\beta_1^2 \cos(\beta_1 a_j) A_j - \beta_1^2 \sin(\beta_1 a_j) B_j - \beta_2^2 \cos(\beta_2 a_j) C_j - \beta_2^2 \sin(\beta_2 a_j) D_j \\
+ \beta_1^2 A_{j+1} + \frac{(GJ)_j}{D} \frac{\pi^2}{b^2} \beta_1 B_{j+1} + \beta_2^2 C_{j+1} + \frac{(GJ)_j}{D} \frac{\pi^2}{b^2} \beta_2 D_{j+1} = 0, \quad (23)
\end{aligned}$$

$$\begin{aligned}
\beta_1^3 \sin(\beta_1 a_j) A_j - \beta_1^3 \cos(\beta_1 a_j) B_j + \beta_2^3 \sin(\beta_2 a_j) C_j - \beta_2^3 \cos(\beta_2 a_j) D_j \\
- \frac{(EI)_j}{D} \left(\frac{\pi}{b} \right)^4 A_{j+1} + \beta_1^3 B_{j+1} - \frac{(EI)_j}{D} \left(\frac{\pi}{b} \right)^4 C_{j+1} + \beta_2^3 D_{j+1} = 0. \quad (24)
\end{aligned}$$

Introducing the following non-dimensional quantities

$$\lambda = \frac{Pb^2}{\pi^2 D}, \quad r_j = \frac{a_j}{b}, \quad \tau_j = \frac{(GJ)_j}{bD}, \quad \omega_j = \frac{(EI)_j}{bD} \quad (j = 1 \sim N), \quad (25)$$

$$\bar{\beta}_1 = \sqrt{\frac{\lambda}{2}} - 1 + \sqrt{\frac{\lambda}{2} \left(\frac{\lambda}{2} - 2 \right)}, \quad \bar{\beta}_2 = \sqrt{\frac{\lambda}{2}} - 1 - \sqrt{\frac{\lambda}{2} \left(\frac{\lambda}{2} - 2 \right)}$$

the boundary conditions for the simply supported continuous plate equations (11)–(14), can be written as

$$A_1 + C_1 = 0, \quad (26)$$

$$\bar{\beta}_1^2 A_1 + \bar{\beta}_2^2 C_1 = 0, \quad (27)$$

$$\bar{\beta}_1^2 \cos(\bar{\beta}_1 r_N \pi) A_N + \bar{\beta}_1^2 \sin(\bar{\beta}_1 r_N \pi) B_N + \bar{\beta}_2^2 \cos(\bar{\beta}_2 r_N \pi) C_2 + \bar{\beta}_2^2 \sin(\bar{\beta}_2 r_N \pi) D_N = 0, \quad (28)$$

$$\cos(\bar{\beta}_1 r_N \pi) A_N + \sin(\bar{\beta}_1 r_N \pi) B_N + \cos(\bar{\beta}_2 r_N \pi) C_N + \sin(\bar{\beta}_2 r_N \pi) D_N = 0. \quad (29)$$

The conditions of continuity for Case A, equations (16)–(19), are transformed into the following equations:

$$A_{j+1} + C_{j+1} = 0, \quad (30)$$

$$\cos(\bar{\beta}_1 r_j \pi) A_j + \sin(\bar{\beta}_1 r_j \pi) B_j + \cos(\bar{\beta}_2 r_j \pi) C_j + \sin(\bar{\beta}_2 r_j \pi) D_j = 0, \quad (31)$$

$$-\bar{\beta}_1 \sin(\bar{\beta}_1 r_j \pi) A_j + \bar{\beta}_1 \cos(\bar{\beta}_1 r_j \pi) B_j - \bar{\beta}_2 \sin(\bar{\beta}_2 r_j \pi) C_j \\ + \bar{\beta}_2 \cos(\bar{\beta}_2 r_j \pi) D_j - \bar{\beta}_1 B_{j+1} - \bar{\beta}_2 D_{j+1} = 0, \quad (32)$$

$$-\bar{\beta}_1^2 \cos(\bar{\beta}_1 r_j \pi) A_j - \bar{\beta}_1^2 \sin(\bar{\beta}_1 r_j \pi) B_j - \bar{\beta}_2^2 \cos(\bar{\beta}_2 r_j \pi) C_j - \bar{\beta}_2^2 \sin(\bar{\beta}_2 r_j \pi) D_j \\ + \bar{\beta}_1^2 A_{j+1} + \tau_j \pi \bar{\beta}_1 B_{j+1} + \bar{\beta}_2^2 C_{j+1} + \tau_j \pi \bar{\beta}_2 D_{j+1} = 0. \quad (33)$$

For Case B, equations (21)–(24) are rendered into the following form:

$$\cos(\bar{\beta}_1 r_j \pi) A_j + \sin(\bar{\beta}_1 r_j \pi) B_j + \cos(\bar{\beta}_2 r_j \pi) C_j + \sin(\bar{\beta}_2 r_j \pi) D_j - A_{j+1} - C_{j+1} = 0, \quad (34)$$

$$-\bar{\beta}_1 \sin(\bar{\beta}_1 r_j \pi) A_j + \bar{\beta}_1 \cos(\bar{\beta}_1 r_j \pi) B_j - \bar{\beta}_2 \sin(\bar{\beta}_2 r_j \pi) C_j \\ + \bar{\beta}_2 \cos(\bar{\beta}_2 r_j \pi) D_j - \bar{\beta}_1 B_{j+1} - \bar{\beta}_2 D_{j+1} = 0, \quad (35)$$

$$-\bar{\beta}_1^2 \cos(\bar{\beta}_1 r_j \pi) A_j - \bar{\beta}_1^2 \sin(\bar{\beta}_1 r_j \pi) B_j - \bar{\beta}_2^2 \cos(\bar{\beta}_2 r_j \pi) C_j - \bar{\beta}_2^2 \sin(\bar{\beta}_2 r_j \pi) D_j \\ + \bar{\beta}_1^2 A_{j+1} + \tau_j \pi \bar{\beta}_1 B_{j+1} + \bar{\beta}_2^2 C_{j+1} + \tau_j \pi \bar{\beta}_2 D_{j+1} = 0, \quad (36)$$

$$\bar{\beta}_1^3 \sin(\bar{\beta}_1 r_j \pi) A_j - \bar{\beta}_1^3 \cos(\bar{\beta}_1 r_j \pi) B_j + \bar{\beta}_2^3 \sin(\bar{\beta}_2 r_j \pi) C_j - \bar{\beta}_2^3 \cos(\bar{\beta}_2 r_j \pi) D_j \\ - \omega_j \pi A_{j+1} + \bar{\beta}_1^3 B_{j+1} - \omega_j \pi C_{j+1} + \bar{\beta}_2^3 D_{j+1} = 0. \quad (37)$$

For a general N -span continuous plate, we have four equations for boundary conditions in the form of equations (26)–(29). Besides, $4 \times (N - 1)$ equations (four equations for each rib or interior support such as equations (30)–(33) or equations (34)–(37)) can be established from the continuity considerations. Altogether there are $4 \times N$ algebraic equations for the same number of unknown coefficients A_j , B_j , C_j and D_j ($j = 1 \sim N$)

$$[F(\lambda)]_{4 \times N} \{\Delta\}_{N \times 1} = \mathbf{0}, \quad (38)$$

where elements of matrix $[F(\lambda)]$ are composed of such parameters as those denoted in (25) and $\{\Delta\}$ is a column containing A_j , B_j , C_j and D_j . These equations are linear and homogeneous. A non-trivial solution is obtained by setting the determinant of $F(\lambda)$ equal to zero, which yields a transcendental equation whose smallest root is the critical buckling load λ . Having known the buckling load λ , equation (38) is used to determine, to an arbitrary constant multiple, the coefficients A_j , B_j , C_j and D_j which can then be substituted back into equation (9) to obtain the buckling mode shape of the entire plate. Note that, in the special case of plates with equally spaced stiffeners, the finite difference calculus discussed by Wah and Calcote [5] can be used. In this investigation, however, since we will concentrate on the two- or three-span plates with stiffeners not necessarily uniformly spaced, the use of the above-mentioned method is not viable here.

3. A PLATE WITH A SINGLE RIB-STIFFENER

In order to investigate the variation of the buckling mode of the stiffened plate due to a small structural irregularity, here we study the simplest case where there is a single stiffener which is slightly misplaced from the mid-span (Fig. 2). This is also the case where the discreteness of the stiffener has the most pronounced effect on the buckling load.

Let us consider a square plate. Intuitively, we know that the single stiffener should be placed as close as possible to the mid cross-section of the plate to produce the highest reinforcement on the plate. We will use the following non-dimensional notations for specifying the positions of the stiffeners

$$r_1 = \frac{1}{2} - \delta, \quad r_2 = \frac{1}{2} + \delta, \quad \delta = \frac{d}{a}, \quad (39)$$

where d denotes the misplacement of the stiffener, and δ is its non-dimensional counterpart. When d (or δ) is positive, the stiffener is shifted to the right of its designed position; when d (or δ) is negative, the stiffener is located to the left of its designed position. $F(\lambda)$ in equation (38) is now an 8×8 matrix with elements as follows:

$$\begin{aligned} \text{Case A: } F_{11} &= 1, & F_{13} &= 1, & F_{21} &= \bar{\beta}_1^2, & F_{23} &= \bar{\beta}_2^2, & F_{35} &= \bar{\beta}_1^2 \cos(\bar{\beta}_1 r_2 \pi), \\ F_{36} &= \bar{\beta}_1^2 \sin(\bar{\beta}_1 r_2 \pi), & F_{37} &= \bar{\beta}_2^2 \cos(\bar{\beta}_2 r_2 \pi), & F_{38} &= \bar{\beta}_2^2 \sin(\bar{\beta}_2 r_2 \pi), \\ F_{45} &= \cos(\bar{\beta}_1 r_2 \pi), & F_{46} &= \sin(\bar{\beta}_1 r_2 \pi), & F_{47} &= \cos(\bar{\beta}_2 r_2 \pi), \\ F_{48} &= \sin(\bar{\beta}_2 r_2 \pi), & F_{55} &= 1, & F_{57} &= 1, & F_{61} &= \cos(\bar{\beta}_1 r_1 \pi), \\ F_{62} &= \sin(\bar{\beta}_1 r_1 \pi), & F_{63} &= \cos(\bar{\beta}_2 r_1 \pi), & F_{64} &= \sin(\bar{\beta}_2 r_1 \pi), \\ F_{71} &= -\bar{\beta}_1 \sin(\bar{\beta}_1 r_1 \pi), & F_{72} &= \bar{\beta}_1 \cos(\bar{\beta}_1 r_1 \pi), & F_{73} &= \bar{\beta}_2 \cos(\bar{\beta}_2 r_1 \pi), \\ F_{74} &= \bar{\beta}_2 \sin(\bar{\beta}_2 r_1 \pi), & F_{76} &= -\bar{\beta}_1, & F_{78} &= -\bar{\beta}_2, & F_{81} &= -\bar{\beta}_1^2 \cos(\bar{\beta}_1 r_1 \pi), \\ F_{82} &= -\bar{\beta}_1^2 \sin(\bar{\beta}_1 r_1 \pi), & F_{83} &= \bar{\beta}_2^2 \cos(\bar{\beta}_2 r_1 \pi), & F_{84} &= -\bar{\beta}_2^2 \sin(\bar{\beta}_2 r_1 \pi), \\ F_{85} &= \bar{\beta}_1^2, & F_{86} &= \tau_1 \pi \bar{\beta}_1, & F_{87} &= \bar{\beta}_2^2, & F_{88} &= \tau_1 \pi \bar{\beta}_1. \end{aligned} \quad (40)$$

The rest of the elements are zero.

$$\begin{aligned} \text{Case B: } F_{11} &= 1, & F_{13} &= 1, & F_{21} &= \bar{\beta}_1^2, & F_{23} &= \bar{\beta}_2^2, & F_{35} &= \bar{\beta}_1^2 \cos(\bar{\beta}_1 r_2 \pi), \\ F_{36} &= \bar{\beta}_1^2 \sin(\bar{\beta}_1 r_2 \pi), & F_{37} &= \bar{\beta}_2^2 \cos(\bar{\beta}_2 r_2 \pi), & F_{38} &= \bar{\beta}_2^2 \sin(\bar{\beta}_2 r_2 \pi), \\ F_{45} &= \cos(\bar{\beta}_1 r_2 \pi), & F_{46} &= \sin(\bar{\beta}_1 r_2 \pi), & F_{47} &= \cos(\bar{\beta}_2 r_2 \pi), \\ F_{48} &= \sin(\bar{\beta}_2 r_2 \pi), & F_{51} &= \cos(\bar{\beta}_1 r_1 \pi), & F_{52} &= \sin(\bar{\beta}_1 r_1 \pi), \\ F_{53} &= \cos(\bar{\beta}_2 r_1 \pi), & F_{54} &= \sin(\bar{\beta}_2 r_1 \pi), & F_{55} &= -1, & F_{57} &= -1, \\ F_{61} &= -\bar{\beta}_1 \cos(\bar{\beta}_1 r_1 \pi), & F_{62} &= \bar{\beta}_1 \sin(\bar{\beta}_1 r_1 \pi), & F_{63} &= -\bar{\beta}_2 \cos(\bar{\beta}_2 r_1 \pi), \\ F_{64} &= \bar{\beta}_2 \sin(\bar{\beta}_2 r_1 \pi), & F_{66} &= -\bar{\beta}_1, & F_{68} &= -\bar{\beta}_2, & F_{71} &= -\bar{\beta}_1^2 \cos(\bar{\beta}_1 r_1 \pi), \\ F_{72} &= -\bar{\beta}_1^2 \sin(\bar{\beta}_1 r_1 \pi), & F_{73} &= -\bar{\beta}_2^2 \cos(\bar{\beta}_2 r_1 \pi), & F_{74} &= -\bar{\beta}_2^2 \sin(\bar{\beta}_2 r_1 \pi), \\ F_{75} &= -\bar{\beta}_1^2, & F_{76} &= \tau_1 \pi \bar{\beta}_1, & F_{77} &= \bar{\beta}_2^2, & F_{78} &= \tau_1 \pi \bar{\beta}_2, & F_{81} &= \bar{\beta}_1^3 \sin(\bar{\beta}_1 r_1 \pi), \\ F_{82} &= -\bar{\beta}_1^3 \cos(\bar{\beta}_1 r_1 \pi), & F_{83} &= \bar{\beta}_2^3 \sin(\bar{\beta}_2 r_1 \pi), & F_{84} &= -\bar{\beta}_2^3 \cos(\bar{\beta}_2 r_1 \pi), \\ F_{85} &= -\omega_1 \pi, & F_{86} &= \bar{\beta}_1^3, & F_{87} &= -\omega_2 \pi, & F_{88} &= \bar{\beta}_2^3. \end{aligned} \quad (41)$$

The rest of the elements are zero. The column $\{\Delta\}$ is now

$$\{\Delta\} = \{A_1, B_1, C_1, D_1, A_2, B_2, C_2, D_2\}^T. \quad (42)$$

Setting the determinant of $F(\lambda)$ to zero and using the quasi-Newton root searching method, one can find the smallest root of $\det F(\lambda) = 0$, which corresponds to the buckling load of the structure. Then, substituting λ back into equation (38) and taking any seven

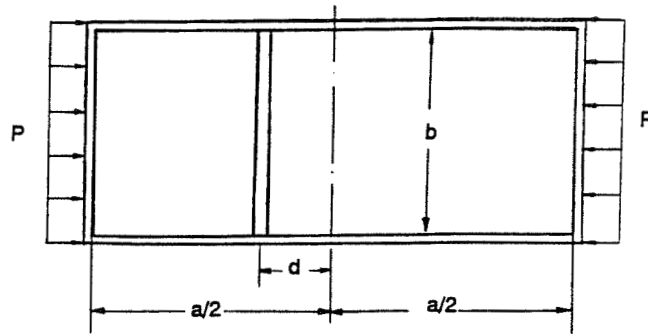


Fig. 2. Uni-axially compressed rectangular plate stiffened with a single misplaced rib.

equations out of the eight equations (38), we can solve for $\{\Delta\}$. The buckling mode reads

$$\begin{aligned}
 w_1(x_1) = & [A_1 \cos(\beta_1 x_1) + B_1 \sin(\beta_1 x_1) \\
 & + C_1 \cos(\beta_2 x_1) + D_1 \sin(\beta_2 x_1)] \sin\left(\frac{\pi y}{b}\right), \quad 0 \leq x_1 \leq \frac{a}{2} - d. \\
 w_2(x_2) = & [A_2 \cos(\beta_1 x_2) + B_1 \sin(\beta_1 x_2) + C_2 \cos(\beta_2 x_2) \\
 & + D_2 \sin(\beta_2 x_2)] \sin\left(\frac{\pi y}{b}\right), \quad 0 \leq x_2 \leq \frac{a}{2} - d.
 \end{aligned} \tag{43}$$

4. A THREE-SPAN STIFFENED PLATE

Now we consider a three-span continuous plate with stiffeners attached to the same positions as the interior supports. The plate is all-round simply supported and subjected to the uni-axial uniform compression in the direction perpendicular to the stiffeners (Fig. 3). For this specific problem, a set of twelve algebraic equations can be established in the form of equation (38). The conditions of continuity of the type discussed in Case A are adopted here.

Suppose that the two stiffeners are located at distances ξ_1 and ξ_2 from the left edge,

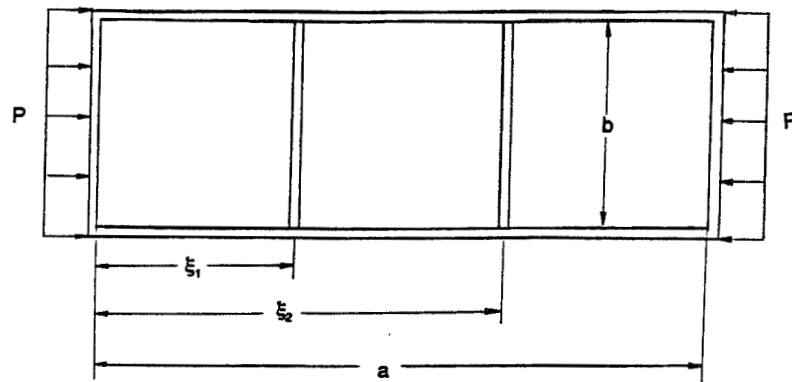


Fig. 3. Uni-axially compressed three-span stiffened plate.

respectively. Following the same procedure as discussed in the last section, the buckling mode for the three spans are expressed as

$$\begin{aligned}
 w_1(x_1) &= [A_1 \cos(\beta_1 x_1) + B_1 \sin(\beta_1 x_1) + C_1 \cos(\beta_2 x_1) \\
 &\quad + D_1 \sin(\beta_2 x_1)] \sin\left(\frac{\pi y}{b}\right), & 0 \leq x_1 \leq \xi_1, \\
 w_2(x_2) &= [A_2 \cos(\beta_1 x_2) + B_2 \sin(\beta_1 x_2) + C_2 \cos(\beta_2 x_2) \\
 &\quad + D_2 \sin(\beta_2 x_2)] \sin\left(\frac{\pi y}{b}\right), & 0 \leq x_2 \leq \xi_2 - \xi_1, \\
 w_3(x_3) &= [A_3 \cos(\beta_1 x_3) + B_3 \sin(\beta_2 x_3) + C_3 \cos(\beta_2 x_3) \\
 &\quad + D_3 \sin(\beta_2 x_3)] \sin\left(\frac{\pi y}{b}\right), & 0 \leq x_3 \leq a - \xi_2.
 \end{aligned} \tag{44}$$

We are interested in the variation of the buckling load and the buckling mode with the small misplacement of the stiffeners. In addition, the optimal position of the stiffeners which yields the highest buckling strength is also sought.

5. NUMERICAL RESULTS AND DISCUSSION

Numerical calculations are performed for both the single rib-stiffened plate and the stiffened three-span continuous plate. Structures with different parameters for the torsional and flexural rigidities are also investigated.

For the plate with a single stiffener, attachment of the stiffener to the mid cross-section of the plate provides the structure with the most favorable load carrying capacity. This conclusion holds true for both Case A and Case B. It is found that for Case A, where there is a support which prevents the vertical displacement of the plate, the magnitude of the nondimensional torsional rigidity τ has only a moderate effect on the buckling load when τ is larger than 10 (Fig. 4). Deviation of the stiffener from its supposed mid-span position reduces the buckling strength, but more importantly, it changes the buckling mode from an overall buckling of the plate to a local buckling of the plate segment with longer span. The more misplaced the stiffener, the greater the reduction in buckling load will be, and the more localized the buckling mode becomes, that is, the deflection of the plate on one side of the stiffener is much greater than that on the other side. For example, for Case A with a torsional rigidity of $\tau = 20.0$, the ratio of the maximum deflection in the left segment to that in the right segment is 4.5 when $\delta = 0.01$. If a bigger misplacement is involved, say $\delta = 0.02$, then the ratio of the maximum deflections in the two segments increases to 7.0. However, for the stiffener with torsional rigidity $\tau < 5$, small misplacement does not significantly affect the buckling load; for instance, when $\tau = 2$, a deviation of magnitude $\delta = 0.05$ produces only 4% reduction in buckling load. Figures 5 and 6 show the buckling mode shape of the plate in Case A for different values of τ . With a stiffener of τ larger than 30, the shorter segment of the plate is almost undeflected as buckling mode is localized in the longer segment. For Case B, the flexural rigidity of the stiffener plays a more important role in the buckling strength than the torsional rigidity, although the influence of torsional rigidity is still remarkable in the buckling mode shape. For example, it can be seen from Fig. 7 that only the stiffener with flexural rigidity $\omega \geq 5$ has noticeable strengthening effect, and that when ω falls below two, the position of the stiffener becomes almost irrelevant for the magnitude of the buckling load. When a plate is reinforced with a rib of moderate flexural stiffness, the longer segment of the plate is severely deflected at

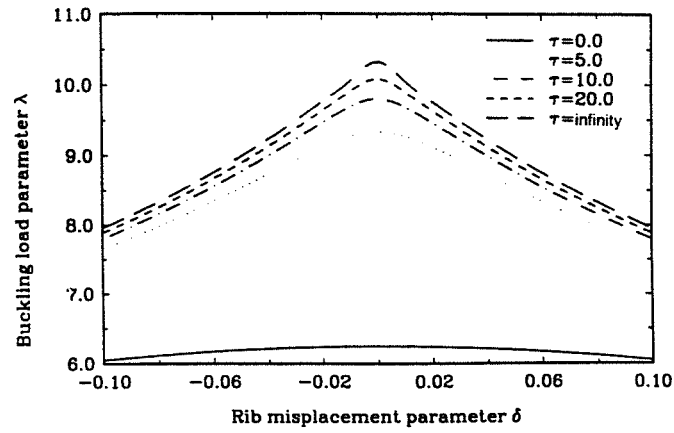


Fig. 4. Loci of buckling loads for a plate stiffened by a single rib with different values of τ (Case A).

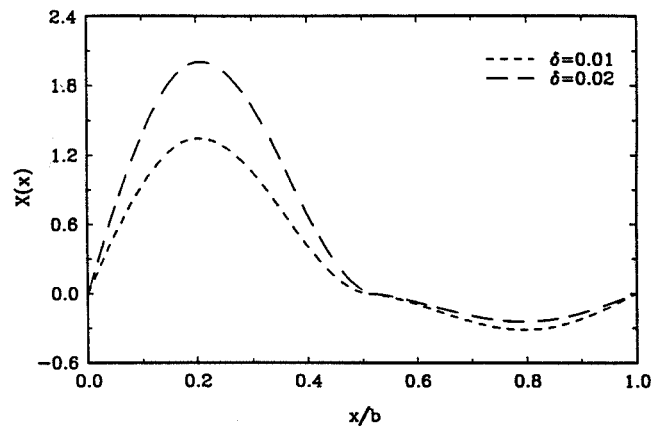


Fig. 5. Buckling mode localization for a plate stiffened with a single rib of $\tau = 20.0$ (Case A).

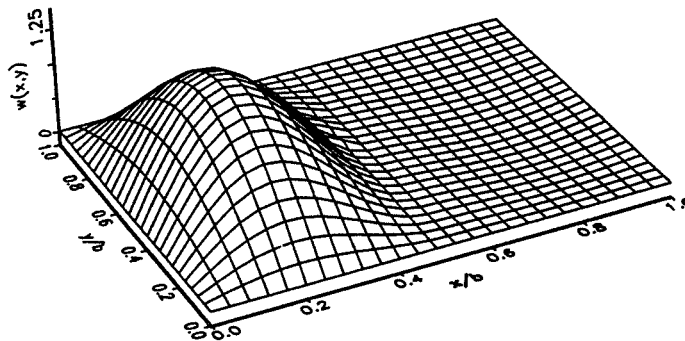


Fig. 6. Buckling mode shape for a plate stiffened by a single rib with misplacement $\delta = 0.02$ (Case A).

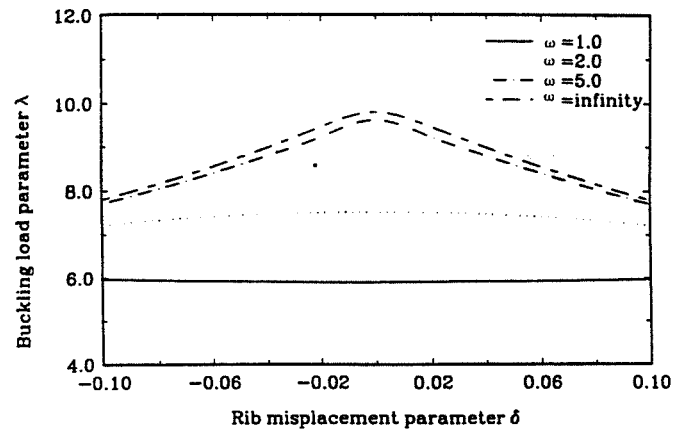


Fig. 7. Loci of buckling loads for a plate stiffened by a single rib with different values of ω ($\tau = 10.0$, Case B).

the onset of buckling while the short segment experiences only a scant deformation. So the buckling is still fairly localized, as can be seen from the mode shapes depicted in Figs 8 and 9. It is interesting to note that the cut-down in the overall strength of the plate by mispositioning a stronger stiffener can be greater. For instance, when $\tau = 30$ and $\omega = 20$, a 5% deviation from the mid-point produces 13% decrease in the buckling strength. Thus we can see, a unilateral increase in the stiffener's strength may make the whole structure highly sensitive to the misplacement (which can be regarded as a special kind of initial imperfection) in the sense that a small misplacement of the stiffener or interior support can lower the buckling load of the plate, and more importantly, localize the buckling mode shape.

For the three-span continuous plate, numerical results show that, as far as the buckling load is concerned, equally spaced stiffeners such that the three spans of the plate have the same length are not most beneficial. As compared with the single rib-stiffened plate, the three-span plate is even more sensitive to the misplacement of the stiffener. For example, if one stiffener is fixed at $\xi_1 = a/3$, the other stiffener is supposed to be located at $\xi_2 = 2a/3$ but somehow it deviates from this position by, say, $\delta_2 = -0.02$ (the negative sign representing the misplacement is in the negative x direction), the buckling load is

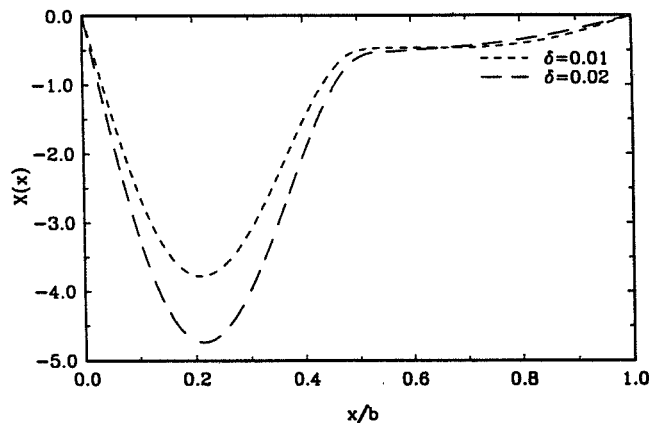


Fig. 8. Buckling mode localization for a plate stiffened by a single rib of $\tau = 20.0$ and $\omega = 10.0$ (Case B).

decreased by 9.5% from its counterpart without misplacement. Interestingly enough, some patterns of the misplacement are detrimental, while others can be helpful. For instance, suppose the stiffeners are designed to be located at $\xi_1 = a/3$ and $\xi_2 = 2a/3$, respectively. The combination of the misplacement by the magnitude $\delta_1 = \delta_2 = 0.02$ (meaning the misplacement are all in the positive x direction) from $\xi_1 = a/3$ and $\xi_2 = 2a/3$, respectively, cuts down the buckling load by 9.6%. However, misplacement of $\delta_1 = -\delta_2 = -0.02$ (meaning the left stiffener has been moved slightly to the left and the right stiffener to the right) boosts the buckling strength by 11% (Fig. 10). As for the buckling mode, in the majority of the situations, the buckling is still severely localized (Fig. 11). This is shown by Fig. 12 where a small misplacement $\delta_2 = -0.01$ of the right stiffener triggers the onset of the local buckling in the third span of the plate at a lower load than its counterpart without the misplacement. When this happens, the other two spans hardly deflect at all.

Numerical analysis shows the optimal stiffener layout for stiffeners with torsional rigidity $\tau = 20$ is $\xi_1 = 0.329a$ and $\xi_2 = 0.671a$. The corresponding buckling load is 19.6% above the buckling load with two identical stiffeners positioned at $\xi_1 = a/3$ and $\xi_2 = 2a/3$. This result can also be interpreted as follows: for misplacement $\delta_1 = 0.334 - 0.329 = 0.005$ and $\delta_2 = 0.667 - 0.671 = -0.004$, the buckling load is decreased by 16% $((1 - 1/1.19) \times$

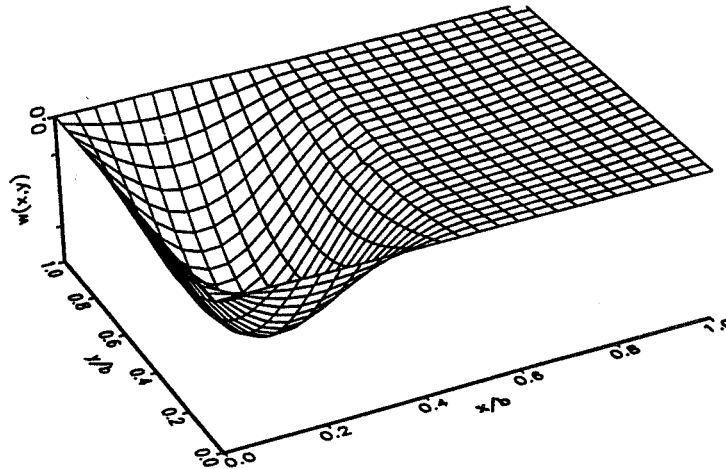


Fig. 9. Buckling mode shape for a plate stiffened by a single rib with misplacement $\delta = 0.01$ (Case B).

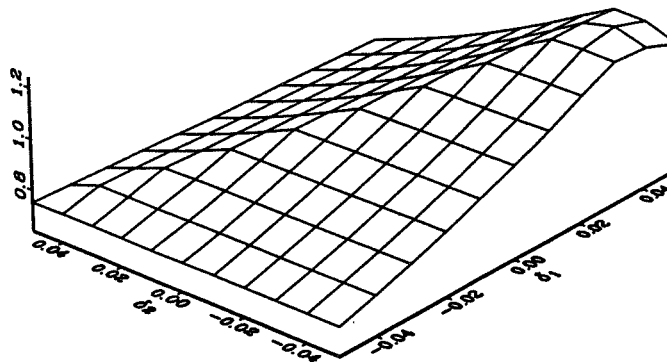


Fig. 10. Effect of misplacements on the buckling load of a stiffened, three-span plate ($\tau_1 = \tau_2 = 20.0$).

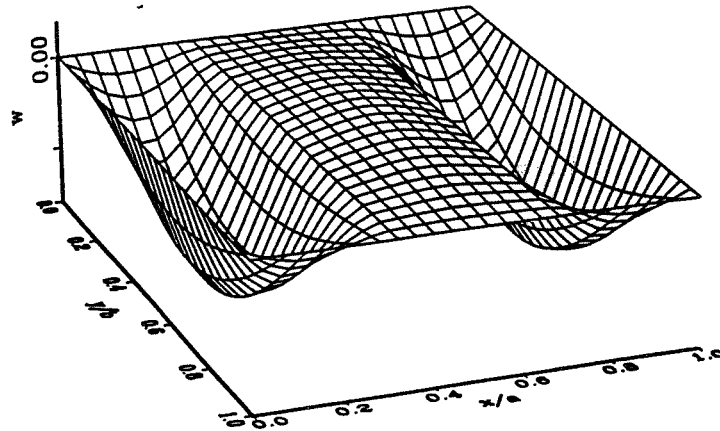


Fig. 11. Buckling mode shape for a stiffened, three-span plate without stiffener misplacement ($\tau_1 = \tau_2 = 20.0$, $\delta_1 = \delta_2 = 0.0$).

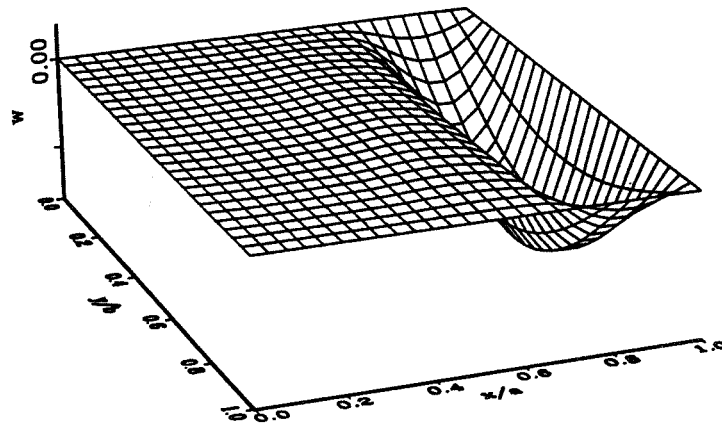


Fig. 12. Buckling mode shape for a stiffened, three-span plate with slight stiffener misplacement ($\tau_1 = \tau_2 = 20.0$, $\delta_1 = 0.0$, $\delta_2 = -0.01$).

100%). This again demonstrates the high sensitivity of optimally designed structures to small imperfections. This phenomenon was discussed by Budiansky and Hutchinson [18] as well as Zyczkowski and Gajewski [19]. Moreover, it is found here that the optimal pattern of the stiffener layout is almost independent of the specific value of τ , as long as the two stiffeners are identical. For example, even when the torsional rigidity τ is decreased to 5.0, the most favorable positions of two stiffeners are hardly changed, as they are now $\xi_1 = 0.330a$ and $\xi_2 = 0.670a$. Figure 13 depicts the buckling mode for such a situation, from which we can observe that with the optimal stiffener layout the buckling mode is a global one, that is, all parts of the plate deflect to comparable degree and the potential capability of the structure is fully tapped.

In conclusion, the buckling mode localization phenomenon due to small misplacements in the stiffened or continuous plates should not be overlooked, especially in those applications where the mode shape is a significant concern. Due to the imprecision in the fabrication, the misplacement is always present and can to the large extent affect the buckling characteristics of the structure. When the structure is designed in terms of the

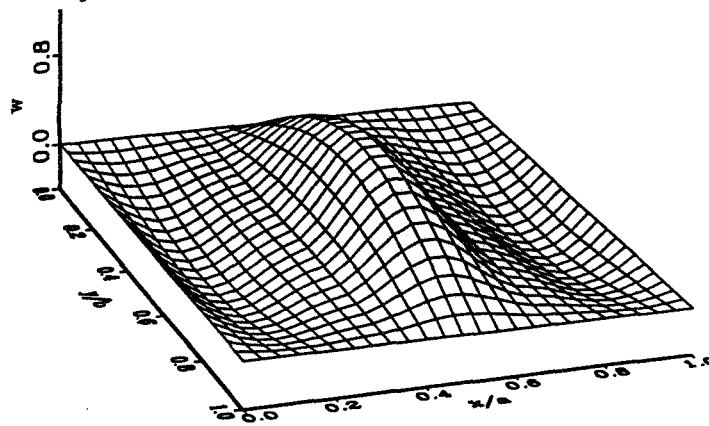


Fig. 13. Buckling mode shape for a stiffened three-span plate with optimal stiffener placement ($\tau_1 = \tau_2 = 20.0$, $\xi_1 = 0.329a$, $\xi_2 = 0.671a$).

optimal stiffener layout, misplacement reduces the buckling load and causes the buckling mode to become highly localized in a manner that one segment of the structure deflects appreciably while the capability of the other parts of the structure has not been brought into full play.

Acknowledgement—Support provided by NASA Langley Research Center, through Grant NAG-1-1310 is gratefully appreciated.

REFERENCES

1. D. O. Brush and B. O. Almroth, *Buckling of Bars, Plates and Shells*. McGraw-Hill, New York (1975).
2. D. McFarland, B. Smith and W. Bernhart, *Analysis of Plates*. Spartan Books, New York (1972).
3. P. S. Bulson, *The Stability of Flat Plates*. Elsevier, New York (1969).
4. K. M. Liew and C. M. Wang, Elastic buckling of rectangular plates with curved internal supports, *Journal of Structural Engineering*, **118**, 1480–1493 (1990).
5. T. Wah and L. R. Calcote, *Structural Analysis by Finite Difference Calculus*. Van Nostrand Reinhold (1970).
6. F. Bleich, *Buckling Strength of Metal Structures*, pp. 275–288. McGraw-Hill, New York (1952).
7. P. W. Anderson, Absence of diffusion in certain random lattices, *Physical Review*, **109**(5), 1492–1505 (1958).
8. C. Pierre and R. H. Plaut, Curve veering and mode localization in a buckling problem, *Journal of Applied Mathematics and Physics (ZAMP)*, **40**, 758–761 (1989).
9. A. H. Nayfeh and M. Hawwa, Buckling mode localization in multi-span columns, *Proceedings of 35th AIAA/ASME/ASCE/AHS/ASC Structures, Structural Dynamics, and Materials Conference*, 18–20 April, pp. 277–289, Hilton Head, SC.
10. S. T. Ariaratnam and W. C. Xie, Buckling mode localization in randomly disordered continuous beams, manuscript (1993).
11. V. Tvergaard and A. Needleman, On the development of localized buckling patterns, in *Collapse: The Buckling of Structures in Theory and Practice*, edited by J. M. T. Thompson and G. W. Hunt, pp. 299–332. Cambridge University Press, Cambridge (1983).
12. G. Q. Cai and Y. K. Lin, Localization of wave propagations in disordered periodic structures, *A.I.A.A. Journal*, **29**(3), 450–456 (1991).
13. M. S. El Naschie, Localized diamond shaped buckling patterns of axially compressed cylindrical shells, *A.I.A.A. Journal*, **13**, 837–838 (1975).
14. M. S. El Naschie, Local postbuckling of compressed cylindrical shells, *Proceedings of the Institution of Civil Engineers*, Part 2, vol 59, pp. 523–525 (1975).
15. M. S. El Naschie, Nonlinear isometric bifurcation and shell buckling, *Zeitschrift für angewandte Mathematik und Mechanik*, **57**, 293–296 (1977).
16. M. S. El Naschie, *Stability and Chaos in Structural Engineering: an Energy Approach*. McGraw-Hill, London (1990).
17. S. P. Timoshenko and J. M. Gere, *Theory of Elastic Stability*. McGraw-Hill, New York (1961).

18. B. Budiansky and J. W. Hutchinson, Buckling: progress and challenge, in *Trends in Solid Mechanics*, W. T. Koiter 65th Anniversary Volume, edited by J. F. Besseling and A. M. A. van der Heijden, pp. 93–116. Delft University Press (1979).
19. M. Zyczkowski and A. Gajewski, Optimal structural design under stability constraints, in *Collapse: The Buckling of Structures in Theory and Practice*, edited by J. M. T. Thompson and G. W. Hunt, pp. 299–232. Cambridge University Press, Cambridge (1983).



0020-7462(95)00054-2

ON VIBRATIONAL IMPERFECTION SENSITIVITY OF AUGUSTI'S MODEL STRUCTURE IN THE VICINITY OF A NON-LINEAR STATIC STATE

I. Elishakoff,* S. Marcus[†] and J. H. Starnes Jr[‡]

* Department of Mechanical Engineering, Florida Atlantic University, Boca Raton,
 FL 33431-0991, U.S.A.;

[†] Department of Mathematics, Israel Institute of Technology, Haifa 32000, Israel;

[‡] NASA Langley Research Center, Hampton, VA 23664-5225, U.S.A.

(Received 29 May 1994)

Abstract—In this paper we present a closed-form solution for vibrational imperfection sensitivity—the effect of small imperfections on the vibrational frequencies of perturbed motion around the static equilibrium state of Augusti's model structure (a rigid link, pinned at one end to a rigid foundation and supported at the other by a linear extensional spring that retains its horizontality as the system deflects). We also treat a modified version of that model with attendant slightly different dynamics. It is demonstrated that the vibrational frequency decreases as the initial imperfections increase.

Keywords: dynamics of rigid links, influence of imperfections on link vibrations, rigid body dynamics

INTRODUCTION

The theory of dynamic imperfection sensitivity was put forward in a number of studies by Budiansky and Hutchinson [1–3] as a counterpart to the static framework developed by Koiter [4]. Whereas the latter investigation yielded the maximum (limit) load which can be sustained by the structure under static conditions, the former studies resorted to a step-load applied to the system in order to find the effect of unavoidable small imperfections on the maximum dynamic load. A general framework for the problems of suddenly loaded structures was considered by Simitses [5].

In recent years, dynamic imperfection sensitivity has also been studied in a different context, namely, with the system loaded statically up to some specific load level at which it is dynamically perturbed. The resulting motion possesses frequencies which are influenced both by the load level and by the initial imperfections. (For details, the reader is referred to the papers by Rosen and Singer [6], Singer and Prucz [7], Elishakoff *et al.* [8], Hui and Leissa [9, 10], Shilkrut and Virlan [11], Nash [12] and Valishvili [13].) Here, the general behavior can be elucidated by examining the various effects involved on model structures. One such model structure was pioneered by Budiansky and Hutchinson [1–3], and the influence of the initial imperfections and its vibrational frequencies was studied by Elishakoff *et al.* [14]. Another interesting model in the static context was thoroughly investigated by Augusti [15] and by Thompson and Hunt [16]; Yizhak *et al.* [17] studied the dynamic buckling loads of this model, with relevant closed-form expressions. Other models were considered by Souza [18] and by Kounadis *et al.* [19]. We will now deal with the original Augusti model and its modified version, with regard to their vibrational imperfection sensitivity in the vicinity of a non-linear static state.

ANALYSIS

Consider the cantilever shown in Fig. 1(a); it consists of a rigid link (of length L) pinned to a rigid foundation and supported by a linear extensional spring (of stiffness k) which retains its horizontality as the system deflects. The initial imperfection is modeled by the angular deflection α_0 from the vertical position, and the non-dimensional total displacement is denoted by x . We first consider the static case.

NLS

S2-39

CWAIVED

408908

PR

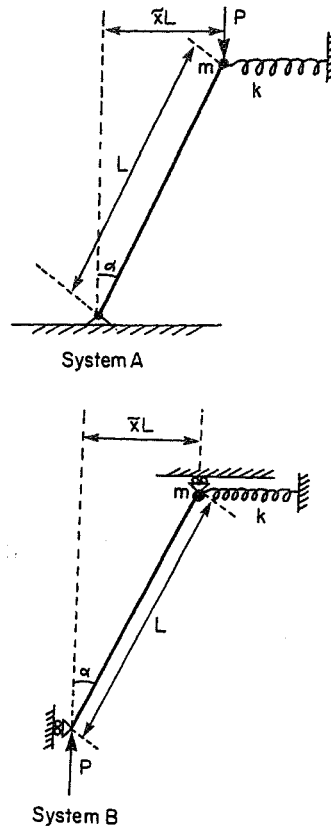


Fig. 1.

Due to the equilibrium, we have

$$\sum M_A = PxL - k(x - x_0)\sqrt{1 - x^2}L = kL[\sigma x - (x - x_0)\sqrt{1 - x^2}] = 0 \quad (1)$$

where

$$\sigma = \frac{P}{P_{cl}}, \quad P_{cl} = kL, \quad (2)$$

P_{cl} being the classical buckling load. From equation (1):

$$\sigma = \left(1 - \frac{x_0}{x}\right)\sqrt{1 - x^2}. \quad (3)$$

The limit load is given as the maximum load the system can support, so that

$$\frac{d\sigma}{dx} = 0, \quad \frac{d\sigma}{dx} = \frac{x_0 - x^3}{x^2\sqrt{1 - x^2}} \quad (4)$$

leading to

$$x_s = x_0^{1/3} \quad (5)$$

$$\sigma_s = (1 - x_0^{2/3})^{3/2} \quad (6)$$

which coincides with the formulae of Augusti [15] and Thompson and Hunt [16]; x_s is the total displacement at which the static limit load σ_s is achieved.

Let us now consider the dynamic case. At some load level σ , which corresponds to the total displacement x , we superimpose the perturbation $w(t)$, so that the total displacement becomes

$$\tilde{x}(t) = x + w(t). \quad (7)$$

The equation of motion reads

$$\dot{\sum} M_A = m\ddot{\alpha}L^2 \quad (8)$$

where the dot denotes differentiation with respect to time.

Denoting

$$\omega_0^2 = k/m, \quad (9)$$

ω_0 being the natural frequency of the mass m under small motion. Equation (8) is rewritten as

$$\omega_0^{-2} \ddot{\alpha} = \sigma \tilde{x} - (\tilde{x} - x_0) \sqrt{1 - \tilde{x}^2} \quad (10)$$

where (see Fig. 1):

$$\tilde{x} = \sin \alpha \quad (11)$$

$$\ddot{\alpha} = \frac{\ddot{\tilde{x}}}{\sqrt{1 - \tilde{x}^2}} + \frac{(\dot{\tilde{x}})^2}{(1 - \tilde{x}^2)^{3/2}} = (1 - \tilde{x}^2)^{-1/2} \left[\ddot{w} + \frac{(\dot{w})^2}{1 - \tilde{x}^2} \right]. \quad (12)$$

We seek a solution in the form

$$w(t) = W e^{i\omega t} \quad (13)$$

subject to restrictions such that instead of equation (12), we arrive at:

$$\omega_0^{-2} \ddot{w} = [\sigma \tilde{x} - (\tilde{x} - x_0) \sqrt{1 - \tilde{x}^2}] \sqrt{1 - \tilde{x}^2}. \quad (14)$$

With equation (13) in mind, we have

$$\omega_0^{-2} \ddot{w} = -\Omega^2 W e^{i\omega t} \quad (15)$$

where

$$\Omega = \frac{\omega}{\omega_0}. \quad (16)$$

Denoting

$$f(x) = (x - x_0) \sqrt{1 - x^2}, \quad (17)$$

equations (1) and (14) are rewritten as follows:

$$\sigma x = f(x) \quad (18)$$

$$\Omega^2 w = [f(\tilde{x}) - \sigma \tilde{x}] \sqrt{1 - \tilde{x}^2}. \quad (19)$$

We note that at the limit load, and after linearization, we obtain:

$$0 = \frac{d\sigma}{dx} = \frac{f'(x) - \sigma}{x} \quad (20)$$

$$\Omega^2 = [f'(x) - \sigma] \sqrt{1 - x^2} \quad (21)$$

or, by equation (3):

$$\Omega^2 = \frac{d\sigma}{dx} x \sqrt{1 - x^2}. \quad (22)$$

Noting that at the limit load $d\sigma/dx = 0$, and by inspecting equation (22), we arrive at the important conclusion that at that level the natural frequency Ω vanishes identically:

$$\sigma = \sigma_s; \quad \Omega^2 = 0. \quad (23)$$

Bearing in mind equations (4)–(6), we obtain the following interesting representation:

$$\Omega^2 = \frac{x_0 - x^3}{x} \quad (24)$$

which must be solved in conjunction with equation (3).

The following question now arises: "How does the non-dimensional squared frequency Ω^2 change, for fixed loading $\sigma = \text{const}$ ($\sigma < 1$) as the imperfection increases from $x_0 = 0$ (i.e. $\Omega^2 = 1 - \sigma$) to $x_0 = (1 - \sigma^{2/3})^{3/2}$, at which $\Omega^2 = 0$?"

From equation (3) we deduce

$$\Omega^2 = 1 - x^2 - \frac{\sigma}{\sqrt{1-x^2}} \quad (25)$$

which is a decreasing function of x . Also, observing that

$$\left. \frac{d\sigma}{dx} \right|_{x_0=\text{const}} = \frac{x_0 - x^3}{x^2 \sqrt{1-x^2}} > 0 \quad (26)$$

and

$$\left. \frac{d\sigma}{dx_0} \right|_{x=\text{const}} = -\frac{\sqrt{1-x^2}}{x} < 0 \quad (27)$$

we conclude that

$$\left. \frac{dx}{dx_0} \right|_{\sigma=\text{const}} > 0 \quad (28)$$

and

$$\frac{d(\Omega^2)}{dx_0} < 0 \quad (29)$$

implying that Ω^2 decreases monotonically.

In order to interrelate Ω^2 , x_0 and σ , we recast equation (3) in the form of the polynomial equation:

$$p_4(x) = x^4 - 2x_0x^3 - \gamma x^2 + 2x_0x - x_0^2 = 0 \quad (30)$$

where

$$\gamma = 1 - \sigma^2 - x_0^2. \quad (31)$$

Now, for $\sigma < 1$, $x_0 < 1$, we arrive at

$$\sigma^2 + x_0^2 < \sigma^{2/3} + x_0^{2/3} \leq 1 \quad (32)$$

that is, γ is always positive.

Now equation (24) also can be written as a polynomial equation:

$$q_3(x) = x^3 + \Omega^2 x - x_0 = 0. \quad (33)$$

We are looking for the conditions under which equations (30) and (33) have a common root. Equation (30) could be put as or:

$$p_3(x) = -p_4(x) + xq_3(x) = 2x_0^3x + (\gamma + \Omega^2)x^2 - 3x_0x + x_0^2 = 0 \quad (34)$$

$$q_2(x) = p_3(x) + 2x_0q_3(x) = (\gamma + \Omega^2)x^2 - (3 + 2\Omega^2)x_0x + 3x_0^2 = 0. \quad (35)$$

Instead of equation (33), we resort to

$$\tilde{q}_2(x) = [q^3(x)x_0 + p_3(x)]/x = 3x_0x^2 + (\gamma + \Omega^2)x + (\Omega^2 - 3)x_0 = 0. \quad (36)$$

For $q_2(x) = 0$ and $\tilde{q}_2(x) = 0$ to have a common root, it is necessary and sufficient that their resultant $R(q_2, \tilde{q}_2)$ vanish:

$$R(q_2, \tilde{q}_2) = \begin{vmatrix} \gamma + \Omega^2 & -(3 + 2\Omega^2)x_0 & 3x_0^2 & 0 \\ 0 & \gamma + \Omega^2 & -(3 + 2\Omega^2)x_0 & 3x_0^2 \\ 3x_0 & \gamma + \Omega^2 & (\Omega^2 - 3)x_0 & 0 \\ 0 & 3x_0 & \gamma + \Omega^2 & (\Omega^2 - 3)x_0 \end{vmatrix} = 0 \quad (37)$$

which yields the final equation

$$2(x_0^2 - \sigma^2) - 27x_0^2\lambda^2 + \gamma^3 + (\gamma^2 - 3\gamma)\Omega^4 + \Omega^8 = 0. \quad (38)$$

Two particular cases associated with this equation are:

$$(a) x_0 = 0: \Omega^2 = 1 - \sigma \tag{39}$$

$$(b) \sigma = 0: \Omega^2 = 1 - x_0^2. \tag{40}$$

Figure 2 shows the dependence of the non-dimensional frequency upon the initial imperfection parameter x_0 , for different values of the loading σ . For a zero initial imperfection, the curves initiate at $(1 - \sigma)$ and descend as the initial imperfection increases. Figure 3 shows the non-dimensional frequencies vs the non-dimensional loading, for different initial imperfections.

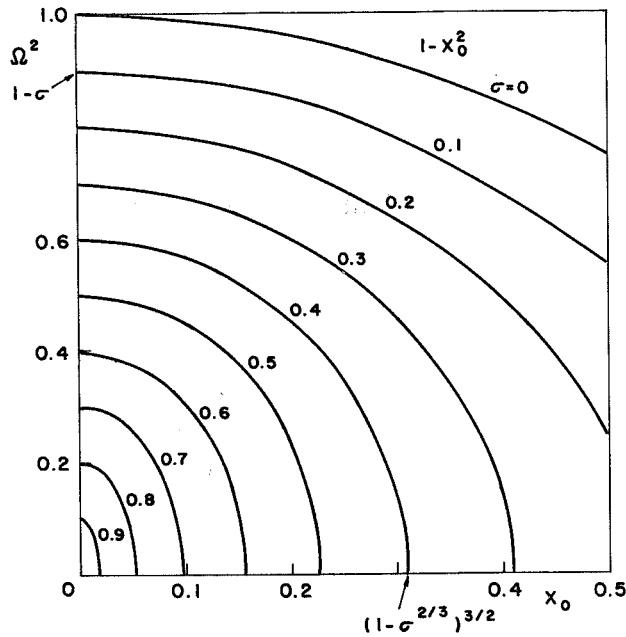


Fig. 2.

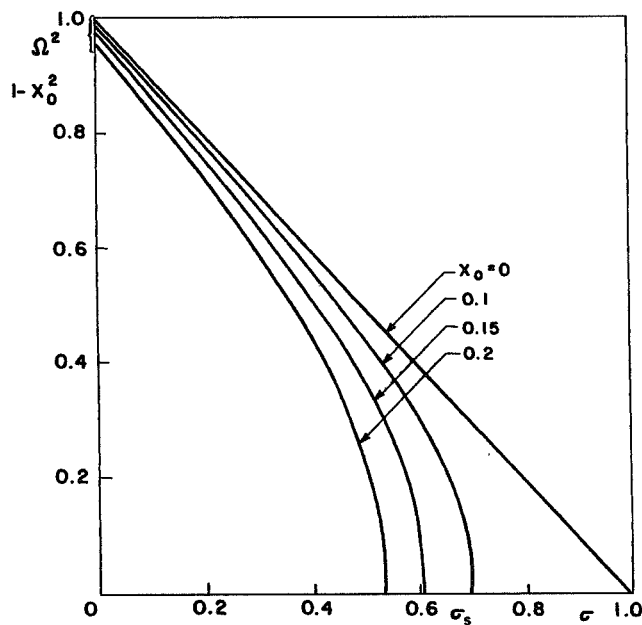


Fig. 3.

MODIFIED AUGUSTI MODEL

Consider now a slightly modified Augusti model, statically equivalent to the original version but with different dynamics [Fig. 1(b)]. The equation of motion now reads

$$m\ddot{x}L = P \frac{x}{\sqrt{1-x^2}} - F \quad (41)$$

where F is the force in the spring.

This equation could be rewritten as

$$\omega_0^{-2} \ddot{x} = \frac{\sigma x}{\sqrt{1-x^2}} - (x - x_0) \quad (42)$$

where x_0 is again the imperfection.

Equation (42) in conjunction with (13) yields

$$\Omega^2 = -\frac{\sigma}{(\sqrt{1-x^2})^2} + 1. \quad (43)$$

This expression again reveals that Ω^2 is a decreasing function of x ; equivalent to the latter equation is

$$\Omega^2 = \frac{x_0 - x^3}{x(1-x^2)} = 1 - \frac{x - x_0}{x(1-x^2)}. \quad (44)$$

or

$$\Omega^2 = 1 - \frac{(x - x_0)x}{1 - x^2} - \frac{\sigma}{\sqrt{1-x^2}}. \quad (45)$$

We make the following substitutions:

$$a = x_0^{2/3} = x_0 \quad (46)$$

$$\Delta = \frac{\sigma}{\sigma_s} = \frac{\sigma}{(1-a)^{3/2}}. \quad (47)$$

Hence

$$\Omega^2 = 1 - \frac{z - a}{z(1 - az^2)} \quad (48)$$

yielding

$$(1 - \Omega^2)az^3 + \Omega^2z - a = 0. \quad (49)$$

On the other hand, from equation (3) we arrive at

$$(z - a)^2(az^2 - 1) + \Delta(1 - a)^3 z^2 = 0 \quad (50)$$

or

$$az^4 - 2a^2z^3 - \beta^2z^2 + 2az - a^2 = 0 \quad (51)$$

where

$$\beta = 1 - a^2 - \Delta^2(1 - a)^2. \quad (52)$$

Figure 4 shows the non-dimensional natural frequency squared vs the non-dimensional loading σ . As σ approaches the critical values σ_s , the non-dimensional frequency vanishes identically. At $\sigma = 0$ all curves initiate at $1 - x_0^2$. Figure 5 shows the behavior of Ω^2 as a function of x_0 , and here again, as in Fig. 2, the natural frequencies decrease as x_0 increases.

CONCLUSIONS

We investigated the effect of initial imperfections in Augusti's model structure, in the vicinity of the non-linear static state. Qualitatively, the effect is analogous to that associated with buckling problems, where the buckling load decreases as the initial imperfections increase. Accordingly, the concept of vibrational imperfection sensitivity is seen to be very important for engineering applications, since the vibrational frequency actually experienced

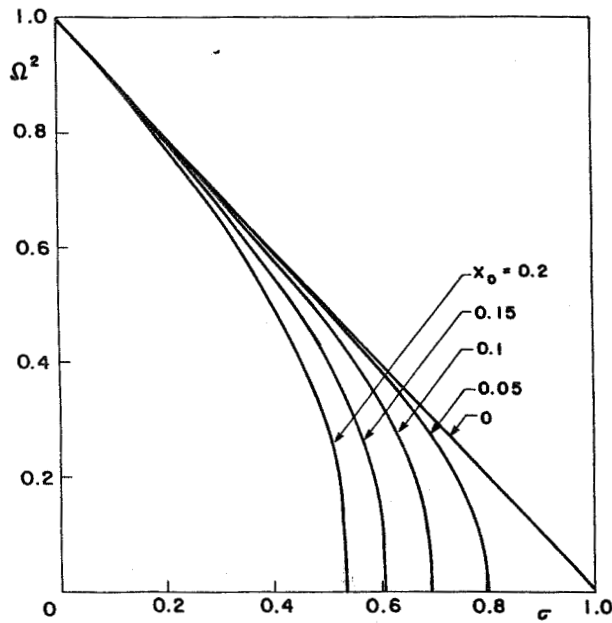


Fig. 4.

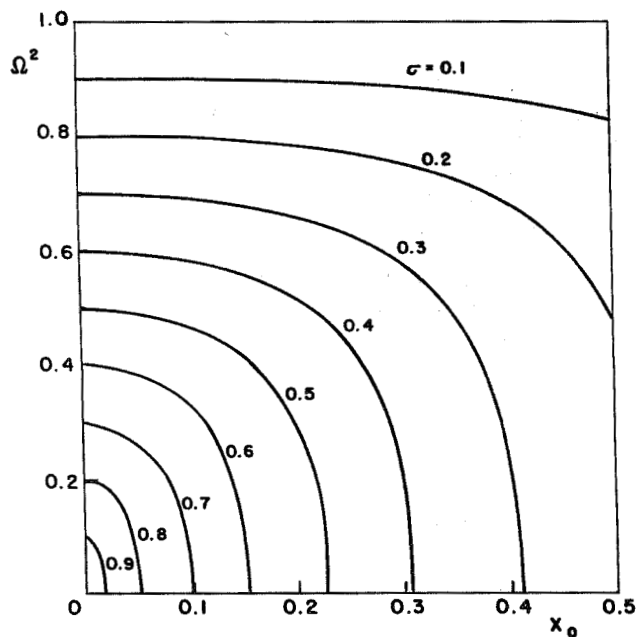


Fig. 5.

by the system could be much lower than the design level. In this paper, the closed form solutions have been derived to serve as benchmark solutions for the vibrational imperfection sensitivity.

Acknowledgement—Support provided by the NASA Langley Research Center through grant No. NAG-1-1310 is gratefully acknowledged and appreciated.

REFERENCES

1. B. Budiansky and J. W. Hutchinson, Dynamic buckling of imperfection sensitive structures. In *Proceedings of the Eleventh International Congress of Applied Mechanics*, H. Göbtrler (ed.), Munich, Germany, pp. 636-651 (1964).

2. B. Budiansky, Dynamic buckling of elastic structures: criteria and estimates. In *Dynamic Stability of Structures*, G. Herrmann (ed.), pp. 83–106. Pergamon Press, Oxford (1967).
3. J. W. Hutchinson and B. Budiansky, Dynamic buckling estimates. *AIAA J.* **4**, 525–530 (1966).
4. W. T. Koiter, On the stability of elastic equilibrium, Ph.D. thesis, Delft University of Technology, N.J. Paris, Amsterdam (in Dutch). English translations: (a) NASA TTF-10, 833 (1967); (b) AFFDL-TR-70-25 (1970).
5. G. J. Simitses, *Dynamic Stability of Suddenly Loaded Structures*. Springer, Berlin (1990).
6. A. Rosen and J. Singer, Effect of axisymmetric imperfections on the vibrations of cylindrical shells under axial compression. *AIAA J.* **12**, 995–997 (1974).
7. J. Singer and J. Prucz, Influence of initial geometrical imperfections on vibrations of axially compressed stiffened cylindrical shells. *J. Sound Vibr.* **80**, 117–143 (1982).
8. I. Elishakoff, V. Birman and J. Singer, Small vibration of an imperfect panel in the vicinity of a nonlinear static state. *J. Sound Vibr.* **114**, 57–63 (1987).
9. D. Hui and A. Leissa, Effects of uni-directional geometric imperfections on vibrations of pressurized shallow shells. *Int. J. Non-Linear Mech.* **18**, 279–285 (1983).
10. D. Hui and A. Leissa, Effects of geometric imperfections on vibrations of biaxially compressed rectangular flat plates. *J. Appl. Mech.* **50**, 750–756 (1984).
11. D. I. Shilkrut and P. M. Virlan, Dynamic study of the stability of all equilibria of geometrically nonlinear shallow spherical shells. *Stroitel'naya Mekhanika i Raschet Sooruzhenii*, pp. 54–58 (1975) (in Russian).
12. W. A. Nash, Free vibrations of initially imperfect cylindrical shells. In *Proceedings of the 8th Canadian Congress of Applied Mechanics*, Moncton, pp. 365–366 (1988).
13. N. V. Valishvili, *Computer Aided Design of Shells of Revolution*, pp. 265–271. Mashinostroenie, Moscow (1976) (in Russian).
14. I. Elishakoff, V. Birman and J. Singer, Effect of imperfections on the vibrations of loaded structures. *J. Appl. Mech.* **51**, 191–193 (1984).
15. G. Augusti, *Stabilità di Strutture Elastiche Elementari in Presenza di Grandi Spostamenti*, Publication No. 172, Department of Structural Sciences, Faculty of Engineering, University of Naples, Italy (1964).
16. J. M. T. Thompson and G. W. Hunt, *A General Theory of Elastic Stability*. John Wiley, London (1973).
17. E. Yithak, I. Elishakoff and M. Baruch, Dynamic imperfection sensitivity of a simple spring model structure. *J. Mech. Struct. Machines* **16**, 187–199 (1988).
18. M. A. de Souza, Dynamic behaviour of structural elements liable to buckling. In *Proceedings of the IUTAM Symposium on the Inelastic Behaviour of Plates and Shells*, PUC/RJ-Rio de Janeiro, Brazil, 5–9 August (1985).
19. A. N. Kounadis, J. Raftoyiannis and J. Mallis, Dynamic buckling of an arch model under impact loading. *J. Sound Vibr.* **134**, 193–202 (1989).



0960-0779(95)0110-7

Imperfection Sensitivity Due to the Elastic Moduli in the Roorda–Koiter Frame

NLS

I. ELISHAKOFF and Y. W. LI

Department of Mechanical Engineering, Florida Atlantic University, FL 33431-0991, USA

and

J. H. STARNES JR

NASA Langley Research Center, Hampton, VA 23665-5225, USA

(Accepted 13 November 1996)

52-39

408915

358932

P 8

Abstract—In this study, it is demonstrated through a simple example of the Roorda–Koiter frame that the unavoidable dissimilarity in the distribution of elastic moduli may further reduce the load-carrying capacity in addition to the well-recognized effect of initial geometric imperfections. Copyright © 1996 Elsevier Science Ltd.

INTRODUCTION

The works by Koiter [1, 2], Budiansky and Hutchinson [3] established that the initial geometric imperfection—deviation from the nominally ideal shape—plays a major role in the reduction of the load-carrying capacity of structures. An additional source of such a reduction was identified recently by Koiter *et al.* [4, 5] as a non-uniform thickness of the structure. To the best of the authors' knowledge, there is only a single work, by Ikeda and Murota [6], that points out that the symmetry breaking in the distribution of elastic moduli may cause additional reduction in the loads the system is able to sustain. In particular, they analyzed the von Mises truss in such a context. In this note, we perform analytical and numerical investigation on a frame structure to study the effect of dissimilarity of elastic moduli on the load-carrying capacity of the structure.

ANALYSIS

In 1965, Roorda [7] conducted a set of experiments on the two-bar frame, subjected to an eccentric load. Koiter [8] performed an initial-imperfection analysis of this frame, referred to in the literature since then as the Roorda–Koiter frame [9]. Roorda and Chilver [10] and Bažant and Cedolin [11] analyzed this structure from different perspectives; El Naschie studied a discrete analog of the Roorda–Koiter frame [12] (for additional references, see also the text of Brush and Almroth [13]). In this note, the vertical and the horizontal segments of the two-bar frame (Fig. 1) may have different lengths L_1 and L_2 and different Young's moduli E_1 and E_2 . Our aim is to study the effect of a small

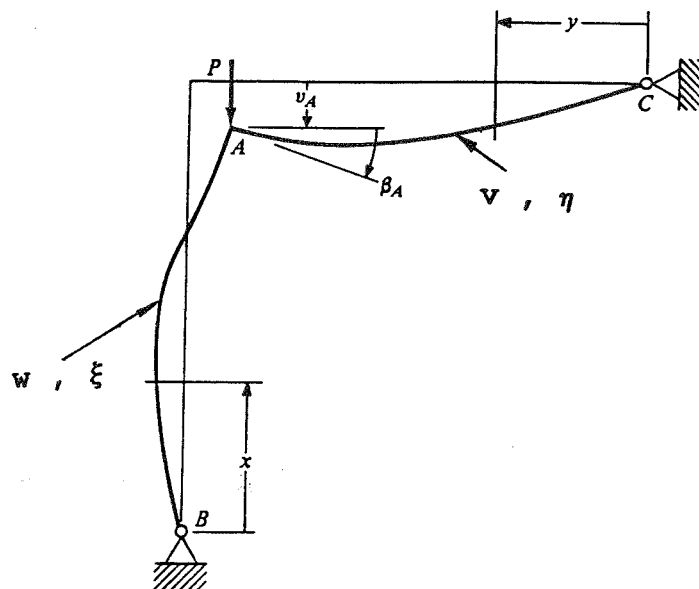


Fig. 1. Roorda-Koiter frame.

difference in the elastic moduli between the two segments, namely, the vertical and the horizontal bars, of the frame structure. It is such a difference that may trigger the dissimilarity in the elastic moduli of the structure.

Following those previous investigators, we first analyze the perfect structure.

The total potential energy of the two-bar frame is

$$\begin{aligned} \Pi = & \int_0^{L_1} \left\{ \frac{E_1 A}{2} \left[\frac{d\xi}{dx} + \frac{1}{2} \left(\frac{dw}{dx} \right)^2 \right]^2 + \frac{E_1 I}{2} \left(\frac{d^2 w}{dx^2} \right)^2 \right\} dx \\ & + \int_0^{L_2} \left\{ \frac{E_2 A}{2} \left[\frac{d\eta}{dy} + \frac{1}{2} \left(\frac{dv}{dy} \right)^2 \right]^2 + \frac{E_2 I}{2} \left(\frac{d^2 v}{dy^2} \right)^2 \right\} dy - P v_A. \end{aligned} \quad (1)$$

The change in potential energy is obtained by letting

$$\xi \rightarrow \xi_0 + \bar{\xi}, \quad \eta \rightarrow \eta_0 + \bar{\eta}, \quad v \rightarrow v_0 + \bar{v}, \quad w \rightarrow w_0 + \bar{w} \quad (2)$$

where

$$\eta_0 = v_0 = w_0 = 0, \quad \xi_0 = -\frac{Px}{EA} \quad (3)$$

represents an equilibrium state on the primary equilibrium path in the neighborhood of the bifurcation point A. The energy expression may take the following form

$$\Delta \Pi = \frac{1}{2!} \delta^2 \Pi + \frac{1}{3!} \delta^3 \Pi + \frac{1}{4!} \delta^4 \Pi \quad (4)$$

where

$$\begin{aligned} \frac{1}{2!} \delta^2 \Pi = & \int_0^{L_1} \left\{ \frac{E_1 A}{2} \left(\frac{d\bar{\xi}}{dx} \right)^2 - \frac{P}{2} \left(\frac{d\bar{w}}{dx} \right)^2 + \frac{E_1 I}{2} \left(\frac{d^2 \bar{w}}{dx^2} \right)^2 \right\} dx \\ & + \int_0^{L_2} \left\{ \frac{E_2 A}{2} \left(\frac{d\bar{\eta}}{dy} \right)^2 + \frac{E_2 I}{2} \left(\frac{d^2 \bar{v}}{dy^2} \right)^2 \right\} dy \end{aligned} \quad (5)$$

$$\frac{1}{3!} \delta^3 \Pi = \int_0^{L_1} \frac{E_1 A}{2} \frac{d\bar{\xi}}{dx} \left(\frac{d\bar{w}}{dx} \right)^2 dx + \frac{E_2 A}{2} \int_0^{L_2} \frac{d\bar{\eta}}{dy} \left(\frac{d\bar{v}}{dy} \right)^2 dy \quad (6)$$

$$\frac{1}{4!} \delta^4 \Pi = \int_0^{L_1} \frac{E_1 A}{8} \left(\frac{d\bar{w}}{dx} \right)^4 dx + \frac{E_2 A}{8} \int_0^{L_2} \left(\frac{d\bar{v}}{dy} \right)^4 dy \quad (7)$$

correspond to second, third and fourth variations of the potential energy, respectively.

According to Koiter's initial postbuckling theory [1], in the initial postbuckling range, the incremental displacement components are of the form of the classical buckling mode

$$\bar{\xi} = \beta_A \xi_1, \quad \bar{\eta} = \beta_A \eta_1, \quad \bar{v} = \beta_A v_1, \quad \bar{w} = \beta_A w_1 \quad (8)$$

where ξ_1 , η_1 , v_1 , w_1 are normalized classical buckling load. β_A is the rotation angle at bifurcation point A , and could be viewed as the amplitude parameter.

Substituting the above into the second variation leads to

$$\begin{aligned} \frac{1}{2!} \delta^2 \Pi = & \frac{1}{2} \int_0^{L_1} \left[E_1 A \left(\frac{d\xi_1}{dx} \right)^2 - P \left(\frac{dw_1}{dx} \right)^2 + \frac{E_1 I}{2} \left(\frac{d^2 w_1}{dx^2} \right)^2 \right] dx \beta_A^2 \\ & + \frac{1}{2} \int_0^{L_2} \left[E_2 A \left(\frac{d\eta_1}{dy} \right)^2 + E_2 I \left(\frac{d^2 v_1}{dy^2} \right)^2 \right] dy \beta_A^2. \end{aligned} \quad (9)$$

Performing variation on the above expression, we obtain, according to the Trefftz criterion,

$$\begin{aligned} \delta \left(\frac{1}{2!} \delta^2 \Pi \right) = & \int_0^{L_1} \left[E_1 A \left(\frac{d\xi_1}{dx} \right) \frac{d(\delta\xi_1)}{dx} - P \left(\frac{dw_1}{dx} \right) \frac{d(\delta w_1)}{dx} + \frac{E_1 I}{2} \left(\frac{d^2 w_1}{dx^2} \right) \frac{d^2(\delta w_1)}{dx^2} \right] dx \beta_A^2 \\ & + \int_0^{L_2} \left[E_2 A \left(\frac{d\eta_1}{dy} \right)^2 \frac{d(\delta\eta)}{dy} + E_2 I \left(\frac{d^2 v_1}{dy^2} \right) \frac{d^2(\delta v_1)}{dy^2} \right] dy \beta_A^2 = 0. \end{aligned} \quad (10)$$

Integration by parts and rearrangement gives

$$\begin{aligned} & \left[E_A \frac{d\xi_1}{dx} \delta\xi_1 \right]_0^{L_1} + \left[E_2 A \frac{d\eta_1}{dy} \delta\eta_1 \right]_0^{L_2} - \left[\left(E_1 I \frac{d^3 w_1}{dx^3} + P \frac{dw_1}{dx} \right) \delta w_1 \right]_0^{L_1} \\ & - \left[E_2 I \frac{d^3 v_1}{dy^3} \delta v_1 \right]_0^{L_2} + \left[E_1 I \frac{d^2 w_1}{dx^2} \frac{d(\delta w_1)}{dx} \right]_0^{L_1} + \left[E_2 I \frac{d^2 v_1}{dy^2} \frac{d(\delta v_1)}{dy} \right]_0^{L_2} \\ & - \int_0^{L_1} E_1 A \frac{d^2 \xi_1}{dx^2} \delta\xi_1 dx - \int_0^{L_2} E_2 A \frac{d^2 \eta_1}{dy^2} \delta\eta_1 dy + \int_0^{L_1} \left(E_1 I \frac{d^4 w_1}{dx^4} + P \frac{d^2 w_1}{dx^2} \right) \delta w_1 dx \\ & + \int_0^{L_2} E_2 I \frac{d^4 v_1}{dy^4} \delta v_1 dy = 0. \end{aligned} \quad (11)$$

The satisfaction of the above equation results in boundary conditions (using $\xi|_{x=L_1} = -v|_{y=L_2}$; $\eta|_{y=L_2} = w|_{x=L_2}$);

$$\frac{d^2 w_1}{dx^2} = 0 \quad \text{at } x = 0; \quad \frac{d^2 v_1}{dy^2} = 0 \quad \text{at } y = 0 \quad (12)$$

$$E_1 A \frac{d\xi_1}{dx} + E_2 I \frac{d^3 v_1}{dy^3} = \frac{d^2 w_1}{dx^2} + \frac{d^2 v_1}{dy^2} = 0 \quad \text{at } x = L_1, y = L_2 \quad (13)$$

$$E_2 A \frac{d\eta_1}{dy} - E_1 I \frac{d^3 v_1}{dx^3} - P \frac{dw_1}{dx} = 0; \quad \text{at } x = L_1, y = L_2 \quad (14)$$

and governing equations:

$$\begin{aligned} \frac{d^2\xi_1}{dx^2} = 0, \quad E_1 I \frac{d^4 w_1}{dx^4} + P \frac{d^2 w_1}{dx^2} = 0 \\ \frac{d^2\eta_1}{dy^2} = 0, \quad \frac{d^4 v_1}{dy^4} = 0. \end{aligned} \quad (15)$$

Integration of the above equations gives

$$\begin{aligned} \beta_A \xi_1 = C_1 \frac{x}{E_1 A}, \quad \beta_A \eta_1 = C_2 \frac{y}{E_2 A} \\ \beta_A w_1 = C_3 \sin(kx) + C_4 x, \quad \beta_A v_1 = C_5 y + C_6 y^3 \end{aligned} \quad (16)$$

where $k^2 = P/E_1 I$, and C_i ($i = 1, 2, \dots, 6$) are integration constants.

Using boundary conditions at $x = L_1$, $y = L_2$:

$$w = \eta: C_3 \sin(kL_1) + C_4 L_1 = \frac{L_2}{E_2 A} C_2 \quad (17)$$

$$\xi = -v: C_5 L_2 + C_6 L_2^3 = \frac{L_1}{E_1 A} C_1 \quad (18)$$

$$\frac{dw}{dx} = -\beta_A: kC_3 \cos(kL_1) + C_4 = -\beta_A \quad (19)$$

$$\frac{dv}{dy} = -\beta_A: C_5 + 3C_6 L_2^2 = -\beta_A \quad (20)$$

$$E_1 A \frac{d\xi_1}{dx} + E_2 I \frac{d^3 v_1}{dy^3} = 0: C_1 + 6E_2 I C_6 = 0 \quad (21)$$

$$\frac{d^2 w_1}{dx^2} + \frac{d^2 v_1}{dy^2} = 0: -k^2 C_3 \sin(kL_1) + 6C_6 L_2 = 0 \quad (22)$$

$$E_2 A \frac{d\eta_1}{dy} - E_2 I \frac{d^3 v_1}{dx^3} - P \frac{dw_1}{dx} = 0: C_2 - P[kC_3 \cos(kL_1) + C_4] = 0. \quad (23)$$

The above seven equations are linear, homogeneous algebraic equations in terms of β_A , C_1, \dots, C_6 . The non-triviality condition leads to

$$\begin{aligned} 6(kL_1) \cos(kL_1) - \frac{6E_2 I}{E_1 A L_2^2} (kL_1)^2 \sin(kL_1) - 6 \sin(kL_1) - 2(kL_1)^2 \frac{L_2}{L_1} \sin(kL_1) \\ + \frac{P}{E_1 A} \frac{6E_1 I}{E_1 A L_1 L_2} (kL_1)^2 \sin(kL_1) + 2(kL_1)^2 \frac{P}{E_2 A} \left(\frac{L_2}{L_1} \right)^2 \sin(kL_1) = 0. \end{aligned} \quad (24)$$

Since our discussion is limited to the elastic range, terms containing $P/E_1 A$, $6E_2 I/E_1 A L_2^2$, $P/E_2 A$ and $6E_1 I/E_1 A L_1 L_2$ are negligibly small, and could be omitted in the first approximation. Thus, we have an approximate characteristic equation as the following

$$\tan(kL_1) \approx \frac{kL_1}{1 + \frac{1}{3}(kL_1)^2 \frac{L_2}{L_1}} \quad (25)$$

from which, the critical buckling load parameter k_{cl} can be determined. The normalized classical buckling mode is found to be

$$\begin{aligned}
\xi_1 &= \frac{3P_{cl}}{E_1 A (k_{cl} L_1)^2} x \\
\eta_1 &= \frac{3P_{cl}}{E_1 A (k_{cl} L_2)^2} y \\
w_1 &= \frac{3}{(k_{cl} L_1)^2} \left[x - L_1 \frac{\sin(k_{cl} x)}{\sin(k_{cl} L_1)} \right] \\
v_1 &= \frac{1}{2} y \left(1 - \frac{y^2}{L_2^2} \right), \quad P = P_{cl} + (\lambda - 1) P_{cl}.
\end{aligned} \tag{26}$$

For the case $L_1 = L_2 = L$, the buckling load parameter is found to be $k_{cl} L = 3.72$. Substituting the above expressions, we have

$$\frac{1}{2!} \delta^2 \Pi = \left(0.478 P_{cl} L + 0.109 \frac{E_2}{E_1} P_{cl} L - 0.587 \lambda \right) \beta_A^2. \tag{27}$$

If we assume that there is a dissimilarity in the distribution of elastic moduli, i.e. generally $E_1 \neq E_2$

$$E_2 = E_1 (1 + \varepsilon) \tag{28}$$

then equation (29) reads

$$\frac{1}{2!} \delta^2 \Pi = 0.587 (1 + 0.186 \varepsilon - \lambda) P_{cl} L \beta_A^2. \tag{29}$$

The third variation is

$$\frac{1}{3!} \delta^3 \Pi = 0.149 P_{cl} L \beta_A^3. \tag{30}$$

The approximate expression for the potential energy increment $\Delta \Pi$ is the sum of the second and third variations of the energy expressions. For equilibrium, $d(\Delta \Pi)/d\beta_A = 0$. For $\beta_A \neq 0$, we obtain

$$\lambda = 1 + 0.186 \varepsilon + 0.381 \beta_A \tag{31}$$

or, we can re-write equation (31) as

$$\lambda_1 = \frac{P}{P'_{cl}} = 1 + \frac{0.381}{1 + 0.186 \varepsilon} \beta_A; \quad P'_{cl} = P_{cl} (1 + 0.186 \varepsilon). \tag{32}$$

We now proceed with the analysis of the geometrically imperfect structure. For an eccentric load applied at a distance ϕL to the right of point A , the potential energy expression must be modified by adding a term [13]

$$\Omega_\phi = -PL\phi\beta_A = -\lambda_1 P'_{cl} L \phi \beta_A \tag{33}$$

and the second variation and the third variation take the form

$$\begin{aligned}
\frac{1}{2!} \delta^2 \Pi &= A_2 (1 - \lambda_1) P'_{cl} L \beta_A^2 \\
\frac{1}{3!} \delta^3 \Pi &= A_3 (1 - \lambda) P'_{cl} L \beta_A^3
\end{aligned} \tag{34}$$

where $A_2 = 0.587/(1 + 0.186 \varepsilon)^2$ and $A_3 = 0.149/(1 + 0.186 \varepsilon)$. Then

$$\Delta\Pi = \frac{1}{2!}\delta^2\Pi + \frac{1}{3!}\delta^3\Pi + \Omega_\phi = [(1 - \lambda_1)A_2\beta_A^2 + A_3\beta_A^3 - \lambda_1\phi\beta_A]P'_{cl}L. \quad (35)$$

For the equilibrium, we have $d(\Delta\Pi)/d\beta_A = 0$:

$$\lambda_1 = 1 + \frac{3A_3}{2A_2}\beta_A - \frac{1}{2A_2}\frac{\phi}{\beta_A}\lambda_1 \quad (36)$$

or, in another form,

$$\lambda_1\beta_A = \beta_A + \frac{3A_3}{2A_2}\beta_A^2 - \frac{1}{2A_2}\phi\lambda_1. \quad (37)$$

Differentiating both sides of the above equation with respect to β_A , we have

$$\beta_A\frac{d\lambda_1}{d\beta_A} + \lambda_1 = 1 + \frac{3A_3}{A_2}\beta_A - \frac{1}{2A_2}\phi\frac{d\lambda_1}{d\beta_A}. \quad (38)$$

Setting $d\lambda_1/d\beta_A$ equal to zero, we obtain the limit-point load factor λ_L for the imperfect structure

$$\lambda_L = 1 + \frac{3A_3}{A_2}\beta_A \quad (39)$$

or

$$\beta_A = \frac{(\lambda_L - 1)A_2}{3A_3}. \quad (40)$$

Substituting back into equation (36), we have

$$\lambda_L = 1 - \frac{(3A_3\lambda_L)^{1/2}}{A_2}(-\phi)^{1/2}. \quad (41)$$

As a first approximation, we can set $\lambda_L = 1$ at the right-hand side of the above equation, and we arrive at

$$\lambda_L \approx 1 - \frac{(3A_3)^{1/2}}{A_2}(-\phi)^{1/2} = 1 - a(-\phi)^{1/2}, \quad a = \frac{(3A_3)^{1/2}}{A_2} \quad (42)$$

where a is a parameter describing the imperfection sensitivity of the structure. For $\varepsilon = 0$, $a = 1.15$; $\varepsilon = 0.1$, $a = 1.17$; $\varepsilon = -0.1$, $a = 1.11$. Using these data, we can plot the relationship between the buckling load and the initial imperfection parameter. This is depicted in Fig. 2, where the three curves correspond to three different cases of elastic moduli.

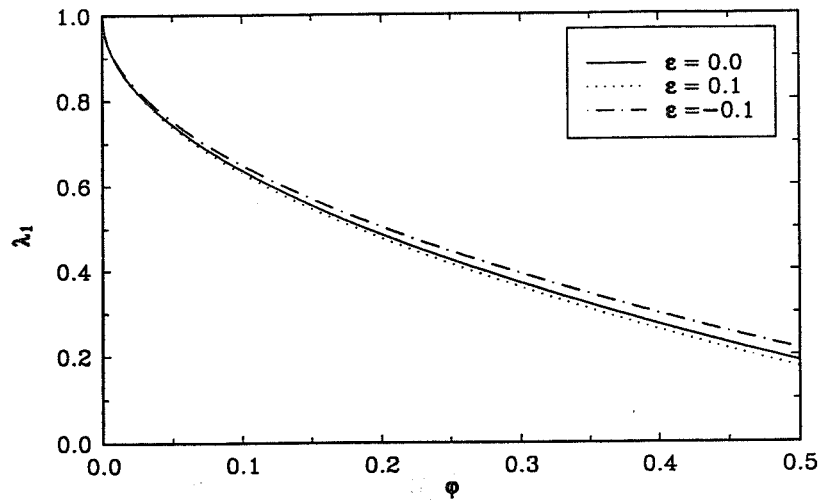
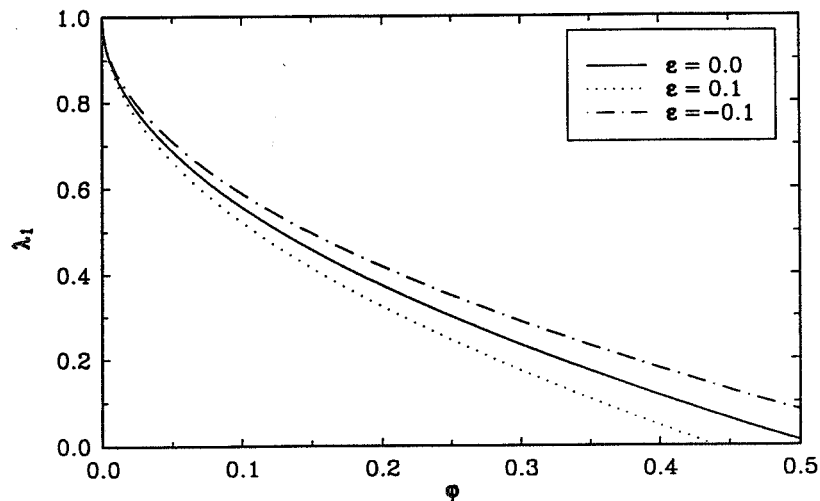
For the case where $L_2/L_1 = 0.5$, the buckling load parameter obtained from equation (25) is $(k_{cl}L_1) = 3.97$. Following the same procedure as above, we again end up with expression (42). However, A_2 and A_3 now have the following expressions

$$A_2 = \frac{0.37}{(1 + 0.51\varepsilon)^2}, \quad A_3 = \frac{0.09}{1 + 0.51\varepsilon} \quad (43)$$

For $\varepsilon = 0$, $a = 1.40$; $\varepsilon = 0.1$, $a = 1.51$; $\varepsilon = -0.1$, $a = 1.30$. Having these, we can plot the curves of buckling load reduction as in Fig. 3.

DISCUSSION

Figures 2 and 3 demonstrate the usual pattern of the buckling load reduction due to initial imperfection. However, what is worth noticing here is a further reduction in buckling

Fig. 2. Buckling load reduction ($L_2/L_1 = 1.0$).Fig. 3. Buckling load reduction ($L_2/L_1 = 0.5$).

load because of the presence of dissimilarity in the elastic moduli and the geometric configuration. When ε is positive, it means that the horizontal bar possesses a bigger elastic modulus than the vertical bar, which results in a stiffer structure. Likewise, when L_2/L_1 is less than unity (the horizontal bar is shorter), the overall stiffness of the structure is again increased. On the one hand, a stiffer structure has a larger buckling load. On the other hand, Figs 2 and 3 show that the stiffer the structure is, the more sensitive it is to the initial imperfection. As we can see also from those two figures, when the stiffness is decreased either through a reduced elastic modulus ($\varepsilon < 0$) or from an increased length ($L_2/L_1 > 1$), the structure becomes less sensitive to the initial imperfection. The change in the overall stiffness of the structure comes, as is shown here, from the dissimilarity. Thus, one may conclude that the dissimilarity in elastic moduli could contribute to the change in sensitivity of the structure to the initial imperfection. One may intentionally introduce such a

dissimilarity in elastic moduli so that the structure has a decreased sensitivity to initial imperfections. In this simple two-bar structure, the decrease in sensitivity due to dissimilarity in elastic modulus is not remarkable when the two segments of the frame have the same length, namely, $L_1 = L_2$. However, for other geometric configurations, the effect may become more pronounced. For $L_1 = 2L_2$ (Fig. 3), say, at $\phi = 0.25$, $\lambda = 0.3$ for $\varepsilon = 0$, and $\lambda = 0.24$ for $\varepsilon = 0.1$, which indicates 20% decrease in the limit load; for $\varepsilon = -0.1$, $\lambda = 0.3$, which amounts to 17% increase in load-carrying capacity. It appears that the subject is worth pursuing in the direction of shell structures to see how important the effect of non-homogeneity of elastic moduli is on the imperfection sensitivity.

Acknowledgement—Support provided by NASA Langley Research Center, through grant NAG-1-1310 is gratefully appreciated.

REFERENCES

1. W. T. Koiter, On the stability of elastic equilibrium, Ph.D. dissertation, Delft (1945). (English translation: *NASA Tech. Trans. F* 10, 833, 1967).
2. W. T. Koiter, The effect of axisymmetric imperfections on the buckling of cylindrical shells under axial compression, *Proceedings of Royal Netherlands Academy of Sciences*, Amsterdam, Series 13, Vol. 66, pp. 265–279 (1963).
3. B. Budiansky and J. W. Hutchinson, Dynamic buckling of imperfection-sensitivity structures. *Proceedings of the Eleventh International Congress of Applied Mechanics*, edited by H. Goertler, Munich, pp. 636–651 (1964).
4. W. T. Koiter, I. Elishakoff, Y. W. Li and J. H. Starnes, Buckling of an axially compressed cylindrical shell of variable thickness. *Int. J. Solids and Structures* 31, 797–805 (1994).
5. W. T. Koiter, I. Elishakoff, Y. W. Li and J. H. Starnes, Buckling of an axially compressed imperfect cylindrical perfect shell of variable thickness. *Proceedings of 35th AIAA ASME/ASCE/AHS/ASC Structures, Structural Dynamics and Materials Conference*, Hilton Head, SC, pp. 277–289 (1994).
6. K. Ikeda and K. Murota, Critical initial imperfection of structures. *Int. J. Solids and Structures*, 26, 865–886 (1990).
7. J. Roorda, Stability of structures with small imperfections, *J. Engineering Mechanics Division* 91, 87–95 (1965).
8. W. T. Koiter, Postbuckling analysis of simple two-bar frames. *Recent Progress in Applied Mechanics*, edited by B. Broberg *et al.*, p. 337. Almquist and Wiksell, Göteborg (1967).
9. Z. Bažant and L. Cedolin, *Stability of Structures*. Oxford University Press, Oxford (1991).
10. J. Roorda and A. M. Chilver, Frame buckling: an illustration of the perturbation technique, *Int. J. Non-linear Mechanics* 5, 235–246 (1970).
11. Z. Bažant and L. Cedolin, Initial postcritical analysis of asymmetric bifurcation in frames, *J. Structural Engineering*, 115, 2845–2857 (1989).
12. M. S. El Naschie, *Stress, Stability and Chaos in Structural Engineering: An Energy Approach*, pp. 431–433. McGraw–Hill, London (1990).
13. D. D. Brush and B. O. Almroth, *Buckling of Bars, Plates and Shells*. McGraw–Hill, New York (1975).
14. J. Roorda, An experience in equilibrium and stability, Technical Report No. 3, Solid Mechanics Division, University of Waterloo (1971).

Reprinted from

CHAOS, SOLITONS & FRACTALS

Vol. 5, No. 6, pp. 955-969

1115

54-39

408929

p 16

358936 (WAIVED)

BUCKLING MODE LOCALIZATION IN A MULTI-SPAN
PERIODIC STRUCTURE WITH A DISORDER IN A
SINGLE SPAN

I. ELISHAKOFF

Center for Applied Stochastics Research and Department of Mechanical Engineering, Florida Atlantic University,
Boca Raton, FL 33431-0991, USA



PERGAMON

1995



0960-0779(94)00211-8

Buckling Mode Localization in a Multi-span Periodic Structure with a Disorder in a Single Span

Y. W. LI and I. ELISHAKOFF

Center for Applied Stochastics Research and Department of Mechanical Engineering, Florida Atlantic University,
Boca Raton, FL 33431-0991, USA

and

J. H. STARNES JR

NASA Langley Research Center, Hampton, VA 23664-5225, USA

(Received 13 July 1994)

Abstract—This paper investigates the buckling mode localization in the periodic multi-span beam with disorder occurring in an arbitrary single span. The analytical finite difference calculus is used in conjunction with the conventional displacement method to derive the transcendental equations from which buckling load is calculated. The underlying treatment is general and the solution thus obtained is exact. Numerical results show that the buckling mode is highly localized in the vicinity of the disordered span of the beam.

1. INTRODUCTION

Large-scale periodic structures are often encountered in engineering practice. They appear in different forms, such as beams on equidistant supports, gridwork structures with equally spaced and geometrically similar stiffening components, plates and shells with uniformly distributed stiffeners. Periodic structures have drawn substantial interest among researchers, and many mathematical methods have been developed, starting from the pioneering work by Brillouin [1]. The reader may also consult with studies by Lin and McDaniel [2], Mead [3], Sen Gupta [4], Abramovich and Elishakoff [5], Zhu *et al.* [6] and others. However, in reality, although these structures are designed to be completely identical for every constituent component, they seldom exhibit perfect periodicity. The deviation from complete periodicity is commonly known as disorder or irregularity. Disorders may arise from various imprecisions in the fabrication process or from geometric and material variations in the different parts of the structures. From the standpoint of structural analysis, if the constituent units of the structure are different from one another, we have to analyze each of them separately, with attendant satisfaction of continuity conditions from one unit to another. This procedure usually results in matrices of high order if the structure is composed of a large number of units. Owing to the fact that the inversion and other operations on such matrices may be involved in the calculations, the numerical errors are almost unavoidable. Therefore, it is often desirable to reduce the order of the matrices as far as possible. Fortunately, many large-scale engineering structures are essentially periodic and disorders often take place in some localized areas of the structure. For the analysis of perfectly periodic structures, the method of the finite difference calculus [7, 8] appears to

be very instrumental. For the treatment of periodic structures, this method has decisive advantages over the conventional matrix methods used in the structural analysis. The method usually leads to a determinative matrix that can be orders of magnitude smaller than those necessary in the force or displacement method, or in the conventional finite element method. With the size of the matrix reduced, the numerical accuracy is improved and the computational effort is cut down dramatically. However, the applicability of this method is only confined to those structures which are uniform in the spacing and stiffness characteristics of the constituent elements. When the periodicity is disturbed, this method can no longer be applied.

Analysis of disordered structures has become of interest more recently, mainly due to the localization phenomenon which arises with disorders. In the past, most of the research on the localization phenomena have been conducted in connection with vibrations [9–12]. The localization phenomenon relative to buckling problem was first addressed by Pierre and Plaut [13], who examined the occurrence of buckling mode localization in a simple two-span disordered column. Ariaratnam and Xie [14] investigated the localization in the buckling of a system of rigid bars connected with springs, in the stochastic setting. Recently, Nayfeh and Hawwa [15] studied the similar problem in a more complex setting of multi-span columns by use of the transfer matrix method. The deterministic buckling localizations in cylindrical shells and in elastic plates were investigated, respectively, in several studies by El Naschie [16–19] and by the present authors [20]. Here, we discuss the general N -span beam with torsional springs at supports, which is structurally periodic except that one of the spans of the beam contains a disorder. By combining the finite difference calculus with the conventional displacement method, we present the exact solution for the buckling of a large-scale, multi-span periodic beam having disorder in an arbitrary, single span of the beam. It is shown that even a single disorder could be responsible for the highly localized pattern of buckling modes.

2. BASIC EQUATIONS

The governing differential equation for the typical i th span of the axially compressed, continuous beam with uniform cross-section reads

$$EI \frac{d^2 y}{dx_i^2} + Py = M_{i-1}^R \left(\frac{x_i}{a_i} - 1 \right) - M_i^L \frac{x_i}{a_i} \quad (1)$$

or

$$\frac{d^2 y}{dx_i^2} + k^2 y = \frac{M_{i-1}^R}{EI} \left(\frac{x_i}{a_i} - 1 \right) - \frac{M_i^L}{EI} \frac{x_i}{a_i} \quad (2)$$

where $k = \sqrt{P/EI}$; P is the axial load on the beam; E is the Young's modulus, and I is the moment of inertia of the cross-section of the beam; y is the deflection of the beam and a_i is the length of the i th span (Fig. 1); M_{i-1}^R , M_i^L are the bending moments at two supports of that span, respectively. The superscript 'R' ('L') indicates that span of the beam is to the right (left) of the support in question.

The general solution to equation (2) is

$$y = C_i \sin(kx_i) + D_i \cos(kx_i) + \frac{M_{i-1}^R}{P} \left(\frac{x_i}{a_i} - 1 \right) - \frac{M_i^L}{P} \frac{x_i}{a_i} \quad (3)$$

where C_i and D_i are arbitrary constants which are to be determined by the use of boundary conditions.

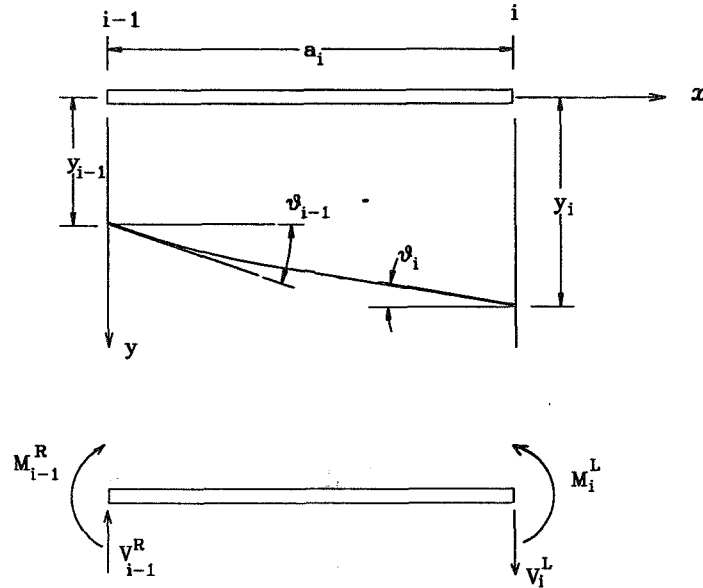


Fig. 1. Notations and positive directions.

Here we discuss the case of transversely rigid supports. Thus, the boundary conditions at the supports are

$$(1) y = 0 \text{ at } x_i = 0; \quad (2) y = 0 \text{ at } x_i = a_i \quad (4)$$

from which C_i and D_i can be evaluated as

$$C_i = -\frac{M_{i-1}^R \cos(ka_i)}{P \sin(ka_i)} + \frac{M_i^L}{P \sin(ka_i)}, \quad D_i = \frac{M_{i-1}^R}{P}. \quad (5)$$

Substitution into equation (3) results in

$$y = \frac{M_{i-1}^R}{P} \left[-\frac{\cos(ka_i)}{\sin(ka_i)} \sin(kx_i) + \cos(kx_i) + \frac{x_i}{a_i} - 1 \right] + \frac{M_i^L}{P} \left[-\frac{\sin(kx_i)}{\sin(ka_i)} + \frac{x_i}{a_i} \right] \quad (6)$$

from which

$$y' = \frac{M_{i-1}^R}{P} \left[\frac{1}{a_i} - k \frac{\sin(ka_i) \sin(kx_i) + \cos(ka_i) \cos(kx_i)}{\sin(ka_i)} \right] - \frac{M_i^L}{P} \left[\frac{1}{a_i} - \frac{k \cos(kx_i)}{\sin(ka_i)} \right]. \quad (7)$$

In the following, use will be made of the analytical finite difference calculus [8]. We will use the angles of rotation at supports as principal variables, since the deflections at all the supports are zero. The angles of rotation at supports $i-1$ and i are obtained from equation (7) by setting x_i equal to 0 and a_i , respectively:

$$\theta_{i-1} = \frac{M_{i-1}^R}{k^2 a_i EI} \left[1 - \frac{ka_i \cos(ka_i)}{\sin(ka_i)} \right] - \frac{M_i^L}{k^2 a_i EI} \left[1 - \frac{ka_i}{\sin(ka_i)} \right], \quad (8)$$

$$\theta_i = \frac{M_{i-1}^R}{k^2 a_i EI} \left[1 - \frac{ka_i}{\sin(ka_i)} \right] - \frac{M_i^L}{k^2 a_i EI} \left[1 - \frac{ka_i \cos(ka_i)}{\sin(ka_i)} \right]. \quad (9)$$

We may also express M_{i-1}^R , M_i^L , the bending moments at supports $i-1$ and i respectively, in terms of the rotational angles θ_i and θ_{i+1} as follows:

$$\begin{aligned} M_{i-1}^R &= \frac{2EI}{a_i} [2c_1 \theta_{i-1} + c_2 \theta_i] \\ M_i^L &= -\frac{2EI}{a_i} [2c_1 \theta_i + c_2 \theta_{i-1}] \end{aligned} \quad (10)$$

where

$$\begin{aligned} c_1 &= \frac{ka_i [\sin(ka_i) - ka_i \cos(ka_i)]}{4[2 - 2 \cos(ka_i) - ka_i \sin(ka_i)]} \\ c_2 &= \frac{ka_i [ka_i - \sin(ka_i)]}{2[2 - 2 \cos(ka_i) - ka_i \sin(ka_i)]}. \end{aligned} \quad (11)$$

Note that the above derivation could also be done straightforwardly by using the stability function [21]. Equilibrium at a typical i th support requires that

$$M_i^L - M_i^R = J \theta_i \quad (12)$$

where J is the torsional modulus of the spring (Fig. 1), θ_i is the rotational angle at support i .

Using equation (10), we obtain

$$c_2(\theta_{i+1} + \theta_{i-1}) + 4(c_1 + \nu)\theta_i = 0 \quad (13)$$

where $\nu = Ja/8EI$.

Introducing the shifting operator E [8] which is defined as $E\theta_i = \theta_{i+1}$, equation (13) can be rewritten as

$$[c_2(E + E^{-1}) + 4(c_1 + \nu)]\theta_i = 0. \quad (14)$$

Equation (14) is a second-order finite difference equation, whose solution is obtained by letting

$$\theta = \exp(\phi i). \quad (15)$$

A direct substitution of equation (15) into equation (14) yields

$$\cosh \phi = -\frac{2(c_1 + \nu)}{c_2}. \quad (16)$$

Three different cases must be considered.

Case A. $-2(c_1 + \nu)/c_2 \geq 1$.

The solution of equation (16) has the following form

$$\phi_{1,2} = \pm \phi; \quad \phi = \cosh^{-1} \left[-\frac{2(c_1 + \nu)}{c_2} \right]. \quad (17)$$

The attendant solution for θ_i reads

$$\theta_i = Ae^{\phi i} + Be^{-\phi i} \quad (18)$$

where A and B are arbitrary constants.

Case B. $-2(c_1 + \nu)/c_2 \leq -1$.

The solution to equation (16) takes the form

$$\phi_{1,2} = \pm(\alpha + j\pi); \quad \alpha = \cosh^{-1} \left[\frac{2(c_1 + \nu)}{c_2} \right], \quad j = \sqrt{-1} \quad (19)$$

and the solution for θ_i is

$$\theta_i = [A \cosh(\alpha i) + B \sinh(\alpha i)] \cos(\pi i). \quad (20)$$

Case C. $-1 \leq -2(c_1 + \nu)/c_2 \leq 1$.

The solution to equation (16) now becomes

$$\phi_{1,2} = \pm\beta; \quad \beta = \cos^{-1} \left[-\frac{2(c_1 + \nu)}{c_2} \right] \quad (21)$$

and, for θ_i , we have

$$\theta_i = A \cos(\beta i) + B \sin(\beta i). \quad (22)$$

Suppose that we have an N -span beam (Fig. 2), which is periodic except that its $(q + 1)$ th span contains a span length imperfection which makes that span slightly longer or shorter than the other spans of the structure, i.e.

$$a_i = a \quad \text{for} \quad i = 1, \dots, q, q + 2, \dots, N; \quad a_{q+1} = b \quad (a \neq b). \quad (23)$$

As a particular case $b = a$, we recover the original, perfectly periodic structure.

To facilitate the solution of the problem, we can treat the entire beam as being composed of three segments. The first q -span periodic beam constitutes segment I; the $(q + 1)$ th span, namely, the disordered span, constitutes segment II; and the last $(N - q - 1)$ spans of periodic beam represent segment III. Assume first that both segment I and III themselves contain a large number of spans. For segments I and III *per se*, the finite difference calculus is applicable due to their structural periodicity. As to the disordered span, segment II, a separate consideration should be made, and the conventional displacement method is used here. By following this procedure, we construct a solution composed of three parts with each part corresponding to a specific segment of the beam. Continuity conditions between those adjacent segments are utilized in combination with boundary conditions at the ends of the beam to establish an eigenvalue problem.

For the first q spans of periodic beam, we perform the finite difference calculus analysis

$$\theta_r = \theta_r^I; \quad (r = 0, 1, \dots, q) \quad (24)$$

where the superscript denotes the sequence number of the segment in question; θ_r^I takes

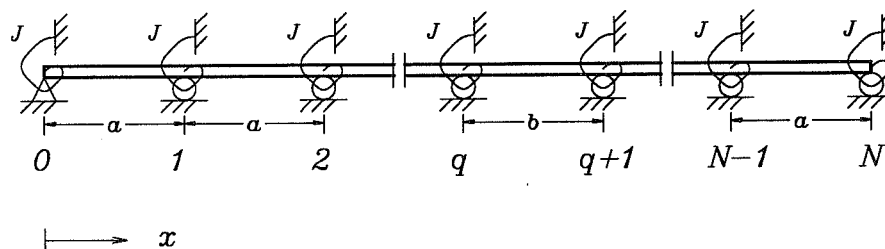


Fig. 2. A multi-span beam with a single disorder in the $(q + 1)$ th span.

one of the three forms represented by equations (18), (20) and (22), depending on the physical and geometrical conditions of the segment.

For the disordered span, recalling equation (10), we have

$$\begin{aligned} M_q^R &= \frac{2EI}{b} [2\bar{c}_1\theta_0^{\text{II}} + \bar{c}_2\theta_1^{\text{II}}] \\ M_{q+1}^L &= -\frac{2EI}{b} [2\bar{c}_1\theta_1^{\text{II}} + \bar{c}_2\theta_0^{\text{II}}] \end{aligned} \quad (25)$$

or in another form

$$\begin{aligned} \theta_0^{\text{II}} &= \frac{b}{2EI} \frac{2\bar{c}_1 M_q^R + \bar{c}_2 M_{q+1}^L}{4\bar{c}_1^2 - \bar{c}_2^2} \\ \theta_1^{\text{II}} &= -\frac{b}{2EI} \frac{2\bar{c}_1 M_{q+1}^L + \bar{c}_2 M_q^R}{4\bar{c}_1^2 - \bar{c}_2^2} \end{aligned} \quad (26)$$

where

$$\begin{aligned} \bar{c}_1 &= \frac{kb[\sin(kb) - kb \cos(kb)]}{4[2 - 2 \cos(kb) - kb \sin(kb)]} \\ \bar{c}_2 &= \frac{kb[kb - \sin(kb)]}{2[2 - 2 \cos(kb) - kb \sin(kb)]} \end{aligned} \quad (27)$$

Note that \bar{c}_1 and \bar{c}_2 are obtained from equation (11) by formally replacing a_i with b .

The treatment of the last $N - q - 1$ spans of periodic beam is similar to that of segment I,

$$\theta_s = \theta_{s-q-1}^{\text{III}}; \quad (s = q + 1, q + 2, \dots, N) \quad (28)$$

where $\theta_{s-q-1}^{\text{III}}$ again adopts one of the three forms denoted by equations (18), (20) and (22).

Consider now a beam simply supported at its two ends (other boundary conditions can be treated in a similar manner). Then the boundary condition at the left end of the beam can be represented as

$$-M_0^R = J\theta_0^{\text{I}} \quad \text{or} \quad (2c_1 + 4\nu)\theta_0^{\text{I}} + c_2\theta_1^{\text{I}} = 0 \quad (29)$$

while the boundary condition at the right end of the beam reads

$$M_N^L = J\theta_{N-q-1}^{\text{III}} \quad \text{or} \quad (2c_1 + 4\nu)\theta_{N-q-1}^{\text{III}} + c_2\theta_{N-q-2}^{\text{III}} = 0. \quad (30)$$

Conditions of continuity between the periodic spans and the disordered span of the beam, namely, between segment I and segment II, are

$$\begin{aligned} M_q^L - M_q^R &= J\theta_q \quad \text{or} \quad (2c_1 + 4\nu)\theta_q^{\text{I}} + c_2\theta_{q-1}^{\text{I}} + \frac{a}{2EI}M_q^R = 0 \\ \theta_q^{\text{I}} &= \theta_0^{\text{II}} \quad \text{or} \quad \theta_q^{\text{I}} - \frac{b}{a(4\bar{c}_1^2 - \bar{c}_2^2)} \left(2\bar{c}_1 \frac{a}{2EI} M_q^R + \bar{c}_2 \frac{a}{2EI} M_{q+1}^L \right) = 0. \end{aligned} \quad (31)$$

Analogously, the continuity conditions between the second and the third segments are

$$\begin{aligned} M_{q+1}^L - M_{q+1}^R &= J\theta_0^{\text{III}} \quad \text{or} \quad (2c_1 + 4\nu)\theta_0^{\text{III}} + c_2\theta_1^{\text{III}} - \frac{a}{2EI}M_{q+1}^L = 0 \\ \theta_1^{\text{III}} &= \theta_0^{\text{II}} \quad \text{or} \quad \theta_0^{\text{III}} + \frac{b}{a(4\bar{c}_1^2 - \bar{c}_2^2)} \left(\bar{c}_2 \frac{a}{2EI} M_q^R + 2\bar{c}_1 \frac{a}{2EI} M_{q+1}^L \right) = 0. \end{aligned} \quad (32)$$

Equations (31) and (32) should be formulated in terms of the three different cases, because in each case, the resulting expressions are different.

For Case A, the rotation angles in the first and third segments can be expressed as

$$\begin{aligned}\theta_r^I &= A_1 e^{\phi r} + B_1 e^{-\phi r} & (r = 0, 1, \dots, q) \\ \theta_{s-q-1}^{III} &= A_2 e^{\phi(s-q-1)} + B_2 e^{-\phi(s-q-1)} & (s = q + 1, \dots, N).\end{aligned}\quad (33)$$

Substituting the above expressions in the boundary conditions (29) and (30) and the continuity conditions (31) and (32), we obtain six homogeneous algebraic equations,

$$(2c_1 + 4\nu + c_2 e^\phi)A_1 + (2c_1 + 4\nu + c_2 e^{-\phi})B_1 = 0 \quad (34)$$

$$[(2c_1 + 4\nu)e^{\phi q} + c_2 e^{\phi(q-1)}]A_1 + [(2c_1 + 4\nu)e^{-\phi q} + c_2 e^{-\phi(q-1)}]B_1 + \bar{M}_q^R = 0 \quad (35)$$

$$e^{\phi q}A_1 + e^{-\phi q}B_1 - \frac{2\bar{c}_1}{4\bar{c}_1^2 - \bar{c}_2^2} \left(\frac{b}{a}\right) \bar{M}_q^R - \frac{\bar{c}_2}{4c_1^2 - \bar{c}_2^2} \left(\frac{b}{a}\right) \bar{M}_{q+1}^L = 0 \quad (36)$$

$$(2c_1 + 4\nu + c_2 e^\phi)A_2 + (2c_1 + 4\nu + c_2 e^{-\phi})B_2 - \bar{M}_{q+1}^L = 0 \quad (37)$$

$$A_2 + B_2 + \frac{\bar{c}_2}{4\bar{c}_1^2 + \bar{c}_2^2} \left(\frac{b}{a}\right) \bar{M}_q^R + \frac{2\bar{c}_1}{4c_1^2 - \bar{c}_2^2} \left(\frac{b}{a}\right) \bar{M}_{q+1}^L = 0 \quad (38)$$

$$[(2c_1 + 4\nu)e^{\phi(N-q-1)} + c_2 e^{\phi(N-q-2)}]A_2 + [(2c_1 + 4\nu)e^{-\phi(N-q-1)} + c_2 e^{-\phi(N-q-2)}]B_2 = 0 \quad (39)$$

where

$$\bar{M}_q^R = \frac{M_q^R a}{2EI}; \quad \bar{M}_{q+1}^L = \frac{M_{q+1}^L a}{2EI}. \quad (40)$$

For Case B, the solutions for the first and third segments are as below.

$$\begin{aligned}\theta_r^I &= A_1 \cosh(\alpha r) \cos(\pi r) + B_1 \sinh(\alpha r) \cos(\pi r) & (r = 0, 1, \dots, q) \\ \theta_{s-q-1}^{III} &= A_2 \cosh[\alpha(s-q-1)] \cos[\pi(s-q-1)] \\ &+ B_2 \sinh[\alpha(s-q-1)] \cos[\pi(s-q-1)] & (s = q + 1, \dots, N)\end{aligned}\quad (41)$$

and performing the substitution similar to that in Case A, we arrive at the following six homogeneous equations

$$[2c_1 + 4\nu - c_2 \cosh(\alpha)]A_1 - c_2 \sinh(\alpha)B_1 = 0 \quad (42)$$

$$\begin{aligned}\{(2c_1 + 4\nu) \cosh(\alpha q) \cos(\pi q) + c_2 \cosh[\alpha(q-1)] \cos[\pi(q-1)]\}A_1 \\ \{(2c_1 + 4\nu) \sinh(\alpha q) \cos(\pi q) + c_2 \sinh[\alpha(q-1)] \cos[\pi(q-1)]\}B_1 + \bar{M}_q^R = 0\end{aligned}\quad (43)$$

$$\cosh(\alpha q) \cos(\pi q)A_1 + \sinh(\alpha q) \cos(\pi q)B_1 - \frac{2\bar{c}_1}{4\bar{c}_1^2 - \bar{c}_2^2} \left(\frac{b}{a}\right) \bar{M}_q^R - \frac{\bar{c}_2}{4c_1^2 - \bar{c}_2^2} \left(\frac{b}{a}\right) \bar{M}_{q+1}^L = 0 \quad (44)$$

$$[2c_1 + 4\nu - c_2 \cosh(\alpha)]A_2 - c_2 \sinh(\alpha)B_2 - \bar{M}_{q+1}^L = 0 \quad (45)$$

$$A_2 + \frac{\bar{c}_2}{4\bar{c}_1^2 + \bar{c}_2^2} \left(\frac{b}{a}\right) \bar{M}_q^R + \frac{2\bar{c}_1}{4c_1^2 - \bar{c}_2^2} \left(\frac{b}{a}\right) \bar{M}_{q+1}^L = 0 \quad (46)$$

$$\begin{aligned}\{(2c_1 + 4\nu) \cosh[\alpha(N-q-1)] \cos[\pi(N-q-1)] \\ + c_2 \cosh[\alpha(N-q-2)] \cos[\pi(N-q-2)]\}A_2 \\ \times \{(2c_1 + 4\nu) \sinh[\alpha(N-q-1)] \cos[\pi(N-q-1)] \\ + c_2 \sinh[\alpha(N-q-2)] \cos[\pi(N-q-2)]\}B_2 = 0.\end{aligned}\quad (47)$$

For Case C, the solutions are in the following form

$$\begin{aligned}\theta_r^I &= A_2 \cos(\beta r) + B_1 \sin(\beta r) & (r = 0, 1, \dots, q) \\ \theta_{s-q-1}^{III} &= A_2 \cos[\beta(s-q-1)] + B_2 \sin[\beta(s-q-1)] & (s = q+1, \dots, N)\end{aligned}\quad (48)$$

and the corresponding equations are

$$[2c_1 + 4\nu + c_2 \cos(\beta)]A_1 + c_2 \sin(\beta)B_1 = 0 \quad (49)$$

$$\begin{aligned}\{(2c_1 + 4\nu) \cos(\beta q) + c_2 \cos[\beta(q-1)]\}A_1 \\ + \{(2c_1 + 4\nu) \sin(\beta q) + c_2 \sin[\beta(q-1)]\}B_1 + \bar{M}_q^R = 0\end{aligned}\quad (50)$$

$$\cos(\beta q)A_1 + \sin(\beta q)B_1 - \frac{2\bar{c}_1}{4\bar{c}_1^2 - \bar{c}_2^2} \left(\frac{b}{a}\right) \bar{M}_q^R - \frac{\bar{c}_2}{4\bar{c}_1^2 - \bar{c}_2^2} \left(\frac{b}{a}\right) \bar{M}_{q+1}^L = 0 \quad (51)$$

$$[2c_1 + 4\nu + c_2 \cos(\beta)]A_2 + c_2 \sin(\beta)B_2 - \bar{M}_{q+1}^L = 0 \quad (52)$$

$$A_2 + \frac{\bar{c}_2}{4\bar{c}_1^2 - \bar{c}_2^2} \left(\frac{b}{a}\right) \bar{M}_q^R + \frac{2\bar{c}_1}{4\bar{c}_1^2 - \bar{c}_2^2} \left(\frac{b}{a}\right) \bar{M}_{q+1}^L = 0 \quad (53)$$

$$\begin{aligned}\{(2c_1 + 4\nu) \cos[\beta(N-q-1)] + c_2 \cos[\beta(N-q-2)]\}A_2 \\ + \{(2c_1 + 4\nu) \sin[\beta(N-q-1)] + c_2 \sin[\beta(N-q-2)]\}B_2 = 0.\end{aligned}\quad (54)$$

Thus, for each case, we have six homogeneous algebraic equations, which can be expressed in a matrix form as follows

$$[F(K)]_{6 \times 6} \{\delta\}_{6 \times 1} = 0 \quad (55)$$

where $[F(K)]$ is the coefficient matrix, $K = ka$ and $\{\delta\}^T = \{A_1, B_1, \bar{M}_q^R, \bar{M}_{q+1}^L, A_2, B_2\}$.

Non-triviality of $\{\delta\}$ requires that the determinant of the coefficient matrix vanish,

$$\text{Det}[F(K)] = 0 \quad (56)$$

which constitutes a transcendental equation for the non-dimensional buckling load parameter K . Once the buckling load parameter K is determined, we can use equation (6) to calculate, span by span, the buckling mode shapes for the entire structure.

It is worth mentioning that, if the disorder occurs in the first or last span of the beam, the whole beam can be partitioned into two segments; one is the disordered span and the other is the $N-1$ spans of periodic beam. If this happens, only four equations are needed to characterize the problem so that instead of having a 6×6 matrix for $[F(K)]$, we will have a 4×4 determinant matrix (see Appendix for details).

3. EXAMPLES AND DISCUSSION

In the following numerical examples, the non-dimensional spring constant ν is fixed at 0.3 since this particular case for perfectly periodic beam was considered by Wah and Calcote [8] and a comparison can be made with their results.

As a first example, we discuss a simply supported, 100-span continuous beam. The disorder arises from a span length imperfection characterized by $b/a = 1.1$, where a and b are the lengths of periodic spans and the disordered span, respectively. Since $b/a > 1$, the disordered span is longer than other spans of the structure. The disorder may appear in any span of the beam. Figure 3 depicts the results of the buckling load parameter K for the beams with or without torsional springs. The most critical situation for the beam without

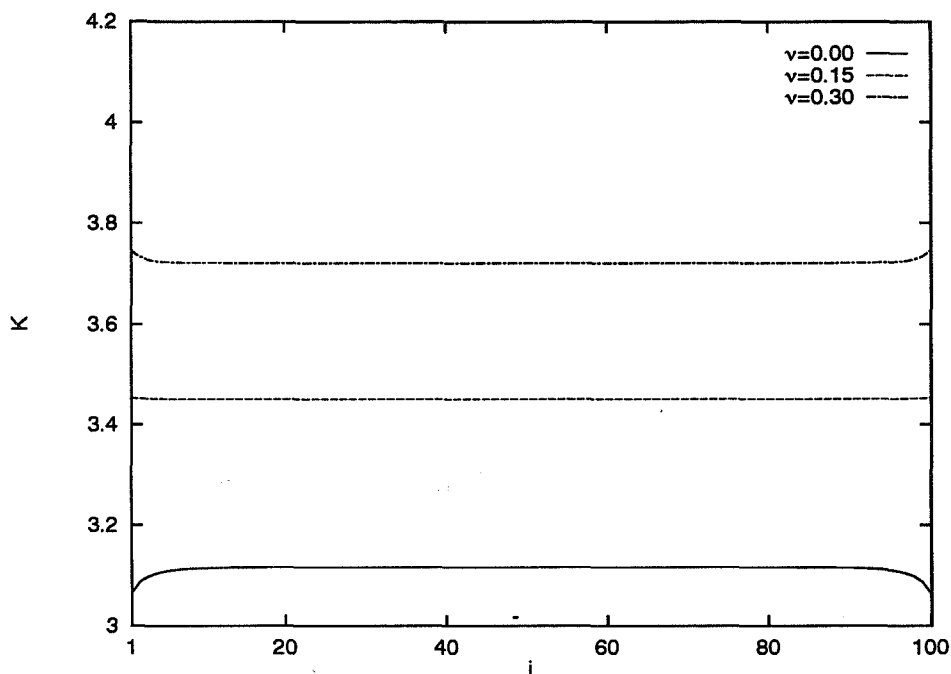


Fig. 3. Change of buckling load with the location of the disorder (i —the sequence number of the span where the disorder occurs).

torsional springs occurs when the disorder occurs at either the first or the last span, for which the buckling load parameter K equals 3.05. If the disorder appears in one of the spans close to the center of the beam, the buckling load increases. However, for beams with torsional springs, numerical results display a quite different picture. For this case, the occurrence of disorder near the boundaries may be more advantageous, since the buckling load decreases as the disorder moves away from the boundaries. Nevertheless, for both cases, the buckling load remains almost unchanged with the location of disorder, once the disorder is 10 spans away from both boundaries. This means that the effect of the boundary dies out if the disorder is sufficiently far from the boundary. The location of the disorder has almost no effect on the buckling load if the spring modulus $\nu = 0.15$. If we refer to the buckling load in the absence of disorder as the classical buckling load, then the classical buckling load parameter K equals π for the case without torsional springs, and has a value of 3.760 for the beam with torsional springs of $\nu = 0.3$ [8]. With the disorder present, numerical results show that the buckling load parameter K is below the corresponding classical value. For instance, K is less than 3.12 for the beam without torsional springs, and is no more than 3.72 for the beam with torsional springs of $\nu = 0.3$. Thus, we can see that such a disorder, namely, the span length imperfection, may have a degrading effect on the load-carrying capacity of the structure.

The second example is mainly devoted to the discussion of the buckling mode shapes for disordered periodic beam. Figures 4 and 5 depict the buckling mode shapes for an 11-span beam with the disorder appearing at different locations of the beam. Again, the disorder is introduced by a span length imperfection specified by $b/a = 1.1$. A significant phenomenon is that the buckling mode shapes exhibit a strong localization in the disordered span, when the torsional springs are used at supports. The larger the moduli of the torsional springs, the more localized the mode shape becomes. Thus, the torsional spring weakens the

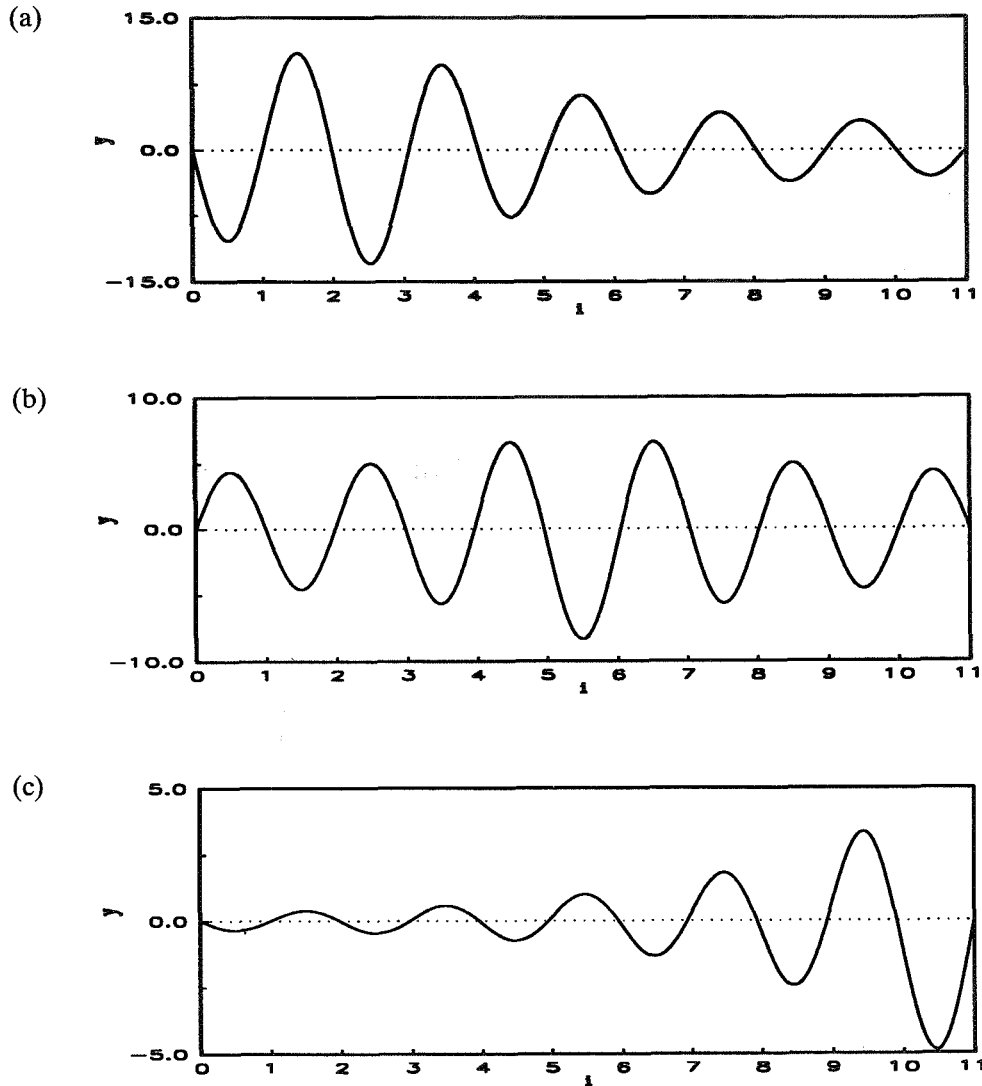


Fig. 4. Buckling mode shapes for a disordered 11-span beam without torsional spring (i -support sequence number, y -deflection). (a) Disorder occurs in the third span; (b) disorder occurs in the mid-span (sixth span); (c) disorder occurs in the last span.

coupling between different spans of the structure. This observation is consistent with that found by Pierre and Plaut [13] for the two-span beam.

In passing, it is worthwhile to point out that, although the underlying treatment makes it possible to obtain an exact solution to the buckling problem of disordered periodic beams with any number of spans by dealing with a determinative matrix of very low order (the matrix is 6×6 if only one disorder occurs in the span neither the first nor the last), some numerical problem can occur when N , the number of spans, is a large number, say $N \geq 50$. This is because, in our calculations, we have to evaluate terms $e^{\phi(N-q-1)}$, $\cosh[\alpha(N-q-1)]$, which can be so large when q is small, that they may exceed the upper limit of a digital computer. To avoid this numerical difficulty, we may divide the corresponding equation by a relevant, large term, for example, $e^{\phi(N-q-1)}$ or

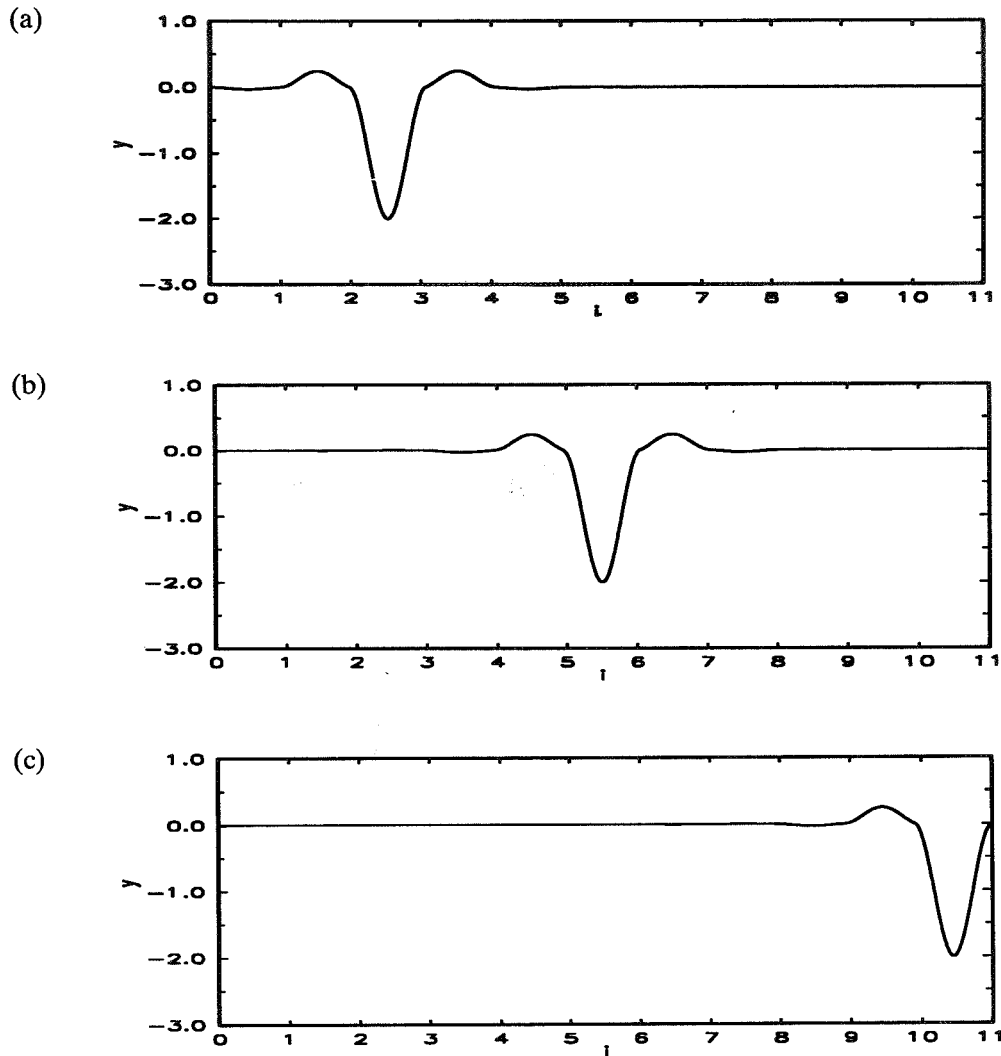


Fig. 5. Buckling mode shapes for a disordered 11-span beam with torsional spring of $\nu=10$ (i —support sequence number, y —deflection). (a) Disorder occurs in the third span; (b) disorder occurs in the mid-span (sixth span); (c) disorder occurs in the last span.

$\cosh[\alpha(N - q - 1)]$, and manipulate the resulting equation by making an asymptotic approximation

$$\frac{\sinh[\alpha(N - q - 1)]}{\cosh[\alpha(N - q - 1)]} \rightarrow 1 \quad \text{for } q \ll N. \quad (57)$$

It follows that only equations (39) and (47) need to be modified and they adopt, after the approximations, the following forms, respectively:

$$[(2c_1 + 4\nu) + c_2 e^{-\phi}]A_2 = 0 \quad (58)$$

and

$$\begin{aligned} &\{(2c_1 + 4\nu) \cos[\pi(N - q - 1)] + c_2 e^{-\alpha} \cos[\pi(N - q - 2)]\}A_2 \\ &+ \{(2c_1 + 4\nu) \cos[\pi(N - q - 1)] + c_2 e^{-\alpha} \cos[\pi(N - q - 2)]\}B_2 = 0. \end{aligned} \quad (59)$$

Figure 6 depicts the buckling modes of a 100-span beam and a 400-span beam with torsional springs of $\nu = 0.3$; both beams contain a disorder in the 40th span. From Fig. 6, it is clear that the deflection of the beam at buckling dies out quickly as the distance from the disordered span increases. The envelope of the buckling mode is depicted in Fig. 7. If we take a logarithm of the function, we obtain Fig. 8, which displays a nearly straight line. Thus we establish that the deflection at buckling decays exponentially. The exponential decay constant [12], sometimes referred to as the Lyapunov exponent [14] in the literature, (its counterpart in vibration problems is commonly known as the logarithmic decrement [22]) equals -0.260 .

In the above examples, we have dealt with the disorder of 'detrimental' character; that is, the disordered span is longer than the periodic spans, and such a disorder leads to a reduction in the buckling load of the structure. As a third example, we consider also another possibility with attendant opposite effect; that is, the disordered span being shorter than the other spans ($b/a < 1$). In this case, the disorder turns out to be 'beneficial' because it results in slightly higher buckling loads. For example, for a perfectly periodic 11-span beam with torsional springs of non-dimensional modulus $\nu = 0.3$, the buckling load parameter K is, as mentioned earlier, 3.76; for the same structure but with disorder, K varies in the range from 3.79 to 3.82, depending on the location of the disorder. Thus, we

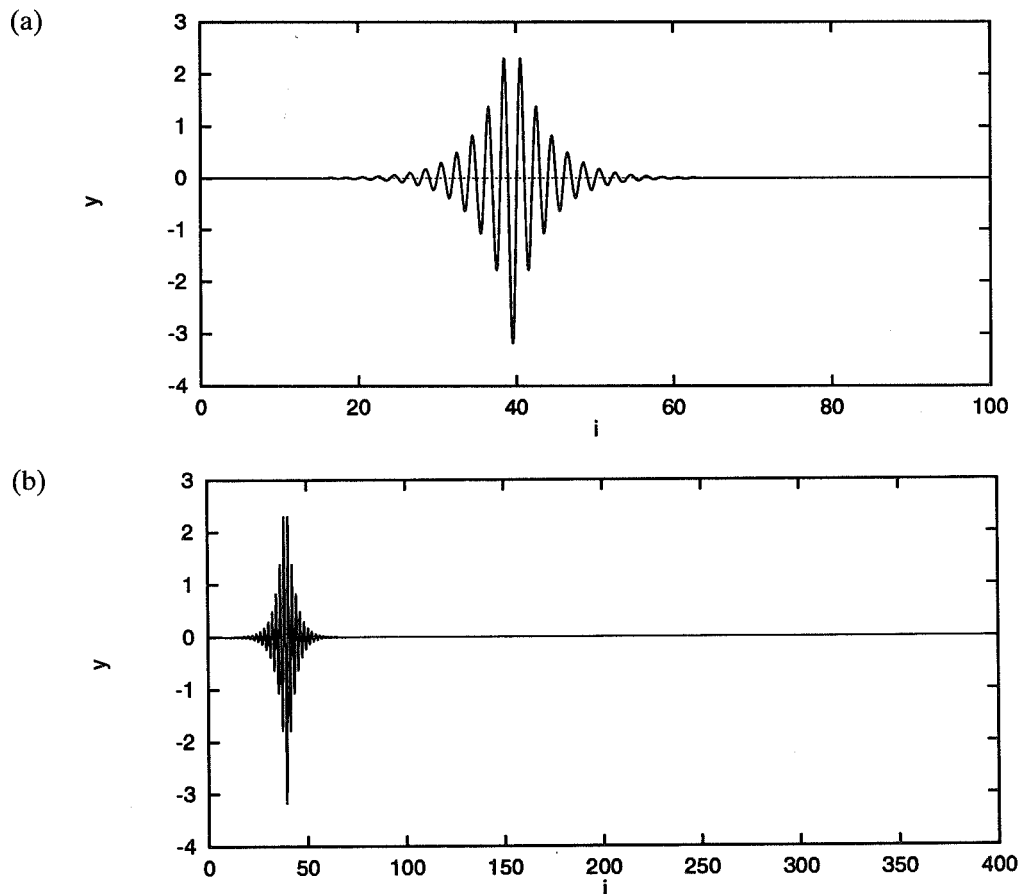


Fig. 6. Buckling mode localization in multi-span beams with torsional springs of $\nu = 0.3$ (the disorder occurs in the 40th span). (a) Buckling mode for a 100-span beam; (b) buckling mode of a 400-span beam.

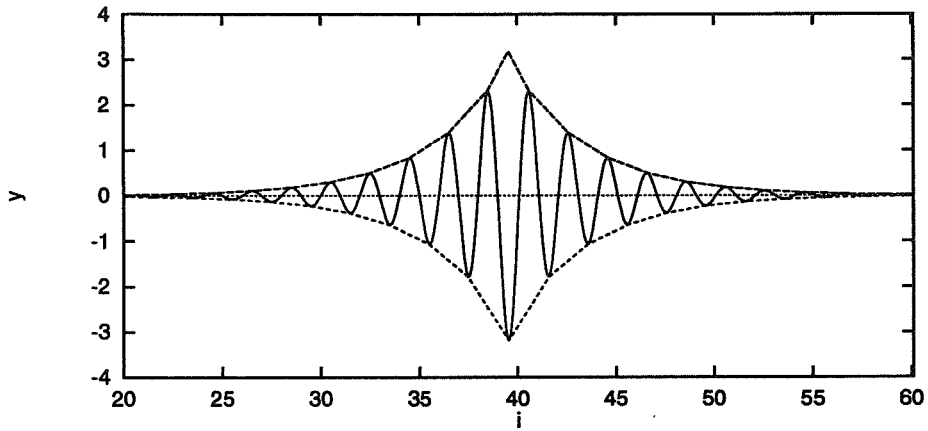


Fig. 7. Envelope of the buckling mode shape for a 100-span beam.

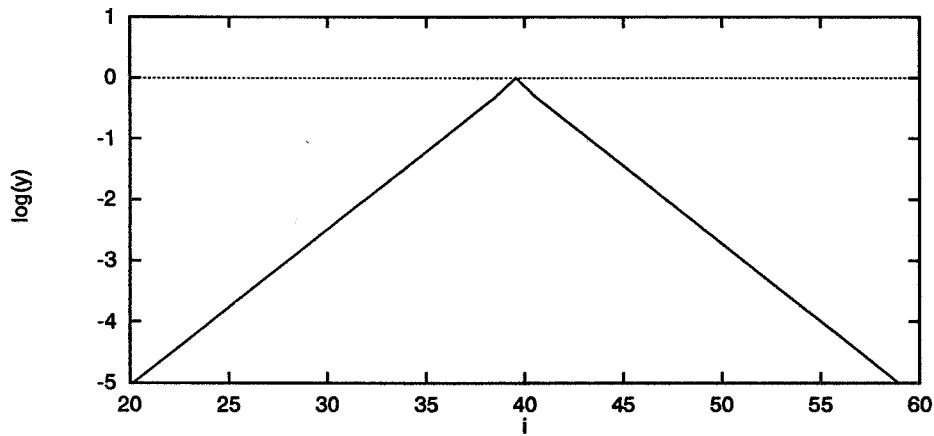


Fig. 8. Logarithmic plot of the envelope function.

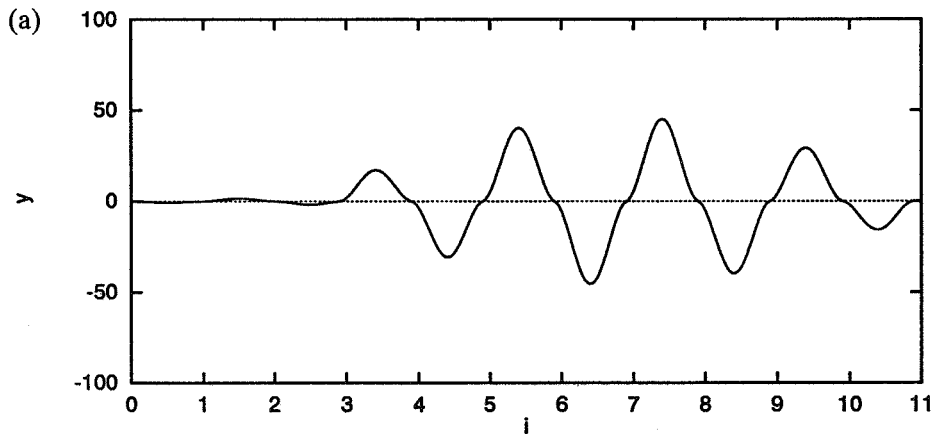


Fig. 9.(a).

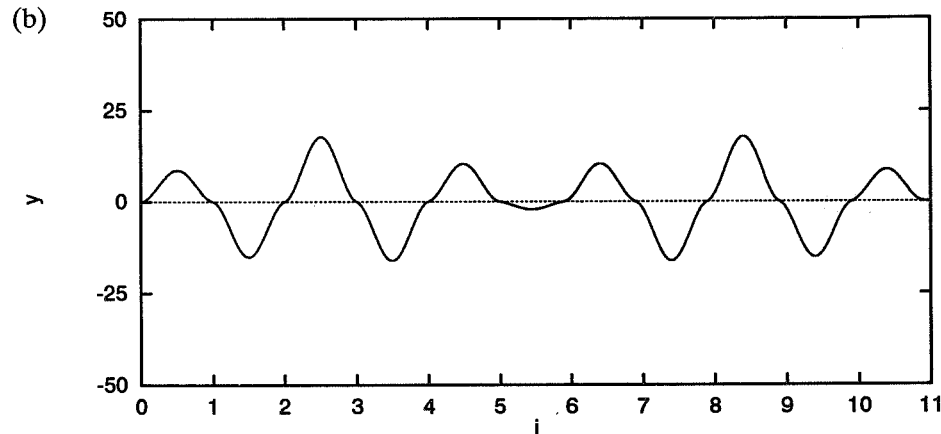


Fig. 9. Buckling mode shapes for a disorder 11-span beam (disordered span is shorter than the periodic span). (a) Disorder occurs in the third span; (b) disorder occurs in the mid-span (sixth span).

can see that the ‘beneficial’ effect of such a disorder on the buckling load is very small—the increase in buckling load is less than 2%. However, the impact of disorder on the buckling mode shape is noteworthy. Figure 9 portrays the buckling mode shapes of 11-span beams containing such a disorder, from which it can be seen that the change in buckling mode is significant, especially when the disorder occurs near the boundaries. Interestingly enough, the localization phenomenon has not been observed in this ‘beneficial’ case.

Finally, it should be noted that the present study can be generalized to other more complicated problems. The work is underway and will be reported elsewhere.

Acknowledgement—Support provided by NASA Langley Research Center, through Grant NAG-1-1310 is gratefully appreciated. Discussion with Professor S. T. Ariaratnam of the University of Waterloo is appreciated.

REFERENCES

1. L. Brillouin, *Wave Propagation in Periodic Structures*. Dover, New York (1953).
2. Y. K. Lin and T. J. McDaniel, Dynamics of beam type periodic structures, *Journal of Engineering for Industry* **93**, 1133–1141 (1969).
3. D. J. Mead, Free wave propagation in periodically supported infinite beams, *Journal of Sound and Vibration*, **11**, 181–197 (1971).
4. G. Sen Gupta, Natural flexural wave and the normal modes of periodically supported beams and plates, *Journal of Sound and Vibration* **13**, 89–101 (1970).
5. H. Abramovich and I. Elishakoff, Application of the Krein’s method for determination of natural frequencies of periodically supported beam based on simplified Bresse–Timoshenko equations, *Acta Mechanica* **66**, 39–59 (1987).
6. L. P. Zhu, I. Elishakoff and Y. K. Lin, Free and forced vibrations of periodic multi-span beams, *Shock and Vibration* **1**, 217–232 (1994).
7. F. Bleich *Buckling Strength of Metal Structures*. McGraw-Hill, New York (1952).
8. T. Wah and L. R. Calcote, *Structural Analysis by Finite Difference Calculus*. Van Nostrand Reinhold, New York (1970).
9. G. Q. Cai and Y. K. Lin, Localization of wave propagation in disordered periodic structures, *AIAA Journal* **29**, 450–456 (1988).
10. C. Pierre and E. H. Dowell, Localization of vibrations by structural irregularity, *Journal of Sound and Vibration* **114**, 549–564 (1987).
11. C. Pierre and P. D. Chat, Strong mode localization in nearly periodic disordered structures, *AIAA Journal* **27**, 227–241 (1989).
12. C. Pierre, Weak and strong vibration localization in disordered structures: a statistical investigation, *Journal of Sound and Vibration* **139**, 111–132 (1990).
13. C. Pierre and R. H. Plaut, Curve veering and mode localization in a buckling problem, *Journal of Applied Mathematics and Physics (ZAMP)* **40**, 758–761 (1984).

14. S. T. Ariaratnam and W. C. Xie, Buckling mode localization in randomly disordered continuous beams, manuscript (1993).
15. A. H. Nayfeh and M. Hawwa Buckling mode localization in multi-span columns, in *Proceedings of 35th AIAA/ASME/ASCE/AHS/ASC Structures, Structural Dynamics, and Materials Conference*, April 18–20, Hilton Head, SC, pp. 277–289.
16. M. S. El Naschie, Local postbuckling of compressed cylindrical shells, in *Proceedings of the Institution of Civil Engineers*, Part 2, vol 59, pp. 523–525 (1975).
17. M. S. El Naschie, Nonlinear isometric bifurcation and shell buckling, *Zeitschrift für angewandte Mathematik und Mechanik*, 57, 293–296 (1977).
18. M. S. El Naschie, *Stability and Chaos in Structural Engineering: an Energy Approach*. McGraw-Hill, London (1990).
19. M. S. El Naschie, Localized diamond shaped buckling patterns of axially compressed cylindrical shells, *AIAA Journal* 13, 837–838 (1975).
20. I. Elishakoff, Y. W. Li and J. H. Starnes Jr, Buckling mode localization in elastic plates due to misplacement in the stiffener location, *Chaos, Solitons & Fractals* to appear.
21. M. R. Horne, *Stability of Frames*. Pergamon, Oxford (1965).
22. W. T. Thompson, *Theory of Vibration with Applications*, 2nd Edition pp. 30–34. Prentice-Hall, Englewood Cliffs, NJ (1981).

APPENDIX

Consider the case when the disorder occurs in the first span. We have the following set of equations for boundary and continuity conditions.

- (1) Boundary condition at the left end

$$-M_0^R = J\theta_0^L \quad \text{or} \quad \left[8\nu \left(\frac{b}{a} \right) \frac{\bar{c}_1}{4c_1^2 - c_2^2} + 1 \right] \bar{M}_0^R + 4\nu \left(\frac{b}{a} \right) \frac{\bar{c}_2}{4\bar{c}_1^2 - \bar{c}_2^2} \bar{M}_1^L = 0. \quad (\text{A1})$$

- (2) Equilibrium equation for support 1

$$M_1^L - M_1^R = J\theta_0^H \quad \text{or} \quad \bar{M}_1^L - (2c_1 + 4\nu)\theta_0^H - c_2\theta_1^H = 0. \quad (\text{A2})$$

- (3) Continuity condition between segments I and II

$$\theta_1^L = \theta_0^H \quad \text{or} \quad \theta_0^H + \frac{b}{a(4\bar{c}_1^2 - \bar{c}_2^2)} (\bar{c}_2 \bar{M}_0^R + 2\bar{c}_1 \bar{M}_1^L) = 0. \quad (\text{A3})$$

- (4) Boundary condition at the right end

$$M_N^L = J\theta_{N-1}^H \quad \text{or} \quad (2c_1 + 4\nu)\theta_{N-1}^H + c_2\theta_{N-2}^H = 0. \quad (\text{A4})$$

Again, three different cases have to be considered separately. The expressions for θ_s^H in those three cases are as follows.

$$\text{Case A: } \theta_s^H = A_2 e^{\alpha s} + B_2 e^{-\alpha s}$$

$$\text{Case B: } \theta_s^H = A_2 \cosh(\alpha s) \cos(\pi s) + B_2 \sinh(\alpha s) \cos(\pi s) \quad (\text{A5})$$

$$\text{Case C: } \theta_s^H = A_2 \cos(\beta s) + B_2 \sin(\beta s) \quad (s = 0, 1, 2, \dots, N-1).$$

Substituting equation (A5) into equations (A1)–(A4), one obtains four homogeneous algebraic equations for each case. These four equations can be expressed in a matrix form

$$[F(K)]_{4 \times 4} \{\delta\}_{4 \times 1} = 0, \quad (\text{A6})$$

where $[F(K)]$ is a coefficient matrix, and $\{\delta\}^T = \{\bar{M}_0^R, \bar{M}_1^L, A_2, B_2\}$.

It is of interest to note that the above equations can be formally obtained from equation (55) by letting $q = 0$ and $A_1 = B_1 = 0$. As to the case where the disorder occurs in the last span of the beam, a similar treatment can be made accordingly and the problem again reduces to a set of four homogeneous algebraic equations.

N15
55-39
408 936
QUAILED
358955 p 16

Prediction of Natural Frequency and Buckling Load Variability Due to Uncertainty in Material Properties by Convex Modeling

Y.W. Li, I. Elishakoff

Mechanical Engineering Department
Florida Atlantic University
Boca Raton FL 33431-0991 USA

J. H. Starnes, Jr.

NASA Langley Research Center
Hampton VA 23664-5225, USA

M. Shinozuka

Department of Civil Engineering
University of Southern California
Los Angeles CA 90089-0242 USA

1 Introduction

Composite materials are widely used in various types of engineering structures. Previous studies have been based on the assumption that the properties of the composite materials are characterized by pre-determined elastic moduli, and no uncertainties of these moduli have been considered (Vinson and Sierakowski [1986], Tennyson [1975], Whitney [1987]). However, the composite materials are subject to a certain amount of scatter in their measured elastic moduli (Tewary [1978]). Such uncertainties in elastic moduli are due to many factors which influence the actual properties of composites. For example, among other things, misalignment of fibers or imperfect bonding between the fibers and the matrix may contribute to the scattered values of the measured elastic moduli. To a large extent, the properties of composite materials are dependent on the fabrication process. But even the composite materials manufactured by the same process may demonstrate differences in their elastic properties. For design purposes, one should be aware of the potential variations in load-carrying capacity and dynamic behavior of such structures that can arise due to the uncertainty in elastic moduli. A more realistic analysis of composite structures should be performed with the variations of the elastic moduli being taken into consideration at the same time.

Scatter in material properties is usually treated within the realm of the stochastic finite element method (Anantha and Ganesan [1993]). However, as Shinozuka

1991 *Mathematics Subject Classification*. Primary: 73K20; Secondary: 73K15, 73H05.

[1987] mentions: "...it is recognized that it is rather difficult to estimate experimentally the auto-correlation function, or in the case of weak homogeneity, the spectral density function of the stochastic variation of material properties. In view of this, the upper bound results are particularly important, since the bounds derived ... do not require knowledge of the autocorrelation function." In the stochastic context, Shinozuka [1987], and Shinozuka and Deodatis [1988] and Deodatis and Shinozuka [1989] derived upper and lower bounds on the probabilistic characteristics of the response in terms of probabilistic characteristics of the material variability.

Recently, in a private correspondence, Ariaratnam [January, 1992] advocated placing bounds on elastic moduli and deriving appropriate bounds for certain structural properties such as the buckling loads and natural frequencies. This idea is implemented in this investigation. Here, we use *convex modeling* (Ben-Haim and Elishakoff [1990]), a newly-developed analytical tool, which incorporates uncertainties in elastic moduli into the structural analysis. Since it came into being, convex modeling has been used under different circumstances for solving a variety of engineering problems (Elishakoff and Ben-Haim [1990], Elishakoff, Li and Starnes [1994]).

The present paper is a generalization of the previous study of Elishakoff, Li and Starnes [1994], where the influence of uncertainty in elastic moduli on the *axial buckling load* was discussed. Here, we consider another case of buckling, that is, shells under *uniform external pressure*. In addition, this paper deals with the variability of *natural frequencies* by use of *convex modeling*, which is apparently the first study of this kind in the literature. A numerical approach to the uncertainty problem is nonlinear programming, which we apply to solve the same problem to generate a set of comparable numerical data. The results from both methods show good agreement throughout. Thus, the effectiveness of the analytic convex modeling is clearly demonstrated. The bounds of the natural frequency and the buckling load provide the designer with a better view of the vibrational behavior and the actual load carrying capacities possessed by the composite structure.

2 Basic Equations

We use the Donnell shell theory (Timoshenko and Gere [1961]) for the analysis of buckling of cylindrical shells of composite materials. The strain-displacement relations are

$$\begin{aligned}
 \epsilon_x &= \frac{\partial u}{\partial x}, & \kappa_x &= -\frac{\partial^2 w}{\partial x^2} \\
 \epsilon_y &= \frac{\partial v}{\partial y} + \frac{w}{R}, & \kappa_y &= -\frac{\partial^2 w}{\partial y^2} \\
 \gamma_{xy} &= \frac{\partial v}{\partial x} + \frac{\partial u}{\partial y}, & \kappa_{xy} &= -2\frac{\partial^2 w}{\partial x \partial y}
 \end{aligned} \tag{2.1}$$

where x and y are the axial and circumferential coordinates in the shell middle surface; u and v are the shell displacement along axial and circumferential directions, and w is the radial displacement, positive outward; ϵ_x , ϵ_y and γ_{xy} are strain components; κ_x , κ_y and κ_{xy} are middle surface curvatures of the shell; R is the radius of the cylindrical shell. The constitutive relations for the composite laminate

read

$$\begin{pmatrix} N_x \\ N_y \\ N_{xy} \\ M_x \\ M_y \\ M_{xy} \end{pmatrix} = \begin{pmatrix} A_{11} & A_{12} & A_{16} & B_{11} & B_{12} & B_{16} \\ A_{12} & A_{22} & A_{26} & B_{12} & B_{22} & B_{26} \\ A_{16} & A_{26} & A_{66} & B_{16} & B_{26} & B_{66} \\ B_{11} & B_{12} & B_{26} & D_{11} & D_{12} & D_{16} \\ B_{12} & B_{22} & B_{26} & D_{12} & D_{22} & D_{26} \\ B_{16} & B_{26} & B_{66} & D_{16} & D_{26} & D_{66} \end{pmatrix} \begin{pmatrix} \epsilon_x \\ \epsilon_y \\ \epsilon_{xy} \\ \kappa_x \\ \kappa_y \\ \kappa_{xy} \end{pmatrix} \quad (2.2)$$

where N_x , N_y and N_{xy} are stress resultants, M_x , M_y and M_{xy} are bending and twisting moments, acting on a laminate; the laminate stiffnesses A_{ij} , B_{ij} and D_{ij} are defined as

$$(A_{ij}, B_{ij}, D_{ij}) = \int_{-h/2}^{h/2} \bar{Q}_{ij}^{(k)}(1, z, z^2) dz$$

where h is the total thickness of the laminate, and z is the coordinate in the direction of the laminate thickness; $\bar{Q}_{ij}^{(k)}$ are the transformed reduced stiffnesses and can be expressed in terms of the lamina orientation and four independent engineering material constants in principal material directions, i.e., E_1 , E_2 , ν_{12} and G_{12} Jones [1975].

The equilibrium equations of the cylindrical shell read

$$\begin{aligned} \frac{\partial N_x}{\partial x} + \frac{\partial N_{xy}}{\partial y} &= 0 \\ \frac{\partial N_{xy}}{\partial x} + \frac{\partial N_y}{\partial y} &= 0 \\ \frac{\partial^2 M_x}{\partial x^2} + 2 \frac{\partial^2 M_{xy}}{\partial x \partial y} + \frac{\partial^2 M_y}{\partial y^2} - \frac{1}{R} N_y + N_x \frac{\partial^2 w}{\partial x^2} + 2N_{xy} \frac{\partial^2 w}{\partial x \partial y} + N_y \frac{\partial^2 w}{\partial y^2} - \rho \frac{\partial^2 w}{\partial t^2} &= 0 \end{aligned} \quad (2.3)$$

where ρ is the mass per unit volume of the shell and t is the time variable.

Using equations (2.1) and (2.2), equation (2.3) can be written as

$$\begin{pmatrix} L_{11} & L_{12} & L_{13} \\ L_{21} & L_{22} & L_{23} \\ L_{31} & L_{32} & L_{33} \end{pmatrix} \begin{pmatrix} u \\ v \\ w \end{pmatrix} = \begin{pmatrix} 0 \\ 0 \\ N_x \frac{\partial^2 w}{\partial x^2} + 2N_{xy} \frac{\partial^2 w}{\partial x \partial y} + N_y \frac{\partial^2 w}{\partial y^2} - \rho \frac{\partial^2 w}{\partial t^2} \end{pmatrix} \quad (2.4)$$

where the operators L_{ij} are

$$\begin{aligned}
L_{11} &= A_{11} \frac{\partial}{\partial x^2} + 2A_{16} \frac{\partial^2}{\partial x \partial y} + A_{66} \frac{\partial^2}{\partial y^2} \\
L_{12} &= A_{16} \frac{\partial^2}{\partial x^2} + (A_{12} + A_{66}) \frac{\partial^2}{\partial x \partial y} + A_{26} \frac{\partial^2}{\partial y^2} \\
L_{13} &= \frac{1}{R} (A_{12} \frac{\partial}{\partial x} + A_{26} \frac{\partial}{\partial y}) - B_{11} \frac{\partial^2}{\partial x^2} \\
&\quad - 3B_{16} \frac{\partial^3}{\partial x^2 \partial y} - (B_{12} + B_{66}) \frac{\partial^3}{\partial x \partial y^2} - B_{26} \frac{\partial^3}{\partial y^3} \\
L_{22} &= A_{66} \frac{\partial^2}{\partial x^2} + 2A_{26} \frac{\partial^2}{\partial x \partial y} + A_{22} \frac{\partial^2}{\partial y^2} \\
L_{23} &= \frac{1}{R} (A_{26} \frac{\partial}{\partial x} + A_{22} \frac{\partial}{\partial y}) - B_{22} \frac{\partial^3}{\partial y^3} \\
&\quad - 3B_{26} \frac{\partial^3}{\partial x \partial y^2} - (B_{12} + 2B_{66}) \frac{\partial^3}{\partial x^2 \partial y} - B_{16} \frac{\partial^3}{\partial x^3} \\
L_{33} &= -\frac{2}{R} (B_{12} \frac{\partial^2}{\partial x^2} + 2B_{26} \frac{\partial^2}{\partial x \partial y} + B_{22} \frac{\partial^2}{\partial y^2}) + \frac{A_{22}}{R^2} + D_{11} \frac{\partial^4}{\partial x^4} \\
&\quad + 4D_{16} \frac{\partial^4}{\partial x^3 \partial y} + 2(D_{12} + 2D_{66}) \frac{\partial^4}{\partial x^2 \partial y^2} + 4D_{26} \frac{\partial^4}{\partial x \partial y^3} + D_{22} \frac{\partial^4}{\partial y^4}
\end{aligned} \tag{2.5}$$

We consider the cylindrical shell with simply supported boundary conditions which are satisfied by the following displacement functions,

$$\begin{pmatrix} u \\ v \\ w \end{pmatrix} = \sum_{m=1}^{\infty} \sum_{n=0}^{\infty} \begin{pmatrix} U_{mn} \cos(\lambda_m x) \cos(\lambda_n y) e^{i\omega t} \\ V_{mn} \sin(\lambda_m x) \sin(\lambda_n y) e^{i\omega t} \\ W_{mn} \sin(\lambda_m x) \cos(\lambda_n y) e^{i\omega t} \end{pmatrix} \tag{2.6}$$

where $\lambda_m = m\pi/L$, $\lambda_n = n/R$ and ω is the natural frequency of the shell.

Similar to Tasi [1966] and Hirano [1979], here the coupling stiffnesses ($A_{16}, A_{26}, B_{16}, B_{26}, D_{16}, D_{26}$) are neglected. They actually vanish for symmetric cross-ply laminates. As for symmetric angle-ply laminates, B_{16} and B_{26} are zero, and A_{16}, A_{26}, D_{16} and D_{26} can be neglected for laminates with many layers.

Substitution of equations (2.1) and (2.2) into equation (2.4) leads to a set of homogeneous linear algebraic equations, and the existence of non-trivial solutions requires that the determinant of the coefficient matrix vanish,

$$\det \begin{pmatrix} C_{11} & C_{12} & & C_{13} \\ C_{21} & C_{22} & & C_{23} \\ C_{31} & C_{32} & C_{33} - \lambda_m^2 N_x - \lambda_m \lambda_n N_{xy} - \lambda_n^2 N_y + \rho\omega^2 & \\ & & & \end{pmatrix} = 0 \tag{2.7}$$

where elements C_{ij} 's are expressed as

$$\begin{aligned}
 C_{11} &= A_{11}\lambda_m^2 + A_{66}\lambda_n^2 \\
 C_{22} &= A_{22}\lambda_n^2 + A_{66}\lambda_m^2 \\
 C_{33} &= D_{11}\lambda_m^4 + 2(D_{12} + 2D_{66})\lambda_m^2\lambda_n^2 + D_{22}\lambda_n^4 + \frac{A_{22}}{R^2} + 2\frac{B_{22}}{R}\lambda_n^2 + 2\frac{B_{12}}{R}\lambda_m^2 \\
 C_{12} &= C_{21} = (A_{12} + A_{66})\lambda_m\lambda_n \\
 C_{23} &= C_{32} = (B_{12} + 2B_{66})\lambda_m^2\lambda_n + \frac{A_{22}}{R}\lambda_n + B_{22}\lambda_n^3 \\
 C_{13} &= C_{31} = \frac{A_{12}}{R}\lambda_m + B_{11}\lambda_m^3 + (B_{12} + 2B_{66})\lambda_m\lambda_n^2
 \end{aligned} \tag{2.8}$$

From equation (2.7), the following expression can be readily derived for the natural frequency

$$\begin{aligned}
 \rho\omega^2 = C_{33} + \frac{(2C_{12}C_{23} - C_{13}C_{22})C_{13} - C_{23}^2C_{11}}{C_{12}^2 - C_{11}C_{22}} \\
 + \lambda_m^2 N_x + \lambda_m\lambda_n N_{xy} + \lambda_n^2 N_y \equiv \rho\omega_{mn,N}^2
 \end{aligned} \tag{2.9}$$

where the subscript "N" indicates the presence of external loading acting in the mid-surface of the shell.

If the shell in question is free from external loading, i.e. $N_x = N_y = N_{xy} = 0$, the natural frequency becomes

$$\omega_{mn,0}^2 = \frac{1}{\rho} \left[C_{33} + \frac{(2C_{12}C_{23} - C_{13}C_{22})C_{13} - C_{23}^2C_{11}}{(C_{12}^2 - C_{11}C_{22})} \right] \tag{2.10}$$

where the subscript zero indicates that the external loads acting in the mid-surface of the shell are absent.

To determine the fundamental natural frequency for a cylindrical shell with given dimensions and material properties, one determines those integer values of m and n which minimize ω_{mn} .

If $\omega = 0$, equation (2.9) yields an expression for the buckling load. The case of static axial buckling of composite shells has been discussed in our previous study Elishakoff, Li and Starnes [1994]. Here we will confine ourselves to the investigation of the buckling of shells under external pressure p , for which

$$N_y = -pR, \quad N_x = -\frac{pR}{2}, \quad N_{xy} = 0 \tag{2.11}$$

The expression for the critical external pressure can be readily derived as follows

$$p = \frac{2}{(\lambda_m^2 + 2\lambda_n^2)R} \left[C_{33} + \frac{(2C_{12}C_{23} - C_{13}C_{22})C_{13} - C_{23}^2C_{11}}{C_{12}^2 - C_{11}C_{22}} \right] \equiv p_{mn} \tag{2.12}$$

Again, one has to perform a search with respect to integer variables m and n to minimize the objective function p_{mn} in order to obtain the critical external pressure p_{cr} for a cylindrical shell with given dimensions and material properties.

3 Convex Modeling of Uncertain Moduli

As has been stated in the previous section, the objective function (the natural frequency $\omega_{mn,0}$ or the critical external pressure p_{mn}) of the structure depends on the four basic elastic moduli. (One can also discuss the natural frequency $\omega_{mn,N}$ if the external pressure is present, provided that the external pressure is below its critical value.) For the sake of generality, in the following analysis, a generic formula for the objective function is adopted instead of relying on a more concrete expression such as equation (2.10) or (2.12).

The objective function is written in the following generic form,

$$F = F(E_1, E_2, \nu_{12}, G_{12}), \quad F = \omega_{mn,0} \text{ or } p_{mn} \quad (3.1)$$

or more simply,

$$F = F(E_i), \quad (i = 1, 2, 3, 4) \quad (3.2)$$

where $E_3 = \nu_{12}$ and $E_4 = G_{12}$. The function F in the above equation also depends on the form of structure, boundary conditions as well as geometric properties.

Let E_i^0 ($i = 1, 2, 3, 4$) be the nominal values of the elastic moduli, which might be visualized as the nominal values of the elastic moduli, or the average values derived from test data. Then, the elastic moduli of values different from those nominal values could be denoted as $E_i^0 + \delta_i$, δ_i being deviations from nominal values. The objective function corresponding to these elastic moduli, retaining only the first order terms in δ_i , is written as follows:

$$F(E_i^0 + \delta_i) = F(E_i^0) + f^T \delta \quad (3.3)$$

where

$$\delta^T = (\delta_1, \delta_2, \delta_3, \delta_4), \quad f^T = \left(\frac{\partial F(E_i^0)}{\partial E_1}, \frac{\partial F(E_i^0)}{\partial E_2}, \frac{\partial F(E_i^0)}{\partial E_3}, \frac{\partial F(E_i^0)}{\partial E_4} \right) \quad (3.4)$$

The deviation δ from the nominal elastic moduli is assumed to vary in the following *ellipsoidal* set:

$$Z(\alpha, e) = \left\{ \delta : \sum_{i=1}^4 \frac{\delta_i^2}{e_i^2} \leq \alpha^2 \right\} \quad (3.5)$$

where the size parameter α and the lengths of semi-axes e_i ($i = 1, 2, 3, 4$) of the ellipsoid are based on the experimental data available, and will be discussed later.

The problem is formulated as follows: given an ellipsoid of the elastic moduli (equation (3.5)), find the extremal natural frequency (or the critical external pressure)

$$F_{ext} = \text{extremum} \\ \delta \in Z(\alpha, e)(F(E_i^0) + f^T \delta). \quad (3.6)$$

In equation (3.6), F_{ext} is the lowest or the highest value of the fundamental natural frequency (or the critical external pressure) of the composite structure with the elastic moduli varying within the range of the ellipsoidal set Z . Since equation (3.6) calls for finding the extremum of the linear functional $f^T \delta$ on the convex set $Z(\alpha, e)$, the extremal values take place on the set of the extreme points, or the boundary, of the set Z as discussed by Ben-Haim and Elishakoff [1990].

To arrive at the extreme values, we use the method of Lagrange multipliers. Since the analysis which follows is mathematically analogous to that described in the monograph Ben-Haim and Elishakoff [1990], here we only list the final result. The extremal values of the objective function F result in the following expressions

$$\begin{aligned}
 \omega_{mn,\max} &= \langle \omega_{mn,0} \rangle \left[1 + \alpha \sqrt{\sum_{i=1}^4 \left(\frac{e_i}{\langle \omega_{mn,0} \rangle} \frac{\partial \omega_{mn,0}(E_i^0)}{\partial E_i} \right)^2} \right] \\
 \omega_{mn,\min} &= \langle \omega_{mn,0} \rangle \left[1 - \alpha \sqrt{\sum_{i=1}^4 \left(\frac{e_i}{\langle \omega_{mn,0} \rangle} \frac{\partial \omega_{mn,0}(E_i^0)}{\partial E_i} \right)^2} \right] \\
 p_{cr,\max} &= \langle p_{cr} \rangle \left[1 + \alpha \sqrt{\sum_{i=1}^4 \left(\frac{e_i}{\langle p_{cr} \rangle} \frac{\partial p_{cr}(E_i^0)}{\partial E_i} \right)^2} \right] \\
 p_{cr,\min} &= \langle p_{cr} \rangle \left[1 - \alpha \sqrt{\sum_{i=1}^4 \left(\frac{e_i}{\langle p_{cr} \rangle} \frac{\partial p_{cr}(E_i^0)}{\partial E_i} \right)^2} \right]
 \end{aligned} \tag{3.7}$$

where $\langle \omega_{mn,0} \rangle = \omega_{mn,0}(E_1^0, E_2^0, E_3^0, E_4^0)$ and $\langle p_{cr} \rangle = p_{cr}(E_1^0, E_2^0, E_3^0, E_4^0)$ are values of the natural frequency and critical external pressure calculated at the average values of the elastic moduli.

From the above equation, the upper and lower bounds of the natural frequency ω and the critical external pressure p_{cr} can be calculated if we use the appropriate expression for F . Equation (3.7) shows explicitly that the uncertainties in elastic moduli have a direct effect on the values of the natural frequency and the buckling load of the structure. It is seen here that the products of lengths of semi-axes of the uncertainty ellipsoid and the sensitivity derivatives play an important role in the variation profile of the objective function in the convex modeling.

4 Determination of Convex Set from Measured Data

Before any prediction can be made on the vibratory properties of the composite structure, the values of α and e_i ($i = 1, 2, 3, 4$) should be known in advance. In fact, these values are dependent on the manufacturing process by which the composite structure has been fabricated. It is understandable that the more advanced the manufacturing process and the better the workmanship, the smaller these parameters will be in value. Besides, the evaluation of these parameters is also linked with the amount of information one has about the properties of the composite considered. In this study, the parameter α is set equal to unity. As long as α is fixed, the other parameters could be readily determined by the evaluation of the existing experimental data. Normally, if a sufficient amount of experimental data is available, the average value of these data could be used as the nominal value E_i^0 for the corresponding elastic modulus, whereas parameters e_i 's could be chosen as the proper deviations from the average values of the corresponding measured data. Even if one has only limited knowledge of the uncertain elastic moduli, it is still possible to make judgement on what value the natural frequency of the composite structure will be, provided the variation ranges of these elastic moduli are known.

Suppose that from the experimental data we deduce that the elastic moduli are varying in the following ranges:

$$E_i^L \leq E_i \leq E_i^U \quad (i = 1, 2, 3, 4) \quad (4.1)$$

where E_i^U and E_i^L correspond to upper and lower bounds of the elastic modulus E_i respectively. By using the method described in Elishakoff, Li and Starnes [1994], the nominal values of the elastic moduli and the semi-axes of the ellipsoid can be determined respectively as

$$E_i^0 = (E_i^U + E_i^L)/2, \quad e_i = E_i^U - E_i^L, \quad (i = 1, 2, 3, 4) \quad (4.2)$$

Thus, once the experimental data are available, the semi-axes of the ellipsoid can be determined, and the analysis of convex modeling can be carried out.

5 Numerical Analysis by Nonlinear Programming

The above problem can also be treated as a nonlinear programming problem with bounds, which is mathematically stated as follows:

$$\begin{aligned} \text{Find} \quad & \min F(E_1, E_2, E_3, E_4) \quad \text{or} \quad \max F(E_1, E_2, E_3, E_4) \quad (5.1) \\ & \text{subject to} \quad E_i^L \leq E_i \leq E_i^U, \quad \text{for } i = 1, 2, 3, 4 \end{aligned}$$

For this problem, it is not advisable to apply the gradient methods or Davidon-Fletcher-Powell method (Himmelblau [1972]) which are used most often in nonlinear optimization, since the directional derivative of the objective function F can not be easily calculated analytically. So, a direct search should be implemented. Here we choose the *complex method* (Himmelblau [1972], Beveridge and Schechter [1970]) which is based exclusively on function comparison and no derivatives are used. In the search for a minimum F , the complex method starts with $2n$ ($n = 4$ in our case) points $\mathbf{E}^{(1)}, \mathbf{E}^{(2)}, \dots, \mathbf{E}^{(2n)}$, where $\mathbf{E}^{(i)} = \{E_1^{(i)}, E_2^{(i)}, E_3^{(i)}, E_4^{(i)}\}$. At each search cycle, a new point is generated by a certain rule in terms of the previous $2n$ points and the worst point $\mathbf{E}^{(j)}$, which has the largest value of F among these $2n$ points, is rejected and replaced by the new point. Whenever the new point generated is beyond the bound, it will be set to the bound. Progress will continue with repeated rejection and regeneration until some criteria is met. For a complete description of this method, one may consult Himmelblau [1972], Beveridge and Schechter [1970]. Nowadays, with many commercial software packages available for numerical analysis, such as IMSL [1989], performing non-linear programming could also be realized through use of such computational tools as gradient projection, feasible direction and penalty-function methods (Kirsh [1981]). As was shown above, since the expression of the natural frequency and buckling load is available explicitly, one can choose to optimize a two-term or three-term Taylor expression (Ben-Haim and Elishakoff [1990]), of the natural frequency and the buckling load about the nominal values of elastic moduli subject to nonlinear quadratic constraint function. The constraint function, given in equation (3.5), represents the equation of the ellipsoid of minimum volume that encloses the rectangular parallelepiped representing the original inequality constraints.

It appears remarkable that there is a basic philosophical difference with the classical optimization studies, whereas in classical optimum design of structures one

looks for the maximization of the buckling loads and natural frequencies, here we look for the least favorable scenarios; namely, we determine, for the design purposes, minimum natural frequencies and minimum buckling loads. This procedure has been dubbed in Elishakoff [1991a] “*anti-optimization*”.

6 Numerical Example and Discussion

We now proceed to investigate several cases of the free vibration and buckling problem of composite shells with a view of gaining some insight into the effect of uncertainties in the material properties on the load-carrying capacity and the dynamic behavior of these structures.

In the following analysis, elastic moduli used are from real material tests (Goggin [1973]). The material of the lamina is composed of carbon fibers and resin matrix, with a volume fraction of fiber being 40%. From the figures in Goggin [1973], the following data were deduced

$$\begin{aligned} E_1^U &= 100\text{GPa}(14.5 \times 10^6 \text{psi}), & E_1^L &= 90\text{GPa}(13.0 \times 10^6 \text{psi}) \\ E_2^U &= 7.3\text{GPa}(1.06 \times 10^6 \text{psi}), & E_2^L &= 6.8\text{GPa}(.99 \times 10^6 \text{psi}) \\ E_3^U &= 0.28, & E_3^L &= 0.22 \\ E_4^U &= 3.2\text{GPa}(.46 \times 10^6 \text{psi}), & E_4^L &= 2.6\text{GPa}(0.38 \times 10^6 \text{psi}) \end{aligned} \quad (6.1)$$

From these data, the nominal elastic moduli E_i^0 and the semi-axes e_i can be evaluated, by use of equation (4.2), as the following

$$\begin{aligned} E_1^0 &= 13.75 \times 10^6 \text{psi}, & e_1 &= 1.5 \times 10^6 \text{psi} \\ E_2^0 &= 1.03 \times 10^6 \text{psi}, & e_2 &= 0.07 \times 10^6 \text{psi} \\ E_3^0 &= 0.25, & e_3 &= 0.06 \\ E_4^0 &= 0.42 \times 10^6 \text{psi}, & e_4 &= 0.08 \times 10^6 \text{psi} \end{aligned} \quad (6.2)$$

The natural frequency and the critical external pressure of the composite cylindrical shell are given by equation (2.10) and equation (2.12), respectively. It should be noted here that the basic elastic moduli E_i are implicitly contained in the flexural stiffnesses A_{ij} and D_{ij} .

The shells investigated have a radius 6.0 inch, are composed of 0.012-inch thick layers. The following two cases are considered:

Case 1: the 10-layer laminated shell, with ply angle being $[\theta, -\theta, \theta, -\theta, \theta, -\theta]_{sym}$, θ ranging from 0° to 90° .

Case 2: the 5-layer laminated shell, with ply angle being $[\theta, -\theta, \theta_{1/2}]_{sym}$, θ ranging from 0° to 90° .

In order to quantify the variability of the natural frequency or the critical external pressure of the composite structure, a percentage variability β is defined as follows

$$\beta = \frac{F_u - F_l}{2F_n} \times 100\% \quad (6.3)$$

where subscripts u , l and n denote the upper-bound, lower-bound, and the nominal value, respectively.

Figures 1 and 2 portray the variability of the fundamental natural frequency due to the uncertainty in elastic moduli for the above two cases. Figures 3 and 4 depict the variation profile for the critical external pressure of a set of 10-layer and 5-layer laminated shells. Note that the abrupt turns at some points of these

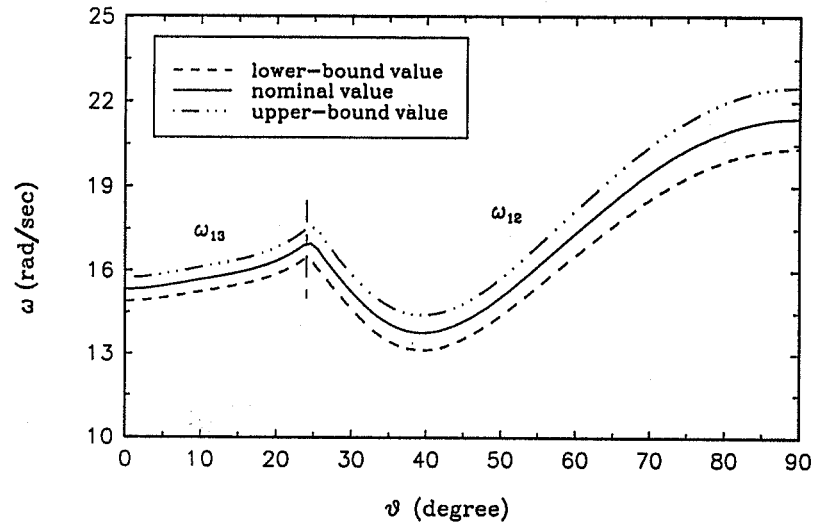


Figure 1 Variability of fundamental natural frequency for a set of 10-layer laminated cylindrical shells

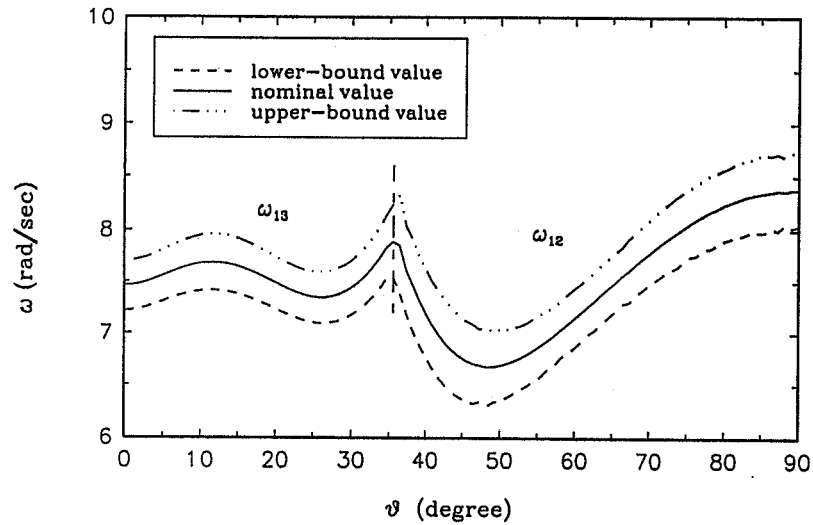


Figure 2 Variability of fundamental natural frequency for a set of 5-layer laminated cylindrical shells

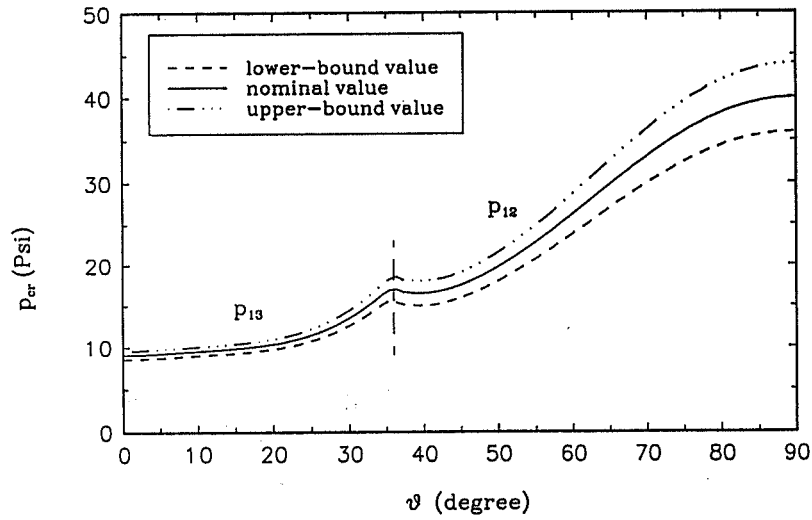


Figure 3 Variability of critical external pressure for a set of 10-layer laminated cylindrical shells

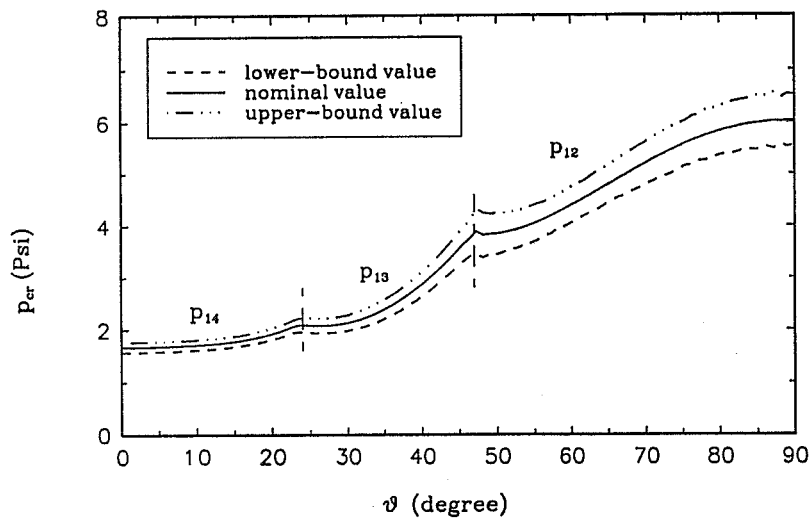


Figure 4 Variability of critical external pressure for a set of 5-layer laminated cylindrical shells

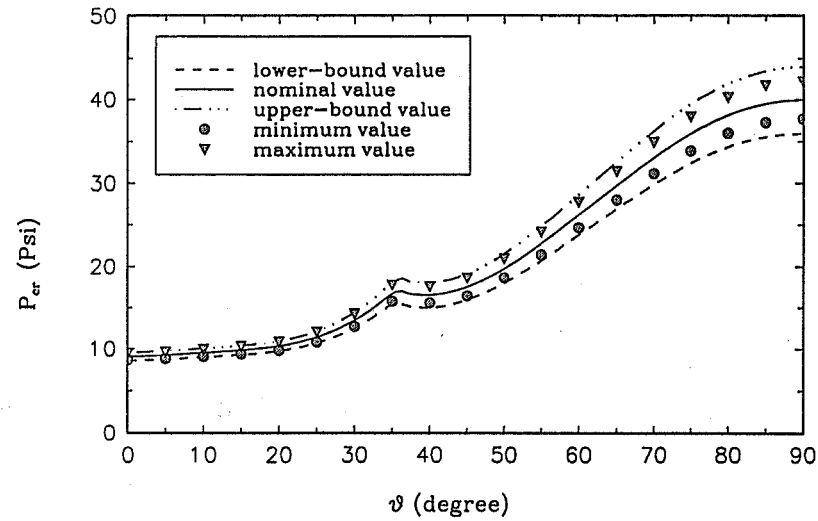


Figure 5 Comparison of results for critical external pressure from the convex modelling and numerical nonlinear programming

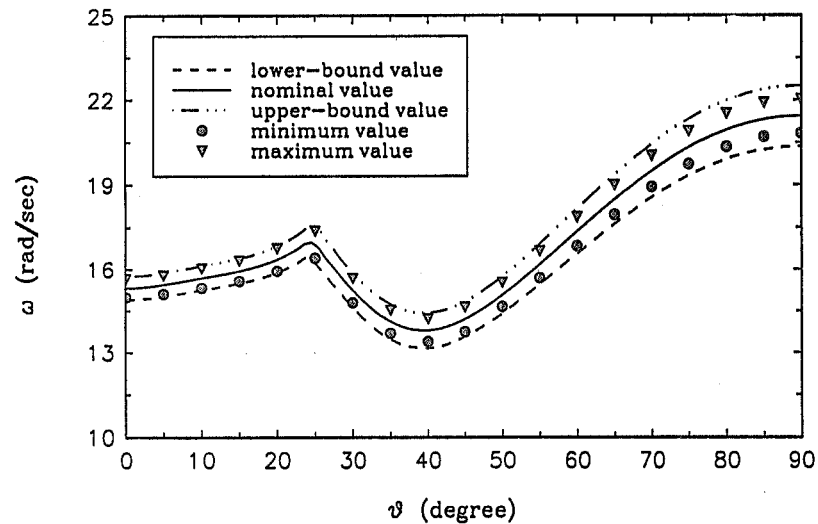


Figure 6 Comparison of results for fundamental natural frequency from convex modelling and numerical nonlinear programming

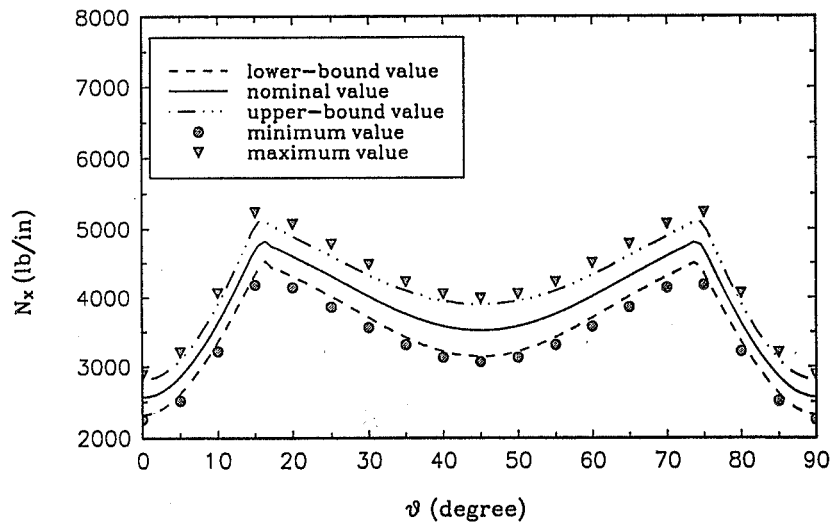


Figure 7 Comprison of results for axial buckling load from convex modelling and numerical nonlinear programming

curves are due to the change of vibration or buckling mode. The effect of uncertainty in elastic moduli on both the critical external pressure and the natural frequency varies greatly with the laminate configuration and the number of layers which make up the laminated shell. For instance, for the 10-ply shells under the external pressure, the variability of the critical external pressure β goes from the minimum 5.5% at $\theta = 0^\circ$ to the maximum 10% at $\theta = 90^\circ$, whereas, for the 5-ply shells under the same loading conditions, β varies between 5.9% at $\theta = 0^\circ$ and 11% at $\theta = 47^\circ$. In comparison, the variability of the fundamental natural frequency due to the uncertainty in elastic moduli is smaller. For example, the uncertainty in elastic moduli brings about a maximum 5% and 6% variability of fundamental natural frequency around its nominal value for the 10-layer and 5-layer shells, respectively. However, the lamination angle corresponding to the maximum variability is different: $\theta = 90^\circ$ for the 10-layer shell and $\theta = 43^\circ$ for the 5-layer shell. In order to evaluate the accuracy of the above simple, analytic convex modeling analysis, we perform a numerical analysis of the critical external pressure and the natural frequency for a set of 10-ply laminated cylindrical shells by nonlinear programming. The results are displayed in Figures 5 and 6, which demonstrate a very good overall agreement between the results from the two different methods. Thus, once again, analytic convex modeling is proved very effective. It can also be seen from these two figures that when the lamination angle θ is less than 45° , the results from convex modeling almost overlap with those from nonlinear programming. When θ is greater than 45° , convex modeling predicts a slightly bigger variability than nonlinear programming. As far as the natural frequency and the critical external pressure are concerned, a design based on convex modeling results seems more conservative. However, it appears difficult to generalize this conclusion since it has been found that sometimes convex modeling may under-estimate the

variability of certain structural behavior. For instance, for the same 10-layer composite cylindrical shells as above, if the loading condition is axial compression, the buckling load results generated by nonlinear programming can lie slightly outside the variation pattern predicted by convex modeling (Figure 7).

It should be brought to the attention of the designer that, whenever one is confronted with imprecisely measured elastic moduli or with a collection of scattered data on elastic moduli, it is advisable to evaluate the potential variability of the structural properties, since such a variability may lead to the degradation in the load-carrying capability and dynamic behavior of the structure. Besides, it is worthy to note that, in many circumstances, while the traditional deterministic analysis based on using nominal values may lead to under-designing of the structure, and the probabilistic analysis may not be performed due to the insufficiency of the available data (especially when an extremely low probability of failure is required for the designed structure), the proposed non-stochastic, convex modeling, method may serve as a viable alternative to both deterministic and probabilistic methods.

7 Conclusion

Both analytical convex modeling and numerical nonlinear programming are utilized to evaluate the variability of buckling load and natural frequency of the composite shells due to the uncertainties in elastic moduli. Based on the experimental data for the elastic moduli, the lower and upper bounds of the buckling load and natural frequency are evaluated. The bounds are very useful in practice and could be directly incorporated into design. It is remarkable that this simple non-stochastic, convex modeling enables the engineer to predict accurately the variation profile of certain structural behavior due to uncertainty in moduli, even when the experimental data are limited and hence the conventional probabilistic approach can not be utilized.

Acknowledgement

Support provided by NASA Langley Research Center, through Grant NAG-1-1310 is gratefully appreciated. The authors also thank the reviewers of the paper for their constructive discussions.

References

- Anantha Ramu, S. and Ganesan, R. [1993], *Parametric stability of stochastic columns*, International Journal of Solids and Structures, **30**, 1339-1354.
- Ariaratnam, S. T. [January, 1992], Private communication to I. Elishakoff.
- Ben-Haim, Y. and Elishakoff, I. [1990], *Convex Models of Uncertainty in Applied Mechanics*, Elsevier.
- Beveridge, G. and Schechter, R. [1970], *Optimization: Theory and Practice*, McGraw-Hill, New York, 453-456.
- Deodatis, G. and Shinozuka, M. [1989], *Bounds on response variability of stochastic systems*, Journal of Engineering Mechanics, **115**, 2543-2563.
- Elishakoff, I. [1991a], *Convex versus probabilistic modeling of uncertainty in structural dynamics*, Structural Dynamics Recent Advances, ed. by M. Petyt, H.F. Wolfe, and C. Mei, Elsevier Applied Science, London, 3-21.

- Elishakoff, I. [1991b], *Essay on probability, convexity and earthquake engineering*, Proceedings of the 5th Italian National Conference on Earthquake Engineering, L'Ingegneria Sismica in Italia, **2**, 907-935.
- Elishakoff, I. [1991c], *Essay on reliability index, probabilistic interpretation of safety factor, and convex models of uncertainty*, Reliability Problems: General Principles and Applications in Mechanics of Solids and Structures, (Casciati, F. and Roberts, J.B. ed.) Springer, Berlin, 237-271.
- Elishakoff, I. and Ben-Haim, Y. [1990], *Dynamics of a thin cylindrical shell under impact with limited deterministic information on its initial imperfections*, Journal of Structural Safety, **8**, 103-112.
- Elishakoff, I. Cai, G. C., and Starnes, J. H. Jr. [1993], *Nonlinear buckling of a column with initial imperfection via stochastic and non-stochastic, convex models*, International Journal of Nonlinear Mechanics, **29**, 71-82.
- Elishakoff, I. and Colombi, P. [1993], *Combination of probabilistic and convex models of uncertainty when scarce knowledge is present on acoustic excitation parameters*, Computer Methods in Applied Mechanics and Engineering, **104**, 187-209.
- Elishakoff, I., Gana-Shvili, Y., and Givoli, D. [1991], *Treatment of uncertain imperfections as a convex optimization problems*, Proceedings of the Sixth International Conference on Applications of Stochastics and Probability in Civil Engineering, (Esteve, L. and Ruiz, S.E., ed.) Mexico City, **1**, 150-157.
- Elishakoff, I., Li, Y.W., and Starnes, J. H. Jr. [1994], *A deterministic method to predict the buckling load variability due to uncertain elastic moduli*, Computer Methods in Applied Mechanics and Engineering, **111**, 155-167.
- Engineering Materials Handbook* [1987], **1**, Composites, ASM International, 445-446.
- Goggin, P. R. [1973], *The elastic constants of Carbon-fiber composites*, Journal of Materials Science, **8**, 233-244.
- Himmelblau, D. M. [1972], *Applied Nonlinear Programming*, McGraw-Hill, New York, 177-178.
- Hirano, Y. [1979], *Buckling of angle-ply laminated circular cylindrical shells*, Journal of Applied Mechanics, **46**, 233-234.
- IMSL [1989], *Fortran Subroutines for Mathematical Applications*, Version 1.1, IMSL Inc.
- Jones, R. M. [1975], *Mechanics of Composite Materials*, Hemisphere Publishing Co., 45-54.
- Kirsh, U. [1981], *Optimum Structural Design*, McGraw-Hill, New York.
- Shinozuka, M. [1987], *Structural response variability*, Journal of Engineering Mechanics, **113**, 825-842.
- Shinozuka, M. and Deodatis, G. [1988], *Response variability of stochastic finite element systems*, Journal of Engineering Mechanics, **114**, 499-519.
- Tasi, J. [1966], *Effect of heterogeneity on the stability of composite cylindrical shells under axial compression*, A.I.A.A. Journal, **4**, 1059-1062.

- Tennyson, R. C. [1975], *Buckling of laminated composite cylinders: a review*, Composite, 17-24.
- Tewary, V.K. [1978], *Mechanics of Fiber Composites*, John Wiley & Sons, 108-121.
- Timoshenko, S.P. and Gere, J. M. [1961], *Theory of Elastic Stability*, McGraw-Hill Book Co., 462-466.
- Vinson, J.R. and Sierakowski, R.L. [1986], *The Behavior of Structures Composed of Composite Materials*, Martinus Nijhoff Publishers, 63-171.
- Whitney, J. M. [1987], *Structural Analysis of Laminated Anisotropic Plates*, Technomic Publishing Company, Lancaster, PA, 151-156.



Derivation of Multi-Dimensional Ellipsoidal Convex Model for Experimental Data

L. P. ZHU AND I. ELISHAKOFF

Department of Mechanical Engineering, Florida Atlantic University
Boca Raton, FL 33431, U.S.A.

J. H. STARNES, JR.

NASA Langley Research Center, Hampton, VA 23664-5225, U.S.A.

(Received June 1994; accepted March 1995)

Abstract—This paper deals with determination of the best ellipsoidal model fitting the available limited experimental data. The problem is defined as that of finding the minimum volume ellipsoid containing all experimental data. A general transformation matrix for the rotation of N -dimensional coordinate system is first obtained by the Gramm-Schmidt orthogonalization procedure. The use of this matrix makes it possible to search in all possible directions to find an ellipsoid with a minimum volume. The general procedure is illustrated by examples in which the real data is utilized. An invariance property of the response with uncertain parameters of different physical nature is also discussed.

Keywords—Convex modeling, Experimental data, Uncertainty analysis.

1. INTRODUCTION

The availability of uncertain, limited, information for the parameters either in a structure or in a excitation to which the structure is subjected, or in both, is often encountered in various branches of engineering; this is partially due to high cost of the measurements. For this case, Ben-Haim and Elishakoff [1,2] developed a novel approach, dubbed as *convex modelling*, to analyze vibration and buckling of beams, plates, and shells due to uncertain excitation or uncertain geometrical parameters. When the excitation is of the stochastic nature with some imbedded uncertain but nonstochastic parameters, the method of random vibration must be combined with convex modelling. These considerations led Elishakoff and Colombi [3] to propose a new, hybrid probabilistic and convex-theoretic approach to analyze dynamic response of structures. In the special case when the set of uncertain parameters is an ellipsoid, closed-form solutions were derived for the upper and lower bounds of the mean-square displacements of the structure. The direct comparison of probabilistic and convex analyses was performed by Elishakoff, Cai and Starnes [4].

Uncertainty modeling by methods alternative to probabilistic modeling was dealt in various contexts by Leitmann [5], Chernousko [6] and Schweppe [7]. Applications to structures include papers by Drenick [8], Shinozuka [9], Deodatis and Shinozuka [10], Lindberg [11], Köylüoğlu, Cakmak and Nielsen [12]. The analysis of structures based on convex model for uncertain parameters consists of two parts: one is the formulation of a deterministic objective function, namely, the stress, strain or displacement of the structure; the other is modeling of uncertain parameters,

The study reported herein was supported by the NASA Langley Center. This support is gratefully appreciated.

Typeset by AMS-TEX

which are represented as belonging to a convex set. In this paper, we focus on the second part, namely, determination of convex model. It is obvious that the response or the buckling load of the structure depend on the associated convex model. Hence, the problem of determining the best convex model for a limited available information about the uncertainty parameters becomes of paramount importance. In the previous studies [1,2], for numerical convenience, the axes of the ellipsoids appearing in the convex models for the uncertain parameters were taken as directed along the coordinate axes. Thus, the results obtained based on such ellipsoidal set may be somewhat conservative for engineering design, since the volume of this ellipsoid may not possess the minimal property amongst all possible ellipsoids which can be constructed. In this study, we abandon this restrictive assumption. A general transformation matrix for rotation of N -dimensional coordinate system is first obtained by the Gramm-Schmidt orthogonalization procedure. The use of this matrix makes it possible to search in all directions to find an ellipsoid with a minimum volume. The general procedure is illustrated by an example in which real data is utilized.

2. N -DIMENSIONAL ELLIPSOIDAL CONVEX MODEL

Assume that there are N uncertain parameters a_i ($i = 1, 2, \dots, N$) describing either in the structural properties or in the excitation. These parameters constitute an N -dimensional parameter space, namely, $\mathbf{a}^T = \{a_1, a_2, \dots, a_N\}$. Assume that we have limited information on these parameters, represented by M experimental points, $\mathbf{a}^{(r)}$ ($r = 1, 2, \dots, M$) in this N -dimensional space. The convex model assumes that all these experimental points belong to an ellipsoid

$$(\mathbf{a} - \mathbf{a}^0)^T \mathbf{G} (\mathbf{a} - \mathbf{a}^0) \leq 1, \quad (1)$$

where \mathbf{a}^0 is the state vector of the central point of the ellipsoid, and \mathbf{G} is its characteristic matrix

$$\mathbf{G} = \begin{bmatrix} g_{11} & g_{12} & \cdots & g_{1N} \\ g_{21} & g_{22} & \cdots & g_{2N} \\ \vdots & \vdots & & \vdots \\ g_{N1} & g_{N2} & \cdots & g_{NN} \end{bmatrix}, \quad (2)$$

which determines the size and the orientation of the ellipsoid. The matrix \mathbf{G} is diagonal only when the axes of the ellipsoid are directed along the axes of the coordinates. Once \mathbf{G} and \mathbf{a}^0 are found, the ellipsoid is determined. The best ellipsoidal convex model in the class of the ellipsoids is identified with the one which contains all given experimental points but has a minimum volume. The possible steps to search for such an ellipsoid include the rotation of the coordinate system and construction of an ellipsoid whose axes are along the principle axes in the rotated coordinate system. If we can rotate the coordinate system in all possible directions, there must exist a direction along which the ellipsoid has a minimum volume. The proposed algorithm to achieve this goal is described as follows.

2.1. Transformation Matrix for Rotation of Coordinate System

We first construct the transformation matrix for rotation of an N -dimensional coordinate system. The new coordinates \mathbf{b} are related with original ones \mathbf{a} as follows

$$\mathbf{b} = \mathbf{T}_N \mathbf{a}, \quad (3)$$

where \mathbf{T}_N is a transformation matrix

$$\mathbf{T}_N = \mathbf{T}_N(\theta_1, \theta_2, \dots, \theta_{N-1}), \quad (4)$$

which represents a $N \times N$ square matrix and is dependent on $N - 1$ parameters, $\theta_1, \theta_2, \dots, \theta_{N-1}$, for the general N -dimensional case; for example, for the two-dimensional case there is one parameter θ_1 in \mathbf{T}_2 , whereas for the three-dimensional case there are two parameters θ_1 and θ_2 in \mathbf{T}_3 .

The transformation matrix \mathbf{T}_N can be constructed by any set of orthogonal vectors. One of the approaches to generate these orthogonal vectors is the Gram-Schmidt orthogonalization procedure, which is briefly presented as follows: assume \mathbf{V}_k ($k = 1, \dots, N$) to be a set of linear independent vectors. We first normalize one of the vectors, say, \mathbf{V}_1

$$\mathbf{U}_1 = \frac{\mathbf{V}_1}{\sqrt{\mathbf{V}_1^T \mathbf{V}_1}}. \quad (5)$$

Let a new vector \mathbf{W}_2 be defined as

$$\mathbf{W}_2 = \mathbf{V}_2 - c_1 \mathbf{U}_1. \quad (6)$$

We require orthogonality of \mathbf{W}_2 to \mathbf{U}_1

$$\mathbf{U}_1^T \mathbf{W}_2 = 0, \quad (7)$$

from which the constant c_1 is obtained

$$c_1 = \mathbf{U}_1^T \mathbf{V}_2. \quad (8)$$

Again, we normalize \mathbf{W}_2 to yield

$$\mathbf{U}_2 = \frac{\mathbf{W}_2}{\sqrt{\mathbf{W}_2^T \mathbf{W}_2}}. \quad (9)$$

Analogously, the general form of the k^{th} orthogonal vector and its normalized form can be obtained as follows:

$$\begin{aligned} \mathbf{W}_k &= \mathbf{V}_k - \sum_{i=1}^{k-1} (\mathbf{U}_i^T \mathbf{V}_k) \mathbf{U}_i \neq 0, \quad k \leq N, \\ \mathbf{U}_k &= \frac{\mathbf{W}_k}{\sqrt{\mathbf{W}_k^T \mathbf{W}_k}}. \end{aligned} \quad (10)$$

The initial vectors \mathbf{V}_k can be chosen from any set of linear independent vectors. Here a set of \mathbf{V}_k are chosen as follows:

$$\mathbf{V}_1 = \begin{Bmatrix} \cos \theta_1 \\ \sin \theta_1 \cos \theta_2 \\ \sin \theta_1 \sin \theta_2 \cos \theta_3 \\ \vdots \\ \sin \theta_1 \sin \theta_2 \cdots \sin \theta_{N-2} \cos \theta_{N-1} \\ \sin \theta_1 \sin \theta_2 \cdots \sin \theta_{N-2} \sin \theta_{N-1} \end{Bmatrix}; \quad \mathbf{V}_k = \begin{Bmatrix} 0 \\ \vdots \\ \delta_{i,k-1} \\ \vdots \\ 0 \end{Bmatrix}, \quad (11)$$

$$0 \leq \theta_{k-1} \leq \frac{\pi}{2}, \quad (i = 1, 2, \dots, N; k = 2, 3, \dots, N),$$

where $\delta_{i,m}$ is the Kronecker delta, and the components in \mathbf{V}_1 are chosen to be the spherical coordinates in N -dimensional space [14]. Obviously, the vector \mathbf{V}_k satisfies the following relation

$$\mathbf{V}_k^T \mathbf{V}_k = 1; \quad (k = 1, 2, \dots, N). \quad (12)$$

By using equation (10), a set of orthogonal vectors \mathbf{U}_k ($k = 1, 2, \dots, N$) is derived as follows:

$$\mathbf{U}_1 = \mathbf{V}_1; \quad \mathbf{U}_k = \left\{ \begin{array}{c} \mathbf{O}_{k-2} \\ \bar{\mathbf{U}}_k \end{array} \right\}; \quad k = 2, 3, \dots, N, \quad (13)$$

where \mathbf{O}_{k-2} is a vector with $k-2$ zero components and $\bar{\mathbf{U}}_k$ is a vector with $N-k+2$ components

$$\bar{\mathbf{U}}_k = \left\{ \begin{array}{c} -\sin \theta_{k-1} \\ \cos \theta_{k-1} \cos \theta_k \\ \vdots \\ \cos \theta_{k-1} \sin \theta_k \cdots \sin \theta_{N-2} \cos \theta_{N-1} \\ \cos \theta_{k-1} \sin \theta_k \cdots \sin \theta_{N-2} \sin \theta_{N-1} \end{array} \right\}. \quad (14)$$

Thus, the transformation matrix \mathbf{T}_N for the rotation of the N -dimensional coordinate system reads

$$\mathbf{T}_N(\theta_1, \theta_2, \dots, \theta_{N-1}) = [\mathbf{U}_1, \mathbf{U}_2, \dots, \mathbf{U}_N], \quad (15)$$

which is an orthogonal matrix. From the general N -dimensional transformation matrix, the specific cases can be obtained. For $N = 2$

$$\mathbf{T}_2(\theta_1) = \begin{bmatrix} \cos \theta_1 & -\sin \theta_1 \\ \sin \theta_1 & \cos \theta_1 \end{bmatrix}. \quad (16)$$

For $N = 3$

$$\mathbf{T}_3(\theta_1, \theta_2) = \begin{bmatrix} \cos \theta_1 & -\sin \theta_1 & 0 \\ \sin \theta_1 \cos \theta_2 & \cos \theta_1 \cos \theta_2 & -\sin \theta_2 \\ \sin \theta_1 \sin \theta_2 & \cos \theta_1 \sin \theta_2 & \cos \theta_2 \end{bmatrix}. \quad (17)$$

The coordinate system for $\mathbf{T}_2(\theta_1)$ is shown in Figure 1. Note that the $\mathbf{T}_3(\theta_1, \theta_2)$ can be represented as the product of two transformation matrices

$$\mathbf{T}_3(\theta_1, \theta_2) = \mathbf{T}_3^{(1)}(\theta_2) \mathbf{T}_3^{(2)}(\theta_1), \quad (18)$$

where

$$\mathbf{T}_3^{(1)}(\theta_2) = \begin{bmatrix} 1 & 0 & 0 \\ 0 & \cos \theta_2 & -\sin \theta_2 \\ 0 & \sin \theta_2 & \cos \theta_2 \end{bmatrix}; \quad (19)$$

$$\mathbf{T}_3^{(2)}(\theta_1) = \begin{bmatrix} \cos \theta_1 & -\sin \theta_1 & 0 \\ \sin \theta_1 & \cos \theta_1 & 0 \\ 0 & 0 & 1 \end{bmatrix}; \quad (20)$$

which represent two consecutive rotations around axis 1 and axis 3', respectively (see Figure 3). The rotational coordinate systems corresponding to $\mathbf{T}_3^{(1)}(\theta_2)$ and $\mathbf{T}_3^{(2)}(\theta_1)$ are given in Figures 2a and 2b, respectively.

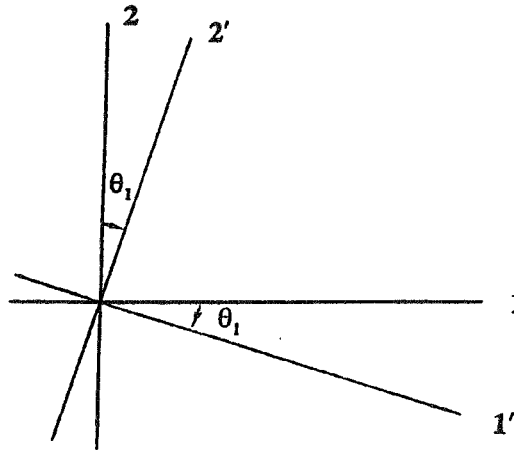
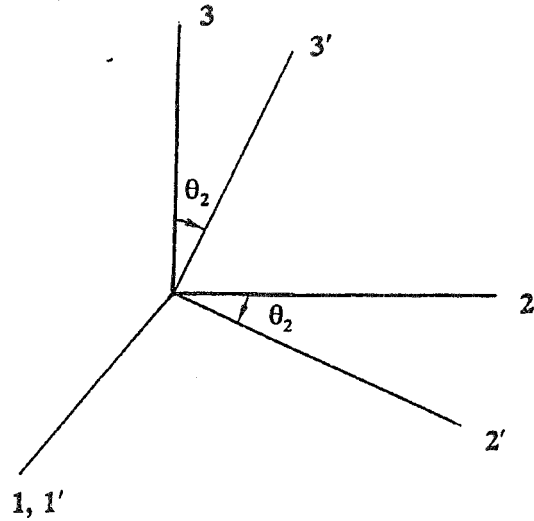
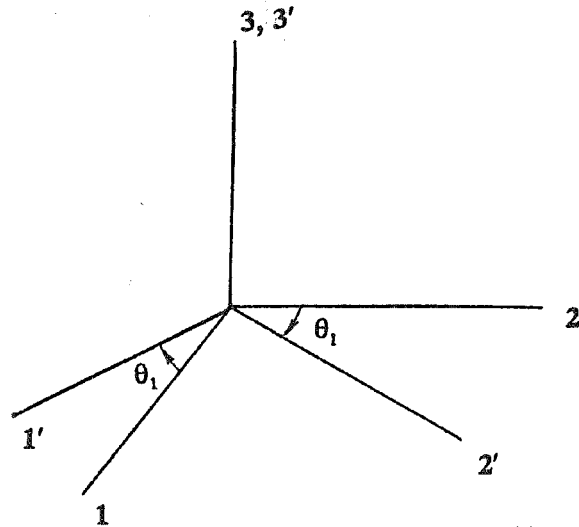


Figure 1. Rotation of coordinate system associated with $\mathbf{T}_2(\theta_1)$.



(a) Rotation of coordinate system associated with $T_3^{(1)}(\theta_2)$.



(b) Rotation of coordinate system associated with $T_3^{(2)}(\theta_1)$.

Figure 2.

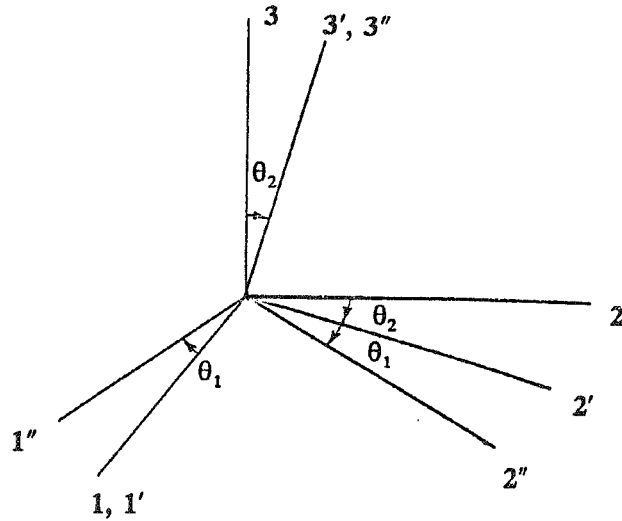


Figure 3. Rotation of coordinate system associated with $T_3(\theta_1, \theta_2)$.

2.2. Ellipsoid in Rotated Coordinate System

By using transformation matrix \mathbf{T}_N given in equation (4), the given M points in the rotated coordinate system will have their new coordinates denoted by $\mathbf{b}^{(r)}$ ($r = 1, 2, \dots, M$). To obtain the ellipsoid, let us first examine an N -dimensional box of the form

$$|\mathbf{b} - \mathbf{b}^0| \leq \mathbf{d}, \quad (21)$$

which contains all M points. The vector of semi-axes $\mathbf{d}^\top = \{d_1, d_2, \dots, d_N\}$ and the vector of central points $\mathbf{b}^{0\top} = \{b_1^0, b_2^0, \dots, b_N^0\}$ of the "box" in the rotated coordinate system are given by

$$\begin{aligned} d_k &= \frac{1}{2} \left[\max_r \{b_k^{(r)}\} - \min_r \{b_k^{(r)}\} \right], \\ b_k^0 &= \frac{1}{2} \left[\max_r \{b_k^{(r)}\} + \min_r \{b_k^{(r)}\} \right], \end{aligned} \quad (r = 1, 2, \dots, M; k = 1, 2, \dots, N). \quad (22)$$

We now enclose this box by an ellipsoid

$$\sum_{k=1}^N \frac{(b_k - b_k^0)^2}{g_k^2} \leq 1, \quad (23)$$

where g_k are the semi-axes of the ellipsoid. There are infinite number of ellipsoids which contain the box given in equation (21). Clearly, the best choice is the one with the minimum volume. The volume of an N -dimensional ellipsoid is given by

$$V_e = C_N \prod_{k=1}^N g_k, \quad (24)$$

where C_N is a constant, depending on the dimensionality of the ellipsoid; for example, $C_2 = \pi$, $C_3 = 4\pi/3$, etc; \prod denotes the product. The surface of the ellipsoid should pass through the corner points of the "box" (see equation (21)). Therefore,

$$\sum_{k=1}^N \frac{d_k^2}{g_k^2} = 1. \quad (25)$$

We are interested in minimizing the volume V_e of the ellipsoid, subject to constraint (25). We use the Lagrange multiplier technique. The Lagrangian reads

$$L = C_N \prod_{k=1}^N g_k + \lambda \left(\sum_{k=1}^N \frac{d_k^2}{g_k^2} - 1 \right). \quad (26)$$

By requiring

$$\frac{\partial L}{\partial g_k} = 0, \quad (k = 1, 2, \dots, N), \quad (27)$$

we obtain a set of equations

$$C_N \prod_{k=1, k \neq i}^N g_k - 2\lambda \frac{d_i^2}{g_i^3} = 0, \quad (i = 1, 2, \dots, N). \quad (28)$$

Multiplying equation (28) by g_i and summing up the results with respect to i , we obtain

$$NV_e - 2\lambda \sum_{i=1}^N \frac{d_i^2}{g_i^2} = 0. \quad (29)$$

Combining equations (25) and (29), we arrive at

$$\lambda = \frac{N}{2} V_e. \quad (30)$$

Substitution of equation (30) into equation (28) results in

$$\frac{V_e}{g_i} - NV_e \frac{d_i^2}{g_i^3} = 0. \quad (31)$$

Since V_e is nonzero, we get

$$g_i = \sqrt{N} d_i, \quad (i = 1, 2, \dots, N). \quad (32)$$

Thus, once the size of the box equation (21) is known, the semi-axes of the minimum-volume ellipsoid enclosing the box of the experimental data are readily determined by utilizing equation (32). If there are no experimental points at the corner of the box, the size of such an ellipsoid may further be reduced until one of the experimental points reaches the surface of the ellipsoid. The semi-axes of the ellipsoid in this case may be replaced by ηg_k , where the factor η is determined from the condition

$$\eta = \sqrt{\max_r \sum_{k=1}^N \frac{[b_k^{(r)} - b_k^0]^2}{g_k^2}} \leq 1; \quad (r = 1, 2, \dots, M). \quad (33)$$

If there are some experimental points in the corner of the multidimensional box, the factor η equals unity. The ellipsoid (23) can be rewritten in the form

$$\{\mathbf{b} - \mathbf{b}^0\}^T \mathbf{D} \{\mathbf{b} - \mathbf{b}^0\} \leq 1, \quad (34)$$

in which \mathbf{b}^0 is the vector of central points whose components are given by equation (22), and \mathbf{D} is a diagonal matrix

$$\mathbf{D} = \text{diag} \left\{ (\eta g_1)^{-2}, (\eta g_2)^{-2}, \dots, (\eta g_N)^{-2} \right\}. \quad (35)$$

2.3. The Ellipsoid with Minimum Volume

The volume of the ellipsoid now reads

$$V_e = C_N \eta^N \prod_{k=1}^N g_k, \quad (36)$$

which is a function of a set of parameters θ_k ($k = 1, 2, \dots, N - 1$). Therefore, the best ellipsoid among these ellipsoids is the one which contains all given points and possesses the minimum volume, i.e.,

$$V_e = \min_{\theta_1, \theta_2, \dots, \theta_{N-1}} \{V_e(\theta_1, \theta_2, \dots, \theta_{N-1})\}. \quad (37)$$

A possible approach to determine this ellipsoid is to search among all possible cases by increasing θ_k ($k = 1, 2, \dots, N - 1$) from 0 to $\pi/2$ in sufficiently small increments $\Delta\theta_k$, and to compare the volumes of so obtained ellipsoids. Once one finds the ellipsoid with minimum volume in one direction, say θ_k^0 ($k = 1, 2, \dots, N - 1$), the ellipsoid can be transformed back into the original coordinate system by applying the transformation matrix \mathbf{T}_N . Hence, the vector \mathbf{a}^0 of central point and the characteristic matrix \mathbf{G} in equation (1) become

$$\mathbf{a}^0 = \mathbf{T}_N^T \mathbf{b}^0, \quad \mathbf{G} = \mathbf{T}_N^T \mathbf{D} \mathbf{T}_N, \quad (38)$$

where $\mathbf{T}_N = \mathbf{T}_N(\theta_1^0, \theta_2^0, \dots, \theta_{N-1}^0)$ is given by equation (15); vector \mathbf{b}^0 and matrix \mathbf{D} are given by equations (22) and (35), respectively. It can be shown that \mathbf{G} is a symmetric and positive-definite matrix which is nondiagonal in the general case.

3. NUMERICAL EXAMPLES AND INVARIANCE PROPERTY

As an example, a set of uncertain parameters obtained from real tests on shell buckling [14] are chosen. These parameters represent Fourier coefficients of the half-wave cosine and half-wave sine representations, respectively, of the initial imperfections of shells. Chosen four parameters form the four-dimensional space. The values of Fourier coefficients of initial geometric imperfection derived in eight tests are represented by eight points in this space. They are listed in Tables 1 and 3, respectively.

Table 1. The values of uncertain parameters A_k for half-wave cosine representation.

k	1	2	3	4
$A_k^{(1)}$	1.800×10^{-2}	-5.000×10^{-3}	6.700×10^{-2}	7.000×10^{-3}
$A_k^{(2)}$	3.400×10^{-2}	-3.000×10^{-3}	0.653	2.800×10^{-2}
$A_k^{(3)}$	2.300×10^{-2}	-6.000×10^{-3}	8.300×10^{-2}	2.000×10^{-2}
$A_k^{(4)}$	1.100×10^{-2}	2.000×10^{-3}	-2.300×10^{-2}	0.000
$A_k^{(5)}$	2.000×10^{-3}	1.000×10^{-3}	1.600×10^{-2}	0.000
$A_k^{(6)}$	2.000×10^{-3}	0.000	2.400×10^{-2}	0.000
$A_k^{(7)}$	3.000×10^{-3}	0.000	6.600×10^{-2}	1.000×10^{-3}

Table 2. Minimum volume of ellipsoid obtained by different increments, $\Delta\theta$.

Increment $\Delta\theta$	Orientation θ_i			Volume A_e
	θ_1	θ_2	θ_3	
5°	90°	90°	50°	1.7623×10^{-6}
3°	90°	3°	87°	5.6886×10^{-7}
2°	90°	2°	88°	4.4827×10^{-7}
1°	90°	2°	87°	4.2200×10^{-7}

Table 3. The values of uncertain parameters B_k for half-wave sine.

k	1	2	3	4
$B_k^{(1)}$	3.700×10^{-2}	-1.600×10^{-2}	6.600×10^{-2}	9.000×10^{-3}
$B_k^{(2)}$	2.600×10^{-2}	-1.000×10^{-2}	0.611	4.500×10^{-2}
$B_k^{(3)}$	5.600×10^{-2}	-1.000×10^{-2}	7.500×10^{-2}	-6.000×10^{-3}
$B_k^{(4)}$	2.900×10^{-2}	8.000×10^{-3}	-1.900×10^{-2}	1.000×10^{-3}
$B_k^{(5)}$	9.000×10^{-3}	4.000×10^{-3}	6.000×10^{-3}	1.000×10^{-3}
$B_k^{(6)}$	-2.000×10^{-3}	5.000×10^{-3}	2.000×10^{-2}	0.000
$B_k^{(7)}$	3.000×10^{-3}	5.000×10^{-3}	4.900×10^{-2}	8.000×10^{-3}

Table 4. Minimum volume of ellipsoid obtained by different increments of $\Delta\theta$.

Increment $\Delta\theta$	Orientation θ_i			Volume A_e
	θ_1	θ_2	θ_3	
5°	25°	0°	85°	5.2986×10^{-6}
3°	15°	0°	87°	7.2538×10^{-6}
2°	26°	0°	86°	5.0534×10^{-6}
1°	25°	0°	86°	5.0479×10^{-6}

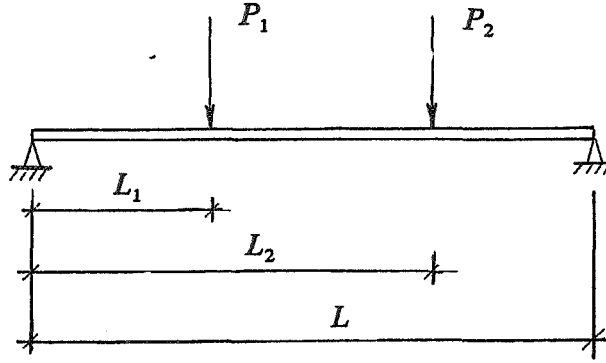


Figure 4. A simply supported beam with concentrated loading.

Tables 2 and 4, respectively, list the minimum volumes and orientations of the ellipsoid obtained by different increments $\Delta\theta$. The size of the increment is reduced so as to achieve the practical numerical convergence. The process of reducing $\Delta\theta$ is completed if the volumes of so constructed ellipsoids change by less than one percent. The minimum volume of an ellipsoid depends on the value of the increment $\Delta\theta$. The axes of the ellipsoid with the minimum volume are usually along the general, nonprincipal directions.

An additional simple example of beam with simply supported ends and under two concentrated loads is shown in Figure 4. We are interested in the invariance property of convex modelling. To this end we assume that two hypothetical independent investigations use two different unit systems, for example, SI system and English system to analyze the same experimental data. The most and least favorable response of a structure based on the convex analysis read [2]

$$\left. \begin{array}{l} R_{\max} \\ R_{\min} \end{array} \right\} = R(\mathbf{a}^0) \pm \sqrt{\mathbf{r}^T \mathbf{G}^{-1} \mathbf{r}}, \quad \mathbf{r}^T = \left[\frac{\partial R(\mathbf{a})}{\partial a_1}, \frac{\partial R(\mathbf{a})}{\partial a_2}, \dots, \frac{\partial R(\mathbf{a})}{\partial a_N} \right]_{\mathbf{a}=\mathbf{a}^0}. \quad (39)$$

The invariance property of the convex model will assure that the responses obtained by two different unit systems are identical. Let us investigate a simple example. The bending moment at the midpoint of the simply supported beam (Figure 4) subjected to two concentrated loads P_1 and P_2 reads

$$M = \frac{1}{2} [P_1 L_1 + P_2 (L - L_2)]. \quad (40)$$

First, we assume that two span lengths $a_1 = L_1$ and $a_2 = L_2$ are uncertain parameters with a limited measurements represented by four points in two-dimensional space as shown in Figures 5 and 6 in different units, and $P_1 = 1 \text{ kN}$ (0.2248 klb_f), $P_2 = 2 \text{ kN}$ (0.4496 klb_f) and $L = 3 \text{ m}$ (9.843 ft). The ellipsoidal convex model and the maximum values of moment at the midpoint of beam are evaluated in two different units as follows: for SI system (m, kN)

$$\begin{aligned} \theta^0 &= 65^\circ, \quad \mathbf{a}^0 = \{1.0721 \text{ m}, 2.0003 \text{ m}\}, \\ \mathbf{G} &= \begin{bmatrix} 37.1723 & 9.4686 \\ 9.4686 & 21.2821 \end{bmatrix}, \end{aligned} \quad (41)$$

and

$$R_{\max} = M_{\max}^{(\text{SI})} = 1.53575 + 0.27217 = 1.80792 \text{ kN} \cdot \text{m}, \quad (42)$$

for English system (ft, klb_f)

$$\begin{aligned} \theta^0 &= 65^\circ, \quad \mathbf{a}^0 = \{3.5176 \text{ ft}, 6.5631 \text{ ft}\}, \\ \mathbf{G} &= \begin{bmatrix} 3.45585 & 0.88065 \\ 0.88065 & 1.97794 \end{bmatrix}, \end{aligned} \quad (43)$$

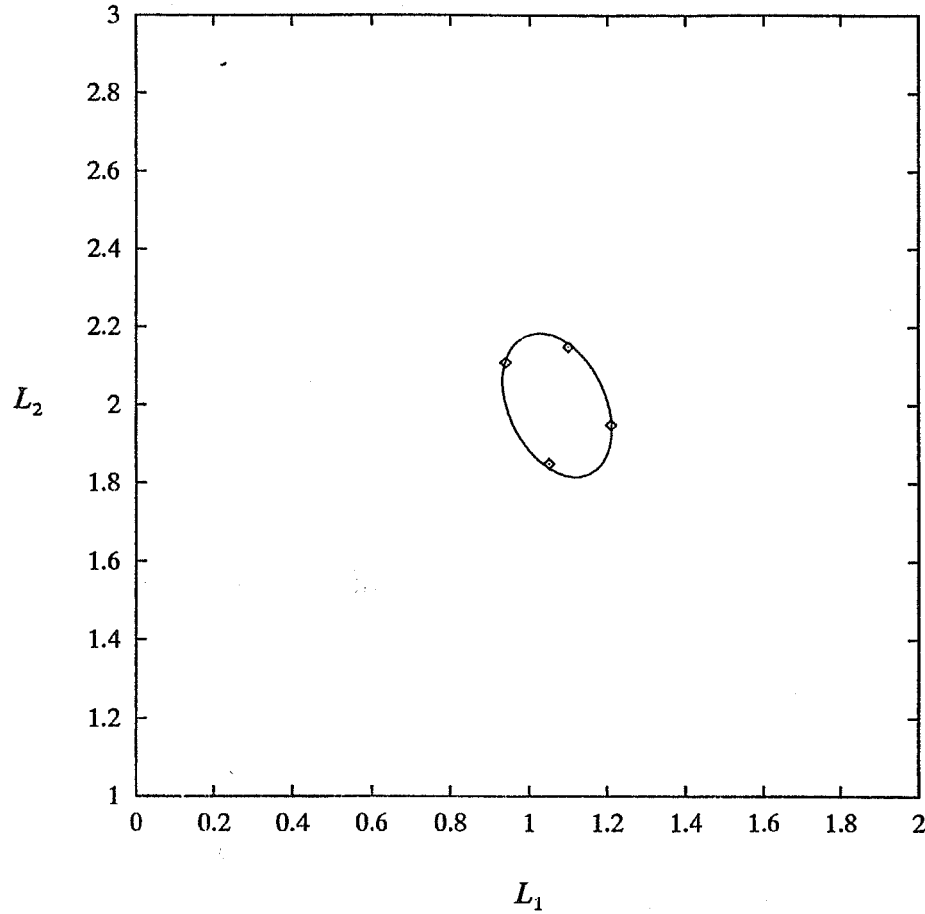


Figure 5. Ellipse of uncertain parameters L_1 and L_2 in SI units (m).

and

$$R_{\max} = M_{\max}^{(\text{EG})} = 1.13272 + 0.20072 = 1.33344 \text{ klb}_f \cdot \text{ft}. \quad (44)$$

Note that the unit factors for force and length λ_P and λ_L are

$$\begin{aligned} \lambda_P &= 1 \text{ kN} = 0.2248 \text{ klb}_f, \\ \lambda_L &= 1 \text{ m} = 3.281 \text{ ft}. \end{aligned} \quad (45)$$

Thus,

$$\lambda_L \lambda_P M_{\max}^{(\text{SI})} = 0.73757 \times 1.80792 = 1.33346 \text{ klb}_f \cdot \text{ft} \equiv M_{\max}^{(\text{EG})}. \quad (46)$$

It is shown that two results are identical, as expected.

Consider now the case that two uncertain parameters have different dimensions. In order to maintain the invariance property of the responses with different units, nondimensional uncertain parameters are suggested to be used in the convex analysis. For example, assume in our previous example that uncertain parameters are $L_1 = a_1 \lambda_L$ and $P_2 = a_2 \lambda_P$, where a_1 and a_2 are nondimensional uncertain parameters. The other, fixed parameters are $L_2 = 2 \lambda_L$, $P_1 = 1 \lambda_P$ and $L = 3 \lambda_L$. Thus, the bending moment at the midpoint of the beam from (40) becomes, in view of equation (40)

$$\begin{aligned} M(a_1, a_2) &= \frac{1}{2} (a_1 + a_2) \lambda_P \lambda_L \equiv m(a_1, a_2) \lambda_P \lambda_L, \\ \mathbf{F}^\top(a_1, a_2) &= \text{grad}^\top \{M(a_1, a_2)\} = \left\{ \frac{1}{2}, \frac{1}{2} \right\} \lambda_P \lambda_L \equiv f^\top(a_1, a_2) \lambda_P \lambda_L, \end{aligned} \quad (47)$$

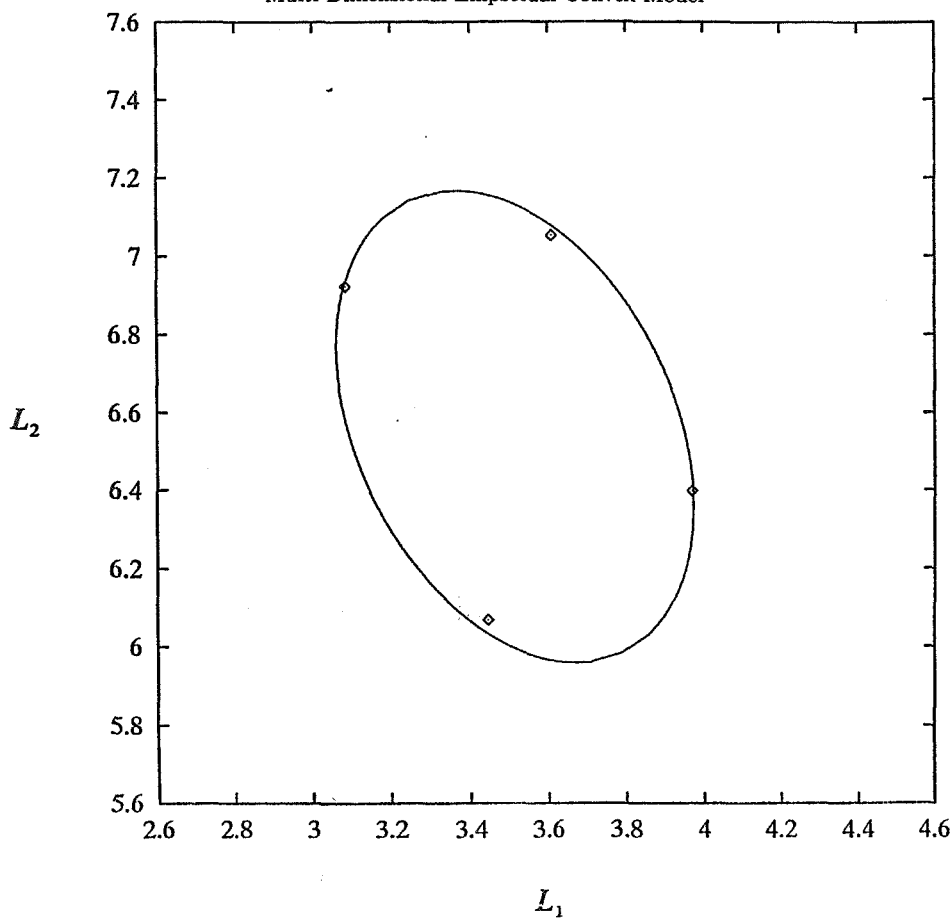


Figure 6. Ellipse of uncertain parameters L_1 and L_2 in customary units (ft).

where $m(a_1, a_2)$ and $f(a_1, a_2)$ have nondimensional values. Since a_1 and a_2 are nondimensional, the \mathbf{a}^0 and \mathbf{G} (or \mathbf{G}^{-1}) obtained by convex analysis in equation (38) are also nondimensional. Hence, the maximum value of the response becomes, in view of equation (39)

$$\begin{aligned} M_{\max} &= M(a_1^0, a_2^0) + \sqrt{\mathbf{F}^T(a_1^0, a_2^0) \mathbf{G}^{-1} \mathbf{F}(a_1^0, a_2^0)} \\ &= \left\{ m(a_1^0, a_2^0) + \sqrt{f^T(a_1^0, a_2^0) \mathbf{G}^{-1} f(a_1^0, a_2^0)} \right\} \lambda_L \lambda_P, \end{aligned} \quad (48)$$

where $\mathbf{a}^0 = \{a_1^0, a_2^0\}$ is the nominal vector or central point of ellipse given by equation (38). As is seen the choice of the units can be arbitrary.

4. CONCLUSION

A general transformation matrix for rotation of N -dimensional coordinate system was constructed by using Gramm-Schmidt orthogonalization procedure. It was shown that the use of this matrix makes it possible to search in all directions to find the N -dimensional ellipsoid with a minimum volume. Several numerical examples have been chosen for illustration. It is shown that the axes of the ellipsoid with the minimum volume have the general orientation in the parameter space. The invariance property of the response of structure with uncertain parameters of different units was investigated. It is shown that, with the nondimensional formulation, the invariance property of the response is retained.

REFERENCES

1. Y. Ben-Haim and I. Elishakoff, *Convex Models of Uncertainty in Applied Mechanics*, Elsevier Science, Amsterdam, (1990).

2. I. Elishakoff and Y. Ben-Haim, Dynamics of a thin cylindrical shell under impact with limited deterministic information on its initial imperfections, *Journal of Structural Safety* **8**, 103–112 (1990).
3. I. Elishakoff and P. Colombi, Combination of probabilistic and convex models of uncertainty when scarce knowledge is present on acoustic excitation parameters, *Computer Methods in Applied Mechanics and Engineering* **104**, 187–209 (1993).
4. I. Elishakoff, G.Q. Cai and J.H. Starnes, Jr., Nonlinear buckling of a column with initial imperfection via stochastic and nonstochastic convex modes, *International Journal of Nonlinear Mechanics* **29**, 71–82 (1994).
5. G. Leitmann, One approach to the control of uncertain systems, *Journal of Dynamic Systems, Measurement and Control* **115**, 362–373 (1993).
6. F.L. Chernousko, *State Estimation for Dynamic Systems*, CRC Press, Boca Raton, (1994).
7. F.C. Schweppe, *Uncertain Dynamics Systems*, Prentice Hall, Englewood Cliffs, (1973).
8. R.F. Drenick, Model-free design of aseismic structures, *Journal of Engineering Mechanics* **96**, 483–493 (1970).
9. M. Shinozuka, Maximum structural response to seismic excitations, *Journal of Engineering Mechanics* **96**, 729–738 (1970).
10. G. Deodatis and M. Shinozuka, Bounds on response variability of stochastic systems, *Journal of Engineering Mechanics* **115**, 2543–2563 (1989).
11. H. Lindberg, Convex models for uncertain imperfection control in multimode dynamic buckling, *Journal of Applied Mechanics* **59**, 937–945 (1992).
12. H.U. Köylüoğlu, A.S. Cakmak and S.R. Nielsen, Applications of interval algebra in mechanics for structural uncertain and pattern loading, In *Proceedings of the Second International Conference on Computational Stochastic Mechanics*, (Edited by S.P. Spanos), pp. 125–133, Athens, 1994.
13. G. Masaglia, Choosing a point from the surface of a sphere, *Ann. Math. Stat.* **43**, 645–646 (1972).
14. J. Arbocz and H. Abramovich, The initial imperfection data bank at the Delft University of Technology, Part I, Report LR-290, (December 1979).



PII: S0960-0779(96)00057-4

Passive Control of Buckling Deformation Via Anderson Localization Phenomenon

I. ELISHAKOFF and Y. W. LI

Department of Mechanical Engineering, Florida Atlantic University, Boca Raton, FL 33431-0991, USA

and

J. H. STARNES JR

NASA Langley Research Center, Hampton, VA 23664-5225, USA

(Accepted 16 May 1996)

Abstract—Buckling problems of two types of multi-span elastic plates with transverse stiffeners are considered using a method based on the finite difference calculus. The discreteness of the stiffeners is accounted for. It is found that the torsional rigidity of the stiffener plays an important role in the buckling mode pattern. When the torsional rigidity is properly adjusted, the stiffener can act as an isolator of deformation for the structure at buckling so that the deflection is only limited to a small area. Copyright © 1997 Elsevier Science Ltd

1. INTRODUCTION

Multi-span plates are used in many engineering applications where different parts of the plate are connected with one another and strengthened by stiffeners and interior supports to cover a large space. When the supports and stiffeners are equi-distantly spaced and all the constituent components look exactly alike so that the structure is periodic, the analytical finite difference calculus [1] is usually an appropriate method to use. However, the use of this method is normally limited to perfectly periodic structures. The finite difference calculus fails if the periodicity is disturbed due to misplacement in the location of the stiffener or support, which may find its way into the structure through the manufacturing process.

In reality, although some periodic structures are designed to be completely identical for every constituent unit, they are seldom perfectly periodic. The deviation from complete periodicity is commonly known as *disorder* or *irregularity*. In this paper, we will address a particular type of disorder, namely, misplacement of stiffener or support.

It has been found that in the presence of small misplacement of stiffeners or interior supports, the buckling mode shapes of certain structures display a localization in the neighborhood where an irregularity occurs. Localization phenomenon was first uncovered by the Nobel laureate P. W. Anderson [2] in physics. Its occurrence in structures has recently attracted much attention. Among others, Pierre and Plaut [3] considered the two-span column case. A more general case, the multi-span column, was recently discussed by Nayfeh and Hawwa [4] through the transfer matrix method and by the present authors [5] using a method based on the finite difference calculus. The deterministic buckling localization in cylindrical shells was investigated by El Naschie [6-12] and Hunt *et al.*

358977
 NIS
 57-39
 408952
 @WAIVED p18

[13–16], whereas probabilistic aspects were studied by Xie [17]. Localization in a beam on elastic support was studied recently by Ariaratnam and Xie in ref. [23]. As for the plate, we used, in our previous study [18], a method based on a direct integration of the general governing differential equation. Such a method is effective, because it can account for the discrete nature of stiffeners so that the localization phenomena of the buckling mode can be discussed. However, a major drawback of the method is the large amount of computational effort involved, especially when the number of spans is large, because each span of the plate is considered separately and a large determinative matrix results.

In this study, we combine the above method with the finite difference calculus to discuss (1) the general N -span plate with transverse stiffeners and interior supports, which is structurally periodic except that one of the spans of the plate contains a disorder; (2) a piecewise periodic multi-span plate whose constituent segments are periodic themselves if the plate is partitioned into several segments. Unlike some other studies [19] which assumed a zero rigidity in torsion for the stiffeners, the contribution from the torsional rigidity is considered in the analysis. The entire treatment is theoretically exact and leads to a relatively simple formulation. It is shown in these two types of multi-span plates that even a single disorder could be responsible for the localized pattern of buckling modes and that the localization phenomenon can also occur in the piecewise periodic structures, though traditionally localization is discussed in the context of non-periodic structures.

This study represents a generalization of two previous investigations: (a) on one hand ref. [18] which dealt with multispan columns; and (b) on the other ref. [21] which was devoted to passive control in columns. This study deals exclusively with elastic plates.

2. PROBLEM FORMULATION

The differential equation of the deflection surface of the plate subjected to a uniform compression P in the x -direction (Fig. 1) is

$$D_c \left(\frac{\partial^4 w}{\partial x^4} + 2 \frac{\partial^4 w}{\partial x^2 \partial y^2} + \frac{\partial^4 w}{\partial y^4} \right) + P \frac{\partial^2 w}{\partial x^2} = 0 \quad (1)$$

where w is the transverse displacement, downward positive; D_c is the flexural rigidity of the plate. For rectangular plates whose boundaries parallel to the x -axis are simply supported, the solution of eqn (1) can be represented in the following form [18]

$$w(x) = W(x) \sin\left(\frac{\pi y}{b}\right), \quad W(x) = A \cos(\beta_1 x) + B \sin(\beta_1 x) + C \cos(\beta_2 x) + D \sin(\beta_2 x) \quad (2)$$

where A , B , C and D are unknown constants, which are to be determined by use of continuity and boundary conditions; and parameters β_1 and β_2 are denoted by

$$\beta_1 = \frac{\pi}{b} \sqrt{\left[\frac{\lambda}{2} - 1 + \sqrt{\left(\frac{\lambda}{2} - 2 \right)} \right]}, \quad \beta_2 = \frac{\pi}{b} \sqrt{\left[\frac{\lambda}{2} - 1 - \sqrt{\left(\frac{\lambda}{2} - 2 \right)} \right]},$$

$$\lambda = \frac{Pb^2}{\pi^2 D_c}, \quad (3)$$

here b stands for the width of the plate.

Catering to a single, arbitrary j th span, the solution can be written as

$$w_j = W_j \sin\left(\frac{\pi y}{b}\right), \quad W_j = A_j \cos(\beta_1 x_j) + B_j \sin(\beta_1 x_j) + C_j \cos(\beta_2 x_j) + D_j \sin(\beta_2 x_j),$$

$$0 \leq x_j \leq a_j, \quad (4)$$

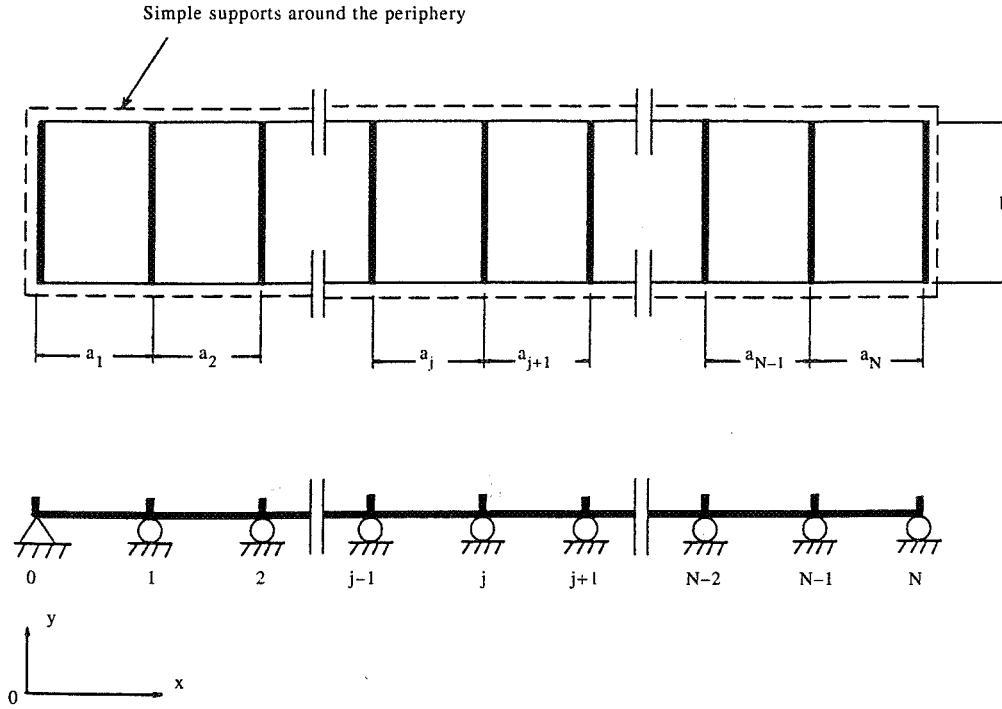


Fig. 1. A multi-span continuous plate reinforced with transverse stiffeners.

where a_j is the length of the j th span and j ranges from one to N for an N -span plate.

Here we consider a simplified case where there is a roller support under each interior stiffener. (The more complicated situation, namely, the plate without the interior support, is addressed in the Appendix.) In reality, we may deviate somehow from this condition. Instead of the presence of the interior supports, a more common occurrence in engineering practice is the use of girders or joists with plate structures, and sometimes the flexure rigidity of these girders can be so large that the deflection of the girders is negligible. If this happens, the deflection along the stiffeners can be regarded as zero.

Using boundary conditions for an arbitrary j th span

$$\begin{aligned}
 (1) \quad & w_j|_{x_j=0} = 0 \\
 (2) \quad & w_j|_{x_j=a_j} = 0 \\
 (3) \quad & \frac{dw_j}{dx_j} \Big|_{x_j=0} = \theta_{j-1}; \quad \theta_{j-1} = \Theta_{j-1} \sin \frac{\pi y}{b} \\
 (4) \quad & \frac{dw_j}{dx_j} \Big|_{x_j=a_j} = \theta_j; \quad \theta_j = \Theta_j \sin \frac{\pi y}{b},
 \end{aligned} \tag{5}$$

coefficients A_j , B_j , C_j and D_j can be determined with the aid of *Mathematica* [20]

$$\begin{aligned}
 A_j &= \frac{1}{S_j} \{ [\beta_2 \sin(\beta_1 a_j) - \beta_1 \sin(\beta_2 a_j)] \Theta_j + [-\beta_2 \cos(\beta_2 a_j) \sin(\beta_1 a_j) \\
 &\quad + \beta_1 \cos(\beta_1 a_j) \sin(\beta_2 a_j)] \Theta_{j-1} \} \\
 B_j &= \frac{1}{S_j} \{ \beta_2 [-\cos(\beta_1 a_j) + \cos(\beta_2 a_j)] \Theta_j + [\beta_2 \cos(\beta_1 a_j) \cos(\beta_2 a_j) - \beta_2 \\
 &\quad + \beta_1 \sin(\beta_1 a_j) \sin(\beta_2 a_j)] \Theta_{j-1} \}
 \end{aligned}$$

$$C_j = \frac{1}{S_j} \{ [-\beta_2 \sin(\beta_1 a_j) + \beta_1 \sin(\beta_2 a_j)] \Theta_j + [\beta_2 \cos(\beta_2 a_j) \sin(\beta_1 a_j) - \beta_1 \cos(\beta_1 a_j) \sin(\beta_2 a_j)] \Theta_{j-1} \} \quad (6)$$

$$D_j = \frac{1}{S_j} \{ \beta_1 [\cos(\beta_1 a_j) - \cos(\beta_2 a_j)] \Theta_j + [-\beta_1 + \beta_1 \cos(\beta_1 a_j) \cos(\beta_2 a_j) + \beta_2 \sin(\beta_1 a_j) \sin(\beta_2 a_j)] \Theta_{j-1} \}$$

$$S_j = 2\beta_1 \beta_2 [-1 + \cos(\beta_1 a_j) \cos(\beta_2 a_j)] + (\beta_1^2 + \beta_2^2) \sin(\beta_1 a_j) \sin(\beta_2 a_j).$$

The expression for the bending moment is

$$M_x = -D_c \left(\frac{\partial^2 w_j}{\partial x_j^2} + \nu \frac{\partial^2 w_j}{\partial y^2} \right). \quad (7)$$

Using eqn (4), a moment-slope relationship can be established as follows

$$M_{j-1}^R = M_x|_{x_j=0} = m_{j-1}^R \sin \frac{\pi y}{b}; \quad m_{j-1}^R = \frac{D_c}{a_j} [c_1 \Theta_{j-1} + c_2 \Theta_j] \quad (8)$$

$$M_j^L = M_x|_{x_j=a_j} = m_j^L \sin \frac{\pi y}{b}; \quad m_j^L = \frac{D_c}{a_j} [c_1 \Theta_j + c_2 \Theta_{j-1}],$$

where M_{j-1}^R , M_j^L are the bending moments at the two supports of the span, respectively. The superscript 'R' ('L') indicates that span of the plate is to the right (left) of the support in question (Fig. 2). The coefficients c_1 and c_2 are defined as

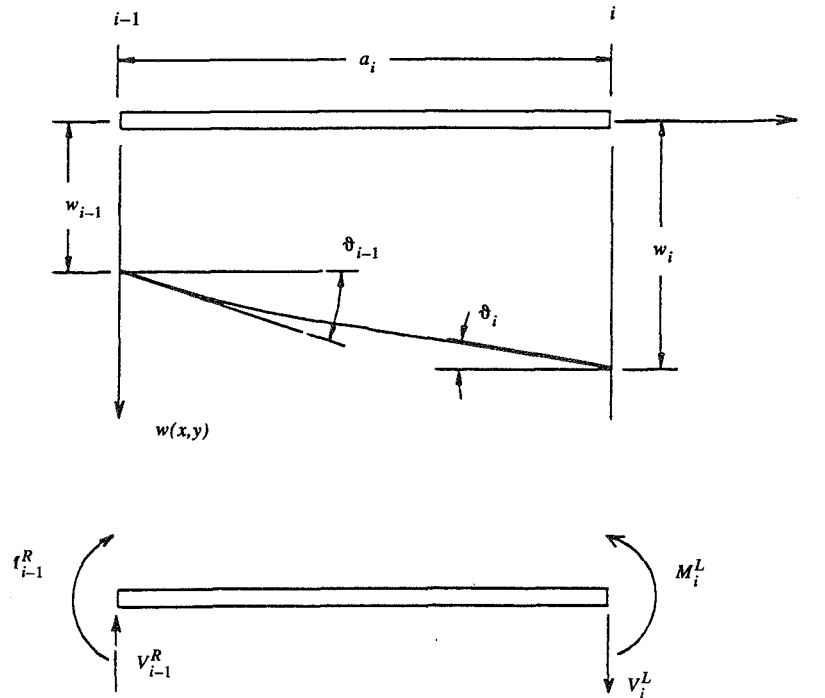


Fig. 2. Notations and positive directions.

$$c_1 = \frac{a_j}{S_j}(\beta_1^2 - \beta_2^2)[- \beta_2 \cos(\beta_2 a_j) \sin(\beta_1 a_j) + \beta_1 \cos(\beta_1 a_j) \sin(\beta_2 a_j)] \quad (9)$$

$$c_2 = \frac{a_j}{S_j}(\beta_1^2 - \beta_2^2)[\beta_2 \sin(\beta_1 a_j) - \beta_1 \sin(\beta_2 a_j)].$$

If a number of spans of the plate have the common length $a_j = a$ and are made of the same material, then the finite difference calculus may be applied in the discussion of that part of the plate. Equilibrium at a typical support, r , reads

$$M_r^R - M_r^L = GJ \frac{\partial^2 \theta_r}{\partial y^2}, \quad (10)$$

where GJ is the torsional rigidity of the transverse stiffener. Substituting eqn (8) into the above, we have

$$(2c_1 + k)\Theta_r + c_2(\Theta_{r+1} + \Theta_{r-1}) = 0, \quad (11)$$

where $k = \pi^{(2)} a GJ / b^2 D_c$.

Introducing the shifting operator \mathbf{E} which is defined as $\mathbf{E}\theta_i = \theta_{i+1}$, eqn (11) can be rewritten as

$$[c_2(\mathbf{E} + \mathbf{E}^{-1}) + (2c_1 + k)]\Theta_r = 0. \quad (12)$$

Equation (12) is a second-order finite difference equation, whose solution is obtained by letting

$$\Theta_r = e^{\phi r}. \quad (13)$$

Substitution into eqn (12) results in

$$\cosh(\phi) = -\frac{2c_1 + k}{2c_2}. \quad (14)$$

Three different cases may arise and deserve separate considerations:

Case 1 $-(2c_1 + k)/2c_2 \geq 1$

The solution of eqn (14) has the following form

$$\phi_{1,2} = \pm \alpha; \quad \alpha = \cosh^{-1} \left[-\frac{2c_1 + k}{2c_2} \right]. \quad (15)$$

The attendant solution for Θ_i reads

$$\Theta_i = A e^{\alpha i} + B e^{-\alpha i}, \quad (16)$$

where A and B are arbitrary constants.

Case 2 $-(2c_1 + k)/2c_2 \leq -1$

The solution to eqn (14) takes the form

$$\phi_{1,2} = \pm(\alpha + j\pi); \quad \alpha = \cosh^{-1} \left[\frac{2c_1 + k}{2c_2} \right], \quad j = \sqrt{-1} \quad (17)$$

and the solution for Θ_i is

$$\Theta_i = [A \cosh(\alpha i) + B \sinh(\alpha i)] \cos(\pi i). \quad (18)$$

Case 3 $-1 \leq -(2c_1 + k)/2c_2 \leq 1$

The solution to eqn (14) now becomes

$$\phi_{1,2} = \pm \alpha; \quad \alpha = \cos^{-1} \left[-\frac{2c_1 + k}{2c_2} \right] \quad (19)$$

and, for Θ_i , we obtain

$$\Theta_i = A \cos(\alpha i) + B \sin(\alpha i). \quad (20)$$

Introducing the following notations

$$\begin{aligned} f_1(\alpha, r) &= e^{\alpha r}, & f_2(\alpha, r) &= \cosh(\alpha r) \cos(\pi r), & f_3(\alpha, r) &= \cos(\alpha r) \\ g_1(\alpha, r) &= e^{-\alpha r}, & g_2(\alpha, r) &= \sinh(\alpha r) \cos(\pi r), & g_3(\alpha, r) &= \sin(\alpha r) \end{aligned} \quad (21)$$

the three cases have a unified expression

$$\Theta_{r,i} = A_1 f_i(\alpha, r) + B_1 g_i(\alpha, r), \quad i = 1, 2, 3, \quad (22)$$

where $\Theta_{r,i}$ corresponds to the three different cases when the subscript i varies from 1 to 3.

We will consider two different kinds of continuous plates. The first kind of multi-span plate is structurally periodic except for a single disordered span that contains an imperfection. The second kind is a two-piecewise-periodic plate, which means that its first q th spans and the rest of the $N-q$ spans are periodic *per se* but they do not have the same periodicity.

Suppose that we have an N -span plate (Fig. 3), which is periodic except that its $(q+1)$ th span contains a span length imperfection which makes that span slightly longer or shorter than the other spans of the structure, i.e.

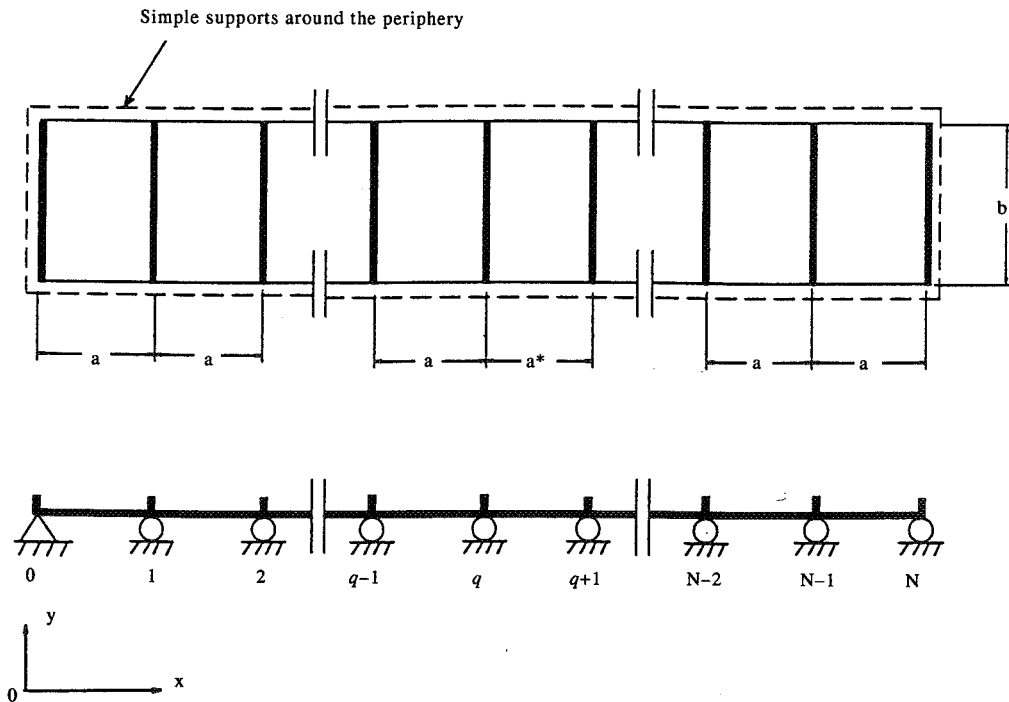


Fig. 3. An N -span continuous plate with a single disorder in the $(q+1)$ th span.

$$a_i = a \quad \text{for} \quad i = 1, \dots, q, \quad q + 2, \dots, N; \quad a_{q+1} = a^* \quad (a \neq a^*). \quad (23)$$

For a particular case $a^* = a$, we recover the original, perfectly periodic structure.

To facilitate the solution of the problem, we can treat the entire continuous plate as being composed of three segments. The first q -span periodic plate constitutes segment I, the $(q + 1)$ th span, namely, the disordered span, constitutes segment II and the last $(N - q - 1)$ spans of periodic plate represent segment III. Assume first that both segments I and III themselves contain a large number of spans. For segments I and III, the finite difference calculus is applicable due to their structural periodicity. As to the disordered span, segment II, a separate consideration should be made. By following this procedure, we construct a solution composed of three parts with each part corresponding to a specific segment of the plate. Continuity conditions between those different segments are utilized in combination with boundary conditions at the ends of the plate to establish an eigenvalue problem.

For the first q spans of periodic plate, we perform the finite difference calculus analysis

$$\theta_r = \theta_r^I = \Theta_r^I \sin \frac{\pi y}{b}; \quad (r = 0, 1, \dots, q), \quad (24)$$

where the superscript denotes the sequence number of the segment in question; Θ_r^I takes on one of the three forms represented by eqns (16), (18) and (20), depending on the physical and geometrical conditions of the segment.

For the disordered span, recalling eqn (8), we have

$$\begin{aligned} M_q^R &= \frac{D_c}{a^*} [\bar{c}_1 \theta_0^{\text{II}} + \bar{c}_2 \theta_1^{\text{II}}] \\ M_{q+1}^L &= -\frac{D_c}{a^*} [\bar{c}_1 \theta_1^{\text{II}} + \bar{c}_2 \theta_0^{\text{II}}]. \end{aligned} \quad (25)$$

Or, in another form,

$$\begin{aligned} \theta_0^{\text{II}} &= \frac{a^*}{D_c} \frac{\bar{c}_1 M_q^R + \bar{c}_2 M_{q+1}^L}{\bar{c}_1^2 - \bar{c}_2^2} \\ \theta_1^{\text{II}} &= -\frac{a^*}{D_c} \frac{\bar{c}_1 M_{q+1}^L + \bar{c}_2 M_q^R}{\bar{c}_1^2 - \bar{c}_2^2}, \end{aligned} \quad (26)$$

where \bar{c}_1 and \bar{c}_2 are obtained from the expressions for c_1 and c_2 by formally replacing a_i in eqn (9) with a^* . The treatment of the last $N - q - 1$ spans of periodic beam is similar to that of segment I,

$$\theta_s = \theta_{s-q-1}^{\text{III}}; \quad (s = q + 1, q + 2, \dots, N). \quad (27)$$

Consider now a plate simply supported at its two ends (other boundary conditions can be treated in a similar manner). Then the boundary condition at the left end of the plate can be represented as

$$M_0^R = GJ_1 \frac{\partial^2 \theta_0^I}{\partial y^2} \quad \text{or} \quad (c_1 + k_1) \Theta_0^I + c_2 \Theta_1^I = 0, \quad (28)$$

while the boundary condition at the right end of the plate reads

$$-M_N^L = GJ_1 \frac{\partial^2 \theta_{N-q-1}^{\text{III}}}{\partial y^2} \quad \text{or} \quad (c_1 + k_1) \Theta_{N-q-1}^{\text{III}} + c_2 \Theta_{N-q-2}^{\text{III}} = 0, \quad (29)$$

where GJ_1 is the torsional rigidity of the transverse stiffeners at the two boundaries. In order to have a purely periodic structure, the stiffeners at the boundaries should have half the stiffness of those interior stiffeners, i.e. $GJ_1 = GJ/2$ or $k_1 = k/2$. This 'half-stiffener' concept has been used widely in ref. [1].

Conditions of continuity between the periodic spans and the disordered span of the beam, namely, between segment I and segment II, are

$$\begin{aligned} -M_q^L + M_q^R &= GJ \frac{\partial^2 \theta_q}{\partial y^2} \quad \text{or} \quad (c_1 + k)\Theta_q^I + c_2\Theta_{q-1}^I + \frac{a}{D_c} m_q^R = 0 \\ \theta_q^I &= \theta_0^{\text{II}} \quad \text{or} \quad \Theta_q^I - \frac{a^*}{a(\bar{c}_1^2 - \bar{c}_2^2)} \left(\bar{c}_1 \frac{a}{D_c} m_q^R + \bar{c}_2 \frac{a}{D_c} m_{q+1}^L \right) = 0. \end{aligned} \quad (30)$$

Analogously, the continuity conditions between the second and the third segments are

$$\begin{aligned} -M_{q+1}^L + M_{q+1}^R &= GJ \frac{\partial^2 \theta_0^{\text{III}}}{\partial y^2} \quad \text{or} \quad (c_1 + k)\Theta_0^{\text{III}} + c_2\Theta_1^{\text{III}} - \frac{a}{D} m_{q+1}^L = 0 \\ \theta_1^{\text{II}} &= \theta_0^{\text{III}} \quad \text{or} \quad \Theta_0^{\text{III}} + \frac{a^*}{a(\bar{c}_1^2 - \bar{c}_2^2)} \left(\bar{c}_2 \frac{a}{D_c} m_q^R + \bar{c}_1 \frac{a}{D} m_{q+1}^L \right) = 0. \end{aligned} \quad (31)$$

Using the unified expression, equation (22), the rotation angles in the first and third segments can be expressed as

$$\begin{aligned} \Theta_r^I &= A_1 f_i(\alpha, r) + B_1 g_i(\alpha, r) \quad (r = 0, 1, \dots, q) \\ \Theta_{s-q-1}^{\text{III}} &= A_2 f_i(\alpha, s - q - 1) + B_2 g_i(\alpha, s - q - 1) \quad (s = q + 1, \dots, N). \end{aligned} \quad (32)$$

Substituting the above expressions in the boundary conditions (28) and (29) and the continuity conditions (30) and (31), we obtain six homogeneous algebraic equations,

$$[(c_1 + k_1)f_i(\alpha, 0) + c_2 f_i(\alpha, 1)]A_1 + [(c_1 + k_1)g_i(\alpha, 0) + c_2 g_i(\alpha, 1)]B_1 = 0 \quad (33)$$

$$[(c_1 + k)f_i(\alpha, q) + c_2 f_i(\alpha, q - 1)]A_1 + [(c_1 + k)g_i(\alpha, q) + c_2 g_i(\alpha, q - 1)]B_1 + \bar{m}_q^R = 0 \quad (34)$$

$$f_i(\alpha, q)A_1 + g_i(\alpha, q)B_1 - \frac{\bar{c}_1}{\bar{c}_1^2 - \bar{c}_2^2} \left(\frac{a^*}{a} \right) \bar{m}_q^R - \frac{\bar{c}_2}{c_1^2 - \bar{c}_2^2} \left(\frac{a^*}{a} \right) \bar{m}_{q+1}^L = 0 \quad (35)$$

$$[(c_1 + k)f_i(\alpha, 0) + c_2 f_i(\alpha, 1)]A_2 + [(c_1 + k)g_i(\alpha, 0) + c_2 g_i(\alpha, 1)]B_2 - \bar{m}_{q+1}^L = 0 \quad (36)$$

$$A_2 + B_2 + \frac{\bar{c}_2}{\bar{c}_1^2 + \bar{c}_2^2} \left(\frac{a^*}{a} \right) \bar{m}_q^R + \frac{\bar{c}_1}{c_1^2 - \bar{c}_2^2} \left(\frac{a^*}{a} \right) \bar{m}_{q+1}^L = 0 \quad (37)$$

$$\begin{aligned} [(c_1 + k_1)f_i(\alpha, N - q - 1) + c_2 f_i(\alpha, N - q - 2)]A_2 + [(c_1 + k_1)g_i(\alpha, N - q - 1) \\ + c_2 g_i(\alpha, N - q - 2)]B_2 = 0, \end{aligned} \quad (38)$$

where

$$\bar{m}_q^R = \frac{m_q^R a}{D_c}; \quad \bar{m}_{q+1}^L = \frac{m_{q+1}^L a}{D_c}. \quad (39)$$

Thus, we have six homogeneous algebraic equations, which can be expressed in a matrix form as follows

$$[F(\lambda)]_{6 \times 6} \{\delta\}_{6 \times 1} = 0 \quad (40)$$

where $[F(\lambda)]$ is the coefficient matrix, and $\{\delta\}^T = \{A_1, B_1, \bar{m}_q^R, \bar{m}_{q+1}^L, A_2, B_2\}$.

Another kind of continuous plate is characterized by

$$a_i = \begin{cases} a & \text{for } i = 1, \dots, q \\ a^* & \text{for } i = q + 1, \dots, N \end{cases} \quad (a \neq a^*). \quad (41)$$

The schematic representation of such a structure is displayed in Fig. 4. For this problem, the first periodic segment which consists of the first q spans of the plate may fall into one of the three different cases, whereas the second periodic segment which is comprised of the remaining $N-q$ spans may present itself in another three different cases. Therefore, there might be nine separate cases altogether, which makes the search for a solution rather complicated.

Recalling eqn (21), a unified solution for this piecewise periodic plate can be written as

$$\Theta_r = \begin{cases} A_1 f_i(\alpha_1, r) + B_1 g_i(\alpha_1, r), & i = 1, 2, 3; \quad r = 0, \dots, q \\ A_2 f_j(\alpha_2, r) + B_2 g_j(\alpha_2, r), & j = 1, 2, 3; \quad r = q + 1, \dots, N \end{cases} \quad (42)$$

Using the boundary conditions (simple supports at two ends)

$$(1) (M_0^R)^I = GJ_1 \frac{\partial^2 \theta_0^I}{\partial y^2}; \quad (2) -(M_N^L)^{II} = GJ_1 \frac{\partial^2 \theta_{N-q}^{II}}{\partial y^2} \quad (43)$$

and the conditions of continuity

$$(1) \theta_q^I = \theta_0^{II}; \quad (2) (M_q^L)^I = (M_0^R)^{II}, \quad (44)$$

the following homogeneous equations are established

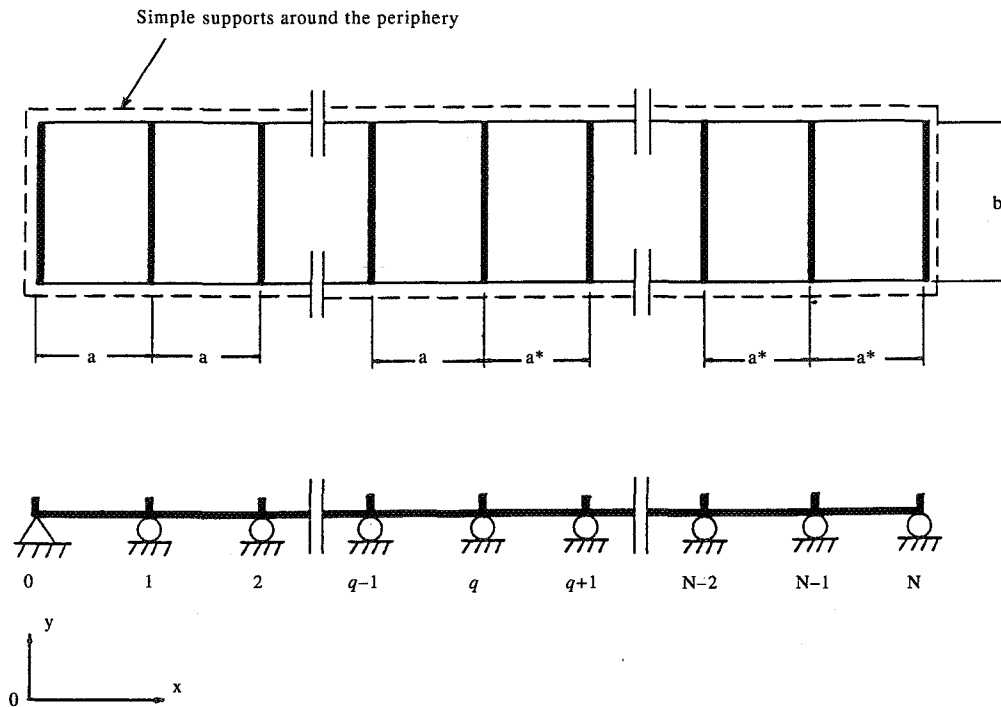


Fig. 4. A piecewise periodic continuous plate.

$$[(k_1 + c_1)f_i(\alpha_1, 0) + c_2f_i(\alpha_1, 1)]A_1 + [(k_1 + c_1)g_i(\alpha_1, 0) + c_2g_i(\alpha_1, 1)]B_1 = 0 \quad (45)$$

$$[(k + \bar{c}_1)f_j(\alpha_2, N - q) + \bar{c}_2f_j(\alpha_2, N - q - 1)]A_2 + [(k + \bar{c}_1)g_j(\alpha_2, N - q) + c_2g_j(\alpha_2, N - q - 1)]B_2 = 0 \quad (46)$$

$$f_i(\alpha_1, q)A_1 + g_i(\alpha_1, q - 1)B_1 - f_j(\alpha_2, 0)A_2 - g_j(\alpha_2, 0)B_2 = 0 \quad (47)$$

$$[c_1f_i(\alpha_1, q) + c_2f_i(\alpha_1, q - 1)]A_1 + [c_1g_i(\alpha_1, q - 1) + c_2g_i(\alpha_1, q - 1)]B_1 - \left(\frac{a}{a^*}\right)[\bar{c}_1f_j(\alpha_2, 0) + \bar{c}_2f_j(\alpha_2, 1)]A_2 + \left(\frac{a}{a^*}\right)[\bar{c}_1g_j(\alpha_2, 0) + c_2g_j(\alpha_2, 1)]B_2 = 0, \quad (48)$$

where the sub-indices i and j take on the value of 1, 2 or 3, depending upon which particular case the segments fall into. Again, the above four equations can be written in matrix form

$$[F(\lambda)]_{4 \times 4} \{\delta\}_{4 \times 1} = 0, \quad (49)$$

where $[F(\lambda)]$ is the coefficient matrix, and $\{\delta\}^T = \{A_1, B_1, A_2, B_2\}$.

Both eqns (40) and (49) are homogeneous algebraic equations. Non-triviality of $\{\delta\}$ requires that the determinant of the coefficient matrix vanish

$$\text{Det}[F(\lambda)] = 0 \quad (50)$$

which constitutes a transcendental equation from which the non-dimensional buckling load parameter λ can be solved in terms of other geometric and material properties of the structure in question. Once the buckling load parameter λ is determined, we can use eqn (4) to calculate, span by span, the buckling mode shape for the entire structure, after the type of case has been ascertained.

3. NUMERICAL EXAMPLES AND DISCUSSION

In this section, we discuss the buckling load and mode shapes of the two different types of multi-span plates described in the last section. As the first example, consider the following case:

$$\frac{a}{b} = 1, \quad \frac{a^*}{a} = 1.1, \quad N = 11, \quad q = 5.$$

As is shown in the above data, the plate consists of eleven spans, of which the sixth span contains a length imperfection which makes that span a bit longer than the other spans. Numerical results show that such an imperfection has a slight degrading effect on the buckling load. For instance, when k , the parameter characterizing the torsional rigidity of the stiffener, equals five the buckling load parameter λ is 5.06. Compared with its counterpart of the periodic plate, which is $\lambda = 5.26$, the reduction rate is only 4%. The buckling load reduction remains almost unchanged with the torsional rigidity of the stiffeners. Even when the torsional rigidity doubles, the reduction rate only amounts to 5%. So, the buckling load decrease induced by the presence of the imperfection is not significant. However, the buckling modes are appreciably different for the plates with and without the imperfection (Figs 5–7). Moreover, as k increases, the buckling mode of the disordered plate becomes increasingly localized (Figs 6 and 7). The overall behavior of such plates is very similar to that of the continuous beams with torsional springs discussed in our previous paper [5], despite the difference of structural dimensionality between beams and plates.

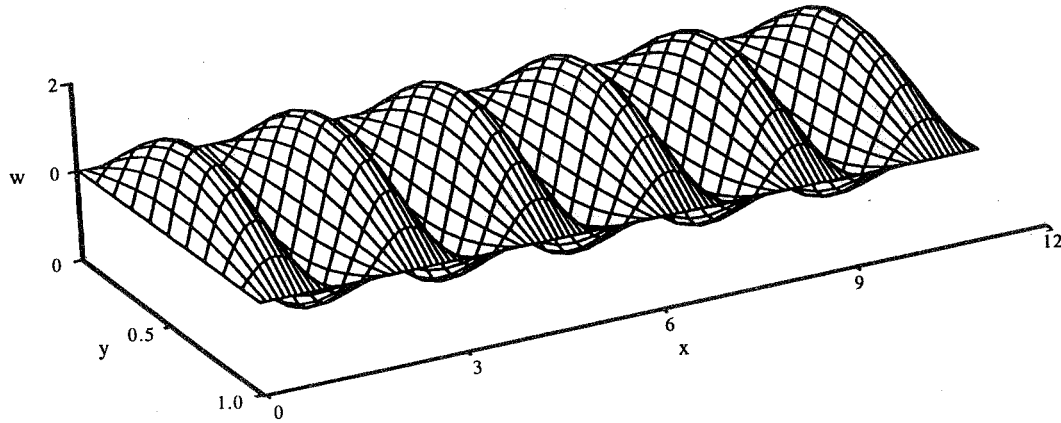
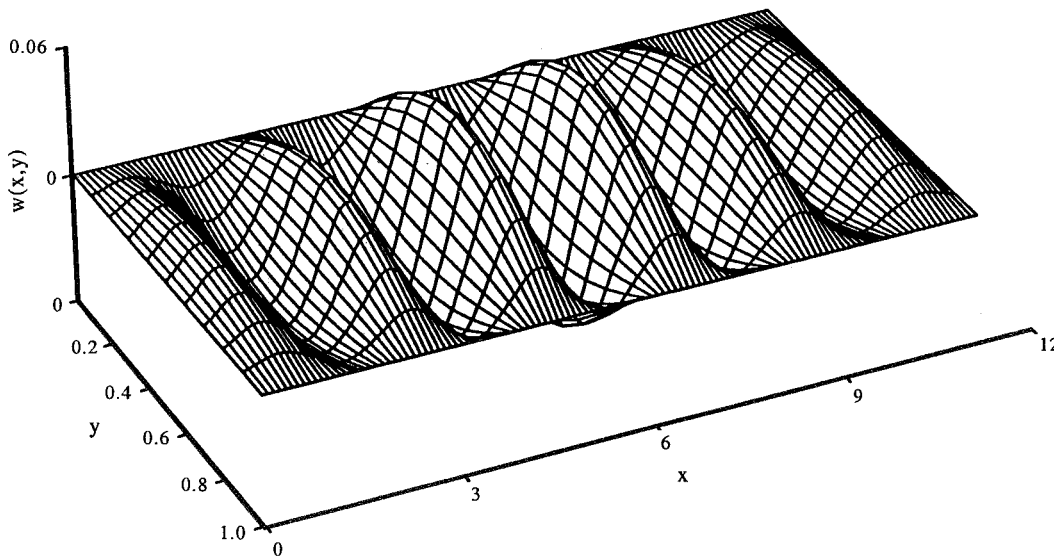


Fig. 5. Buckling mode for an 11-span periodic plate.

Fig. 6. Buckling mode for a disordered 11-span plate ($k = 5$).

The second example is a 10-span, piecewise periodic plate whose first five spans have the length of a and the other five spans have the length of a^* (assuming $a^* > a$), and the plate is reinforced by transverse stiffeners with torsional rigidity of $k = 10$. When the ratio of a^* to a equals unity, the plate reduces to a purely periodic plate. Here we discuss the case where the ratio is different from unity, say, $a^*/a = 1.1$. As far as the buckling load is concerned, the difference between such a structure and the purely periodic plate is relatively minor. For the above structure, the buckling load parameter λ equals 5.35, while, for the corresponding, exactly periodic plate, λ is 5.77. So, the difference in the buckling load between the two is only 7%. More significant, however, is the difference in the buckling mode. For instance, when $a^*/a = 1.1$ and $k = 10$, the deflection of the structure at buckling is largely confined to the left end, while those spans of the plate near the other end hardly experience any deformation (Fig. 8). Figure 9 shows the buckling mode of the same type of structure but with weaker stiffeners ($k = 5$). It is observed from this figure

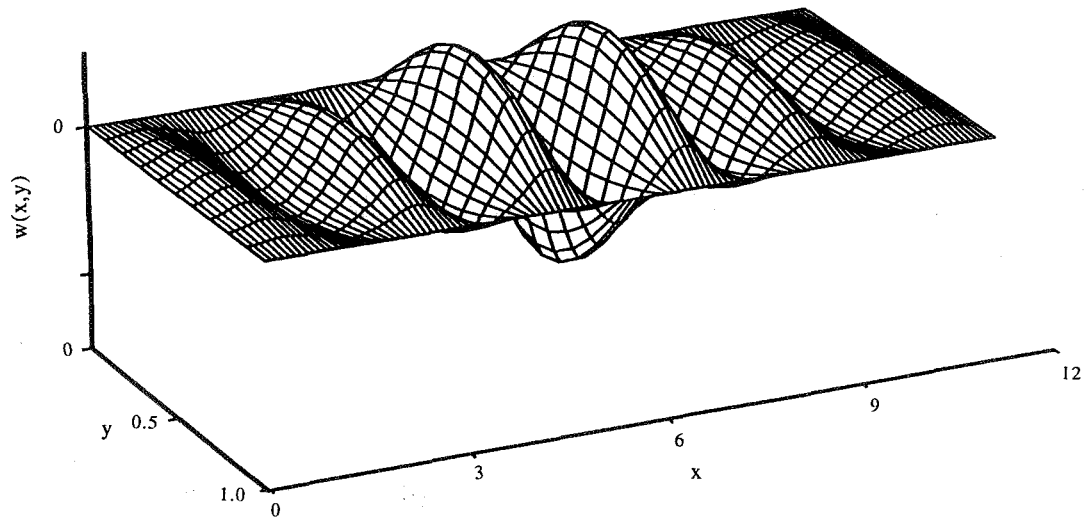


Fig. 7. Buckling mode for a disordered 11-span plate ($k = 10$).

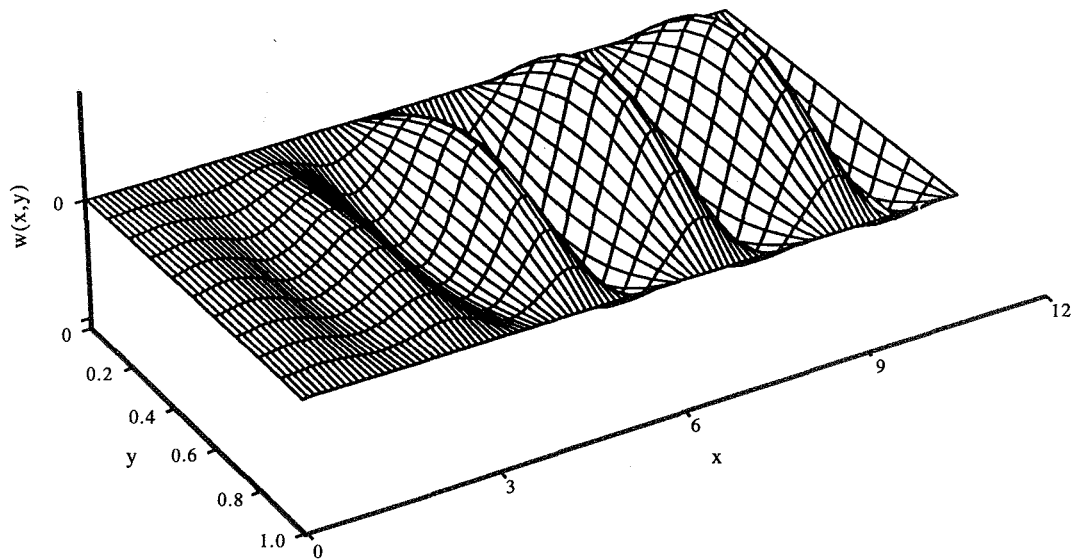


Fig. 8. Buckling mode for a piecewise periodic plate ($k = 5$).

that with a decreased torsional rigidity, the localization of buckling mode becomes less severe, and that deflection spreads from the right end to the left in a gradually attenuating fashion.

From the examples shown above, it is well demonstrated that the torsional stiffness of the stiffeners should not be ignored in the investigation, just for the sake of simplification in analysis. As it turns out, the torsional stiffness plays quite an important role. It not only boosts the strength of the structure, but also localizes the loss of geometric rigidity of the structure at buckling to a small area so that any damage, should it occur, is kept to a minimum.

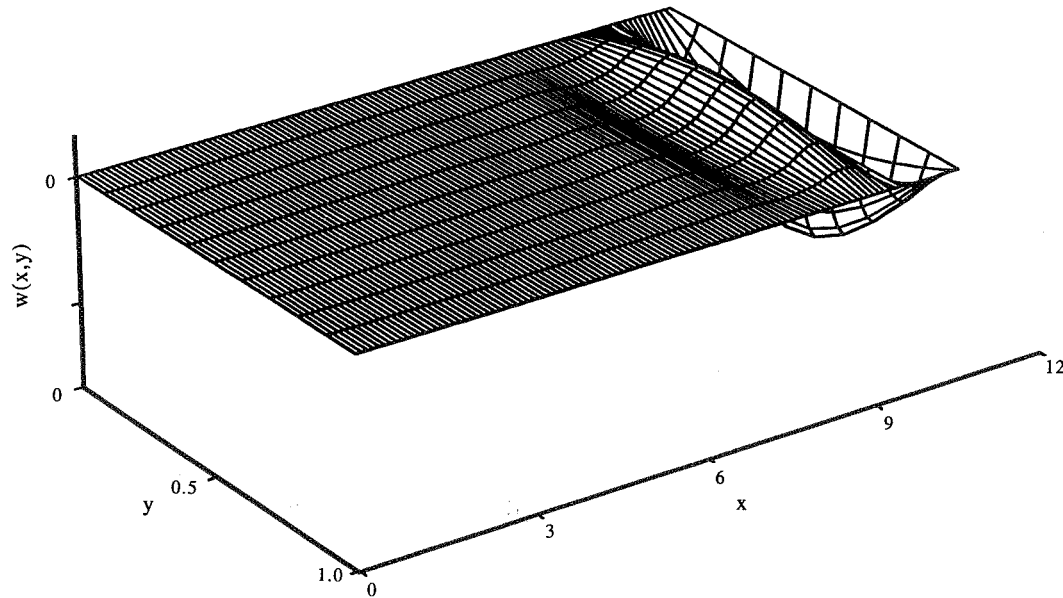


Fig. 9. Buckling mode for a piecewise periodic plate ($k = 10$).

For the plates contemplated here, small structural irregularities do not significantly alter the load-carrying capacity. However, the presence of such irregularities confines the buckling pattern associated with large deflection to a limited fraction of the structure. In this regard, the effect of such irregularities on the buckling loads can be considered favorable. As Nayfeh *et al.* [21] pointed out, by means of inducing 'deliberately' some irregularities in the system, one may confine the structural buckling to a limited part of the system only, which can be regarded as a passive control of the buckling process.

The method used here seems to have a wide application, especially in continuous plates with a large number of spans. In fact, the larger the number of spans, the more advantageous the present method is over the other traditional methods such as the one based on the integration of the governing differential equation [18, 19], since it leads to a determinative matrix that can be orders of magnitude smaller than those necessary in other methods. Besides, the solutions generated by the present method are analytic and exact, and thus can be used as benchmarks for other numerical methods.

4. CONCLUSION

The method of investigation presented here can be applied to discuss essentially periodic structures where irregularities only occur in some local areas. It takes into consideration the discreteness of the stiffeners and, in particular, their torsional rigidity. As it turns out, the torsional rigidity of the stiffeners is important and should not be ignored in the discussion of the buckling mode shape. Adjusting the torsional rigidity of the stiffeners, one can achieve the goal of localizing the deflection of the structure at buckling to a small area.

Acknowledgement—This study was supported by the grant NAG-1-1310 from the NASA Langley Research Center. This support is gratefully appreciated.

REFERENCES

1. T. Wah and L. R. Calcote, *Structural Analysis By Finite Difference Calculus*. Van Nostrand-Reinhold, New York (1970).
2. P. W. Anderson, Absence of diffusion in certain random lattices. *Phys. Rev.* **109**, 1492–1505 (1958).
3. C. Pierre and R. H. Plaut, Curve veering and mode localization in a buckling problem. *J. Appl. Math. Phys. (ZAMP)* **40**, 758–761 (1989).
4. A. H. Nayfeh and M. A. Hawwa, Buckling mode localization in multi-span columns. *Proceedings of the Thirty-Fifth AIAA/ASME/ASCE/AHS/ASC Structures, Structural Dynamics, and Materials Conference*, pp. 2117–2123, Hilton Head, SC (1994).
5. Y. W. Li, I. Elishakoff and J. H. Starnes, Buckling mode localization in a multi-span periodic structure with a disorder in a single span. *Chaos, Solitons & Fractals* **5**, 955–969 (1995).
6. M. S. El Naschie, Localized diamond shaped buckling patterns of axially compressed cylindrical shells. *A.I.A.A. J.* **13**, 837–838 (1975).
7. M. S. El Naschie, Local postbuckling of compressed cylindrical shells. *Proceedings of the Institution of Civil Engineers*, P2, Vol. 59, pp. 523–525 (1975).
8. M. S. El Naschie, Nonlinear isometric bifurcation and shell buckling, *ZAMM* **57**, 293–296 (1977).
9. M. S. El Naschie, *Stability and Chaos in Structural Engineering: An Energy Approach*. McGraw-Hill, London (1990).
10. M. S. El Naschie, Generalized bifurcation and shell buckling as special statical chaos. *ZAMM* **69**, T376–T377 (1989).
11. M. S. El Naschie, Complexity and spacial manifestation of temporal chaos, *Directions in Chaos, Vol. 3: Experimental Study and Characterization of Chaos*, edited by Hao Bai-Lin, pp. 111–131. World Scientific, Singapore (1990).
12. M. S. El Naschie, On certain homoclinic soliton in elastic stability. *J. Phys. Soc. Jap.* **58**, 4310–4321 (1989).
13. A. Champneys and J. Toland, Bifurcation of a plethora of multi-model homoclinic orbits for autonomous Hamiltonian systems. *Nonlinearity*, 665–721 (1993).
14. G. W. Hunt and E. Lucena Neto, Maxwell critical loads for axially-loaded cylindrical shells. *J. Appl. Mech.* **60**, 702–706 (1993).
15. G. W. Hunt and M. K. Wadde, Comparative Lagrangian formulation for localized buckling. *Proc. R. Soc. Lond. Vol. A* **434**, 485–502 (1991).
16. G. W. Hunt, H. M. Bolt and J. M. T. Thompson, Structural localization phenomena and the dynamical phase-space analogy. *Proc. R. Soc. Lond. Vol. A* 245–267 (1989).
17. W.-C. Xie, Buckling mode localization in randomly disordered multispan continuous beams. *AIAA J.* **33**, 1142–1149 (1995).
18. I. Elishakoff, Y. W. Li and J. H. Starnes, Jr, Buckling mode localization in elastic plates due to misplacement in the stiffener location. *Recent Advances in Solids and Structures*, edited by H. H. Chung and Y. W. Kwon, PVP-VI. 321 pp. 153–164. ASME Press, New York (1995).
19. R. Brabré, Stabilität gleichmässig gedrückter Rechteckplatten mit Längs-oder Quersteifen, *Ing. Archiv.* **8**, 117–150 (1937).
20. S. Wolfram, *Mathematica*. Addison-Wesley, Redwood City, CA (1991).
21. A. H. Nayfeh and M. A. Hawwa, The use of mode localization in the passive control of structural buckling. *AIAA J.* **32**, 2131–2133 (1994).
22. *Handbook of Structural Stability*, edited by Column Research Committee of Japan. Corona, Tokyo (1971).
23. S. T. Ariaratnam and W.-C. Xie, Buckling mode localisation in randomly disordered continuous beams using a simplified model. *Chaos, Solitons & Fractals* **7**, 1127–1144 (1996).

APPENDIX

This appendix describes how to analyze the buckling of periodically stiffened plate without the interior supports which were used in the main body of this paper. For such a plate, the deflection of the plate at various stations has to be accounted for. Accordingly, the coefficients A_j , B_j , C_j and D_j in eqn (4) are now expressed, again using *Mathematica* [21], in terms of not only the rotation angles, but also the deflection

$$\begin{aligned}
 A_j = \frac{1}{S_j} \{ & [-\beta_1\beta_2 \cos(\beta_1 a_j) \cos(\beta_2 a_j) + \beta_1\beta_2 \cos^2(\beta_2 a_j) - \beta_2^2 \sin(\beta_1 a_j) \sin(\beta_2 a_j) \\
 & + \beta_1\beta_2 \sin^2(\beta_2 a_j)] W_{j-1} + [\beta_1\beta_2 \cos(\beta_1 a_j) - \beta_1\beta_2 \cos(\beta_2 a_j)] W_j \\
 & + [\beta_2 \cos(\beta_2 a_j) \sin(\beta_1 a_j) - \beta_1 \cos(\beta_1 a_j) \sin(\beta_2 a_j)] \Theta_{j-1} \\
 & + [-\beta_2 \sin(\beta_1 a_j) + \beta_1 \sin(\beta_2 a_j)] \Theta_j \}
 \end{aligned} \tag{A1}$$

$$\begin{aligned}
 B_j = \frac{1}{S_j} \{ & [-\beta_1\beta_2 \cos(\beta_2 a_j) \sin(\beta_1 a_j) + \beta_2^2 \cos(\beta_1 a_j) \sin(\beta_2 a_j)] W_{j-1} \\
 & + [\beta_1\beta_2 \sin(\beta_1 a_j) - \beta_2^2 \sin(\beta_2 a_j)] W_j + [\beta_2 \cos(\beta_1 a_j) - \beta_2 \cos(\beta_2 a_j)] \Theta_j \\
 & + [-\beta_2 \cos(\beta_1 a_j) \cos(\beta_2 a_j) + \beta_2 \cos^2(\beta_2 a_j) - \beta_1 \sin(\beta_1 a_j) \sin(\beta_2 a_j) + \beta_2 \sin^2(\beta_2 a_j)] \Theta_{j-1} \}
 \end{aligned} \tag{A2}$$

$$\begin{aligned}
C_j = & \frac{1}{S_j} \{ [\beta_1 \beta_2 \cos^2(\beta_1 a_j) - \beta_1 \beta_2 \cos(\beta_1 a_j) \cos(\beta_2 a_j) + \beta_1 \beta_2 \sin^2(\beta_1 a_j) - \beta_1^2 \sin(\beta_1 a_j) \sin(\beta_2 a_j)] W_{j-1} \\
& + [-\beta_1 \beta_2 \cos(\beta_1 a_j) + \beta_1 \beta_2 \cos(\beta_2 a_j)] W_j \\
& + [-\beta_2 \cos(\beta_2 a_j) \sin(\beta_1 a_j) + \beta_1 \cos(\beta_1 a_j) \sin(\beta_2 a_j)] \Theta_{j-1} \\
& + [\beta_2 \sin(\beta_1 a_j) - \beta_1 \sin(\beta_2 a_j)] \Theta_j \},
\end{aligned} \tag{A3}$$

where

$$\begin{aligned}
D_j = & \frac{1}{S_j} \{ [\beta_1^2 \cos(\beta_2 a_j) \sin(\beta_1 a_j) - \beta_1 \beta_2 \cos(\beta_1 a_j) \sin(\beta_2 a_j)] W_{j-1} + [-\beta_1^2 \sin(\beta_1 a_j) + \beta_1 \beta_2 \sin(\beta_2 a_j)] W_j \\
& + [\beta_1 \cos^2(\beta_1 a_j) - \beta_1 \cos(\beta_1 a_j) \cos(\beta_2 a_j) + \beta_1 \sin^2(\beta_1 a_j) - \beta_2 \sin(\beta_1 a_j) \sin(\beta_2 a_j)] \Theta_{j-1} \\
& + [-\beta_1 \cos(\beta_1 a_j) + \beta_1 \cos(\beta_2 a_j)] \Theta_j \}
\end{aligned} \tag{A4}$$

$$S_j = 2\beta_1 \beta_2 - (\beta_1^2 + \beta_2^2) \sin(\beta_1 a_j) \sin(\beta_2 a_j) - 2\beta_1 \beta_2 \cos(\beta_1 a) \cos(\beta_2 a). \tag{A5}$$

The moments and shear forces are related to displacement and rotation angles as follows

$$\begin{aligned}
M_{j-1}^R &= m_{j-1}^R \sin \frac{\pi y}{b}; & m_{j-1}^R &= \frac{D_c}{a_j} \left[d_1 \Theta_{j-1} + d_2 \Theta_j + \frac{1}{a_j} (d_3 W_{j-1} + d_4 W_j) \right] \\
M_j^L &= m_j^L \sin \frac{\pi y}{b}; & m_j^L &= -\frac{D_c}{a_j} \left[d_1 \Theta_j + d_2 \Theta_{j-1} - \frac{1}{a_j} (d_3 W_j - d_4 W_{j-1}) \right] \\
V_{j-1}^R &= v_{j-1}^R \sin \frac{\pi y}{b}; & v_{j-1}^R &= \frac{D_c}{a_j^2} \left[-d_7 \Theta_j + d_4 \Theta_{j+1} - \frac{1}{a_j} (d_5 W_{j-1} - d_6 W_j) \right] \\
V_j^L &= v_j^L \sin \frac{\pi y}{b}; & v_j^L &= -\frac{D_c}{a_j^2} \left[d_7 \Theta_j - d_4 \Theta_{j-1} - \frac{1}{a_j} (d_5 W_j - d_6 W_{j-1}) \right],
\end{aligned} \tag{A6}$$

where

$$\begin{aligned}
d_1 &= \frac{a_j}{2S} (\beta_1^2 - \beta_2^2) \{ \beta_1 \sin[(\beta_1 - \beta_2)a_j] + \beta_2 \sin[(\beta_1 - \beta_2)a_j] - \beta_1 \sin[(\beta_1 + \beta_2)a_j] + \beta_2 \sin[(\beta_1 + \beta_2)a_j] \} \\
d_2 &= \frac{a_j}{S} (-\beta_1^2 + \beta_2^2) [\beta_2 \sin(\beta_1 a_j) - \beta_1 \sin(\beta_2 a_j)] \\
d_3 &= \frac{a_j^2}{S} \{ \beta_1^2 [\beta_1 \beta_2 - \beta_1 \beta_2 \cos(\beta_1 a_j) \cos(\beta_2 a) - \beta_1^2 \sin(\beta_1 a_j) \sin(\beta_2 a_j)] \\
& + \beta_1^2 [\beta_1 \beta_2 - \beta_1 \beta_2 \cos(\beta_1 a_j) \cos(\beta_2 a_j) - \beta_1^2 \sin(\beta_1 a_j) \sin(\beta_2 a_j)] \\
& + \frac{\pi^2}{b^2} \{ 2\beta_1 \beta_2 - 2\beta_1 \beta_2 \cos(\beta_1 a_j) \cos(\beta_2 a_j) - (\beta_1^2 + \beta_2^2) \sin(\beta_1 a_j) \sin(\beta_2 a_j) \} \} \\
d_4 &= \frac{a_j^2}{S} \beta_1 \beta_2 (\beta_1^2 - \beta_2^2) [\cos(\beta_1 a_j) - \cos(\beta_2 a_j)] \\
d_5 &= \frac{a_j^2}{2S} \beta_1 \beta_2 (\beta_1^2 - \beta_2^2) \{ \beta_1 \sin[(\beta_1 - \beta_2)a_j] + \beta_2 \sin[(\beta_1 - \beta_2)a_j] + \beta_1 \sin[(\beta_1 + \beta_2)a_j] - \beta_2 \sin[(\beta_1 + \beta_2)a_j] \} \\
d_6 &= \frac{a_j}{S} \beta_1 \beta_2 (\beta_1^2 - \beta_2^2) [\beta_1 \sin(\beta_1 a_j) - \beta_2 \sin(\beta_2 a_j)] \\
d_7 &= -\frac{a_j}{S} \left\{ 2\beta_1^3 \beta_2 + 2\beta_1 \beta_2^3 + \beta_1 \beta_2 \frac{\pi^2}{b^2} (8 - 4\nu) - \left(\beta_1^4 + \beta_1^3 \beta_2 + \beta_1 \beta_2^3 + \beta_2^4 + 2\beta_1^2 \frac{\pi^2}{b^2} + 4\beta_1 \beta_2 \frac{\pi^2}{b^2} \right. \right. \\
& + 2\beta_2^2 \frac{\pi^2}{b^2} - \beta_1^2 \frac{\pi^2}{b^2} \nu - 2\beta_1 \beta_2 \frac{\pi^2}{b^2} \nu - \beta_2^2 \frac{\pi^2}{b^2} \nu \left. \right) \cos[(\beta_1 - \beta_2)a_j] + \left(\beta_1^4 - \beta_1^3 \beta_2 - \beta_1 \beta_2^3 + \beta_2^4 \right. \\
& \left. + 2\beta_1^2 \frac{\pi^2}{b^2} - 4\beta_1 \beta_2 \frac{\pi^2}{b^2} + 2\beta_2^2 \frac{\pi^2}{b^2} - \beta_1^2 \frac{\pi^2}{b^2} \nu + 2\beta_1 \beta_2 \frac{\pi^2}{b^2} \nu - \beta_2^2 \frac{\pi^2}{b^2} \nu \right) \cos[(\beta_1 + \beta_2)a_j] \left. \right\}.
\end{aligned} \tag{A7}$$

Equations of equilibrium now become

$$\begin{aligned}
M_r^R - M_r^L &= GJ \frac{\partial^2 \theta_r}{\partial y^2} \\
V_r^R - V_r^L &= EI \frac{\partial^4 w_r}{\partial y^4}.
\end{aligned} \tag{A8}$$

If the segment of the plate in consideration is periodic, then we have $a_j = a$. On substituting the relations defined by eqn (A6), the equations of equilibrium have the form

$$\begin{aligned} \frac{d_4}{a}(W_{r-1} - W_{r+1}) - 2d_1\Theta_r - d_2(\Theta_{r-1} + \Theta_{r+1}) &= \frac{GJ\pi^2 a}{b^2 D_c}\Theta_r, \\ d_4(\Theta_{r+1} - \Theta_{r-1}) - \frac{1}{a}[2d_5W_r - d_6(W_{r+1} + W_{r-1})] &= \frac{EI\pi^4 a^2}{b^4 D_c}W_r. \end{aligned} \quad (\text{A9})$$

Using the shifting operator \mathbf{E} , the above equations can be rewritten as

$$\begin{aligned} \frac{d_4}{a}(\mathbf{E} - \mathbf{E}^{-1})W_r + [2d_1 + k + d_2(\mathbf{E}^{-1} + \mathbf{E})]\Theta_r &= 0 \\ ad_4(\mathbf{E} - \mathbf{E}^{-1})\Theta_r - [2d_5 + h - d_6(\mathbf{E}^{-1} + \mathbf{E})]W_r &= 0, \end{aligned} \quad (\text{A10})$$

where

$$k = \frac{GJ\pi^2 a}{b^2 D_c}, \quad h = \frac{EI\pi^4 a^2}{b^4 D_c}. \quad (\text{A11})$$

Here EI is the bending stiffness of the plate.

Canceling Θ_r from eqn (A10) leads to

$$\left[\frac{d_4(\mathbf{E} - \mathbf{E}^{-1})}{2d_1 + k + d_2(\mathbf{E}^{-1} + \mathbf{E})} + \frac{2d_5 + h - d_6(\mathbf{E}^{-1} + \mathbf{E})}{d_4(\mathbf{E} - \mathbf{E}^{-1})} \right] W_r = 0. \quad (\text{A12})$$

This is a fourth order difference equation. Assuming the solution is of the form $W_r = e^{\phi r}$, we have the following governing equation

$$\left[\frac{d_4 \sinh(\phi)}{2(2d_1 + k) + d_2 \cosh(\phi)} + \frac{4d_5 + 2h - d_6 \cosh(\phi)}{d_4 \sinh(\phi)} \right] e^{\phi r} = 0 \quad (\text{A13})$$

or

$$A \cosh^2(\phi) + B \cosh(\phi) + C = 0, \quad (\text{A14})$$

where A , B , and C are coefficients defined as

$$A = d_4^2 - d_6 d_2, \quad B = d_2(4d_5 + 2h) - d_6(4d_1 + 2k), \quad C = (4d_5 + 2h)(4d_1 + 2k) - d_4^2. \quad (\text{A15})$$

Solving eqn (A14), we have

$$\cosh(\phi) = \begin{cases} \alpha_1 \\ \alpha_2 \end{cases}; \quad \alpha_{1,2} = \frac{-B \pm \sqrt{(B^2 - 4BC)}}{2A}. \quad (\text{A16})$$

The solution for w_i takes different forms for the different situations:

If $B^2 - 4AC \geq 0$

$$\begin{aligned} W_i &= W_i^{(1)} + W_i^{(2)} \\ W_i^{(1)} &= \begin{cases} A_1 e^{\gamma_1 i} + A_2 e^{-\gamma_1 i}, & \gamma_1 = \cosh^{-1}(\alpha), \quad \text{if } \alpha_1 \geq 1; \\ [A_1 \cosh(\gamma_1 i) + A_2 \sinh(\gamma_1 i)] \cos(\pi i), & \gamma_1 = \cosh^{-1}(\alpha_1), \quad \text{if } \alpha_1 \leq -1; \\ A_1 \cos(\gamma_1 i) + A_2 \sin(\gamma_1 i), & \gamma_1 = \cos^{-1}(\alpha_1), \quad \text{if } -1 \leq \alpha_1 \leq 1; \end{cases} \\ W_i^{(2)} &= \begin{cases} A_3 e^{\gamma_2 i} + A_4 e^{-\gamma_2 i}, & \gamma_2 = \cosh^{-1}(\alpha_2), \quad \text{if } \alpha_2 \geq 1; \\ [A_3 \cosh(\gamma_2 i) + A_4 \sinh(\gamma_2 i)] \cos(\pi i), & \gamma_2 = \cosh^{-1}(\alpha_2), \quad \text{if } \alpha_2 \leq -1; \\ A_3 \cos(\gamma_2 i) + A_4 \sin(\gamma_2 i), & \gamma_2 = \cos^{-1}(\alpha_2), \quad \text{if } -1 \leq \alpha_2 \leq 1. \end{cases} \end{aligned} \quad (\text{A17})$$

If $B^2 - 4AC < 0$

$$W_i = A_1 \cosh(\rho_1 i) \cos(\rho_2 i) + A_2 \cosh(\rho_1 i) \sin(\rho_2 i) + A_3 \sinh(\rho_1 i) \cos(\rho_2 i) + A_4 \sinh(\rho_1 i) \sin(\rho_2 i), \quad (\text{A18})$$

where

$$\begin{aligned} \rho_1 &= \sinh^{-1} \left[\frac{z_1^2 + z_2^2 - 1 + \sqrt{((z_1^2 + z_2^2 - 1)^2 + 4z_2^2)}}{2} \right]^{1/2} \\ \rho_2 &= \cos^{-1} \left[\frac{z_1^2 + z_2^2 + 1 - \sqrt{((z_1^2 + z_2^2 - 1)^2 + 4z_2^2)}}{2} \right]^{1/2}. \end{aligned} \quad (\text{A19})$$

Since the difference equation (eqn (A9)) is of fourth order, it is necessary to have four boundary conditions, i.e. two at each end, fully to specify the problem. If the plate is simply supported at both ends, then the boundary conditions are:

$$\text{At the left end } (i = 0): \quad (1) w_0 = 0; \quad (2) M_0^R = GJ \frac{\partial^2 \theta_0}{\partial y^2} \quad (\text{A20})$$

$$\text{At the right end } (i = N): \quad (3) w_N = 0; \quad (4) M_N^L = -GJ \frac{\partial^2 \theta_N}{\partial y^2}. \quad (\text{A21})$$

Substituting the appropriate form of the solution w_i into the four boundary conditions, we establish a set of four homogenous algebraic equations in terms of four unknowns A_1 , A_2 , A_3 and A_4 :

$$[f(\lambda)]_{4 \times 4} \begin{Bmatrix} A_1 \\ A_2 \\ A_3 \\ A_4 \end{Bmatrix} = 0. \quad (\text{A22})$$

The non-triviality condition dictates that the determinant of the coefficient matrix $[f(\lambda)]$ should vanish

$$\det [f(\lambda)] = 0 \quad (\text{A23})$$

from which the buckling load parameter λ can be evaluated as the lowest positive root of the above transcendental equation. The elements of the determinant are evaluated by using symbolic algebra [20]. Limiting cases of buckling are compared with the comprehensive monograph of ref. [22]. Once the buckling load is known, the buckling mode can be readily calculated following the procedure described in Section 2. In the case that the stiffeners are not uniformly distributed over the plate, partition of the structure may be carried out in order to take advantage of the finite difference calculus, which requires the use of continuity conditions between different segments.



58-39
 408 965
 QWAIVED
 358978
 P14

EFFECT OF THE THICKNESS VARIATION AND
 INITIAL IMPERFECTION ON BUCKLING OF
 COMPOSITE CYLINDRICAL SHELLS: ASYMPTOTIC
 ANALYSIS AND NUMERICAL RESULTS BY
 BOSOR4 AND PANDA2

YI-WEI LI, ISAAC ELISHAKOFF

Department of Mechanical Engineering, Florida Atlantic University, Boca Raton,
 FL 33431-0991, U.S.A.

JAMES H. STARNES, JR

NASA Langley Research Center, Hampton, VA 23664-5225, U.S.A.

and

DAVID BUSHNELL

Lockheed Missiles and Space Company, Inc., Palo Alto, CA 94304, U.S.A.

(Received 18 April 1994; in revised form 1 March 1996)

Abstract—This study is an extension of a previous investigation of the combined effect of axisymmetric thickness variation and axisymmetric initial geometric imperfection on buckling of isotropic shells under uniform axial compression. Here the anisotropic cylindrical shells are investigated by means of Koiter's energy criterion. An asymptotic formula is derived which can be used to determine the critical buckling load for composite shells with combined initial geometric imperfection and thickness variation. Results are compared with those obtained by the software packages BOSOR4 and PANDA2. © 1997 Elsevier Science Ltd.

1. INTRODUCTION

Due to various factors in the manufacturing process, thin cylindrical shells may exhibit variations in wall thickness. In spite of the fact that buckling of uniformly compressed cylindrical shells has been studied intensively for the past several decades, the influence of thickness variation on the buckling load has seldom been studied. In the previous research, we have investigated the effect of thickness variation on the axial buckling of otherwise perfect isotropic shells (Koiter *et al.*, 1994a) and imperfect isotropic shells (Koiter *et al.*, 1994b). These studies resulted in a conclusion that, although the thickness variation pattern in the form of the classical axisymmetric buckling mode may have some deleterious effect on the load-bearing capacity, the most detrimental effect of thickness variation occurs when the wave number of the axisymmetric thickness variation pattern is *twice* that of the classical buckling mode. Asymptotic relationships between the buckling load reduction rate and the thickness variation parameter were established for isotropic shells of non-uniform thickness (Koiter *et al.*, 1994a, 1994b).

The present study aims at the *combined* effect of axisymmetric thickness variation and axisymmetric initial imperfection on the buckling behavior of *composite* shells. We approach this problem by using Koiter's energy criterion of elastic stability (Koiter, 1945, 1966, 1980). Here, we consider the small axisymmetric thickness variation, and as a first approximation, only terms up to the first order of thickness variation parameter are retained. The final product of this discussion is again an asymptotic formula which relates the thickness variation parameter and initial imperfection amplitude to the buckling load of the structure. Therefore, this study is a direct generalization and extension of our former investigation (Koiter *et al.*, 1994a, 1994b) to the anisotropic case. The asymptotic formula obtained herein encompasses the isotropic shell. Comparisons with results obtained by the computer codes BOSOR4 and PANDA2 are provided.

2. FORMULATION BY THE ENERGY CRITERION

The nonlinear strain-displacement relations for cylindrical shells are

$$\begin{aligned}\varepsilon_x &= \frac{\partial u}{\partial x} + \frac{1}{2} \left(\frac{\partial w}{\partial x} \right)^2, & \kappa_x &= -\frac{\partial^2 w}{\partial x^2} \\ \varepsilon_y &= \frac{\partial v}{\partial y} + \frac{w}{R} + \frac{1}{2} \left(\frac{\partial w}{\partial y} \right)^2, & \kappa_y &= -\frac{\partial^2 w}{\partial y^2} \\ \gamma_{xy} &= \frac{\partial v}{\partial x} + \frac{\partial u}{\partial y} + \frac{\partial w}{\partial x} \frac{\partial w}{\partial y}, & \kappa_{xy} &= -2 \frac{\partial^2 w}{\partial x \partial y}\end{aligned}\quad (1)$$

where x and y are the axial and circumferential coordinates in the shell middle surface; u and v are the shell displacements along axial and circumferential directions, and w is the radial displacement, positive outward; ε_x , ε_y and γ_{xy} are strain components; κ_x , κ_y and κ_{xy} are middle surface curvatures of the shell; R is the radius of the cylinder.

Thickness variation of the laminated shell invariably exists due to imprecision involved in the fabrication process. Here we discuss the case that the thickness variation is axis-symmetric and of uniform configurational nature: each lamina has the same variational pattern:

$$h_k(x) = h_{0,k} \left(1 - \varepsilon \cos \frac{2p_1 x}{R} \right) = h_{0,k} H(x) \quad (k = 1 \sim K) \quad (2)$$

where h_k and $h_{0,k}$ are the thickness and the nominal thickness for the k -th layer, respectively; ε and p_1 are the non-dimensional parameters indicating the magnitude and wave number of the thickness variation, assumed to be the same for all the constituent layers; K represents the total number of layers in the laminate. At first sight, the perfect homology of the thickness variation may appear as a restrictive assumption. If the constituent layers are produced by the same manufacturing process according to the same specification, one can not rule out the existence of similar deviations from uniform thickness. Such an assumption may shed some light to the question of thickness variation and lead to a tractable analysis. However, most shells are manufactured by being wound on a mandrel. The inner wall of the shell would probably be flat and the outer wall would have all the thickness variation. In future, some numerical results will be reported for a variable thickness case where the inner surface is at a constant radius and all the thickness variation occurs on the outer surface. Here we assume that the middle surface of the shell with thickness variation only (no geometric imperfection) forms a perfect cylinder.

With the model presented in eqn (2), elements of the stiffness matrices $[A]$, $[B]$ and $[D]$ for the laminated shell with variable thickness become

$$\begin{aligned}A_{ij} &= \sum_{k=1}^K (\bar{Q}_{ij})_k (h_k - h_{k-1}) = H(x) \sum_{k=1}^K (\bar{Q}_{ij})_k (h_{0,k} - h_{0,k-1}) = H(x) a_{ij} \\ B_{ij} &= \frac{1}{2} \sum_{k=1}^K (\bar{Q}_{ij})_k (h_k^2 - h_{k-1}^2) = \frac{1}{2} [H(x)]^2 \sum_{k=1}^K (\bar{Q}_{ij})_k (h_{0,k}^2 - h_{0,k-1}^2) = [H(x)]^2 b_{ij} \\ D_{ij} &= \frac{1}{3} \sum_{k=1}^K (\bar{Q}_{ij})_k (h_k^3 - h_{k-1}^3) = \frac{1}{3} [H(x)]^3 \sum_{k=1}^K (\bar{Q}_{ij})_k (h_{0,k}^3 - h_{0,k-1}^3) = [H(x)]^3 d_{ij}\end{aligned}\quad (i, j = 1, 2, 6) \quad (3)$$

where a_{ij} , b_{ij} and d_{ij} are elements of stiffness matrices for the corresponding uniform laminate with thickness h_0 ; \bar{Q}_{ij} 's are the transformed reduced stiffnesses of the individual lamina and

$$\Pi = U_m + U_b + \Omega \quad (13)$$

or, with use of the constitutive relations (8) and (9):

$$\begin{aligned} \Pi = \frac{1}{2} \int_0^{2\pi R} \int_0^L & \left[A_{11} \varepsilon_x^2 + 2A_{12} \varepsilon_x \varepsilon_y + 2A_{16} \varepsilon_x \gamma_{xy} + 2A_{26} \varepsilon_y \gamma_{xy} + A_{22} \varepsilon_y^2 + A_{66} \gamma_{xy}^2 + D_{11} \kappa_x^2 \right. \\ & \left. + 2D_{12} \kappa_x \kappa_y + 2D_{16} \kappa_x \kappa_{xy} + 2D_{26} \kappa_y \kappa_{xy} + D_{22} \kappa_y^2 + D_{66} \kappa_{xy}^2 - N_0 \left(\frac{\partial w}{\partial x} + \frac{\partial w_0}{\partial x} \right)^2 \right] dx dy. \quad (14) \end{aligned}$$

Substitution of eqn (1) into the above formula leads to the energy expression in terms of displacements u, v, w :

$$\begin{aligned} \Pi = \frac{1}{2} \int_0^{2\pi R} \int_0^L & \left[A_{11} \left[\frac{\partial u}{\partial x} + \frac{1}{2} \left(\frac{\partial w}{\partial x} \right)^2 \right]^2 + 2A_{12} \left[\frac{\partial u}{\partial x} + \frac{1}{2} \left(\frac{\partial w}{\partial x} \right)^2 \right] \left[\frac{\partial v}{\partial y} + \frac{w}{R} + \frac{1}{2} \left(\frac{\partial w}{\partial y} \right)^2 \right] \right. \\ & + 2A_{16} \left[\frac{\partial u}{\partial x} + \frac{1}{2} \left(\frac{\partial w}{\partial x} \right)^2 \right] \left[\frac{\partial u}{\partial y} + \frac{\partial v}{\partial x} + \frac{\partial w}{\partial x} \frac{\partial w}{\partial y} \right] \\ & + 2A_{26} \left[\frac{\partial v}{\partial y} + \frac{w}{R} + \frac{1}{2} \left(\frac{\partial w}{\partial y} \right)^2 \right] \left[\frac{\partial u}{\partial y} + \frac{\partial v}{\partial x} + \frac{\partial w}{\partial x} \frac{\partial w}{\partial y} \right] + A_{22} \left[\frac{\partial v}{\partial y} + \frac{w}{R} + \frac{1}{2} \left(\frac{\partial w}{\partial y} \right)^2 \right]^2 \\ & + A_{66} \left[\frac{\partial u}{\partial y} + \frac{\partial v}{\partial x} + \frac{\partial w}{\partial x} \frac{\partial w}{\partial y} \right]^2 + D_{11} \left(\frac{\partial^2 w}{\partial x^2} \right)^2 + 2D_{12} \frac{\partial^2 w}{\partial x^2} \frac{\partial^2 w}{\partial y^2} \\ & + 4D_{16} \frac{\partial^2 w}{\partial y^2} \frac{\partial^2 w}{\partial x \partial y} + 4D_{26} \frac{\partial^2 w}{\partial y^2} \frac{\partial^2 w}{\partial x \partial y} + D_{22} \left(\frac{\partial^2 w}{\partial y^2} \right)^2 \\ & \left. + 4D_{66} \left(\frac{\partial^2 w}{\partial x \partial y} \right)^2 - N_0 \left(\frac{\partial w}{\partial x} + \frac{\partial w_0}{\partial x} \right)^2 \right] dx dy. \quad (15) \end{aligned}$$

In Koiter's energy criterion of elastic stability, variations of energy are performed at the fundamental (pre-buckling) state.

The second variation of the energy for buckling modes is

$$\begin{aligned} P_2[\underline{u}] = \frac{1}{2} \int_0^{2\pi R} \int_0^L & \left[A_{11} \left(\frac{\partial u}{\partial x} \right)^2 + 2A_{12} \frac{\partial u}{\partial x} \left(\frac{\partial v}{\partial y} + \frac{w}{R} \right) + 2A_{16} \frac{\partial u}{\partial x} \left(\frac{\partial u}{\partial y} + \frac{\partial v}{\partial x} \right) \right. \\ & + 2A_{26} \left(\frac{\partial v}{\partial y} + \frac{w}{R} \right) \left(\frac{\partial u}{\partial y} + \frac{\partial v}{\partial x} \right) + A_{22} \left(\frac{\partial v}{\partial y} + \frac{w}{R} \right)^2 + A_{66} \left(\frac{\partial u}{\partial y} + \frac{\partial v}{\partial x} \right)^2 \\ & + D_{11} \left(\frac{\partial^2 w}{\partial x^2} \right)^2 + 2D_{12} \frac{\partial^2 w}{\partial x^2} \frac{\partial^2 w}{\partial y^2} + 4D_{16} \frac{\partial^2 w}{\partial x^2} \frac{\partial^2 w}{\partial x \partial y} + D_{22} \left(\frac{\partial^2 w}{\partial y^2} \right)^2 \\ & \left. + 4D_{26} \frac{\partial^2 w}{\partial y^2} \frac{\partial^2 w}{\partial x \partial y} + 4D_{66} \left(\frac{\partial^2 w}{\partial x \partial y} \right)^2 - N_0 \left(\frac{\partial w}{\partial x} \right)^2 \right] dx dy. \quad (16) \end{aligned}$$

We will discuss the effect of the most critical type of axisymmetric geometrical imperfection $w_0(x) = -\mu h_0 \cos(2px/R)$ (Koiter, 1963; Tennyson *et al.*, 1971) where h_0 is the nominal thickness of the shell, μ is the non-dimensional parameter giving the amplitude of the imperfection, and p is the wave number of the axisymmetric classical buckling mode, which is given by (Tennyson *et al.*, 1971):

do not depend on the thickness. In the following, use will be made of the transformed stiffness matrices $[A^*]$, $[B^*]$ and $[D^*]$, which are related to the matrices in (3) as follows :

$$[A^*] = [A]^{-1}, [B^*] = [B][A], [D^*] = [D] - [B][A^*][B] \tag{4}$$

Thus

$$A_{ij}^* = \frac{1}{H(x)} a_{ij}^*, B_{ij}^* = H(x)b_{ij}^*D_{ij}^* = [H(x)]^3 d_{ij}^* \tag{5}$$

where $[a^*]$, $[b^*]$ and $[d^*]$ are counterparts, in the uniform laminate, of the transformed stiffness matrices $[A^*]$, $[B^*]$ and $[D^*]$. They are given by

$$[a^*] = [a]^{-1}, [b^*] = [b][a], [d^*] = [d] - [b][a^*][b]. \tag{6}$$

We will deal with symmetric laminates, for which there is no coupling between bending and extension. Thus, we have

$$B_{ij} = 0, B_{ij}^* = 0 \quad (i, j = 1, 2, 6). \tag{7}$$

The constitutive relations for the anisotropic laminate are (Vinson and Sierakowski, 1986)

$$\begin{Bmatrix} N_x \\ N_y \\ N_{xy} \end{Bmatrix} = \begin{pmatrix} A_{11} & A_{12} & A_{16} \\ A_{12} & A_{22} & A_{26} \\ A_{16} & A_{26} & A_{66} \end{pmatrix} \begin{Bmatrix} \epsilon_x \\ \epsilon_y \\ \epsilon_{xy} \end{Bmatrix} \tag{8}$$

$$\begin{Bmatrix} M_x \\ M_y \\ M_{xy} \end{Bmatrix} = \begin{pmatrix} D_{11} & D_{12} & D_{16} \\ D_{12} & D_{22} & D_{26} \\ D_{16} & D_{26} & D_{66} \end{pmatrix} \begin{Bmatrix} \kappa_x \\ \kappa_y \\ \kappa_{xy} \end{Bmatrix} \tag{9}$$

where N_x , N_y and N_{xy} are stress resultants, M_x , M_y and M_{xy} are bending and twisting moments, acting on the mid-surface of a laminate.

Membrane strain energy of a laminated cylindrical shell of length L is

$$U_m = \frac{1}{2} \int_0^{2\pi R} \int_0^L (N_x \epsilon_x + N_y \epsilon_y + N_{xy} \gamma_{xy}) dx dy. \tag{10}$$

Bending strain energy reads

$$U_b = \frac{1}{2} \int_0^{2\pi R} \int_0^L (M_x \kappa_x + M_y \kappa_y + M_{xy} \kappa_{xy}) dx dy. \tag{11}$$

For the shell under axial uniform end compression N_0 , potential energy of the applied load takes the form

$$\Omega = -\frac{1}{2} \int_0^{2\pi R} \int_0^L N_0 \left(\frac{\partial w}{\partial x} + \frac{\partial w_0}{\partial x} \right)^2 dx dy \tag{12}$$

where w_0 is the geometric initial imperfection.

Thus, the total potential energy is

$$p^2 = \frac{R}{4\sqrt{a_{22}^* a_{11}^*}}. \tag{17}$$

We supplement the second variation with the additional bilinear term due to geometric initial imperfection

$$P_{11}[\underline{u}_0, \underline{u}] = -N_0 \int_0^{2\pi R} \int_0^L \frac{\partial w}{\partial x} \frac{dw_0}{dx} dx dy. \tag{18}$$

The third variation of the energy reads

$$\begin{aligned} P_3[\underline{u}] = & \frac{1}{2} \int_0^{2\pi R} \int_0^L \left\{ A_{11} \frac{\partial u}{\partial x} \left(\frac{\partial w}{\partial x} \right)^2 + A_{12} \left[\frac{\partial u}{\partial x} \left(\frac{\partial w}{\partial y} \right)^2 + \left(\frac{\partial w}{\partial x} \right)^2 \left(\frac{\partial u}{\partial y} + \frac{w}{R} \right) \right] \right. \\ & + 2A_{16} \left[\frac{\partial u}{\partial x} \frac{\partial w}{\partial x} \frac{\partial w}{\partial y} + \frac{1}{2} \left(\frac{\partial w}{\partial x} \right)^2 \left(\frac{\partial u}{\partial y} + \frac{\partial v}{\partial x} \right) \right] \\ & + 2A_{26} \left[\left(\frac{\partial v}{\partial y} + \frac{w}{R} \right) \frac{\partial w}{\partial x} \frac{\partial w}{\partial y} + \frac{1}{2} \left(\frac{\partial w}{\partial y} \right)^2 \left(\frac{\partial u}{\partial y} + \frac{\partial v}{\partial x} \right) \right] \\ & \left. + A_{22} \left(\frac{\partial v}{\partial y} + \frac{w}{R} \right) \left(\frac{\partial w}{\partial y} \right)^2 + 2A_{66} \left(\frac{\partial u}{\partial y} + \frac{\partial v}{\partial x} \right) \frac{\partial w}{\partial x} \frac{\partial w}{\partial y} \right\} dx dy. \tag{19} \end{aligned}$$

We now assume that the buckling modes of the shell with a uniform thickness remain a good approximation for the buckling modes of the shell with small thickness variations. We are at least ensured that the critical load obtained in this way is, by the energy principle, an upper bound for the actual critical buckling load.

According to the study of Tennyson *et al.* (1971), the following expression for the buckling mode can be adopted for the laminated cylindrical shell with the aforementioned axisymmetric initial imperfection w_0 :

$$w = b \cos \frac{2px}{R} + C_n \cos \frac{px}{R} \cos \frac{ny}{R} \tag{20}$$

where b and C_n are constants, n is the number of waves in the circumferential direction. If we recall the shell equilibrium equations in terms of displacements u , v and w (Vinson Sierakowski, 1986)

$$\begin{pmatrix} L_{11} & L_{12} & L_{13} \\ L_{12} & L_{22} & L_{23} \\ L_{13} & L_{23} & L_{33} \end{pmatrix} \begin{pmatrix} u \\ v \\ w \end{pmatrix} = \begin{pmatrix} 0 \\ 0 \\ N_0 \frac{\partial^2 w}{\partial x^2} \end{pmatrix} \tag{21}$$

where operators L_{ij} are

$$\begin{aligned} L_{11} = & a_{11} \frac{\partial^2}{\partial x^2} + 2a_{16} \frac{\partial^2}{\partial x \partial y} + a_{66} \frac{\partial^2}{\partial y^2}, & L_{12} = & a_{16} \frac{\partial^2}{\partial x^2} + (a_{12} + a_{66}) \frac{\partial^2}{\partial x \partial y} + a_{26} \frac{\partial^2}{\partial y^2} \\ L_{13} = & \frac{1}{R} \left(a_{12} \frac{\partial}{\partial x} + a_{26} \frac{\partial}{\partial y} \right), & L_{22} = & a_{66} \frac{\partial^2}{\partial x^2} + 2a_{26} \frac{\partial^2}{\partial x \partial y} + a_{22} \frac{\partial^2}{\partial y^2}, \end{aligned}$$

$$L_{23} = \frac{1}{R} \left(a_{26} \frac{\partial}{\partial x} + a_{22} \frac{\partial}{\partial y} \right)$$

$$L_{33} = \frac{a_{22}}{R^2} + d_{11} \frac{\partial^4}{\partial x^4} + 4d_{16} \frac{\partial^4}{\partial x^3 \partial y} + 2(d_{12} + 2d_{66}) \frac{\partial^4}{\partial x^2 \partial y^2} + 4d_{26} \frac{\partial^4}{\partial x \partial y^3} + d_{22} \frac{\partial^4}{\partial y^4} \quad (22)$$

we can obtain the expressions for u and v as follows

$$u = -\frac{a_{12}}{2pa_{11}} b \sin \frac{2px}{R} + Q_n C_n \sin \frac{px}{R} \cos \frac{ny}{R}$$

$$v = K_n C_n \cos \frac{px}{R} \sin \frac{ny}{R} \quad (23)$$

where

$$K_n = -\frac{n(p^2 a_{11} a_{22} + n^2 a_{66} a_{22} - a_{12}^2 p^2 - a_{66} a_{12} p^2)}{(a_{11} p^2 + a_{66} n^2)(a_{66} p^2 a_{22} n^2) - (a_{12} + a_{66})^2 p^2 n^2}$$

$$Q_n = -\frac{pa_{66}(p^2 a_{12} - n^2 a_{22})}{(a_{11} p^2 + a_{66} n^2)(a_{66} p^2 + a_{22} n^2) - (a_{12} + a_{66})^2 p^2 n^2}. \quad (24)$$

It should be mentioned that in deriving solution (23), we used an assumption in the studies of Hirano (1979) and Tasi (1966) that the coupling stiffnesses A_{16} , A_{26} , D_{16} , and D_{26} are zero. They are identically zero for cross-ply laminates. When the laminate is composed of many layers, these coupling stiffnesses are small and can be neglected.

In our previous numerical analysis of composite shells with axisymmetric thickness variations (Li *et al.*, 1994), we have shown that, in the absence of the geometric imperfection, the thickness variation with wave number being twice that of the classical buckling mode ($p_1 = 2p$) has the most degrading effect of the buckling load. This result is also observed for isotropic shells (Koiter *et al.*, 1994a, 1994b). Now we are interested in the combined effect of the most critical geometric imperfection and the most detrimental thickness variation on the load-carrying capacity.

Substituting eqn (20) and (23) into the second and third variations, we obtain, after retaining only the first order terms in ε :

$$P_2[\underline{u}] = \frac{C_n^2 \pi L}{4R^3} [d_{22} n^4 + 2d_{12} n^2 p^2 + 4d_{66} n^2 p^2 + d_{11} p^4 + a_{22} (1 + K_n)^2 R^2$$

$$- N_0 p^2 R^2 + 2a_{12} (1 + K_n n) Q_n p R^2 + a_{11} Q_n^2 p^2 R^2 + a_{66} (K_n p + n Q_n)^2 R^2]$$

$$+ \frac{1}{2R^3} b^2 \left[16d_{11} p^4 \left(1 - \frac{3}{2} \varepsilon \right) - \frac{a_{12}^2 R^2}{a_{11}} \left(1 - \frac{1}{2} \varepsilon \right) + a_{22} R^2 \left(1 - \frac{1}{2} \varepsilon \right) - 4N_0 R^2 p^2 \right] \quad (25)$$

$$P_{11}[\underline{u}_0, \underline{u}] = \frac{4bh_0 N_0 p^2 \mu \pi L}{R} \quad (26)$$

$$P_3[\underline{u}] = \frac{bC_n^2 \pi L}{8R^2} \left\{ a_{12} \left[\left(-1 + \frac{1}{2} \varepsilon \right) p^2 + 4 \left(1 + \frac{1}{2} \varepsilon \right) (1 + K_n n) p^2 \right] + a_{22} \left(1 - \frac{1}{2} \varepsilon \right) n^2 + \frac{a_{12}^2 n^2}{a_{11}} \right.$$

$$\left. \times \left(-1 + \frac{1}{2} \varepsilon \right) + a_{12} \left(1 - \frac{1}{2} \varepsilon \right) p^2 + 4a_{11} p^3 Q_n \left(1 + \frac{1}{2} \varepsilon \right) - 4a_{66} \left(1 + \frac{1}{2} \varepsilon \right) n p (K_n p + Q_n n) \right\}. \quad (27)$$

The energy expression to be considered is

$$P_2[\underline{u}] + P_{11}[\underline{u}_0, \underline{u}] + P_3[\underline{u}]. \quad (28)$$

The equations for the initial post-buckling behavior are furnished by setting the partial derivatives of the energy expression (28) with respect to b and C_n equal to zero:

$$\begin{aligned} & \frac{b}{R^3} \left[16d_{11}p^4 \left(1 - \frac{3}{2}\varepsilon\right) - \frac{a_{12}^2 R^2}{a_{11}} \left(1 - \frac{1}{2}\varepsilon\right) + a_{22}R^2 \left(1 - \frac{1}{2}\varepsilon\right) - 4N_0R^2p^2 \right] \\ & + \frac{4N_0h_0p^2\mu}{R} + \frac{C_n^2}{8R^2} \left\{ a_{12} \left[\left(-1 + \frac{1}{2}\varepsilon\right)p^2 + 4\left(1 + \frac{1}{2}\varepsilon\right)(1 + K_n n)p^2 \right] \right. \\ & + a_{22} \left(1 - \frac{1}{2}\varepsilon\right)n^2 + \frac{a_{12}^2 n^2}{a_{11}} \left(-1 + \frac{1}{2}\varepsilon\right) + a_{12} \left(1 - \frac{1}{2}\varepsilon\right)p^2 \\ & \left. + 4a_{11}p^3Q_n \left(1 + \frac{1}{2}\varepsilon\right) - 4a_{66} \left(1 + \frac{1}{2}\varepsilon\right)np(K_n p + Q_n n) \right\} = 0 \end{aligned} \quad (29)$$

and

$$\begin{aligned} & \frac{C_n}{2R^3} [d_{22}n^4 + 2d_{12}n^2p^2 + 4d_{66}n^2p^2 + d_{11}p^4 + a_{22}(1 + K_n n)^2R^2 \\ & - N_0p^2R^2 + 2a_{12}(1 + K_n n)Q_n pR^2 + a_{11}Q_n^2p^2R^2 + a_{66}(K_n p + nQ_n)^2R^2] \\ & + \frac{bC_n}{4R^2} \left\{ a_{12} \left[\left(-1 + \frac{1}{2}\varepsilon\right)p^2 + 4\left(1 + \frac{1}{2}\varepsilon\right)(1 + K_n n)p^2 \right] + a_{22} \left(1 - \frac{1}{2}\varepsilon\right)n^2 \right. \\ & + \frac{a_{12}^2 n^2}{a_{11}} \left(-1 + \frac{1}{2}\varepsilon\right) + a_{12} \left(1 - \frac{1}{2}\varepsilon\right)p^2 + 4a_{11}p^3Q_n \left(1 + \frac{1}{2}\varepsilon\right) \\ & \left. - 4a_{66} \left(1 + \frac{1}{2}\varepsilon\right)np(K_n p + Q_n n) \right\} = 0. \end{aligned} \quad (30)$$

With the solution $C_n = 0$ from eqn (30), eqn (29) yields

$$b = - \frac{4N_0h_0p^2\mu R^2}{16d_{11}p^4 \left(1 - \frac{3}{2}\varepsilon\right) - \frac{a_{12}^2 R^2}{a_{11}} \left(1 - \frac{1}{2}\varepsilon\right) + a_{22}R^2 \left(1 - \frac{1}{2}\varepsilon\right) - 4N_0R^2p^2}. \quad (31)$$

Bifurcation buckling with respect to the asymmetric mode with amplitude C_n occurs at

$$\begin{aligned} b = & - \frac{2}{R} [d_{22}n^4 + 2d_{12}n^2p^2 + 4d_{66}n^2p^2 + d_{11}p^4 + a_{22}(1 + K_n n)^2R^2 \\ & - N_0p^2R^2 + 2a_{12}(1 + K_n n)Q_n pR^2 + a_{11}Q_n^2p^2R^2 + a_{66}(K_n p + nQ_n)^2R^2] \\ & + \left\{ a_{12} \left[\left(-1 + \frac{1}{2}\varepsilon\right)p^2 + 4\left(1 + \frac{1}{2}\varepsilon\right)(1 + K_n n)p^2 \right] + a_{22} \left(1 - \frac{1}{2}\varepsilon\right)n^2 \right. \\ & + \frac{a_{12}^2 n^2}{a_{11}} \left(-1 + \frac{1}{2}\varepsilon\right) + a_{12} \left(1 - \frac{1}{2}\varepsilon\right)p^2 + 4a_{11}p^3Q_n \left(1 + \frac{1}{2}\varepsilon\right) \\ & \left. - 4a_{66} \left(1 + \frac{1}{2}\varepsilon\right)np(K_n p + Q_n n) \right\}. \end{aligned} \quad (32)$$

Equating the above two expressions for b , we obtain the equation for the critical buckling load N_0

$$\begin{aligned}
 & \left[16d_{11}p^4 \left(1 - \frac{3}{2}\varepsilon \right) - \frac{a_{12}^2 R^2}{a_{11}} \left(1 - \frac{1}{2}\varepsilon \right) + a_{22} R^2 \left(1 - \frac{1}{2}\varepsilon \right) - 4N_0 R^2 p^2 \right] \\
 & \quad \times [d_{22}n^4 + 2d_{12}n^2 p^2 + 4d_{66}n^2 p^2 + d_{11}p^4 + a_{22}(1 + K_n n)^2 R^2 \\
 & \quad - N_0 p^2 R^2 + 2a_{12}(1 + K_n n) Q_n p R^2 + a_{11} Q_n^2 p^2 R^2 + a_{66}(K_n p + n Q_n)^2 R^2] \\
 & \quad - 2N_0 h_0 p^2 \mu R^3 \left\{ a_{12} \left[\left(-1 + \frac{1}{2}\varepsilon \right) p^2 + 4 \left(1 + \frac{1}{2}\varepsilon \right) (1 + K_n n) p^2 \right] + a_{22} \left(1 - \frac{1}{2}\varepsilon \right) n^2 \right. \\
 & \quad + \frac{a_{12}^2 n^2}{a_{11}} \left(-1 + \frac{1}{2}\varepsilon \right) + a_{12} \left(1 - \frac{1}{2}\varepsilon \right) p^2 + 4a_{11} p^3 Q_n \left(1 + \frac{1}{2}\varepsilon \right) \\
 & \quad \left. - 4a_{66} \left(1 + \frac{1}{2}\varepsilon \right) n p (K_n p + Q_n n) \right\} = 0. \tag{33}
 \end{aligned}$$

In solving eqn (33), integer search must be performed with respect to the circumferential wave number n to arrive at the lowest value of N_0 .

We define the non-dimensional critical load parameter λ (sometimes referred to as *knockdown factor* in the literature) as

$$\lambda = \frac{N_0}{N_{cl}} \tag{34}$$

where N_{cl} is the classical buckling load in the absence of both initial imperfection and thickness variation. N_{cl} is given by (Vinson and Sierakowski, 1986)

$$N_{cl} = \min_{m,n} \{ N_{m,n} \}, \quad N_{m,n} = \left(\frac{L}{m\pi} \right)^2 \frac{C_{11} C_{22} C_{33} + 2C_{12} C_{23} C_{13} - C_{13}^2 C_{22} - C_{23}^2 C_{11} - C_{12}^2 C_{33}}{C_{11} C_{22} - C_{12}^2} \tag{35}$$

where

$$\begin{aligned}
 C_{11} &= A_{11} \left(\frac{m\pi}{L} \right)^2 + A_{66} \left(\frac{n}{R} \right)^2, & C_{22} &= A_{22} \left(\frac{n}{R} \right)^2 + A_{66} \left(\frac{m\pi}{L} \right)^2 \\
 C_{33} &= D_{11} \left(\frac{m\pi}{L} \right)^4 + 2(D_{12} + 2D_{66}) \left(\frac{m\pi}{L} \right)^2 \left(\frac{n}{R} \right)^2 + D_{22} \left(\frac{n}{R} \right)^4 + \frac{A_{22}}{R^2} \\
 C_{12} &= (A_{12} + A_{66}) \left(\frac{m\pi}{L} \right) \left(\frac{n}{R} \right), & C_{13} &= \frac{A_{12}}{R} \left(\frac{m\pi}{L} \right), & C_{23} &= \frac{A_{22}}{R} \left(\frac{n}{R} \right) + B_{22} \left(\frac{n}{R} \right)^3. \tag{36}
 \end{aligned}$$

3. RESULTS AND DISCUSSION

Axial buckling loads can be determined from eqn (33) for composite cylindrical shells containing a small axisymmetric initial imperfection and a small axisymmetric thickness variation. For practical purposes, the results thus obtained should be considered conservative, since the most detrimental case of geometric imperfection and thickness variation is investigated. However, since we ignored in our derivation the higher order terms in ε , the results from the present study should not be deemed accurate for shells having large

thickness variation. Also, the results may not be conservative from a design point of view because we are limited here to axisymmetric variations.

As a numerical example, we discuss shells made of carbon/epoxy laminae, whose elastic moduli are $E_1 = 13.75 \times 10^6$ psi, $E_2 = 1.03 \times 10^6$ psi, $\nu_{12} = 0.25$, $G_{12} = 0.42 \times 10^6$ psi. The shell is 6 inches in radius and 30 inches in length and is composed of ten equally thick layers, each being 0.012 inch thick. The laminate configuration is $[\theta/-\theta/\theta/-\theta/\theta]_{sym}$, with the fiber angle θ varying from 0° to 90° .

Solving eqn (33) numerically for the critical load N_0 with integer search performed simultaneously with respect to the circumferential buckling wave number n , and then non-dimensionalizing the result according to (34), we obtain the critical buckling load factor λ for different cases of thickness variation parameter ε and imperfection amplitude μ . The results are plotted in Figs 1 and 2. The results obtained here confirm numerically the previous first-order asymptotic formula

$$\lambda = 1 - \varepsilon \quad (37)$$

which holds only for the axisymmetric buckling cases for composite shells without initial imperfection. It is interesting to note that as long as the axisymmetric buckling mode dominates, the buckling load reduction factor λ remains constant, irrespective of the change in the laminate construction. However, once the shell has an axisymmetric initial imperfection, the buckling mode becomes non-axisymmetric, and the buckling load reduction is strongly influenced by the stacking sequence of the laminae. Figure 3 depicts the results of the buckling load factor λ for shells of different laminate profiles, such as $[45^\circ/-45^\circ/45^\circ/-45^\circ/45^\circ]_{sym}$ and $[16^\circ/-16^\circ/16^\circ/-16^\circ/16^\circ]_{sym}$, together with the results for corresponding isotropic shells. It can be seen from this figure that the load-carrying capacity of composite shells is sensitive to thickness variation, and especially sensitive to initial geometric imperfection. The imperfection sensitivity is comparable to that of an isotropic shell. Although axisymmetric geometric initial imperfections cause most of the buckling load reduction, further degradation in the load-bearing capacity of the shell due to axisymmetric thickness variations should not be overlooked.

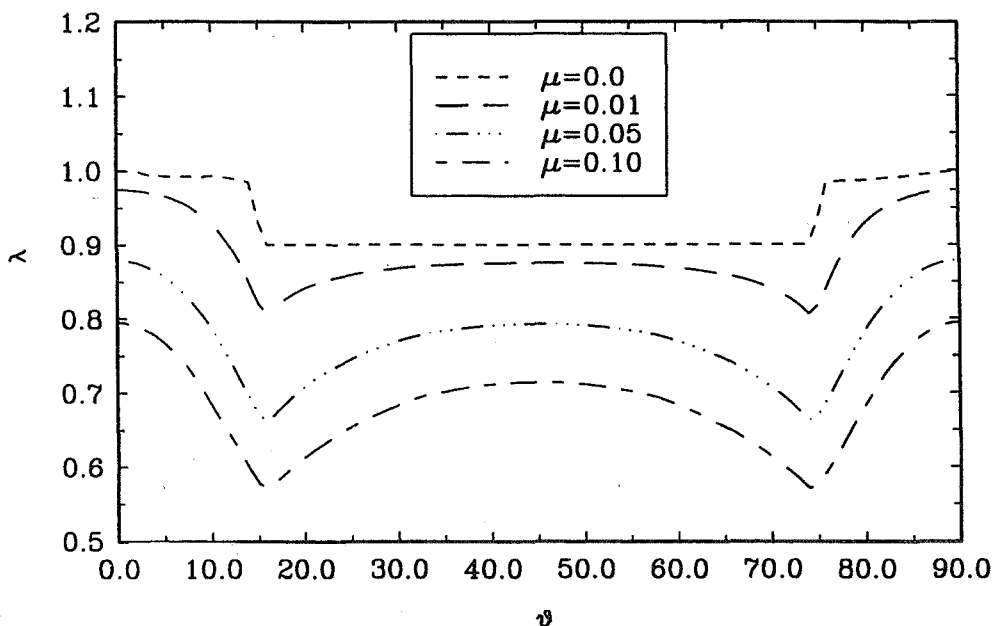


Fig. 1. Effect of thickness variation and imperfection on the buckling load (laminate configuration $[\theta/-\theta/\theta/-\theta/\theta]_{sym}$ thickness variation parameter $\varepsilon = 0.1$).

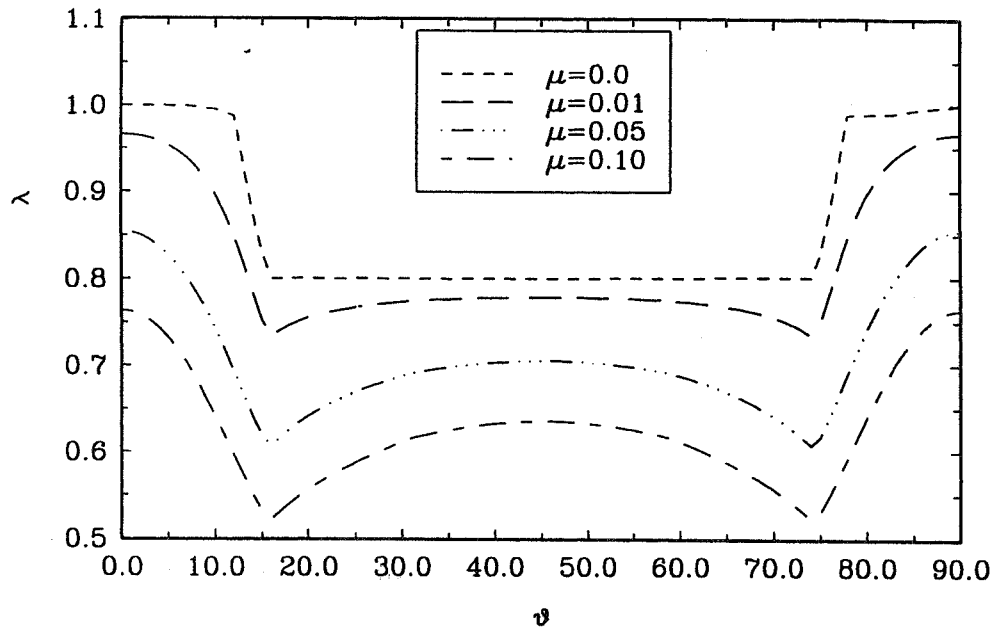


Fig. 2. Effect of thickness variation and imperfection on the buckling load ($[\theta/-\theta/\theta/-\theta/\theta]_{sym}$, $\varepsilon = 0.2$).

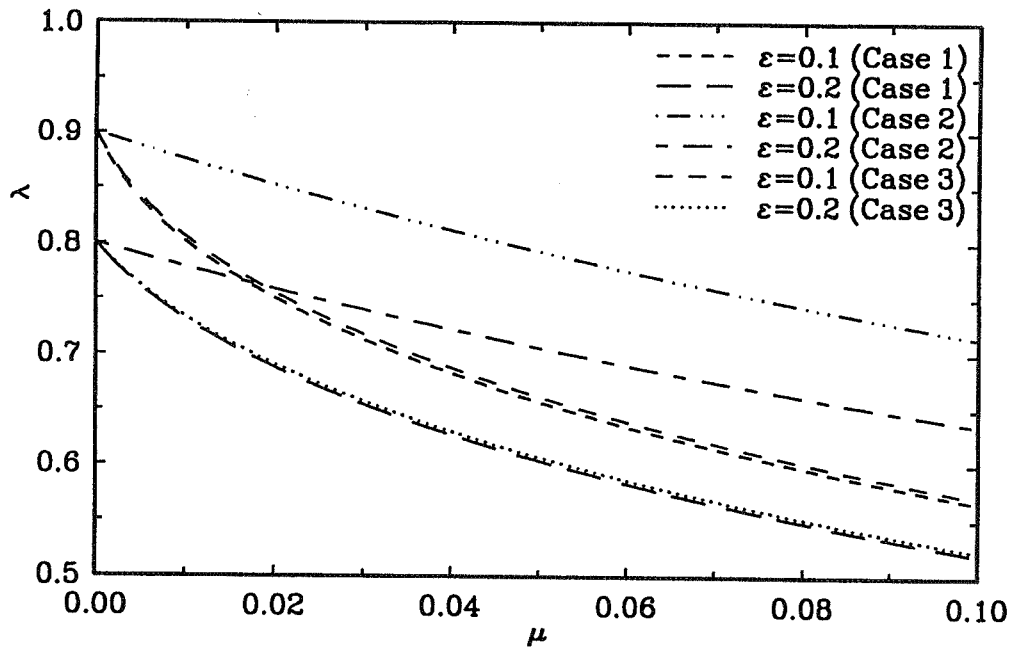


Fig. 3. Buckling load reductions in shells with different laminate configurations (Case 1: isotropic; Case 2: $[45/-45/45/-45/45]_{sym}$; Case 3: $[16/-16/16/-16/16]_{sym}$).

In order to check the accuracy of eqn (33), we used BOSOR4 (Bushnell, 1974), a computer code for stress, buckling and vibration of shells of revolution, to generate a set of comparable data for the non-dimensional critical load parameter λ . Since the classical buckling load has been used to non-dimensionalize the critical buckling load, it is necessary to check the results from eqn (35) with their counterparts from the numerical software so that a common basis can be established for the follow-up comparison of results for non-dimensional critical load λ . For this purpose, software package PANDA2, with use of either the shallow shell or Sanders' theories (Bushnell, 1987, 1996) was run in order to

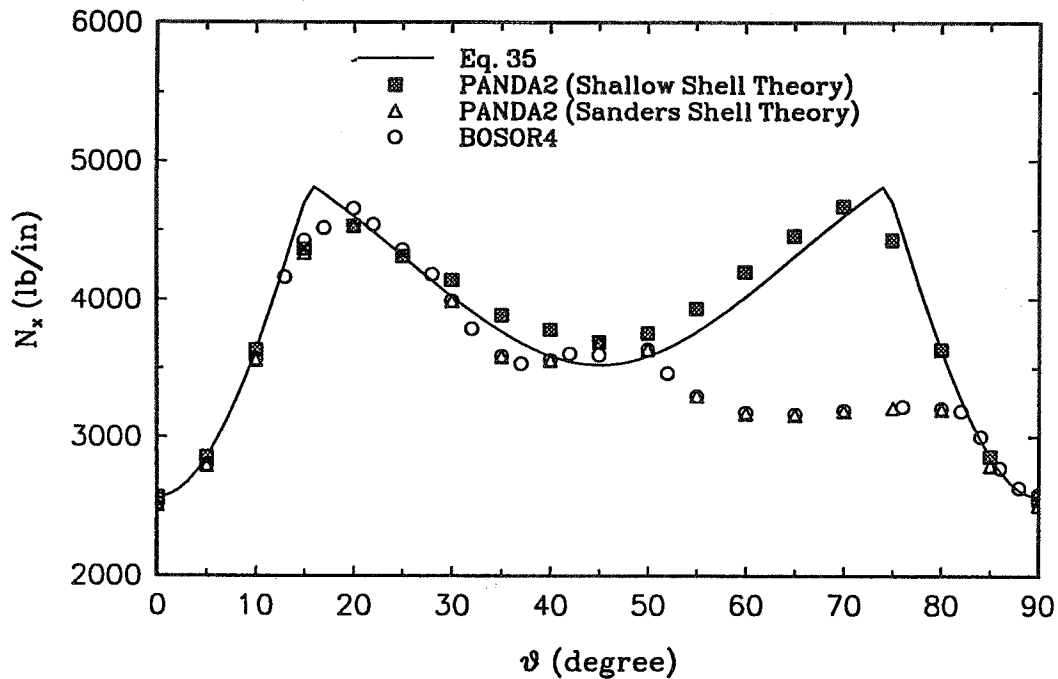


Fig. 4. Comparison of classical buckling load from different methods.

compute the classical buckling load N_{cl} . Predictions are plotted in Fig. 4, together with those from eqn (35) and those from BOSOR4, which is based on Sanders' equations.

Figure 4 shows that the classical buckling loads from different sources agree quite well except in the range $53^\circ < \theta < 80^\circ$. For this range eqn (35) and PANDA2 yield similar predictions with the shallow shell "switch" turned on in PANDA2. However, a significant discrepancy exists between predictions from shallow shell theory and Sander's theory. For $53^\circ < \theta < 80^\circ$ the shallow shell theory is significantly unconservative. A more refined theory is required for the accurate prediction of "classical" buckling load, N_{cl} , in this range of θ .

In the BOSOR4 models of the axisymmetrically imperfect shells, half of the 30 inch length of the cylindrical shell is represented, with symmetry conditions imposed at $x = 15$ inches. The 15 inch long BOSOR4 model is subdivided into six segments in order to get enough nodal points for a good convergence and in order to represent accurately the sinusoidal variation which is equal to the axial wavelength of the axisymmetric buckling mode of the perfect shell. The sixth segment, adjacent to the midlength plane of symmetry, is half as long. BOSOR4 can handle orthotropic walls with meridionally varying thickness. The shell wall in the BOSOR4 model has the same constitutive matrix as the 10-layer laminated shell with fiber angle $\theta = 16^\circ$. (Note: in the BOSOR4 model the same off-diagonal "anisotropic" terms in the integrated constitutive law are assumed to be zero as is the case in the theory presented in this paper.)

Figure 5 displays the results of the non-dimensional critical load parameter λ obtained from the asymptotic formula (eqn 33) and from BOSOR4 for a 10-layer composite shell (laminare configuration: $[16^\circ/-16^\circ/16^\circ/-16^\circ/16^\circ]_{sym}$) which contains both the initial imperfection and the thickness variation. It can be seen from this figure that the asymptotic formula predicts the knockdown factor quite accurately.

Finally, it is worth mentioning that as a special case if we let

$$a_{11} = a_{22} = \frac{Eh_0}{1-\nu^2}, \quad a_{12} = \nu a_{11}, \quad a_{66} = \frac{1-\nu}{2} a_{11}, \quad a_{16} = a_{26} = 0$$

$$d_{11} = d_{22} = \frac{Eh^3}{12(1-\nu^2)}, \quad d_{12} = \nu d_{11}, \quad d_{66} = \frac{1-\nu}{2} d_{11}, \quad d_{16} = d_{26} = 0 \quad (38)$$

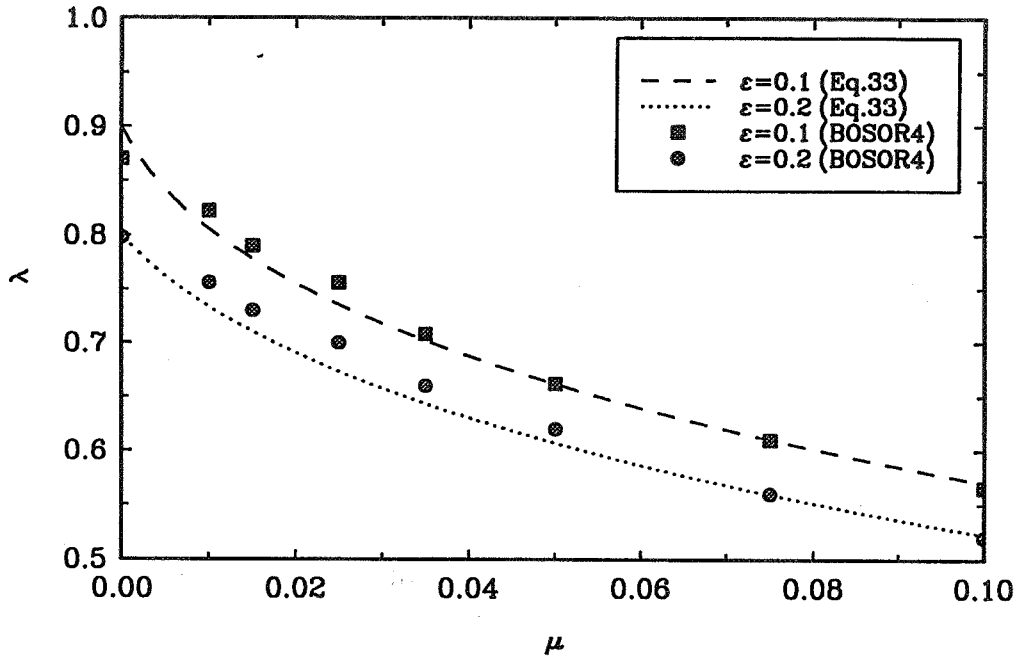


Fig. 5. Comparison of the non-dimensional critical load λ obtained from the asymptotic formula and BOSOR4.

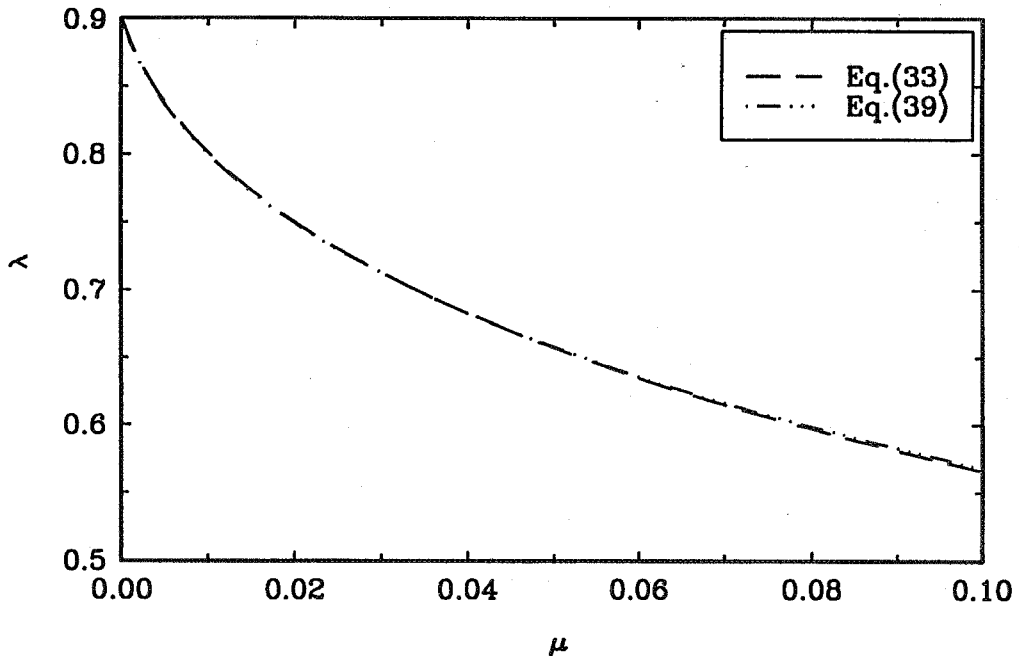


Fig. 6. Comparison of results using Koiter's circle and those using integer search for isotropic shells with thickness variation $\epsilon = 0.2$.

where E is the Young's modulus, and ν is the Poisson's ratio, and furthermore, if we select the asymmetric mode at the top of the Koiter's semi-circle (Koiter, 1980), that is, let $p = n = [\sqrt{3(1-\nu^2)}R^2/2h_0]^{1/2}$, eqn (33) reduces to its counterpart in the isotropic shell case,

$$(1-\lambda)(1-\varepsilon-\lambda) - \frac{3\sqrt{3(1-\nu^2)}}{2} \lambda \mu \left(1 + \frac{1}{6}\varepsilon\right) = 0. \quad (39)$$

Equation (39) is identical to eqn (21) in our previous work (Koiter *et al.*, 1994b) if the small term $\varepsilon/6$ is ignored compared with unity.

Figure 6 shows the comparison of results in the isotropic shell case using Koiter's semi-circle and those using integer search with respect to the circumferential wave number n . It is seen that the agreement is excellent.

One should stress here that in order to obtain good correlation of test and theory, the buckling load of perfect shells with nonlinear bending prebuckling effects should be calculated when the effects of boundary conditions become significant, as in the case for short shells and shells of intermediate length, for which the "boundary layer" length, $(rt)^{1/2}$ comprises a significant fraction of the entire length of the shell.

Acknowledgement—This research has been supported by the NASA Langley Research Center, through Grant NAG-1-1310.

REFERENCES

- Bushnell, D. (1974) Stress, stability and vibration of complex, branched shells of revolution. *Computers and Structures* **4**, 399–435.
- Bushnell, D. (1987) Theoretical basis of the PANDA computer program for preliminary design of stiffened panels under combined in-plane loads. *Computers and Structures* **27**, 541–563.
- Bushnell, D. (1987) PANDA2—program for minimum weight design of stiffened, composite, locally buckled panels. *Computers and Structures* **25**, 469–605.
- Bushnell, D. (1994) Approximate method for the optimum design of ring and stringer stiffened cylindrical panels and shells with local, inter-ring, and general buckling modal imperfections. *Proceedings of AIAA/ASME/ASCE/AHS, Structures, Materials and Structural Dynamics Conference*, 18–20 April, 1994, Hilton Head, SC.
- Bushnell, D. (1996) Recent enhancements to PANDA2. In *Proceedings of 37th AIAA/ASME/ASCE/AHS, Structures, Materials and Structural Dynamics Conference*, 15–17 April, Salt Lake City, UT.
- Hirano, Y. (1979) Buckling of angle-ply laminated circular cylindrical shells. *Journal of Applied Mechanics*, **46**, 233–234.
- Koiter, W. T. (1945) On the stability of elastic equilibrium. Thesis, Delft, in Dutch with extensive English summary. NASA Technical Translation F 10,833 and AFFDL Technical Report 70-25 (English translations (1967) and (1970) by E. Riks).
- Koiter, W. T. (1963) The effect of axisymmetric imperfections on the buckling of cylindrical shells under axial compression. In *Proceedings of Kon. Ned. Ak. Wet.* **B66**, 265–279.
- Koiter, W. T. (1966) General equations of elastic stability for thin shells. In *Proceedings of the Symposium on the Theory of Shells*, 4–6 April 1966, Houston, Texas, U.S.A., pp. 187–227.
- Koiter, W. T. (1980) Buckling of cylindrical shells under axial compression and external pressure. In *Thin Shell Theory. New Trends and Applications*, ed. W. Olszak, CISM Courses and Lectures No. 240. Springer Verlag, Wien and New York, pp. 77–87.
- Koiter, W. T., Elishakoff, I., Li, Y. W. and Starnes, J. H. (1994a) Buckling of an axially compressed cylindrical perfect shell of variable thickness. *International Journal of Solids and Structures* **31**, 797–807.
- Koiter, W. T., Elishakoff, I., Li, Y. W. and Starnes, J. H. (1994b) Buckling of an axially compressed imperfect cylindrical perfect shell of variable thickness. In *Proceedings of 35th AIAA ASME/ASCE/AHS/ASC Structures, Structural Dynamics and Materials Conference*, Hilton Hotel, SC, 18–20 April, pp. 277–289.
- Li, Y. W., Elishakoff, I. and Starnes, J. H. (1995) Axial buckling of composite cylindrical shells with periodic thickness variation. *Computers and Structures* **56**, 65–74.
- Sanders, J. L., Jr (1963) Nonlinear theories for thin shells. *Quarterly of Applied Mechanics* **21**, 21–36.
- Tasi, J. (1966) Effect of heterogeneity on the stability of cylindrical shells under axial compression. *AIAA Journal* **4**, 1058–1062.
- Tennyson, R. C., Chan, M. K. and Muggeridge, D. B. (1971) The effect of axisymmetric shape imperfections on the buckling of laminated anisotropic circular cylinders. *Canadian Aeronautics and Space Institute Transactions* **4**, 131–138.
- Vinson, J. R. and Sierakowski, R. L. (1986) *The Behavior of Structures Composed of Composite Materials*. Martinus Nijhoff Publishers, Dordrecht, pp. 63–171.



59-39
358979 408982 p6
EWAIVED
p6

Worst case estimation of homology design by convex analysis

N. Yoshikawa^{†,*}, I. Elishakoff[‡], S. Nakagiri[†]

[†]*Institute of Industrial Science, The University of Tokyo, 7-22-1, Roppongi, Minato-ku, Tokyo 106, Japan*

[‡]*Center for Applied Stochastics Research and Department of Mechanical Engineering, Florida Atlantic University, Boca Raton, FL 33431-0991, U.S.A.*

Abstract

The methodology of homology design is investigated for optimum design of advanced structures, for which the achievement of delicate tasks by the aid of active control system is demanded. The proposed formulation of homology design, based on the finite element sensitivity analysis, necessarily requires the specification of external loadings. The formulation to evaluate the worst case for homology design caused by uncertain fluctuation of loadings is presented by means of the convex model of uncertainty, in which uncertainty variables are assigned to discretized nodal forces and are confined within a conceivable convex hull given as a hyperellipse. The worst case of the distortion from objective homologous deformation is estimated by the Lagrange multiplier method searching the point to maximize the error index on the boundary of the convex hull. The validity of the proposed method is demonstrated in a numerical example using the eleven-bar truss structure. © 1998 Elsevier Science Ltd. All rights reserved.

1. Introduction

A great deal of attention is paid to structure/control integrated optimum design for advanced structures, such as space structures, adaptive structures and smart structures, which are required to fulfill complicated missions in high quality by the aid of active control systems (see Fig. 1) [1–3]. The precise control of geometrical properties of these structures is stringently demanded for high quality of performance and sophisticated structural design methodology considering the interaction with active control system and mechanism should be devised. Homology design can be a candidate of such structural optimum design for advanced structures, utilizing the concept of *homologous deformation*, in which a prescribed geometrical property at a part of the structure is maintained before, during and after the deformation. The quality of resolution of a huge and precise radio telescope was greatly

enhanced by realizing homologous deformation keeping the shape of the reflector structure parabolic in spite of the deformation caused by its own weight [4, 5]. The control cost of an active system to adjust the shape of a parabolic reflector is greatly reduced and the resolution quality is ensured easily.

Two formulations based on the finite element method have been derived for homology design in static problems [6, 7]. However, the formulations were given in purely deterministic problems, where the external loadings must be specified. The advanced structures are made very flexible owing to lightweight requirement. Thus, the homologous deformation under specified loading appears to be easily disturbed by the uncertain fluctuation of loading. The sensitivity of homologous deformation with respect to such uncertainties should be estimated prior to the application of homology design.

In this study, the formulation of homology design with an illustrative numerical example using the eleven-bar truss structure is given prior to the discussion on the uncertain loading. Use is made of the finite

* Author to whom all correspondence should be addressed.

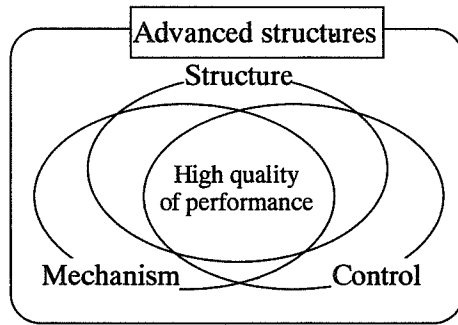


Fig. 1. Concept of advanced structures.

element sensitivity analysis. In the numerical example, the uppermost deck subjected to uniformly distributed vertical load as nominal loading is kept both straight and horizontal, before and after the deformation by homology design. The methodology for the estimation of disturbed homologous deformation is developed based on the convex model of uncertain loadings [8, 9], in which uncertainty variables are assigned to discretized nodal forces and the existence domain of the uncertainty variables is confined within a convex hull of hyperellipse. The worst case of homology design is estimated on the boundary of the convex hull as the point that maximizes the error index. The latter is defined as the square of the Euclidean norm of displacements error from objective homologous deformation. The validity of the proposed method for the worst case estimation of the homology design is demonstrated in a numerical example using the eleven-bar truss structure after homology design.

2. Homology design under deterministic loading

2.1. Formulation by finite element sensitivity analysis

For the sake of specificity, let us consider the static deformation of the linear and elastic structure discretized by the finite elements. The formulation for homology design under deterministic loading is summarized first and is governed by the following stiffness equation in matrix form after the incorporation of the geometrical boundary condition,

$$[K]\{u\} = \{f\} \quad (1)$$

where $[K]$ is the stiffness matrix, $\{u\}$ is the unknown displacement vector, $\{f\}$ is the external nodal force vector and the degrees of freedom of discretized structure are denoted by L . In this formulation, we need a trial design changed to satisfy the constraint of objective homologous deformation, which is given as follows:

$$\{\mathbf{H}(u)\} = \{0\} \quad (2)$$

Eq. (2) consists of J equations with respect to nodal displacements and represents the constraint of the objective homologous deformation. The way of representation is not unique even for the same objective homologous deformation. The success of the objective homology design greatly depends on the manner of determining adequate trial design and represents the homologous constraint neatly. For the sake of simplicity of discussion, we treat only linear homologous deformation, the constraint for which is given by linear equations of nodal displacements, in this study. The homologous constraint equation in this case is represented in matrix form,

$$[C]\{u\} = \{d\} \quad (3)$$

where $[C]$ is the constant constraint matrix of $J \times L$ and $\{d\}$ is the constant vector of J components.

If we find an adequate trial design *a priori*, the nodal displacements obtained by solving the stiffness equation, Eq. (1), satisfy the homologous constraint in Eq. (2) and there is no need to change the trial design. In general, however, it is hard to find the transparent homology design. Therefore we are interested in changing the trial design such that the objective homologous deformation is achieved under specified loading. For the design change, we judiciously select structural parameters p_m and assign the design variables α_m in the form of:

$$p_m = \bar{p}_m(1 + \alpha_m) \quad (4)$$

The upper bar means the value of current trial design hereafter. The effect of the design change caused by design variables is linearly approximated and the change of nodal displacement vector is expressed in the following linear form:

$$\{u\} = \{\bar{u}\} + \sum_{m=1}^M \{u_m^f\} \alpha_m \quad (5)$$

where $\{u_m^f\}$ is the displacement sensitivity vector in the first-order obtained by the finite element sensitivity analysis [10]. Substituting the linearly approximated nodal displacement vector of Eq. (5) into the homologous constraint in Eq. (3), we obtain the governing equation of design variables in the form:

$$\sum_{m=1}^M [C]\{u_m^f\} \alpha_m = \{d\} - [C]\{\bar{u}\} \quad (6)$$

The governing equation of design variables can be rewritten in matrix form:

$$[A]\{\alpha\} = \{b\} \quad (7)$$

where $[A]$ is $J \times M$ rectangular matrix, $\{\alpha\}$ is the design variable vector to be determined and $\{b\}$ is a constant vector. In case that M is greater than J , the

governing equation, Eq. (7), has solutions which in general, are not unique. On the other hand, if J is greater than M , Eq. (7) scarcely has any solutions. The prediction about the solution existence based on the size of the coefficient matrix $[A]$ mentioned above suggests that the increase of the number of design variables enlarges the possibility of success in objective homology design.

The solution to Eq. (7) is efficiently handled with the Moore–Penrose generalized inverse [11]. The general solution of Eq. (7) is given as follows when the condition of solution existence given by Eq. (9) is satisfied:

$$\{\alpha\} = [A]^{-}\{b\} + ([I] - [A]^{-}[A])\{h\} \tag{8}$$

$$([I] - [A]^{-}[A])\{b\} = \{0\} \tag{9}$$

where $[A]^{-}$ is the Moore–Penrose generalized inverse of $[A]$, $[I]$ identity matrix and $\{h\}$ arbitrary vector [11]. The first and second terms of the right-hand side of Eq. (8) are called the *particular* and *complementary solution*, respectively. Eq. (8) indicates that the way of changing current trial design to realize objective homologous deformation in general is not unique, since arbitrariness creeps in the general solution of the design variable vector through the arbitrary vector $\{h\}$. We employ only the particular solution to determine the design variable vector for design change. The solution thus determined is the solution of least design change assuming that the Euclidean norm of design variable vector becomes a minimum owing to the property of the Moore–Penrose generalized inverse.

The objective homologous deformation is not realized strictly by the above determined design variables, since the governing equation, Eq. (7), is derived based on the linear approximation of nodal displacements change. The deficient approximation can be compensated by the iterative renewals of structure, in which the hanged structure according to the design variable solution is used as the trial design of the next renewal. The iterative renewals are stopped when the homologous constraint equation is regarded to be satisfied, that is, the Euclidean norm of $\{H(u)\}$ becomes sufficiently small.

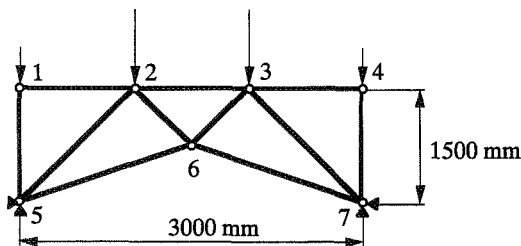


Fig. 2. Eleven-bar truss structure.

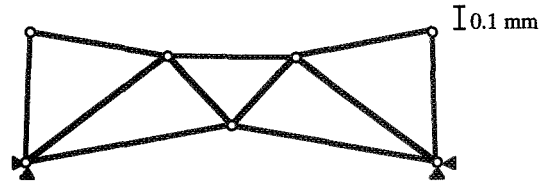


Fig. 3. Deformed structure of initial trial design.

2.2. Numerical example using eleven-bar truss structure

An illustrative example of homology design is demonstrated by using the eleven-bar truss structure illustrated in Fig. 2. The cross-sectional area of all the members is set equal to 100 mm^2 in the initial trial design and the material property of the members is characterized by Young’s modulus, $E = 70.0 \text{ GPa}$. The structure is subjected to a uniformly distributed vertical load of 1.0 N/mm as nominal loading on the uppermost deck. The deformed structure of the initial trial design is depicted in Fig. 3. The measure for displacement is put at the upper right of Fig. 3. The maximum vertical displacement turns out to be 0.133 mm in the initial trial design.

The objective homologous deformation is set so as to keep the uppermost deck straight and horizontal before and after the deformation. The homologous constraint equation is given in the form of

$$\begin{Bmatrix} v_1 - v_m \\ v_2 - v_m \\ v_3 - v_m \\ v_4 - v_m \end{Bmatrix} = \begin{Bmatrix} 0 \\ 0 \\ 0 \\ 0 \end{Bmatrix} \tag{10}$$

where v_i denotes vertical nodal displacement of node i and v_m means the average of vertical nodal displacements on the uppermost deck, that is, $v_m = (v_1 + v_2 + v_3 + v_4)/4$.

The realized homologous deformation by changing the cross-sectional area of all the members is illustrated in Fig. 4. The vertical displacement of the uppermost deck turns out to be 0.0516 mm . The manner for illustration of the deformation is the same as that of Fig. 3. In Fig. 4, the cross-sectional area of the member after homology design is indicated by the number attached to each member. The increase in total weight is 58.7% in this example. Three renewals of trial design are

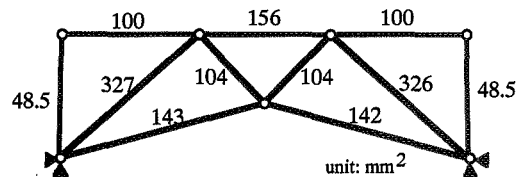


Fig. 4. Realized homologous deformation and changed cross-sectional area.

needed to ensure the sufficiently small Euclidean norm of $\{H(u)\}$, i.e. less than 0.001 mm in this case. One of the transparent homology designs for this example is constructed so as to make the cross-sectional area of vertical and outer horizontal members extremely large. This method inevitably results in an extreme increase of total weight. On the other hand, we take the course of the least design change from the initial design which is chosen judiciously.

3. Convex model of uncertain loading

The legitimate question arises on how sensitive the homology design is to uncertain fluctuation of the loadings. The behavior of the structure is described by the following stiffness equation in the state of the homology design:

$$[K]\{u\} = \{f\} \quad (11)$$

where $[K]$ corresponds to the stiffness matrix of the structure experiencing homology design at the specified nominal loading $\{f^*\}$. The lower bar and asterisk denote the value after homology design and the value under nominal loading, respectively. The fluctuation of loading is represented by introducing N uncertainty variables ε_n assigned to N nodal force components in the form of

$$f_n = f_n^*(1 + \varepsilon_n) \quad (12)$$

The external nodal force vector $\{f\}$ is expressed in the form of Eq. (13) by taking account of the uncertain fluctuation of nodal force components,

$$\{f\} = \{f^*\} + [F]\{\varepsilon\} \quad (13)$$

where $\{\varepsilon\}$ is the uncertainty variable vector which consists of N uncertainty variables. The amplitude of variation $[F]\{\varepsilon\}$ from the nominal loading is assumed to be unknown-but-bounded by a convex hull of hyperellipse with respect to uncertainty variables given in the form of

$$q^2\{\varepsilon\}^T[W]\{\varepsilon\} \leq 1 \quad (14)$$

$[W]$ is a symmetric and positive-definite matrix that defines the shape of the convex hull. The magnification coefficient q governs the expanse of the convex hull. $[W]$ and q are determined from the available information.

4. Worst case estimation of homology design

4.1. Formulation for worst case estimation

In the context of convex analysis the problem is posed as follows: find the most harmful amplitude of variation to maximize the distortion from objective homologous deformation, which is called the worst case. The fluctuation of nodal displacement vector is expressed in the linear approximate form of Eq. (15) by the result of sensitivity analysis with respect to uncertainty variables for the structure governed by the stiffness equation, Eq. (11):

$$\{\underline{u}\} = \{\underline{u}^*\} + \sum_{n=1}^N \{\underline{u}_n^I\} \varepsilon_n \quad (15)$$

$\{\underline{u}^*\}$ is the displacement vector under nominal loading after homology design, i.e. objective homologous deformation, and $\{\underline{u}_n^I\}$ is the rate of change with respect to ε_n . Obviously the homologous constraint in Eq. (3) cannot be satisfied under the uncertain fluctuation of loading. The left-hand side of Eq. (3) after substitution of the fluctuating nodal displacement vector expressed by Eq. (15) is defined as the error vector from exact homologous deformation. The error vector $\{e\}$ is written in the following form:

$$\{e\} = \sum_{n=1}^N [C]\{\underline{u}_n^I\} \varepsilon_n \quad (16)$$

To evaluate the magnitude of the distortion from objective homologous deformation, we introduce a concept of *error index*, which can be defined by using the components of the error vector. In this study, we define the error index Δ^2 as the square of the Euclidean norm of the error vector. The index can be summarized as

Table 1
Estimated error index by convex analysis

Error index, Δ^2 ($\times 10^{-3}$ mm ²)	Uncertainty variables			
	ε_1	ε_2	ε_3	ε_4
2.82	0.707	0.000	0.000	-0.707
2.82	0.500	-0.500	-0.500	0.500
1.94	0.000	-0.707	-0.707	0.000
0.00	0.500	0.500	0.500	0.500

$$\Delta^2 = \{\varepsilon\}^T [D] \{\varepsilon\} \quad (17)$$

where $[D]$ is an $N \times N$ symmetric matrix defined by the rate of change of nodal displacements with respect to uncertainty variables.

The worst case of uncertainty variables, which gives the maximum value of the error index, is searched within the convex hull of Eq. (14). As the error index is expressed in second-order form with respect to uncertainty variables and becomes the convex function, the point of worst case is located on the boundary of convex hull. The search is carried out by the Lagrange multiplier method employing the following functional:

$$\Pi = \Delta^2 - \lambda(q^2\{\varepsilon\}^T [W] \{\varepsilon\} - 1) \quad (18)$$

where λ is the Lagrange multiplier. The uncertainty variables in the worst case are so determined as to satisfy the stationary conditions derived as follows:

$$\frac{\partial \Pi}{\partial \varepsilon} = 2([D] - \lambda q^2 [W]) \{\varepsilon\} = \{0\} \quad (19)$$

$$\frac{\partial \Pi}{\partial \lambda} = q^2 \{\varepsilon\}^T [W] \{\varepsilon\} - 1 = 0 \quad (20)$$

The stationary condition of Eq. (19) results in the eigenvalue problem formed by the eigenvalue λq^2 , which is rewritten by μ , and the eigenvector $\{\varepsilon\}$. On the other hand, the stationary condition of Eq. (20) gives the normalizing condition for the eigenvector. Generally, N eigenpairs are obtained by solving the eigenvalue problem of Eq. (19) under the normalizing condition of Eq. (20). In view of Eqs. (19) and (20), the error index of Eq. (17) becomes

$$\Delta^2 = \{\varepsilon\}^T [D] \{\varepsilon\} = \lambda q^2 \{\varepsilon\}^T [W] \{\varepsilon\} = \lambda = \mu / q^2 \quad (21)$$

as the magnification coefficient q is constant and the maximum value of the error index, i.e. the worst case, is estimated by the maximum eigenvalue obtained by solving Eq. (19). The eigenvector corresponding to maximum eigenvalue gives the uncertainty variable vector for the worst case.

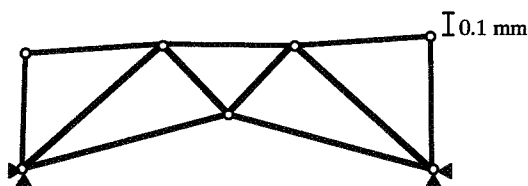


Fig. 5. Deformed structure in worst case 1.

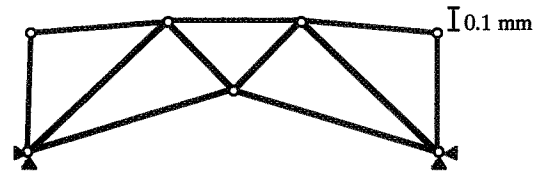


Fig. 6. Deformed structure in worst case 2.

4.2. Numerical example to estimate worst case of homology design

The eleven-bar truss structure obtained from the homology design in Section 2.2 is employed in this numerical example to evaluate the worst case of the distortion from objective homologous deformation caused by uncertain fluctuation of the uniformly distributed vertical load. Four uncertainty variables are assigned to vertical nodal force components for nodes 1, 2, 3 and 4 in Fig. 2. The fluctuation of the uncertainty variables is bounded by hypersphere with radius 1.0, which is expressed by setting q equal to 1.0 and $[W]$ as an identity matrix in Eq. (14). The nodal force components fluctuate from 0 to twice the nominal values in this case.

The result of the worst case estimation obtained by solving the eigenvalue problem of Eq. (19) is shown in Table 1. The error indices estimated by eigenvalue, i.e. $\Delta^2 = \mu / q^2$, are listed in the leftmost column and corresponding uncertainty variables, i.e. eigenvector components, are listed in the right columns. The error index is maximized by two cases of uncertainty variables namely $(\varepsilon_1, \varepsilon_2, \varepsilon_3, \varepsilon_4) = (0.707, 0.0, 0.0, -0.707)$, called worst case 1 and $(\varepsilon_1, \varepsilon_2, \varepsilon_3, \varepsilon_4) = (0.5, -0.5, -0.5, 0.5)$, called worst case 2. The actual error indices evaluated by the analyses employing the nodal force components corresponding to the worst cases 1 and 2 turn out to be equal to $2.82 \times 10^{-3} \text{ mm}^2$ in both cases. The deformations of the eleven-bar truss in the two worst cases are illustrated in Figs. 5 and 6, respectively. The manner of illustration is the same as that employed in Fig. 3.

5. Concluding remarks

A formulation of homology design based on the finite element analysis is reviewed. The change of displacements by design variables is approximated in the first-order by means of the finite element sensitivity analysis and the governing equation for design variables is derived in the matrix form with a rectangular coefficient matrix. The equation is handled with the Moore–Penrose generalized inverse to obtain the least design change solution. The illustrative numerical example using the eleven-bar truss structure demon-

strates that the uppermost deck is maintained straight and horizontal even after the deformation caused by uniformly distributed vertical load.

A methodology to estimate the worst case of homologous deformation caused by uncertain fluctuation of loadings is proposed by means of the convex analysis. The uncertainty variables are assigned to discretized nodal force components and the fluctuation of the uncertainty variables is bounded within a convex hull. The worst case to maximize the error index of homologous deformation is searched on the boundary of the convex hull. The search is carried out by the Lagrange multiplier method. The numerical example using the eleven-bar truss structure proves the validity of the proposed method by demonstrating the identification of the worst case caused by uncertainty variables confined within a hypersphere.

Acknowledgements

The work by I. E. is supported by the NASA Langley Research Center, through grant NAG-1-1310. The supports are gratefully appreciated. This work is a part of a cooperative work between the University of Tokyo and the Florida Atlantic University. The work was performed during the visit of I. E. to the University of Tokyo as Fellow of the Japan Society of Promotion of Science and the visit of N. Y. to the Florida Atlantic University as a Visiting Associate Professor supported by the Foundation for the Promotion of Industrial Science. The views of this publication are those of the authors and do not necessarily represent the views of the sponsoring organizations.

References

- [1] Thomas H L, Sepulveda A E, Schmit L A. Improved approximations for control augmented structural synthesis. *AIAA J.* 1992;30:171–9.
- [2] Kida T, Komatsu K. Vibration control of space structures. *Sci. Mach.* 1993;45:1273–9 (in Japanese).
- [3] Wada B K. Adaptive structure: An overview. *AIAA J. Space Craft* 1990;27:330–7.
- [4] von Hoerner S. Homologous deformation of tilttable telescopes. *J. Struct. Div. Proc. ASCE* 1967;93:461–85.
- [5] Morimoto M, Kaifu N, Takizawa Y, Aoki K, Sakakibara O. Homology design of large antenna. Mitsubishi Elect. Corp., Techn. Rep. 1982;56:495–502 (in Japanese).
- [6] Hangai, Y., Shape analysis of structures. In *Theor. and Appl. Mech.*, Vol. 39. Sci. Council of Japan, University of Tokyo Press, 1990, pp. 11–28.
- [7] Yoshikawa, N. and Nakagiri, S., Homology design of frame structure by finite element method. In *Theor. and Appl. Mech.*, Vol. 42. Sci. Council of Japan, University of Tokyo Press, 1993, pp. 43–51.
- [8] Ben-Haim, Y. and Elishakoff, I., *Convex Models of Uncertainty in Applied Mechanics*. Elsevier, New York, 1990.
- [9] Elishakoff, I. Lin, Y. K. and Zhu, L. P., *Probabilistic and Convex Modeling of Acoustically Excited Structures*. Elsevier, New York, 1994.
- [10] Fox R L. Constraint surface normals for structural synthesis. *AIAA J.* 1965;3:1517–8.
- [11] Rao, C. R. and Mitra, S. K., *Generalized Inverse of Matrices and Its Applications*. John Wiley and Sons, New York, 1971.



NIS

510-39

408 993

©WAINED

358980 p.25

AIAA 97-1242

**Buckling of Structures with Uncertain
Imperfections - Personal Perspective**

I. Elishakoff

Florida Atlantic University

Boca Raton, FL

**38th AIAA/ASME/ASCE/AHS/ASC
Structures, Structural Dynamics, and Materials
Conference and Exhibit
AIAA/ASME/AHS Adaptive Structures Forum
April 7- 10, 1997, Kissimmee, FL**

BUCKLING OF STRUCTURES WITH UNCERTAIN BUT NOT-NECESSARILY
RANDOM IMPERFECTIONS - PERSONAL PERSPECTIVE

Isaac Elishakoff
Dept. of Mechanical Engineering
Florida Atlantic University
Boca Raton, FL 33431-0991

ABSTRACT

The previous review on stochastic buckling of structures was written by Amazigo in 1976. This review summarizes some of the developments which took place in recent two decades. A brief overview is given of the effect on uncertainty in the initial geometric imperfections, elastic moduli, applied forces, and thickness variation. For the benefit of the thinking reader, the review has a critical nature.

It should be noted that this manuscript has yet to be completed. The list of topics to be included is listed below. The final version of the manuscript will be obtainable by informing this writer.

1. INTRODUCTION

The general theory of buckling and postbuckling behavior of elastic structures was worked out by Koiter (1945, 1963). Further contributions were provided by Budiansky and Hutchinson (1964), Arbocz (1985) and other investigators. For a bibliography the reader may consult, for example, with the articles by Budiansky (1974), Budiansky and Hutchinson (1979), Koiter (1985), and Arbocz (1990).

There are many other investigations dealing with the chism that exists between the theoretical analyses and the experimental

results. Most unfortunately, the experimental results "misbehave" their way and do not match the theoretical predictions. In these circumstances it was not unnatural to look for the uncertainty as a responsible factor for the scatter in experimental results. One conceptually understands that there are not two identical shells produced by the same manufacturing procedure. Motivated by this idea, the investigators could ascribe the scatter in buckling loads to the scatter in initial imperfections.

Next step made was to identify uncertainty with randomness and to utilize the probabilistic methods. We find the first hints of these thoughts in the paper by Hoff (1949):

"...The nature and the magnitude of the disturbance must be established from a statistical investigation of the conditions under which the structural element or part of machinery will be used. The safe of the system can be safeguarded if it is made stable for all disturbances which have a probability greater than a required minimum."

This idea, apparently independently, was pursued by Bolotin (1958). He postulated, in brief, that the buckling load λ of a structure can be expressed as a deterministic function of a finite number of parameters $\bar{\xi}_i$, representing the initial imperfections:

$$\lambda = \varphi(\bar{\xi}_1, \bar{\xi}_2, \dots, \bar{\xi}_N) \quad (1)$$

where N is the number of terms taken in expansions. we also assume that we are given a particular function φ , and that joint probability density

$$f_{\bar{X}}(\bar{\xi}_1, \bar{\xi}_2, \dots, \bar{\xi}_N) = \text{Prob} \left[\bigcap_{i=1}^n (\bar{\xi}_i \leq \bar{X}_i \leq \bar{\xi}_i + \Delta\bar{\xi}_i) \right] \quad (2)$$

of random initial imperfection vector, denoted by $X = (\bar{X}_1, \bar{X}_2, \dots, \bar{X}_N)^T$ i.e. the probability that the random components \bar{X}_i of the vector \bar{X} will belong to the interval $(\bar{\xi}_i, \bar{\xi}_i + \Delta\bar{\xi}_i)$, where $\Delta\bar{\xi}_i$ is an increment. Note that the random variables are denoted by capitals, whereas the possible values they can take on are identified by lower-case notation. Bolotin applied this method to a cylindrical panel under uniform compressive load along its curved edges, with the initial imperfections represented by a single normally distributed amplitude parameter. A single-term Galerkin approximation yielded an equation of type (1). Conceptually such an one-term analysis is not complicated. Once relation of type (1) is obtained, and the probability density of the initial imperfection \bar{X}_{i_0} is specified or assumed (i_0 is the index of the governing initial imperfection parameter) one calculates the reliability of the structure. We first note that due to assumed randomness of the initial imperfection, the associated buckling load turns out to be also a random variable, denoted by Λ . The reliability at the load level α is defined as the probability that the structure will not buckle prior to α , or in other words, it will live beyond "age" α :

$$R(\alpha) = \text{Prob}(\Lambda > \alpha) \quad (3)$$

Having determined the reliability of the structure, one proceeds with its design as follows. One should have a codified reliability

r , i.e. the level of reliability below which the performance of the structure is defined as an unacceptable one. The probabilistic design criterion demands that

$$R(\alpha) > r \quad (4)$$

Combining Eqs. (3) and (4) leads to

$$R(\alpha) = \text{Prob}(\Lambda > \alpha) \geq r \quad (5)$$

Inequality (5) leads to a possibility to solve some basic problems of stochastic buckling. If the left and right sides of Eq. (4) are known then one can check if the probabilistic design criterion (4) is met, or it is violated. If some probabilistic characteristic of the initial imperfection, say its variance $d_{i_0}^2$, is unspecified, one can calculate its maximum admissible level of it $\max d_{i_0}$, such that the design criterion is satisfied. The value $\max d_{i_0}$ is obtained by solving an equation

$$R(\alpha) = \text{Prob}(\Lambda > \alpha) = r \quad (6)$$

Solution of this type of problems may then be introduced in the quality control measure; if the variance of the initial imperfection exceeds $\max v_{i_0}$ the structure is declared unacceptable.

This third problem consists in determining the design load α_r , such that if $\alpha \leq \alpha_r$, then the reliability will not be less than r .

The reliability of the structure at the nondimensional load level α can be rewritten as

$$R(\alpha) = \text{Prob} \left(-\bar{\xi}_1 \leq \bar{X}_{i_0} \leq \bar{\xi}_1 \right) \quad (7)$$

where $\bar{\xi}_1$ is the value at which the limit load equals α . This implies that $\bar{\xi}_1$ satisfies an equation:

$$\lambda = \varphi(\bar{\xi}_1) = \alpha \quad (8)$$

Hence

$$\bar{\xi}_1 = \varphi^{-1}(\alpha) \quad (9)$$

If, for example $\bar{X} \equiv \bar{X}_{i_0}$ is a random variable having a normal distribution with zero mean and mean-square deviation d

$$f_{\bar{X}}(\bar{X}) = \frac{1}{\sqrt{2\pi}d} \exp \left[-\frac{\bar{X}^2}{d_{i_0}^2} \right] \quad (10)$$

Then the reliability becomes:

$$R(\alpha) = \text{Prob} \left(-\varphi^{-1}(\alpha) \leq \bar{X} \leq \varphi^{-1}(\alpha) \right) \quad (11)$$

$$= 2 \text{erf} \left[\frac{\varphi^{-1}(\alpha)}{2d_{i_0}} \right] \quad (12)$$

This allows to find the probabilistic design load α_r , such that if $\alpha = \alpha_r$, then the least reliability of the structure equals r :

$$\alpha_r = \varphi \left[2d_{i_0} \text{erf}^{-1} \left(\frac{r}{2} \right) \right] \quad (13)$$

In order to illustrate the stochastic imperfection sensitivity

concepts let us consider a simple structure, namely, a column on a nonlinear elastic foundation

$$EI \frac{d^4 w}{dx^4} + P \frac{d^2 w}{dx^2} + k_1 w - k_3 w^3 = -P \frac{d^2 \bar{w}}{dx^2} \quad (14)$$

where $\bar{w}(x)$ = initial imperfection, $w(x)$ - additional deflection P = axial load, k_1 and k_3 = nonlinear spring coefficients of the foundation. The buckling of the perfect column on a linear foundation is a classical, textbook problem. The imperfect column on a nonlinear softening elastic foundation exhibits imperfections sensitivity in that the limit load the structure may support may turn out to be far less than that of perfect linear counterpart. Application of the Galerkin method for the column that is simply supported at its ends yields in a single-term approximation the following equation, derived by Fraser (1965) in his Ph.D. dissertation:

$$(1 - \lambda)^3 = \frac{81}{32} s \bar{\xi}_m^2 \lambda^2 \quad (15)$$

where $\bar{\xi}_m$ = initial imperfection amplitude associated with m half-sine waves in axial direction, λ = nondimensional limit load, s is a value depending on the physical parameters of the system.

This type of analysis can be demonstrated on the imperfection sensitivity of a shell with a non-axisymmetric periodic imperfections, studied by Koiter (1963):

$$w_0(x) = gh \left[\cos \frac{i_c \pi x}{L} + 4 \cos \frac{i_c \pi x}{2L} \cos \frac{i_c \pi y}{2L} \right] \quad (16)$$

where x = axial coordinate, y circumferential coordinate, g = non-

dimensional initial imperfection amplitude, $i_c =$ the number of half-waves at which the associated perfect shell buckles, $L =$ shell length, $h =$ shell thickness. Koiter (1963) arrived at the following equation relating the buckling load with the initial imperfection amplitude:

$$(1 - \lambda)^2 + 6cg\lambda = 0 \quad (17)$$

when $\lambda = P_{lim}/P_c$, where P_{lim} is the limit load, $P_c =$ classical buckling load of the perfect shell.

The analysis which is based on a single term approximation is quite similar in its general spirit but not in its particulars to the asymptotic analysis developed by Koiter (1945, 1963) and Budiansky and Hutchinson (1964). The asymptotic equations or the equations based on a single-term Galerkin approximations can be utilized for explanatory purposes.

Indeed, we are looking for highly reliable performance, associated with the probability of failure, say 10^{-6} or even less. Realizing this, one immediately should cast a doubt on the possibility that the highly simplified expressions (which are of extreme importance to capture the physical phenomenon itself) would reliably produce the required high reliability. In other words, simplified expressions may be unusable to calculate extremely small probability of failure.

It was perfectly valid to utilize a single-term Galerkin approximation in Bolotin's (1958) early work. Analogously, application of Koiter's (1963) asymptotic expressions by Thompson (1967), Roorda (1972) and Hansen and Roorda (1973) served a purpose

of illustrating the reliability approach in imperfection-sensitive structures. Yet it appears that an industrial firm, for example, cannot use simplified expressions to justify then reafter reliability calculations with attendant extremely small probabilities of failure; taking into account additional terms in Galerkin expansion or additional terms in asymptotic expansions, may significantly alter the resulting probabilities of failure, and invalidate the proposed designs. Yet, some very recent works still utilize the deterministic asymptotic expansions for reliability calculations (see, e.g., Cederbaum et al 1996).

We must assume that these fine points were perfectly understood by some investigators quite early, since they did not follow the single-term or deterministic asymptotic methodologies, superimposed with treating the imperfection amplitude as a random variable.

2. STUDIES BASED ON ERGODICITY ASSUMPTION

In his review paper Amazigo (1976) stresses, relating to the equation (1) postulated by Bolotin (1958):

"It is however a nontrivial problem to obtain on (1) and perform the above analysis for $n > 2$, say. It is this difficulty that limits the effectiveness of this method."

Instead of utilizing the concept of the random variable, as in works by Bolotin (1958) and Thompson (1967), the scholars of the Harvard group correctly decided to adopt the theory for random functions, identifying the initial imperfections as random fields with specified probabilistic characteristics, namely, the mean

initial imperfection function and the covariance function. Apparently first such study dealing with imperfection sensitive structures was undertaken by Frazer and Budiansky (1969). They studied the imperfect column on a nonlinear elastic foundation. The length of the column was taken to be infinity. The following assumptions were made about the initial imperfection field : (a) they were considered to form a homogeneous random field, (b) the assumption of ergodicity of this field was also introduced.

Weak homogeneity implies that the mean initial imperfection function is a constant, whereas the autocorrelation function depends only on the difference $x_2 - x_1$, where x_1 and x_2 are spatial coordinates. This insensitivity to the shift of initial cross-section of reference is possible for infinite domains. Therefore, possibly, this infinite length assumption that was adopted. For solving the problem authors resorted to the classical method of stochastic linearization and the additional assumption, that the output random field, namely the additional deflection of the column, was ergodic too. The main conclusion derived in the paper was that each infinite column in the ensemble has the same buckling load, which depends on the autocorrelation function of the initial imperfection alone, not on a particular realization of any of them. Since then, perhaps because of this surprising conclusion, this problem attracted the attention of other investigators who tackled the problem by various methods. Authors used the method of stochastic linearization (Amazigo et al, 1971), truncated hierarchy (Amazigo, 1969, Amazigo et al, 1971), and perturbation (Amazigo, 1971; Amazigo 1974). In his review Amazigo (1976) comments on the

ergodicity assumption:

"The method...based on the ergodicity hypothesis leads to the conclusion that the structure will buckle statically or dynamically at the corresponding (deterministic, I.E.) load... with probability 1. This result may appear paradoxical. However, to dispel the apparent contradiction we note that no matter how the origin of an infinitely long column is defined the buckling load for such columns with imperfections $\bar{w}(x) = \sin(x + \phi)$ is independent of ϕ and hence independent of any probabilistic distribution we may assign to ϕ ."

It appears to us that the source of this paradoxal result stems from the fact that the authors assumed the ergodicity not only of the input field, but also of the output field. This assumption allowed to facilitate the solutions that were derived. In order to check the validity of such an assumption Scheurkogel et al (1981) undertook an investigation of a model system, which allowed to obtain a closed-form solution. Then the same problem was solved by invoking the ergodicity assumption. A control parameter k was introduced so that one could study the varying behavior of the system as the control parameter was changed. It turned out that, in general the output of the system was *inergodic*. At some value of the parameter, $k = 2$, the ergodicity assumption yielded a result coinciding with the response obtained exactly. This implies that sometimes the error may not affect the estimate of the system's response! In two distinctive ranges of parameter k the behavior turned out to be of different nature. For $0 \leq k < 2$ the ergodicity assumption introduced a small error of the order of

one percent. Yet, for $2 < k \leq 4$ the ergodicity assumption introduced a small error of the order of one percent. Yet, for $2 < k \leq 4$ the ergodicity assumption led to large errors. In particular, when k tends to four the ergodicity-based solution is finite, whereas the exact solution is unbounded. As is seen, extreme caution must be exercised when invoking the ergodicity assumption: the differential equation itself, rather than an analyst, will decide if the output is ergodic or not!

Closely related conclusions were arrived at in another investigation (Scheurkogel et al, 1985) which studied an applied mechanics problem, in which Bolotin (1971) also utilized an ergodicity assumption.

3. MONTE CARLO METHOD

The present author was introduced to stochastic buckling rather incidentally. During the academic year 1977/78, Professor Bernard Budiansky was supposed to spend a sabbatical year at the Department of Aerospace Engineering of the Technion-Israel Institute of Technology. Head of the Structures Group, Professor Joseph Singer recommended me to investigate some problems which may generate an interest of the sabbatical visitor. Without taking an obligation to do so (we all have an academic freedom, don't we?) I decided to study some of the works of Professor Budiansky in more detail.

I read several elegant articles of Budiansky and Hutchinson voted to the imperfection sensitivity of structures. Then, when I

read the article by Frazer and Budiansky (1969), their result of it struck me: the realizations of the columns are different, yet they all share the same, deterministic buckling load! Yes, this load did depend on the probabilistic characteristic of the imperfection, yet it was a constant! Interestingly and surprisingly, this load depended upon the single value of the spectral density of initial imperfections, and was independent, otherwise, on the spectral content of the field.

I have decided that instead of pursuing a new purely analytic approach, in addition to what was already undertaken in Harvard, it would be nice to perform an experiment. Yet, where should we get numerous realizations, I thought, of the real column on nonlinear elastic foundations? If not in the real laboratory, then may be in the virtual one: on the computer? Thus the idea occurred to study the Frazer-Budiansky problem by the Monte Carlo simulation.

The idea did not seem to be very fancy or even new. Indeed, Frazer (1965) performed the Monte Carlo analysis of a column on a nonlinear foundation. Yet, most unfortunately, he limited himself with a single-term approximation which leads, once this assumption is made, to a closed-form solution. Naturally, one does not need the Monte Carlo solution if the exact solution is at hand, except when one wants to illustrate the validity of the Monte Carlo solution in the particular case capable of the exact solution. Once the confidence is gained, one resorts if the multi-mode solution when the exact solution is unavailable.

Multi-term Monte Carlo simulation was conducted by Hansen (1977) in his probabilistic analysis of randomly imperfect shells. However, the analysis performed could be characterized as an

unbalanced one: fancy analytical analysis was superimposed with a naive probabilistic analysis. The assumption was made that all the Fourier coefficients used in the series expansion were identically distributed. Namely, each Fourier coefficient was taken as a normally distributed variable with the same variance. This assumption in essence corresponds to the "white-noise" autocorrelation function of the initial imperfections. Thus, the analysis did not allow the information on general autocovariance function. Some other investigators too, although in a dynamic context, neglected correlations between the various Fourier coefficients, although adopted the nonconstant variances (even a new term was coined for this doubtful proposition: "grey noise," see Lindberg, 1983).

It was realized by this writer that the simulation analysis should start from the mean function and the autocovariance function, and end up with the variance-covariance matrix of initial imperfection's Fourier coefficients. This matrix, in general case, must be a fully populated one: not a diagonal one with identical (Hansen 1977) or different (Lindberg, 1993) elements. In order to study the Frazer-Budiansky model structure the present writer developed a general simulation procedure for solving the stochastic boundary value problems (Elishakoff 1979).

This simulation procedure was applied to the impact buckling of a column (Elishakoff 1978), Hoff's problem of buckling of a column in a testing machine (Elishakoff, 1980) and to the Frazer-Budiansky problem (Elishakoff, 1979). A column of finite length was studied because of several reasons: (1) an assumption of infinite length may simplify the analytical analysis but may

complicate the numerical one, (2) the structures utilized and analyzed by engineers do not possess with the infinite length, (3) the nonlinear column on nonlinear elastic foundation does not have a behavior of the edge-effect to justify for looking for interior solutions as those associated with the infinite structure, and edge effect solutions near the edges. For each realization buckling load was found numerically by transforming the nonlinear algebraic equations to the numerically solved ordinary differential equations. The adopted method of Qiria (1951) and Davidenko (1953) is similar to the arc-length method of Riks (1979), as was communicated to this writer by Professor W. T. Koiter. Reliability of the column was calculated. Following conclusions were drawn:

- (1) Monte Carlo solution yields results that are practically coincident with the exact solution, when the latter is available. This demonstrates that the Monte Carlo solution may exhibit a better performance than the various statistical tests may predict.
- (2) A single-term Galerkin approximation is not sufficient to reliably predict the structural reliability; depending on the system's parameters, various but higher degrees of approximation must be achieved in order reliability estimates to be accurate.
- (3) Design buckling load associated with high reliability may significantly deviate from the average buckling load.
- (4) When the length of the column increases the variance of the buckling load decreases.

The latter conclusion is not in disagreement with the result of Frazer and Budiansky (1969) that for an infinite column the

buckling load is a deterministic quantity. For the realistic finite column the buckling load depends on the particular realization of the initial imperfection function, which in turn depends on the probabilistic measures (mean and covariance function) of the initial imperfections.

In a later analysis Day (1980) showed that in some simple cases the ergodicity assumption may even be dispensed with for the evaluation of the mean buckling load. Yet the analyses yielding mean buckling load alone could hardly be considered practical. Each of us may remember various, sometimes entertaining, objections to average quantities. Anyway, the knowledge of the average buckling load is insufficient for probabilistic design of structures undergoing buckling.

Having a general simulation procedure for initial imperfections with given mean and covariance functions pinpointed the way of introducing the initial imperfection sensitivity into design. It involves three main items:

- (a) Development of accurate deterministic (analytical or numerical) tools, for buckling load prediction.
- (b) Compiling extensive experimental information on imperfections, boundary conditions, elastic properties, scatter in loads etc., in view of deriving mean functions of random fields, and their covariance functions, and assessing their distributions.
- (c) Utilization of the Monte Carlo analysis with simulating brothers and sisters (but not perfect clowns!) of the experimentally measured structures.

This writer was humbled to read in several publications of Arbocz (1991):

"It was not until 1979, when Elishakoff published his reliability study... that a method has been proposed, which made it possible to introduce the results of imperfection surveys into the analysis."

SECTIONS THAT REMAIN TO BE WRITTEN

4. RELIABILITY OF SHELLS OR HOW THE BEAUTIFUL THEORIES ARE KILLED BY UGLY EXPERIMENTAL FACTS
5. A TALE OF THICKNESS VARIATION
6. IS PROBABILISTIC THEORY SO GOOD, AFTER ALL? (PROBABILITY IS NOT A MAGIC WAND)
7. CONVEX MODELING OF INITIAL IMPERFECTIONS
8. OPTIMIZATION AND ANTI-OPTIMIZATION UNDER BUCKLING

FUTURE NEEDS

It appears to this writer that the research should concentrate on several directions:

- (1) Accumulation of data for statistical analysis to check the nature of the distribution of random initial imperfections, elastic moduli, thickness variations, load variations etc.
- (2) Development of techniques of the identification of boundary conditions, which may turn out to have a nonuniform nature. When limited data is provided, the problem of identification may be replaced by establishment of local modifications in boundary conditions, during the use of the structure, via convex modeling.
- (3) Development of finite element codes in stochastic setting, incorporating uncertain imperfections, elastic moduli, boundary conditions, thickness variation, and loading conditions development of buckling post processors to commercially available codes like NASTRAN, ADINA, ALGOR etc.
- (4) Possible establishment of a "NASA-University Buckling Institute," which will establish direct connection between the industry and researchers, to deal with relevant problems.
- (5) Possible launching of new NASA Initiative, at least on a "small fire," so that relevant buckling research would not diminish.

ACKNOWLEDGEMENT

The financial support provided by NASA Langley Research Center, through Grant NAG-1-1310 is gratefully acknowledged. It is also the pleasure to acknowledge cooperation with Dr. James H. Starnes, Head of Aircraft Structures, for continuously posing exciting problems and new challenges.

REFERENCES

Adali S., Elishakoff I., Richter A. and Verijenko V.E., Optimal Design of Symmetric Angle Ply Laminates for Maximum Buckling Load with Scatter in Material Properties, *Proceedings, 5th AIAA/USAF/NASA/ISSMS Symposium on Multidisciplinary Analysis and Optimization*, AIAA Paper 94-4365-CP, AIAA Press, Washington DC, pp. 1041-1045, 1994.

Amazigo J. C., Buckling under Axial Compression of Long Cylindrical Shells with Random Axysymmetric Imperfections, *Quarterly of Applied Mechanics*, Vol. 26, 537-566, 1969.

Amazigo J. C., Budiansky B. and Carrier G. F., Asymptotic Analysis of the Buckling of Imperfect Columns on Nonlinear Elastic Foundation, *International Journal of Solids and Structures*, Vol. 6, 1341-1356, 1971.

Amazigo J. C., and Budiansky B., Asymptotic Formulas for the Buckling Stresses of Axially Compressed Cylinders with Localized or Random Axysymmetric Imperfections, *Journal of Applied Mechanics*, Vol. 39, 179-184, 1972.

Amazigo J. C., Buckling of Stochastically Imperfect Columns on Nonlinear Elastic Foundations, *Quarterly of Applied Mathematics*, Vol. 29, 403-409, 1971.

Amazigo J. C., Buckling of Stochastically Imperfect Structures, *Buckling of Structures* (B. Budiansky, ed.), Springer Verlag, pp. 172-182, Berlin, 1976.

Amazigo J.C., Asymptotic Analysis of the Buckling of Externally Pressurized Cylinders, with Random Imperfections, *Quarterly of Applied Mathematics*, Vol. 31, 429-442, 1974.

Arbocz J., The Imperfection Data Bank, a Means to Obtain Realistic Buckling Loads, *Buckling of Shells, A State-of-the Art Colloquium* (E. Ramm, ed.), University of Stuttgart, pp. 10.1-10.33, 1982.

Arbocz J., Present and Future of Shell Stability Analysis, *Zeitschrift fuer Flugwissenschaften und Wltraumforschung*, Vol. 5, 335-348, 1991.

Arbocz J. and Abramovich H., The Initial Imperfection Data Bank at the Delft University of Technology, Part 1, Report LR-290, Department of Aerospace Engineering, Delft University of Technology, Dec. 1979.

Bolotin V. V. *Application of Methods of Theory of Probability and Theory of Reliability in Analysis of Structures*, Izdatelstvo Literaturny po Stroitelstvu, Moscow, 1971 (in Russian).

Bolotin V. V., Statistical Methods in the Nonlinear Theory of Elastic Shells, *Izvestija Akademii Nauk SSSR, Otdelenie Tekhnicheskikh Nauk*, No. 3, 1958. English translation: NASA TTF-85, pp. 1-16, 1962.

Budiansky B., Theory of Buckling and Postbuckling Behavior of Elastic Structures, in *Advances in Applied Mechanics*, Vol. 14, Academic Press, New York, pp. 1-65, 1974.

Budiansky B. and Hutchinson J.W., Dynamic Buckling of Imperfection Sensitive Structures, *Proceedings of the Eleventh International Congress of Applied Mechanics*, (Görtler M., ed.), pp. 636-651, Munich, 1964.

Cederbaum G. and Arbocz J., On the Reliability of Imperfection-Sensitive Long Isotropic Cylindrical Shells, *Structural Safety*, Vol. 18, 1-9, 1996.

Cederbaum G. and Arbocz J., Reliability of Shells via Koiter Formulas, *Thin-Walled Structures*, Vol. 24, 173-187, 1996.

Davidenko D.F., On a Method of Numerical Solution of the Systems of Nonlinear Equations, *Proceedings of the USSR Academy of Sciences*, Vol. 88, 601-602, 1953 (in Russian).

Day W. B., Buckling of a Column with Nonlinear Restraints and Random Initial Imperfections, *Journal of Applied Mechanics*, Vol. 47, 204-205, 1980.

Elishakoff I., How To Introduce the Imperfection Sensitivity Concept into Design Collapse (J. M. T. Thompson and G. W. Hunt, eds.), Cambridge University Press, pp. 345-357, 1985.

Elishakoff I., Cai G.Q. and Starnes J. H. Jr., Non-linear Buckling of a Column with Initial Imperfection via Stochastic and Non-Stochastic Convex Models, *International Journal of Non-Linear Mechanics*, Vol. 29, 71-82, 1994.

Elishakoff I. and Nordstrand T., Probabilistic Analysis of Uncertain Eccentricities in a Model Structure. *Proceedings of the Sixth International Conference on Applications of Statistics and Probability in Civil Engineering*, (L. Esteva and S. E. Ruiz, eds.), Vol. 1, pp. 250-256, Mexico City, 1991.

Elishakoff I., Li Y.W. and Starnes J. H. Jr., A Deterministic Method to Predict the Buckling Load Variability due to Uncertain Elastic Moduli, *Computer Methods in Applied Mechanics and Engineering*, Vol. 111, 155-1667.

Elishakoff I., Stochastic Simulation of an Initial Imperfection Data Bank for Isotropic Shells with General Imperfections, *Buckling of Structures: Theory and Experiment* (I. Elishakoff, J. Arbocz, C.D. Babcock, Jr. and A. Libai, eds.), Elsevier, Amsterdam, pp. 195-210, 1988.

Elishakoff I., Hoff's Problem in a Probabilistic Setting, *Journal of Applied Mechanics*, Vol. 47, 1-6, 1980.

Elishakoff I., Buckling of a Stochastically Imperfect Finite Column on a Nonlinear Elastic Foundation, *Journal of Applied Mechanics*, Vol. 46, 411-416, 1979.

Elishakoff I., Simulation of Space-Random Fields for Solution of Stochastic Boundary-Value Problems, *Journal of Acoustical Society of America*, Vol. 65, 399-403, 1979.

Elishakoff I., Impact Buckling of Thin Bar via Monte Carlo Method, *Journal of Applied Mechanics*, Vol. 45, 586-590, 1978.

Elishakoff I., *Probabilistic Methods in the Theory of Structures*, Wiley, New York, 1983.

Elishakoff I. and Arbocz J., Reliability of Axially Compressed Cylindrical Shells with Random Axysymmetric Imperfections, *International Journal of Solids and Structure*, Vol. 18, 563-585, 1982.

Elishakoff I., van Manen S., Vermuelen P. and Arbocz, J., First-Order Second-Moment Analysis of the Buckling of Shells with Random Imperfections, *AIAA Journal*, Vol. 25, 1113-1117, 1987.

Elishakoff I. and Fang J. J., Diagnosis of Local Modifications in the Boundary Conditions of a Rectangular Plate via Convex Modeling, *Computer Methods in Applied Mechanics and Engineering*, Vol. 124, 303-319, 1995.

Fersht R., Buckling of Cylindrical Shells with Random Imperfections *Thin Shell Structures: Theory, Experiment and Design* (Y.C. Fung and E. E. Sechler, eds.), Prentice-Hall, Englewood Cliffs, pp. 325-341, 1974.

Frazer W. B. and Budiansky B., The Buckling of a Column with Random Initial Deflection, *Journal of Applied Mechanics*, Vol. 36, 232-240, 1969.

Frazer W. B., Buckling of a Structures with Random Imperfections, Ph.D. Thesis, Division of Engineering and Applied Sciences, Harvard University, 1965.

Hansen J., General Random Imperfections in the Buckling of Axially Loaded Cylindrical Shells, *AIAA Journal*, Vol. 15, 1250-1256, 1977.

Hansen J., Influence of General Imperfections in Axially Loaded Cylindrical Shells, *International Journal of Solids and Structures*, Vol. 11, 1223-1233, 1975.

Hansen J. S. and Roorda J., Reliability of Imperfection Sensitive Structures, *Stochastic Problems in Mechanics* (S. T. Ariaratman and H. H. E. Leipholz, eds.), Waterloo University Press, pp. 229-242, 1973.

Hansen J. S. and Roorda J., On the Probabilistic Stability Theory for Imperfection Sensitive Structures, *International Journal of Solids and Structures*, Vol. 10, 341-359, 1974.

Hoff N. J., The Perplexing Behavior of Thin Circular Cylindrical Shells in Axial Compression, *Israel Journal of Technology*, Vol. 4, 1-28, 1966.

Hoff N. J., *Dynamic Criteria and Buckling*, Engineering Structures Supplement, Butterworth Scientific Publications, London, 1949.

Ikeda K., Murota K. and Elishakoff I., Reliability of Structures Subjected to Normally Distributed Initial Imperfections, *Computers and Structures*, Vol. 59, 463-469, 1996.

Koiter W. T., On the Stability of Elastic Equilibrium (in Dutch), Thesis, Delft University, H. J. Paris; Amsterdam; English translations: (a) NASA TT-F-10, 833, 1967; (b) AFFDL-TR-70-25, 1970.

Koiter W. T., Elishakoff I., Li Y.W. and Starnes J. H. Jr., Buckling of an Axially Compressed Cylindrical Shell of Variable Thickness, *International Journal of Solids and Structures*, Vol. 31, 797-805, 1994.

Koiter W. T., Elishakoff I., Li Y. W. and Starnes J. H. Jr., The Combined Effect of the Thickness Variation and Axisymmetric Initial Imperfection on the Buckling of the Isotropic Cylindrical Shell under Axial Compression, *Proceedings, 35th AIAA/ASME/ASCE/AHS/ASC Structural Dynamics and Materials Conference*, Hilton Head, AIAA, pp 277-289, 1994.

Koiter W. T., Elastic Stability and Postbuckling Behavior, in *Nonlinear Problems* (Langer R. E., ed.), University of Wisconsin Press, Madison, pp. 257-275, 1963.

Li Y.W., Elishakoff I., Starnes J. H. Jr., and Shinozuka M., Nonlinear Buckling of a Structures with Random Imperfection and Random Axial Compression by a Conditional Simulation Technique, *Computers and Structures*, Vol. 56, 59-64, 1995.

Makaroff B. P., Statistical Analysis of Nonideal Cylindrical Shells, *Izvestiya Akademicheskikh Nauk SSSR, Mekhanika Tverdogo Tela*, Vol. 5, No. 1, 97-104, 1970 (in Russian).

Makaroff B. P., Statistical Analysis of Stability of Imperfect Cylindrical Shells, *Proceedings of Seventh All-Union Conference on the Theory of Plates and Shells*, Dnepropetrovsk, pp. 387-391, 1969 (in Russian).

Pantelides C. P., Buckling and Post-Buckling of Stiffened Elements with Uncertainty, *Thin-Walled Structures*, Vol. 26, 1-17, 1996.

Pantelides C. P., Stability of Elastic Bars on Uncertain Foundations using a Convex Model, *International Journal of Solids and Structures*, Vol. 33, 1257-1269, 1996.

Qiria V. S., Motion of the Bodies in Resisting Media, *Proceedings of Tbilisi State University*, Vol. 44, 1-20, 1951 (in Russian).

Riks E., An Incremental Approach to the Solution of Snapping and Buckling Problems, *International Journal of Solids and Structures*, Vol. 15, 524-551, 1979.

Roorda J., *Buckling of Elastic Structures*, University of Waterloo Press, 1980.

Roorda J., Buckling of Shells: An Old Idea with New Twist, *Journal of Engineering Mechanics Division*, Vol. 98, 531-538, 1972.

Scheurkogel A. and Elishakoff I., On the Ergodicity Assumption in an Applied Mechanics Problem, *Journal of Applied Mechanics*, Vol. 52, 133-136, 1985.

Scheurkogel A., Elishakoff I. and Kalker J., On the Error That Can Be Induced by an Ergodicity Assumption, *Journal of Applied Mechanics*, Vol. 48, 654-656, 1981.

Singer J., Abramovich H. and Yaffe R., Initial Imperfection Measurements of Integrally Stringer-Stiffened Cylindrical Shells, *TAE Report 330*, Department of Aeronautical Engineering, Technion-Israel Institute of Technology, Dec. 1978.

Stam A. R., Stability of Imperfect Cylindrical Shells with Random Properties, *AIAA/ASME/ASCE/AHS Structures, Structural Dynamics & Materials Conference*, Vol. 3., pp. 1307-1315, AIAA, New York, 1996.

Thompson J. M. T., Towards a General Statistical Theory of Imperfection Sensitivity in Elastic Post-Buckling, *Journal of Mechanics of Physics and Solids*, Vol. 15, 413-417, 1967.

Verduyn W.D. and Elishakoff I., A Testing Machine for Statistical Analysis of Small Imperfect Shells, *Proceedings of the Seventh International Conference on Experimental Stress Analysis* (A. Betser, ed.), Ayalon Press, Haifa, pp. 545-557, 1982.

Videc B. P. and Sanders J. L., Jr., Application of Khasminskii's Limit Theorem to the Buckling Problem of a Column with Random Initial Deflections, *Quarterly of Applied Mathematics*, Vol. 39, 422-428, 1976.